DYNAMICS OF HEAVY QUARK IN A MEDIUM

Balbeer Singh

DYNAMICS OF HEAVY QUARK IN A MEDIUM

Thesis submitted to
Indian Institute of Technology Gandhinagar
for the award of the degree

of

Doctor of Philosophy

by

Balbeer Singh
[Roll No. 15330015]

under the guidance of

Prof. Hiranmaya Mishra
Senior Professor
Theoretical Physics Division
Physical Research Laboratory, Ahmedabad

DEPARTMENT OF PHYSICS
INDIAN INSTITUTE OF TECHNOLOGY GANDHINAGAR
July 2020

Abstract

Heavy quarks (HQs) like charm (c), bottom (b), and their bounds states such as $J/\psi, \Upsilon$, etc. provide a unique framework and tool to systematically investigate the in-medium properties of strong interaction in high energy nuclear-nuclear collisions. This uniqueness is firstly because of their large mass (M) compared to the inherent QCD scale (Λ_{QCD}) as well as the emergent scales such as temperature (T) in the thermalized medium that is believed to be created in these nuclear collisions. Indeed, due to a large mass threshold, HQs are not produced in the thermal medium for the temperature range achieved in nuclear collision experiments. Thus, both the production mechanism and number of HQs are controlled by the hard scatterings, mainly gluon-gluon fusion during the initial stages of the collision. Secondly, the vacuum properties of HQs and their bound states are quite well understood in pp collision. Therefore, any modification on HQ observables such as jets and quarkonia properties signals the presence of a thermalized bulk medium consisting of light quarks and gluons.

In nuclear collision experiments, the accelerated beam of charged ions is also responsible for the magnetic field generation. Indeed the strongest field in nature, i.e., $\sim 15m_\pi^2$ at LHC with Pb-Pb nuclei at $\sqrt{s} = 2.75$ TeV/A and $\sim m_\pi^2$ at RHIC Au-Au nuclei at $\sqrt{s} = 200$ GeV/A. Even though this magnetic field decreases rapidly in a vacuum, it may be possible that it stays reasonably strong for a longer time and directly affects the dynamics of light partons and HQ through its interaction with the light partons in a magnetized thermal medium as well as in pre-equilibrium phase. This situation may arise in the case when the system develops a finite electrical conductivity during the thermalization process. There have been many efforts to estimate electrical conductivity both in QGP as well as hadronic medium and its effects on the strength of the magnetic field and its phenomenological implications both theoretically as well as experimentally.

In order to characterize the in-medium properties of strong interaction at RHIC and LHC energy scales, perturbative QCD (pQCD) based analysis are not enough.

Since the non-perturbative nature of QCD arising from confinement and chiral symmetry is dominant near $\Lambda_{QCD} \sim 200$ MeV, one needs to go beyond perturbative analysis. Indeed, at finite temperature, this situation arises near a transition temperature of $T_c \approx 170$ MeV.

In this thesis, we study the magnetic field and non-perturbative effects on the in-medium binding potential of HQ and its anti-quark, collisional energy loss, and transport coefficients, namely the drag and diffusion coefficient. In order to see the magnetic field effect on quarkonia decay width, we first estimate modifications of the real and the imaginary part of quarkonia potential. An increase in the imaginary part of the potential with an increase in the magnetic field suggests that quarkonia dissociate earlier in a magnetic medium compared to its counterpart purely thermal medium.

For single HQ, the collisional energy loss in a magnetized medium suggests that the magnetic field may significantly contribute to the jet quenching. This is because the magnetic field contribution to the energy loss is of similar order as to the case of vanishing magnetic field, at least in the strong field limit where HQ is not directly affected by the magnetic field, i.e., $M \gg \sqrt{eB} \gg T \gg g\sqrt{eB}$. Further, in the low momentum regime, the magnetic field gives rise to anisotropy in the diffusion coefficient. In fact, depending on the relative direction of HQ velocity and magnetic field, one can define five diffusion coefficients. For HQ moving parallel to the magnetic field, diffusion in the transverse direction is larger than that of the longitudinal direction, i.e., $\kappa_{TT}^{\parallel} \gg \kappa_{LL}^{\parallel}$. However, for HQ moving perpendicular to the magnetic field, diffusion along the direction of HQ velocity and perpendicular to the magnetic field is gets, and dominant contribution and diffusion perpendicular to both magnetic field and HQ velocity get the least one, i.e., $\kappa_{TL}^{\perp} \gg \kappa_{LT}^{\perp} \gg \kappa_{TT}^{\perp}$. Out of these five diffusion coefficients, $\kappa_{TT}^{\parallel}$ is the dominant one. Similarly, the transverse drag coefficient $\eta_{D;TT}^{\parallel}$ is the largest one out of five drag coefficients. These estimations suggest that the magnetic field can significantly contribute to the elliptic and directed flow of heavy flavor mesons.

In addition to the magnetic field effects, we investigate the non-perturbative contributions that are significantly large near transition temperature on HQ transport coefficients. This is done withing the matrix model of semi-QGP with input parameters as the expectation value of the Polyakov loop and constituent quark mass. It is observed that with the inclusion of constituent quark mass and Polyakov loop, the drag coefficient is significantly large compared to the one estimated within the pQCD framework. On the other hand, the diffusion coefficient decreases with the momentum. Furthermore, with the inclusion of shear and bulk viscosities, it is observed that the momentum diffusion coefficient increases. This, in turn, gives a small value of the spatial diffusion coefficient. The consistency in the results of various models suggests that the non-perturbative effects on HQ transport are indeed very important for heavy ion collision phenomenology.

Keywords: Quark gluon plasma, Thermal field theory, magnetic field, Quarkonia suppresion in QGP, HQ transport coefficient.

Contents

List of Abbreviations

QED	Quantum electrodynamics
QCD	Quantum chromo-dynamics
BCS	Bardeen Cooper schreifer
QGP	Quark gluon plasma
RHIC	Relativistic Heavy Ion Collision
LHC	Large Hadron Collider
HQ	Heavy quark
ITF	Imaginary time formalism
KMS	Kubo-Martin-Schwinger
RTF	Real time formalism
HTL	Hard thermal loop
LL	Landau level
LLL	Lowest Landau Level

List of Figures

CHAPTER 1

Introduction

It is now believed that the strong interaction physics at a fundamental level is described by quantum chromodynamics (QCD) in terms of matter particles called quarks and force carriers called gluons. This interaction has been formulated along the lines of quantum electrodynamics (QED), which has been perhaps the most successful and accurate modern theories. Similar to QED, with gauge theory as the guiding principle and the abelian group U(1) being the underlying gauge group; the interaction of quarks and gluons is described by a gauge theory with SU(3) group being the underlying gauge group which is nonabelian in nature. Similar to QED, the QCD Lagrangian is given by

$$\mathcal{L}(X) = \sum_{f}^{N_f} \bar{\psi}_f(X)(i\not{D} - m)\psi_f(X) - \frac{1}{4}F^a_{\mu\nu}(X)F^{\mu\nu;a}(X) \tag{1.1}$$

In the above f labels the flavors of the quarks (u,d,s,c,b,t), a labels the color indices that transform in the adjoint representation for the gluons and in the fundamental representation for the quarks. The field strength tensor is defined as

$$F^a_{\mu\nu} = \partial_\mu A^a_\nu - \partial_\nu A^a_\mu + g f_{abc} A^b_\mu A^c_\nu \tag{1.2}$$

and D_μ is the covariant derivative on the quark fields is defined by

$$i\not{D}\psi = \gamma^\mu \left(i\partial_\mu + gA_\mu^a \frac{\lambda^a}{2} \right) \psi \tag{1.3}$$

It is the extra non-abelian terms in Eq.(1.2) that lead to the interaction of gluons. Unlike photons that do not have electric charges, the gluons have color charges. Therefore, while in QED one does not have photon-photon scattering, one can have gluon-gluon scatterings.

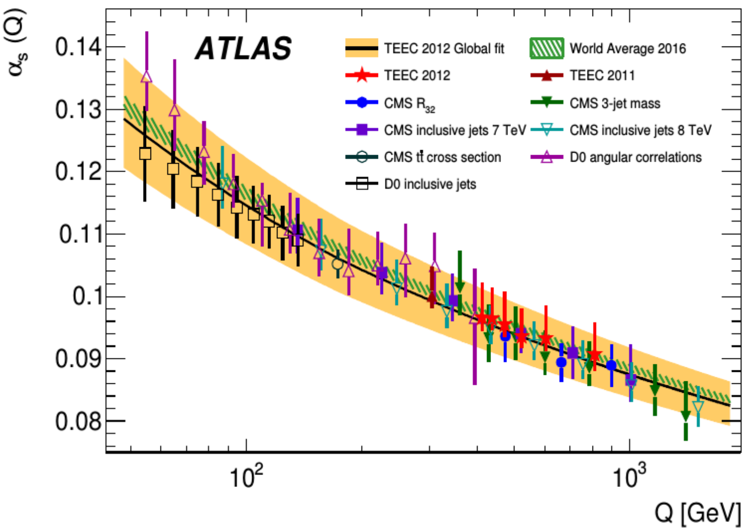

Figure 1.1: Measurement of QCD running coupling as a function of momentum transfer Q. Figure is adapted from Ref.[1].

One of the interesting consequences of the self interaction of the gluons is regarding the behavior of the strength of coupling in QCD as a function of momentum transfer as compared to QED. In any QFT, the vacuum is a medium that screens the charge leading to strength of the interaction depending upon the momentum transfer or the corresponding length scale. In QED, the coupling constant increases as a function of momentum transfer of the corresponding process while in QCD, because of its non-abelian nature, the coupling decreases as the momentum transfer increases. Explicitly the running of the QCD coupling at one-loop level is given by

$$\alpha_s(Q^2) = \frac{g^2}{4\pi} = \frac{4\pi}{\left(11 - \frac{2N_f}{3}\right)\ln\left(\frac{Q^2}{\Lambda}\right)}. \tag{1.4}$$

For higher order contributions see Ref.[6].This has been verified in various experiments as shown in Fig.1.1.

In Eq/1.4, Lambda is the scale parameter of QCD. Typically, it is the scale where QCD coupling becomes strong and is roughly the inverse size of light hadrons. This means that at large momentum transfer processes when the coupling is small one can use the techniques of standard perturbative QCD with confidence. Indeed, explanation of scaling and its violation has been successfully described by perturbative QCD [7, 8]. However, at lower energies when the coupling is strong, one cannot perform any perturbative calculations [9, 10, 11, 12, 13, 14]. On the otherhand, the observed hadrons which are excitations of QCD vacuum have two important properties. The hadrons are colorless, and they are heavy with masses, which are much larger than the mass parameter that enters in the Lagrangian. These are, respectively, the manifestation of confinement and chiral symmetry breaking properties of the QCD vacuum. The Lagrangian is approximately (but for the small current quark masses 'm') chirally symmetric, but in QCD vacuum the quark anti-quark condensate given by $\langle\bar{\psi}\psi\rangle$ is not zero and gives most of the masses of hadrons viewed as a bound state of quarks having 'constituent' masses proportional to the condensates.

1.1 Strongly interacting matter under extreme conditions

To understand the strong interaction physics at low energy, there have been two approaches experimentally. One is related to probing hadronic structure through energetic probes like electron and muons. The other approach has been to understand the phase structure of QCD i.e., studying QCD under extreme conditions. There are several motivations to study extreme QCD. Firstly, extreme conditions exist in nature. Current understanding of big bang cosmology indicates that about a few microseconds after the big bang, the universe passed through a state where the temperature is of the scale of QCD [15]. Later, matter condensed into stars. Some of the stars after exhausting their nuclear fuel, collapse and become neutron stars. While the density of the matter at the center of a neutron star is not known precisely, but almost certainly, it is at densities where the quark degrees of freedom are relevant [16, 17]. Secondly, we cannot properly understand the interaction of hadrons and their structure without understanding the underlying vacuum state, and we cannot understand the vacuum state without understanding how it can be modified. Thirdly, as mentioned, because of asymptotic freedom, QCD simplifies under extreme conditions as extreme conditions of temperature, density or external field, there is a large scale in the problem and one can understand QCD in terms of its fundamental degrees of freedom. Finally, of the many cosmological phase transitions that our universe did undergo during its evolution, the strong interaction phase transition is perhaps the only one that can be realized in the laboratory. With these motivations to study extreme QCD, we next discuss the phase diagram of QCD in the following subsection.

1.1.1 Phase diagram of QCD

The expected phase diagram of QCD in the plane temperature and baryon chemical potential (which is related to baryon density) is shown in Fig.1.2. The Y-axis represents the temperature and the x-axis is the baryon chemical potential associated with a conserved baryon charge and is related to baryonic density. The origin ($T = 0, \mu_B = 0$) correspond to QCD vacuum. At zero temperature, along the x-axis, we have nuclear matter having a saturation density $\rho_0(\sim 0.16/fm^3)$. Along the same direction, if we go in the μ_B axis, the system we have is the neutron star whose central density is about $3-5$ times nuclear matter density and have almost vanishing temperature [16, 17]. At small temperature and low density, one has excited hadrons and the system is a hadron gas. At very high-temperature one expects quark-gluon plasma state. This is because at very high temperature the entropy wins over the order in the sense the states of the system which has minimum free energy has the same symmetry of the Lagrangian. Thus at high temperatures, one would expect the system to be that of a weakly interacting system of gluons and quarks. This expectation, in fact, is reinforced through first principle lattice simulations.

At zero chemical potential one can perform reliable lattice simulation which indicates that there is a cross over transition around $T_c \sim 160 \pm 10$ MeV [18, 19, 20, 21, 22, 23, 24, 25, 26, 27]. This is because with finite quark masses the chiral symmetry is already broken explicitly in the Lagrangian and the corresponding order parameter, the quark condensate decrease continuously as a function of temperature but does not vanish. In the limit of vanishing quark masses, however, the chiral condensate vanishes beyond a critical temperature resulting in a phase transition which is second order. At vanishing chemical potential, these results are quite robust and is obtained from lattice QCD simulation [28, 29, 30]. However, it is difficult to do lattice simulation at finite chemical potential as the probability measure for the Monte Carlo sampling becomes non-positive [31, 32, 33, 34, 35]. However, there have been techniques to avoid this using various techniques but is limited to small chemical potential [36, 37, 38]. On the other hand, different model calculations which capture some features of QCD vacuum like chiral symmetry breaking indicate that the phase transition at high density is first order[39, 40, 41, 42, 43, 44, 45, 2, 46]. If the phase transition is first order at high μ_B and low temperature and a cross-over at small chemical potential then the first order phase transition line separating the QGP and the hadronic phase must end in a critical point where the first order line ends. Much of the current experimental as well as theoretical interest lies in identifying the signature of this critical point and its location in the temperature density plane of the phase diagram of QCD [47, 48].

At low temperature and high density, one has fermi surfaces for quarks- there are actually nine fermi surfaces for the three light quarks (u,d and s) with each flavor coming with three colors. Since there is an attractive interaction in QCD, the quarks will form super-conductors as is known from established Bardeen Cooper Schrieffer (BCS) mechanism [49, 50, 51]. In fact, this phase of color superconductivity is quite rich in its structures as compared to superconductivity in metals where electrons with opposite spin form the BCS pair. The reason being there are more degrees of freedom (color flavor and spin) for the quark matter. This apart, external conditions like charge neutrality both with respect to electric and

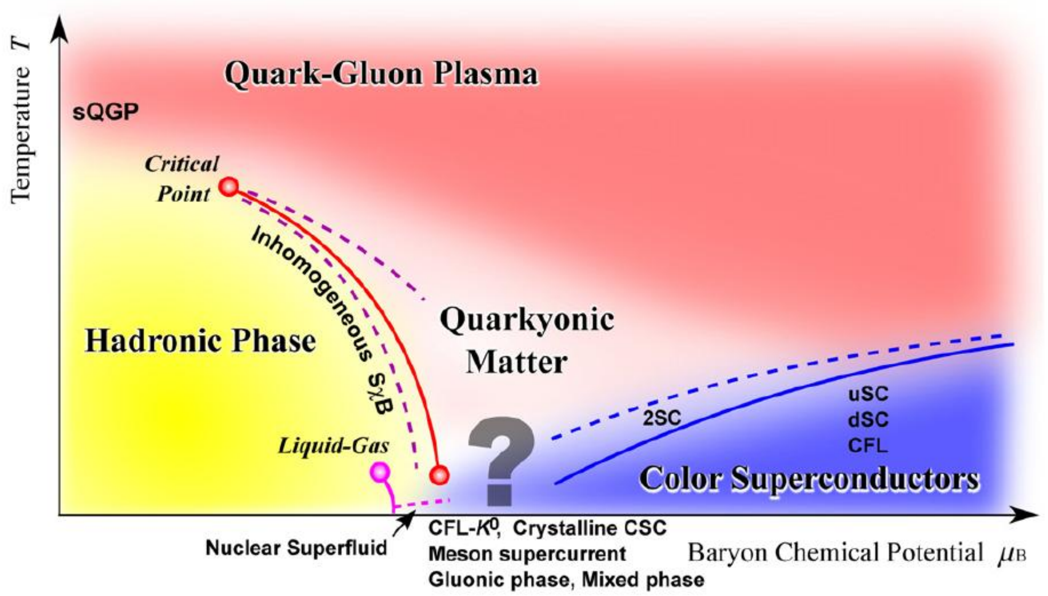

Figure 1.2: QCD phase diagram in temperature-baryon chemical potential ($T - \mu_B$). Figure is adapted from [2].

color charges bring out a host of possible superconducting phases for dense quark matter which include two flavor superconductivity, color flavor locked phase where all the three light flavors take part in BCS pairing, crystalline superconductivity i.e. BCS pairing with finite momentum etc [52, 53, 54, 55, 56].

In the large-N_c limit, there exist another phase known as quarkyonic matter described by both quark and baryon degrees of freedom Ref.[57, 58, 59]. Such a matter may exist at a density larger than the constituent quark mass and a temperature less than the deconfined temperature, i.e., $\mu_q > M_q, T < T_d$ [60, 58]. The quarkyonic matter is described by the quark degrees of freedom below the Fermi surface, where quarks are weakly interacting due to Pauli blocking. Near the Fermi surface, quarks are not affected by Pauli blocking hence interact strongly with each other. However, above the Fermi surface, the quarkyonic matter is described by the strongly interacting baryonic degrees of freedom. Thus, the thermodynamic properties are characterized by weakly interacting quarks inside the Fermi surface and by strongly interacting matter above the Fermi surface. Furthermore, using the PNJL model [14], it has been argued that the transition of quarkyonic matter may be related to the restoration of the chiral symmetry for

$N_c = 3$ [61, 62].

1.1.2 Heavy ion collision and QGP

Heavy-ion collisions (HICs) at Relativistic Heavy Ion Collision (RHIC) and Large Hadron Collider (LHC) create an excellent opportunity to explore the properties of in-medium strong-interaction by creating a deconfined state of strongly interacting matter. As mentioned earlier, QGP existed very early in the universe, i.e., few microseconds after the big bang and possibly exists at the interior of neutron stars which are far away (about few hundred light-years e.g., RX J1856-5-3754 is about 400 light-years away) to be able to systematically study QCD phase diagram in general. It turns out; however, that colliding heavy nuclei at high energy one can create excited strongly interacting matter in the laboratory. By colliding heavy ions with controlled collisional energy one can produce different types of matter in the phase diagram of QCD. In RHIC at Brookhaven, Gold(Au) nuclei after stripping off their electron are accelerated to an energy of 100 GeV/nucleon in two separate beam pipes and smashed head on at different collision points (with $\sqrt{s} = 200$ GeV/A) so that total center-of-mass (CM) energy of each gold ($A = 179$) nuclei is $E_{cm} \approx 40$ TeV. In the case of LHC, the lead(Pb) nuclei are used, and the CM energy per nucleon is 5.5 TeV.

As a result of very high CM energy, the nuclei are contracted along the longitudinal direction. Consequently, as a result of Lorentz contraction, these nuclei are of the disc shape with radius $R_{Pb/Au} \sim 7$ fm, and thickness $2R_{Pb/Au}/\gamma$, where γ is the Lorentz factor. For RHIC and LHC energies, the corresponding Lorentz factor respectively is $\gamma \approx 100$ and $\gamma \approx 1400$ for beam rapidities 5.3 and 8.5. Each of these discs (Lorentz contracted nuclei) in the incoming ion beam consists of quarks and antiquarks with more number of quarks than antiquarks. The quantum fluctuations in the initial quark state create more gluons and quark-antiquark pairs. Moreover, due to relativistic speed, the life-time of these initial state fluctuations is increased by Lorentz factor times. As a result, the density of gluons and quark/antiquark pairs increases with an increase in the energy of incident nuclei. In addition to this, in the high energy limit, the number of gluons outnumber all other partons. Indeed, valence quarks are negligible, and quark/antiquark pairs are suppressed by QCD coupling. In the limit of large occupation number of gluon $\sim \alpha_s^{-1}$, at any order, one must take contribution from an infinite number of Feynmann diagrams. This is done within the framework of Color Glass Condensate (CGC) [63, 64, 65].

At the time of the collision with a CM energy $\sqrt{s}$, most of the energy carried by incident nuclei are deposited in the collision region. For $\sqrt{s} = 200$ GeV/nucleon with Au-Au collision, approximately $\epsilon \sim 5$ Gev/fm^3 amount of energy density is deposited at the collision region. Moreover, during this process, the partons in both the incident nuclei lose their energy. Most of the interactions between two colliding discs are soft; as a result, partons in the final state remains undeflected. However, very few interactions are hard interactions that contribute to the hard probes, i.e., high p_T spectra in the detector. In terms of particles and fields, this can be interpreted as follows; the two incident discs carrying color charges and fields exchange color particles during the collision. As a result, the energy of these discs reduces. After the collision, the space between two receding nuclei is filled with the longitudinal color field that that results in very large entropy production by creating the pair of quark/anti-quark and gluon. Consequently, it is expected to have a deconfined state of quarks and gluons. In fact, lattice QCD predicts that one needs $\epsilon \approx 1$ GeV/fm^3 to create a deconfined state.

The hard processes with momentum exchange $P \geq 10$ GeV begin to develop up to the time $\tau \sim 1/P$ and are responsible for producing hard particles such as the photon, dilepton, hadrons, and hard jets. The transverse momentum of these hard particles is of the order of P. After the hard processes, semi-hard interactions of transverse momentum $P \sim 4$ GeV start dominating after some time around $\tau \approx 0.2$ fm. At this stage, most of the gluons carried by incoming discs are liberated that contribute to final state multiplicity. Moreover, most of the hadrons that appear in the final stage are the result of fragmentation and hadronization of gluons in this stage.

Before the final baryons/mesons that reach the detectors, the system undergoes a phase transition from deconfined to confined/chirally symmetric to the broken phase. In the deconfined phase, the pre-equilibrium interactions among partons lead to a thermal equilibrium system of light thermal partons known as quark-gluon plasma (QGP). This local thermal equilibrium occurs in a small-time $\tau \sim 0.5$

fm. The system further expands owing to the hydrodynamic expansion. This is indeed confirmed by particle spectra of low p_T that obeys Boltzmann distribution in a boosted frame near the freeze-out surface. Eventually, the system cools down, and the interaction between the partons becomes even stronger. As a result, the system hadronizes and confine the color particles to form color neutral bound states baryons and mesons. This transition from deconfined state to the confined state occurs at temperature $T_c \sim 160 \pm 10$ MeV [18, 19].

The system remains hot even after hadronization and creates a dense and hot hadronic medium that continues to expand in all space-time dimensions, i.e., 3+1 for some time. At later stages of the expansion, the interaction between hadrons becomes weak which results in the transition from collective expansion to the free streaming. This free streaming of hadrons that is named as freeze-out continues until particles (hadrons) reach the detector. The main observable here are the momenta spectra of final hadrons. What is interesting is the zero longitudinal momentum in the CM frame of the colliding nuclei, which is the mid rapidity region where one expects the largest energy deposition by the colliding nuclei. For head-on collision at RHIC, there are approximately 650 charged particles per unit rapidity, while at LHC, the corresponding number is about 1000.

The region near the transition temperature is dominated by the non-perturbative effects and can not be treated in the perturbative QCD framework. For small quark chemical potential, these non-perturbative effects in the static limit are studied in the framework of lattice QCD. For heavy ion phenomenology, the non-perturbative effects are also studied in Polyakov loop-based effective models such as Polyakovloop Nambu Jona Lasinio (PNJL), Polyakovloop quark meson (PQM) and matrix model of semi-QGP. We shall discuss the matrix model and the PQM model in chapter6.

1.2 Magnetic field in HIC

The positively charged ions moving with a relativistic velocity in HIC experiments also create a very strong magnetic field in non-central collisions. The magnetic field generation can be thought as follows; the charged heavy ions generate an electrical current, which, according to the laws of electrodynamics, creates a magnetic field in that region. A diagrammatic view transverse plane ($z = 0$) with impact parameter (b) along $\hat{\mathbf{x}}$ and magnetic field along $\hat{\mathbf{y}}$ axis is shown in Fig.1.3. At position $\mathbf{x}$ and time t, the magnetic field is given by the form of Lienard-Wiechert potential as [3]

$$e\mathbf{B}(t, \mathbf{x}) = \alpha \sum_n \frac{Z_n(1 - v_n^2)}{(r_n - \mathbf{r}_n \cdot \mathbf{v}_n)^3}(\mathbf{v}_n \times \mathbf{r}_n) \tag{1.5}$$

where $\alpha \sim 1/137$ is the fine structure constant, $\mathbf{v}_n$ and Z_n respectively are velocity and the charge of the n^{th} particle and summation is over the charged particles in the nucleus. The velocity of the charged particles can be estimated from the CM energy $\sqrt{s}$ by the relation

$$v_n^2 = 1 - \left(\frac{2m_p}{\sqrt{s}}\right)^2 \tag{1.6}$$

where m_p is proton mass. The position vector $\mathbf{r}_n = \mathbf{x} - \mathbf{x}_n$, where $\mathbf{x}_n$ is the position of the n^{th} charge particle at time t. Here, the position $\mathbf{x}_n$ and velocity $\mathbf{v}_n$ of the particle are defined at a retarded time t' while the measurement is taken at time t so that

$$|\mathbf{x}_n - \mathbf{x}_n(t')| = t - t'. \tag{1.7}$$

Here we have put the speed of light $c = 1$. From Eq.(1.5), it is clear that the magnetic field increases with an increase in the velocity of the charged particles. With the symmetry properties of Eq.(1.5), the magnetic field is also proportional to the impact parameter b hence negligible for the small impact parameter. Furthermore, if the beam direction is along $\hat{\mathbf{z}}$-axis and impact parameter is along $\hat{\mathbf{x}}$-axis then the magnetic field is directed along the $\hat{\mathbf{y}}$-axis.

The magnetic field in HIC is of the order of $eB \sim 10^{18}$ G. To appreciate the strength of the magnetic field in HICs, let us compare it with the naturally existed magnetic fields. The estimated value of the magnetic field in a neutron star is $10^{10} - 10^{13}$ G, the magnetic field of the earth is 10^7 G, and the magnetic field generated by the magnetar is 10^{15} G. perhaps, the magnetic field created in the HICs is the strongest field that has ever existed. In fact, for CM energy $\sqrt{s} = 200$ GeV/nucleon, radius of the incoming discs $R = 7$ fm and impact parameter $b = 4$ fm, the magnetic field in HIC is estimated as $eB \sim 1.3m_\pi^2$, where m_π is pion mass.

In the vacuum, the magnetic field decreases rapidly; however, in a bulk medium

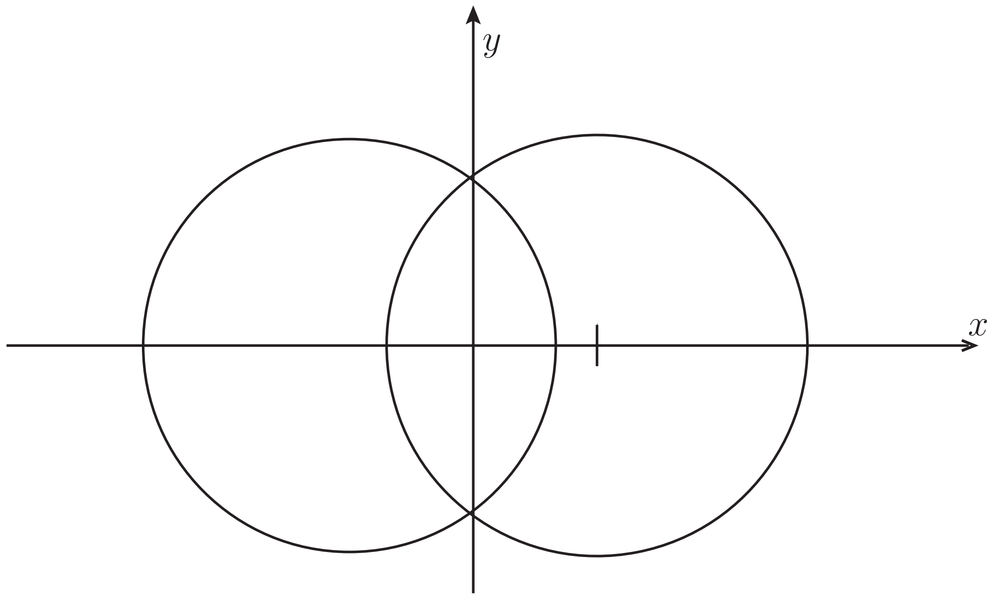

Figure 1.3: The transverse plane in a off central HIC experiment. Beam direction is along $\hat{\mathbf{z}}$-axis and magnetic field along $\hat{\mathbf{y}}$. Figure is adapted from Ref.[3].

like quark-gluon plasma, one must add the medium response by including the electrical conductivity for magnetic field description. In fact, in HICs, a medium known as Glasma exists even before the system thermalizes [66]. Therefore, for a realistic estimation of the magnetic field in HICs must include the electrical conductivity of the system. In a conductive medium with electrical conductivity, the magnetic field satisfies the following diffusion equation [67, 68]

$$\nabla^2 \mathbf{B} = \sigma \frac{\partial \mathbf{B}}{\partial t} \tag{1.8}$$

where σ is the electrical conductivity of QGP which depends on the medium temperature. Taking only the gluon contribution into account, the estimated value of the electrical conductivity on the lattice is [69, 70]

$$\sigma = (5.8 \pm 2.9) \frac{T}{T_c}. \tag{1.9}$$

The diffusion of the magnetic field in a medium affects the rate by which it decreases. In a medium with finite electrical conductivity, the magnetic field remains somewhat more substantial for a longer time. In fact, the magnetic field remains time-independent for time $t < \tau_0$, where $\tau_0 = L^2\sigma/4$ is the relaxation time for the magnetic field [67].

It has repeatedly been argued that the magnetic field can have a profound effect on kinetic, as well as the dynamic properties of the QGP. This may be expected because the magnetic field breaks the spherical symmetry as a result of which particle distribution is asymmetric with respect to the direction of the magnetic field. Furthermore, charged particles moving along the direction of the magnetic field does not experience any Lorentz force; on the other hand, a charged particle moving perpendicular to the magnetic field does. The disparity in the Lorentz force on the charged particles generate an anisotropic azimuthal flow. Indeed, in Ref.[71], using magneto-hydrodynamics at weak coupling limit, it is argued that the magnetic field can enhance the azimuthal anisotropy by 30%.

Azimuthal anisotropy in the QGP medium is the consequence of the momentum transfer's suppression in a direction perpendicular to the magnetic field. This anisotropy manifests itself in the viscous pressure component in that direction. In fact, the viscous pressure component along the magnetic field is twice as large as that of the along reaction plane. This anisotropic nature of viscosity can be anticipated from the fact that particles moving in the direction of the magnetic field does not experience Lorentz force as a result of which viscosity in that direction does not change. In fact, in the presence of the magnetic field, the viscous effects are characterized by seven viscosity coefficients, out of which five are for shear viscosity and two for the bulk viscosity. Therefore, it is crucial to explore the extent to which the magnetic field in the HICs affects the QGP dynamics and corresponding observables.

1.3 Probing QGP with heavy quarks

One of many reasons that make HQs and their bound state an excellent probe of QGP is that their production mechanism and vacuum properties are quite well understood in *pp* collision. Furthermore, their thermal production is negligible in the temperature range accessible in the nuclear collision. Indeed, these are produced during the initial stage hard collision of high momentum transfer processes that are very well separated from the thermal medium.

Now let us first consider the bound states such as $J/\psi, \Upsilon$, etc. Modifications on quarkonium binding are realized due to the presence of Debye screening in the thermal medium [72]. Indeed, the weakening of quarkonia potential with temperature was shown in Ref.[73]. This suggests the suppression of quarkonium states in HICs as a probe of the thermalized QGP medium.

Now let us move to single heavy quarks dynamics that reflect their in-medium interaction in spectra of open heavy meson such as D for the charm and B for bottom quarks. While propagating through the medium, HQ loses its energy via radiating gluons and inelastic scatterings with light partons. This, on the one hand, suggest that high momentum observables such as jets are suppressed in HICs; on the other hand, the in-medium interactions of low momentum HQ can significantly impact its momentum spectrum. The latter is related to the elliptic flow of heavy flavor open mesons.

1.4 Medium modifications on quarkonium binding

The bound state of a heavy quark and its antiquark is generally known as quarkonia. While the hadrons that are made of light quarks get their masses entirely from chiral symmetry breaking, the mass of these hadrons (quarkonia) mostly arises from the bare heavy quark masses. Some known bound states for charm quarks are S-wave state J/ψ (vector) of mass 3.1 GeV, η_c (scalar) of mass 2.98 GeV, and three P-wave states of χ_c (scalar, vector, and tensor) of masses 3.42 GeV, 3.51 GeV, and 3.56 GeV. Similarly, for bottom quark, some known bound states are Υ of mass 9.5 GeV, three states of χ_b, Υ' of masses 10.02 GeV, 10.23 GeV and 10.27 GeV.

The large mass of quarkonia allows a non-relativistic description by using a simple potential model to study the ground and excited-state properties. The potential model known as Cornell potential consists of the Coulomb part that is short-range potential at the asymptotic limit of coupling and the linearly rising string potential responsible for confinement. The study reveals that in comparison to the normal hadrons, the lower excitation states of quarkonia are small, and also, these are of smaller size, i.e., very tightly bound. Apart from potential models, the properties of quarkonia, such as bound state masses, are also explored in lattice simulations.

The presence of the bulk medium weakens the quarkonia binding due to the presence of screening in the medium. When binding in the medium becomes smaller than the size of the quarkonium, Q and $\bar{Q}$ will no longer be able to see each other as a result of which, the quarkonia states will dissociate. In HICs, the heavy quarks and hence the quarkonia are generally formed in the initial stages of the collision. Once quarkonia enter the thermally equilibrated bulk medium of light quarks, depending on time and energy, the corresponding quarkonia state may dissociate or melt. However, the reverse process of regenerating quarkonia is also possible if the sufficient number of quark and anti-quark are present in the medium, although the number of bound states restricted by the initial state.

1.4.1 Potential models at finite temperature

In a vacuum, Cornell potential has both Coulomb as well as the string part of the potential. The potential in a vacuum is given as

$$V(r) = -\frac{\alpha}{r} + \sigma r, \tag{1.10}$$

where $\alpha = C_F g^2/4/\pi$ and σ is string term. The first medium modification on the Cornell potential is realized based on the Debye-Huckle theory [74]. For a $1/r$ form of the potential in an ionized plasma, the medium modified potential in Debye-Huckle formalism is given as

$$V_c(r) = -\frac{\alpha}{r} e^{-\mu r}, \tag{1.11}$$

where $V_c(r)$ stands for standard Coulomb potential. Here, the parameter μ is the screening mass in the medium which is inversely proportional to the screening radius. In the QGP medium, this screening mass is the Debye screening mass (m_D). Using two dimensional Schwinger model arguments, the suggested functional from of the medium modified string part of the potential is [74]

$$V_s(r) = \sigma r \left(\frac{1 - e^{-m_D r}}{m_D r} \right). \tag{1.12}$$

As may be noted in Eqs.(1.11) and (1.12), both the Coulomb and the string part of the potential depends on only one parameter, i.e., Debye mass. In the limit of $m_D \to 0$, both forms of the potentials reduce to their vacuum counterparts. Later on, it was argued that the medium modified form of the string part of the potential also arises from non-zero gluon condensate [75]. In Ref.[75], it is shown that the similar functional form of the medium modified string part of the potential can be obtained by taking the effective string like one-dimensional interaction between quark and anti-quark.

The in-medium properties of the real and the imaginary part of the Cornell potential is studied using the Fourier transform of the retarded gluon propagator in Ref.[76] by incorporating two-dimension gluon condensate to include non-perturbative effects. These non-perturbative effects on the in-medium potential are achieved by adding a term $m_g^2 m_D^2/(p^2 + m_D^2)^3$ in the retarded gluon propagator. As a result, the extra term in the functional form of the real part of string potential looks like

$$\delta V_s(r) = \frac{a\sigma}{4m_D} \left(1 - e^{-m_D r} - m_D r e^{-m_D r} \right), \tag{1.13}$$

where a and m_g are dimensional constant. In the limit $m_D \to 0$, Eq.(1.13) vanishes, and one gets the vacuum form of the Cornell potential. The imaginary part of the potential also gets extra contributions from the non-perturbative terms. For the particular choice $a = 4$, the real part of the potential becomes identical to the one with the entropy contribution potential of Ref.[76]. A similar form of the real part of in-medium string potential is obtained in Ref.[77] by using the system's internal energy.

Furthermore, in Ref.[78], the authors proposed an idea of using the in-medium dielectric permittivity to estimate the medium effects of quarkonia potential. This is achieved by weighting the vacuum potential with the dielectric permittivity as

$$V(\mathbf{p}) = \frac{V(\mathbf{p})_0}{\epsilon(\mathbf{p})}, \tag{1.14}$$

where $V(\mathbf{p})_0$ is Fourier transform of Cornell potential in the vacuum. Using the hard thermal loop (HTL) approximation, the permittivity as a function of momentum and Debye mass is given as [78]

$$\epsilon^{-1}(\mathbf{p}) = \frac{p^2}{p^2 + m_D^2} - i\pi T \frac{|\mathbf{p}| m_D^2}{(p^2 + m_D^2)^2}. \tag{1.15}$$

Taking the inverse Fourier-transform of Eq.(1.14), one can estimate the in-medium quarkonia potential. Note here that the permittivity and hence the in-medium potential depends on one parameter, i.e., Debye mass. The real and the imaginary part of the potential are obtained from the real and the imaginary part of the potential which is given as Ref.[78]

$$\Re V(r) = -\alpha_s m_D \left(1 + \frac{e^{-m_D r}}{1}\right) + \frac{2\sigma}{m_D}\left(1 - \frac{1}{r} + \frac{e^{-m_D r}}{r}\right), \tag{1.16}$$

$$\Im V(r) = -\alpha_s T \phi(m_D r) + \frac{2\sigma T}{m_D^2}\chi(m_D r), \tag{1.17}$$

where

$$\chi(y) = 2\int_0^\infty \frac{dz}{z(1+z^2)^2}\left(1 - \frac{\sin(zy)}{zy}\right), \tag{1.18}$$

$$\phi(y) = 2\int_0^\infty \frac{zdz}{(1+z^2)^2}\left(1 - \frac{\sin(zy)}{zy}\right). \tag{1.19}$$

The medium modified potential above faced some divergence issue in the imaginary part of the potential, which later on rectified in Ref.[79, 80] by the idea of string breaking and bringing together the Gauss law and dielectric permittivity. In this formalism, the real and imaginary part of the in-medium potential are obtained by solving the differential equation

$$-\frac{1}{r^{b+1}}\nabla^2 V(r) + \frac{1+b}{r^{b+2}}\nabla V(r) + 8\pi q n_0 \beta V(r) = 4\pi q \delta(r), \tag{1.20}$$

with appropriate boundry conditions. Taking $b = -1, q = \alpha$ for Coulomb potential and $b = 1, q = \sigma$ for string part of the potential the real and imaginary in-medium potential are given as

$$\Re V(r,T,B) = -\alpha\frac{e^{-m_D r}}{r} - \alpha m_D - \frac{\Gamma(\frac{1}{4})}{2^{\frac{3}{4}}\sqrt{\pi}}\frac{\sigma}{\mu}D_{-\frac{1}{2}}(\sqrt{2}\mu r) + \frac{\Gamma(\frac{1}{4})}{2\Gamma(\frac{3}{4})}\frac{\sigma}{\mu}, \tag{1.21}$$

and

$$\Im V(r,T,B) = -2\alpha T\phi(m_D r) - \frac{\sigma m_{Dg}^2 T}{\mu}\psi(\mu r), \tag{1.22}$$

where

$$\psi(\mu r) = D_{-\frac{1}{2}}(\sqrt{2}\mu r)\int_0^r dx \Re D_{-\frac{1}{2}}(i\sqrt{2}\mu x)x^2 g(m_D x) + \Re D_{-\frac{1}{2}}(i\sqrt{2}\mu r)$$
$$\times \int_r^\infty dx D_{-\frac{1}{2}}(\sqrt{2}\mu x)x^2 g(m_D x) - D_{-\frac{1}{2}}(0)\int_0^\infty dx D_{-\frac{1}{2}}(\sqrt{2}\mu x)x^2 g(m_D x). \tag{1.23}$$

To estimate the medium modified quarkonia potential in a magnetized thermal medium we shall discuss this formalism in detail in Chapter3.

Apart from the perturbative and non-perturbative effects, in HICs, the contribution in the quarkonia suppression and the decay width arising from the magnetic field is also very important. As pointed out in Ref.[81, 82], the magnetic field can give rise to effects such as Lorentz ionization and Zeeman effect, which in turn, can affect quarkonia-binding energy. In this regard, we shall discuss the modified real and imaginary parts of quarkonia potential and decay width in a magnetized thermal medium.

1.5 Heavy quark dynamics in QGP medium

After the formation of a nearly perfect fluid with a minimal value of shear viscosity to entropy ratio η/s, one needs well-calibrated probes to investigate its properties. In this regard, because of their unique properties, heavy quark serves a promising tool to study the bulk properties of QGP. In HICs, the production of HQ is mainly controlled by the interactions in the initial stage of the collision. Furthermore, the thermal production of HQ is suppressed due to small temperature compared to the threshold mass, i.e., $T \ll M$. Therefore, once produced in the initial stage, HQs interact with the bulk medium throughout its evolution. This interaction of HQ with the bulk medium reflects itself in the observation of heavy flavor mesons.

Generally, two processes that affect the dynamics of heavy quark in HICs are radiative and collisional. The radiative process controls the dynamics of the high momentum HQ that mainly contributes to the quenching of high p_T heavy flavor meson associated with the jet quenching [83, 84, 85]. On the other hand, the collisional processes are responsible for the thermalization of HQ in the bulk medium of light thermal partons. It has been argued that the radiative processes may not be sufficient to reproduce the heavy flavor quenching data; therefore, the collisional energy loss may be important for jet quenching.

1.5.1 Heavy quark collisional energy loss

In the framework of perturbative QCD, the first estimation of the energy loss of high momentum quark and gluon via scattering from the thermal partons is estimated in Ref.[86]. The same was determined by considering the tree-level scattering diagrams of exchange gluon momentum q up to logarithmic term with artificial limits on exchange momentum q_{min} and q_{max}. Later on, similar formalism was generalized for the case of a heavy quark, combining the techniques of high-temperature QCD and plasma. In abelian approximation, the energy loss per unit length of quark is given as [87]

$$\frac{dE}{dx} = \frac{vq^a}{t} \Re E^a_{ind}, \tag{1.24}$$

where q^a is the color charge of quark and E^a_{ind} is the induced chromo-electric by a color charge moving with velocity v. The non-abelian effects in energy loss are included via the dielectric permittivity of the medium by incorporating gluon self-energy. Using Maxwell's and continuity equation arguments, the total chromo-electric field can be obtained by using the relation

$$\left[\epsilon_{ij}(\omega, |\mathbf{k}|) - \frac{|\mathbf{k}|^2}{\omega^2}\left(\delta_{ij} - \frac{k_i k_j}{|\mathbf{k}|^2}\right)\right] E^a_{total} = \frac{4\pi}{i\omega} j^a_{ext}(\omega, |\mathbf{k}|), \tag{1.25}$$

where j^a_{ext} is external quark current and $\epsilon_{ij} = \epsilon_T k_i k_j/|\mathbf{k}|^2 + \epsilon_L(\delta_{ij} - k_i k_j/|\mathbf{k}|^2)$ permittivity tensor in the medium. With further simplification of Eq.(1.25) with quark currents, the final form of energy loss becomes

$$\frac{dE}{dx} = -\frac{C_F\alpha_s}{2\pi^2 v}\int d\mathbf{k}\left(\frac{\omega}{|\mathbf{k}|^2}\left[\Im\epsilon_L^{-1} + (v^2|\mathbf{k}|^2 - \omega^2)\Im(\omega^2\epsilon_T - |\mathbf{k}|^2)^{-1}\right]\right)_{\omega=\mathbf{v}\cdot\mathbf{k}}, \quad (1.26)$$

where $\Im$ represents the imaginary part of the respective quantities. Thus, this formalism incorporates the soft scatterings and removes the infrared divergences by introducing the screening of long-range Coulomb potential. The ambiguity of the hard scale scatterings still remained. Finally, including both hard and soft contributions for the heavy-fermion energy loss, the first calculation was performed in Ref.[88] by Braaten ant Thoma. In this formalism, the average energy lost by a heavy-fermion of mass M moving with momentum $\mathbf{p}$ is given as

$$\Delta E = \Delta\tau \int_M^\infty dE'(E - E')\frac{d\Gamma}{dE'}, \quad (1.27)$$

where Γ is interaction rate and $\Delta\tau = \Gamma^{-1}$ is average time. For a heavy-light fermion, i.e., $L(P) + l(K) \to L(P') + l(K')$, the interaction rate is written in terms of scattering amplitude evalutated using the feynman diagram as

$$\begin{aligned}\Gamma(E) &= \frac{1}{2E}\int \frac{d\mathbf{p}'}{2E'}\frac{d\mathbf{k}}{2|\mathbf{k}|}\frac{d\mathbf{k}'}{2|\mathbf{k}'|}\tilde{f}(|\mathbf{k}|)(1 - \tilde{f}(|\mathbf{k}'|))(2\pi)^4 \\ &\times \delta^4(P + K - P' - K')\frac{1}{2}\sum_{spin}|\mathcal{M}|^2, \end{aligned} \quad (1.28)$$

where $d\mathbf{p} = d^3p/(2\pi)^3$, $\tilde{f}$ is Fermi-Dirac distribution function and $|\mathcal{M}|^2$ is matrix element squared for heavy-light fermion scattering. Further, in Eq.(1.28), $d\Gamma/dE'$ is change in interaction rate with respect to the energy of final state heavy fermion. The energy loss of heavy fermion per unit length for average distance $\Delta x = v/\Gamma$ is given as

$$\frac{dE}{dx} = -\frac{1}{v}\int_M^\infty dE'\frac{d\Gamma}{dE'}(E - E'), \quad (1.29)$$

where v is velocity of the heavy fermion. For QGP medium the collisional energy loss is estimated in Refs.[89, 90, 91].

1.6 Diffusion of heavy quark in QGP medium

While the dynamics of high momentum HQ is associated with the jet quenching/energy loss, the low momentum HQ dynamics is related to the diffusion processes. In the QGP medium, the low momentum HQ gets multiple scatterings from the light thermal partons. Since the momentum, $\mathbf{p}^2 \sim 2MT$ of HQ is larger than transfer momentum $\mathbf{q} \sim T$ with the thermal medium; the HQ executes a Brownian motion characterized by the transport coefficient. Furthermore, due to the large mass, HQs do not thermalize with the bulk medium of thermalization time τ. In fact, the thermalization time $\tau_Q = \tau M/T$ of HQ is quite close to the lifetime of the QGP medium. Therefore, HQ interacts with the thermal partons throughout in the QGP medium and retains the relevant interaction information.

Many approaches bases on perturbative QCD framework, effective models, and lattice gauge theory have been made to estimate the drag, momentum, and spatial diffusion coefficient. While the perturbative QCD estimates are at weak coupling limit, effective models such as the T-matrix model [92], dynamical quasi-particle model [93], matrix model of semi-QGP [94], and resonance model [95] have been used to include non-perturbative effects. The first-ever estimation of the spatial diffusion coefficient is done in lattice simulations [96] that predicted a very small spatial diffusion coefficient.

In the following, we shall discuss two widely used approaches to evaluate HQ transport coefficients, namely the drag and the diffusion.

1.6.1 Boltzmann transport equation of heavy quark

Based on kinetic theory framework, the Boltzmann equation for the evolution of the HQ distribution function $f(\mathbf{x}, \mathbf{p}, t)$ is

$$\left[\frac{\partial}{\partial t} + \frac{\mathbf{p}}{E}\frac{\partial}{\partial \mathbf{x}} + \mathbf{F}\frac{\partial}{\partial \mathbf{p}}\right] f(\mathbf{x}, \mathbf{p}, t) = \left.\frac{\partial f}{\partial t}\right|_{collision}, \tag{1.30}$$

where $\mathbf{F}$ is external force on HQ e.g., magnetic field in HIC and $E = \sqrt{\mathbf{p}^2 + M^2}$ is HQ energy. The distribution function f reaches Boltzmann distribution in equilibrium and static medium. In the right side of Eq.(1.30), $\partial f/\partial t$ represents the interaction of HQ with the light thermal partons (light quarks and gluons) of the medium. For $2 \to 2$ scatterings, the collision term is given as [97]

$$\begin{aligned}\frac{\partial f}{\partial t} &= \frac{1}{2E}\int d\mathbf{k}d\mathbf{k}'d\mathbf{p}'\frac{1}{\gamma_Q}|\mathcal{M}|^2(2\pi)^4\delta^4(P+K-P'-K') \\ &\times [f(E')f(E_{k'})-f(E)f(E_k)], \end{aligned} \tag{1.31}$$

where $d\mathbf{k} = d^3k/(2\pi)^3 2E_k$ are phase space integrations and $|\mathcal{M}|^2$ is matrix element squared for $Q(p) + l(k) \to Q(p') + l(k')$ scattering. fs are the distribution function of initial and final state particles. For the inclusion of quantum effects, the distribution functions are replaced by the Fermi-Dirac/Bose-Einstein distribution functions for quark/gluon. In addition, the Bose enhancement and Pauli blocking terms can be added by replacing $f \to (1 \mp f)$ for gluon/quark distribution functions. The contribution of $2 \to 3$ processes, i.e., $Q + l \to Q + l + g$ is discussed in Refs.[98, 99]. It is shown that at small angle, the gluon emission from HQ is suppressed due to its large mass. This phenomenon is also known as dead cone effect. In Chapter6 and Chapter7, we shall discuss this formalism in more detail. In these chapters, we estimate the non-perturbative effects arising from Polyakov loop and chiral symmetry breaking on the drag and the momentum diffusion coefficients within the matrix model of semi-QGP.

1.6.2 Langevin transport equation of heavy quark

Since the HQ momentum is larger than the exchanged momentum, multiple collisions are required to change HQ momentum. Generally, it takes M/T collisions to change HQ momentum by a unit order. In this scenario of getting multiple non-correlated kicks, HQ momentum evolution satisfy the Langevin equation [100]

$$\frac{dp_i}{dt} = \xi_i(t) - \eta_D p_i, \tag{1.32}$$

$$\langle \xi_i(t)\xi_j(t')\rangle = \kappa\delta_{ij}\delta(t-t'). \tag{1.33}$$

Here, η_D is the drag coefficient and κ is momentum diffusion coefficients defined as mean squared momentum transfer. $\xi(t)$ represents the multiple kicks on HQ. The differential equation, i.e., Eq.(1.32) has the following solution for the momentum evolution

$$p_i(t) = \int_{-\infty}^{t} e^{-\eta_D(t-t')}\xi_i(t'.). \tag{1.34}$$

In terms of $xi_i(t)$, the mean squared momentum $\langle p^2 \rangle = 3MT$ is defined as

$$\langle p^2 \rangle = \int dt dt' e^{\eta_D(t+t')}\langle \xi_i(t)\xi_i(t')\rangle = \frac{3\kappa}{2\eta_D}. \tag{1.35}$$

Therefore, momemtum diffusion and drag coefficients are related as

$$\kappa = 2\eta_D MT. \tag{1.36}$$

Similarly, the spatial diffusion coefficient is defined as

$$2D_s t\delta_{ij} = \langle x_i(t)x_j(t)\rangle. \tag{1.37}$$

We shall discuss the detailed analysis of the estimation of the drag and the diffusion coefficient using the Langevin transport equation in Chapter5. In this chapter, we shall discuss the anisotropic diffusion coefficients in the presence of the magnetic field. In Chapter7, we shall discuss the spatial diffusion coefficient in a Polyakov loop background.

1.7 Organization of the thesis

The thesis is organized as follows. In chapter2, a brief discussion on the real and imaginary time formalism of thermal field theory is presented. Further, the solution of the Dirac equation and fermion propagator in a constant magnetic field background are discussed in detail. In chapter3, the real and the imaginary parts of the in-medium quarkonia potential in a strongly magnetized hot medium are investigated. Based on the imaginary part of the potential, it is found that charmonium decay width increases in the presence of the magnetic field. This is followed by a discussion on HQ collision energy loss in the hot magnetized medium within the lowest Landau level (LLL) approximation in chapter4. Here, it is shown that in the weak coupling limit, the collisional energy loss is comparable to the case of vanishing magnetic field, which can be important for the jet quenching. In chapter5, the anisotropic momentum diffusion coefficients of heavy quark within the LLL approximation of the magnetic field are estimated. It is observed that based on the relative directions of HQ velocity and magnetic field, there can be five diffusion coefficients. For the case of $\mathbf{v} \parallel \mathbf{B}$, the diffusion coefficient transverse to the magnetic field is dominant; however, for $\mathbf{v} \perp \mathbf{B}$ the diffusion coefficient transverse to velocity and along the direction of the magnetic field, i.e., κ_{TL} is dominant. Furthermore, in chapter6, the non-perturbative effects arising from the Polyakov loop and constituent quark mass on the HQ drag and diffusion coefficients are investigated. The convergence of the results with the results from the other models indicates that the non-perturbative effects on the HQ transport coefficients are significant. In chapter7, effects of bulk and shear viscosities along with the Polyakov loop on the drag and the diffusion coefficients are discussed. It is found that with the inclusion of viscosities the spatial diffusion coefficient decreases. Finally, in chapter8, the summary of the investigations included in the thesis is presented along with possible future directions.

CHAPTER 2

Field theory in a medium

Thermal ensembles are of great importance in equilibrium statistical mechanics. Generally, one can encounter three types of ensembles depending on the exchange of energy (E) and the number of particles (N) with a thermal reservoir at temperature T. *Micronanonical ensemble* describes an isolated system with fixed E and N at volume V, *canonical ensemble* describe a system that can exchange energy with the reservoir keeping N and V fixed. On the other hand, a *grand canonical ensemble* can exchange energy and particles with the reservoir while keeping chemical potential μ, T, and the volume V fixed. In a relativistic quantum system, where particles number is not conserved (i.e., particles can be created and destroyed e.g., in the QED process $l^+l^- \to l^+l^-l^+l^-$ where l stands for Lapton) observables are evaluated using grand canonical ensemble and a process where $\mu = 0$ observables are evaluated using canonical ensemble. Considering a system at temperature T that can be characterized by Hamiltonian H, one can define the quantity

$$\rho = \exp(-\beta H), \tag{2.1}$$

where $\beta = T^{-1}$ is inverse temperature. Here ρ is known as statistical density matrix that can be used to compute ensemble average for any desired quantum operator $\hat{A}$ as

$$\langle A \rangle = \frac{Tr(\rho\hat{A})}{Tr\rho}, \tag{2.2}$$

where Tr stands for trace, i.e., sum over expectation value in any complete basis. If E_n and $|n\rangle$ are eigenvalues and eigenstates of Hamiltonia H i.e., $H|n\rangle = E_n|n\rangle$ then

$$\langle A \rangle = \frac{1}{Z}\sum_n \langle n|A|n\rangle \exp(-\beta E_n), \tag{2.3}$$

where $Z \approx Tr(\rho) = Tr(\exp(-\beta H))$ is the partition function which is sumed over all thermally excited states $|n\rangle$ that are weighted with the corresponding Boltzmann factor $\exp(-\beta E_n)$. For a system with finite chemical potential μ, Hamiltonian H is replaced by $H - \mu N$.

Thermal field theory (TFT) describes a system of interacting particles including the non-abelian gauge interactions such as QCD in a thermodynamical environment at or near equilibrium [101, 5]. The thermal field theory framework of a relativistic statistical system is different from more familiar many-body or kinetic theory [102, 103] in the sense of using the path integral approach, the treatment of non-abelian gauge interactions and finally the Lorentz covariance of theory.

In particle physics, the usefulness of thermal field theory is mainly realized in the hot and dense plasma studies, phase transition, and cosmology. One good example of thermal field theory application is the study of QCD matter under extreme conditions of temperature and density. Such a state of strongly interacting matter known as QGP that is created in the HIC experiments where the temperature reaches few hundred MeV. In the high temperature limit, i.e., $T \gg \Lambda_{QCD}$ where the coupling is weak due to asymptotic freedom, properties of the deconfined state of quarks/anti-quarks and gluons can be captured within the framework of pQCD. Another important application is in the study of the early universe. Indeed, in the evolution of the universe, one can have a thermalized medium before recombination where the mean free path of the interacting particles is smaller than the system size [104]. This, in fact, is supported by CMB analysis that demonstrates a perfectly black-body spectrum at the time of the last scattering, up to fluctuation as small as $\delta T/T \approx 10^{-5}$ [105].

In both QGP and the early universe, the in-medium interactions of particles are characterized by the thermodynamic parameters associated with the system temperature and density. Even though the questions one may be interested in addressing in the heavy-ion collision and the early universe are different, the calculational techniques are quite similar. The resummation techniques developed in one case can also be used in the other case. In fact, we are more interested in quantifying the observables rigorously by means of finite temperature quantum field theory.

There exist two equivalent formalisms of thermal field theory commonly known as imaginary time formalism (ITF) and real-time formalism (RTF), each with its own convenience and limitations. The former one is developed by Matsubara by incorporating the imaginary time in the evolution of operator [106]. On the other hand, the alternative real-time description was developed by Mills, Schwinger, and Keldysh by appropriately choosing a contour in the complex plane [4, 107]. Below we shall discuss both the formulations in somewhat detail.

2.1 Imaginary time formalism

In the ITF, the time in the evolution operator is taken as purely imaginary. In fact, the exponential factors in Eqs.(2.1) and 2.2 may be regarded as the evolution operator with $it = \tau = \beta$. Therefore, any operator $\mathcal{O}$ can evolve as

$$\mathcal{O}(\tau) = e^{\tau H}\mathcal{O}(0)e^{-\tau H}. \tag{2.4}$$

Here, the transformation is unitary as time is imaginary. For the calculational purpose, it is also possible to use a diagrammtic approach similar to zero temperature by defining a partition function and hence generating functional with a source term. However, the important difference lies in defining the time variable. In fact, with definition $\tau = \beta$, the evolution operator is restricted to be within certain time intervals. This can be seen in the two-point function of any field Φ with space-time arguments $(\tau, \mathbf{x})$ as [5, 108]

$$\langle \Phi(\mathbf{x},\tau)\Phi(\mathbf{y},0)\rangle = \Delta_T(\tau, \mathbf{x}-\mathbf{y})$$

$$\begin{aligned}
&= \frac{1}{Z}Tr(e^{-\beta H}\Phi(\mathbf{x},\tau)\Phi(\mathbf{y},0)) \\
&= \frac{1}{Z}Tr(e^{-\beta H}\Phi(\mathbf{x},\tau)e^{\beta H}\Phi(\mathbf{y},0)e^{-\beta H}) \\
&= \frac{1}{Z}Tr(e^{-\beta H}\Phi(\mathbf{x},\tau)\Phi(\mathbf{y},\beta)) \\
&= \langle\Phi(\mathbf{x},\tau)\Phi(\mathbf{y},\beta)\rangle = \Delta_T(\tau-\beta,\mathbf{x}-\mathbf{y}). \qquad (2.5)
\end{aligned}$$

This relation is known as Kubo-Martin-Schwinger (KMS) relation. For any field Φ satisfying commutation or anti-commutation relation one can have

$$\Phi(\mathbf{x},0) = \pm\Phi(\mathbf{x},\beta). \qquad (2.6)$$

Here plus sign stands for fields satisfying commutation relation and minus sign for fields satisfying anti-commutation relation. KMS relation shows that the fields are either periodic, e.g., bosonic or antiperiodic, e.g., fermionic with imaginary time β. In fact, owing to KMS relation, the propagator of a scalar field can be written as

$$\Delta_T(\tau,\mathbf{x}-\mathbf{y}) = \Delta_T(\tau+n\beta,\mathbf{x}-\mathbf{y}), \qquad n\in\mathbb{Z}. \qquad (2.7)$$

The consequence of Eqs.2.6 and 2.7 is that the imaginary time is restricted in interval $[0,\beta]$. Thus, the real-time dependence of correlation functions are lost in the ITF. One can obtain the static thermodynamic properties of a system, e.g., like pressure, energy density, etc. The time-dependent quantities are obtained by performing an analytic continuation from imaginary to real-time after evaluating all relevant Feynman diagrams.

Similar to the case of zero temperature where Feynman diagram evaluation is easy in the momentum space here one can evaluate the diagrams in frequency space. In fact, one can write the fields in terms of these frequencies named after Matsubara as

$$\Phi(\mathbf{x},\tau) = T\sum_{n=-\infty}^{+\infty}\tilde{\Phi}(\mathbf{x},\omega_n)e^{i\omega_n\tau}. \qquad (2.8)$$

Here, the Matsubara frequencies $\omega_n = 2n\pi T$ and $\omega_n = (2n+1)\pi T$ are respectively for bosonic and fermionic fields. The discrete frequency arises in ITF as the (imaginary) time is restricted to the finite interval. Therefore, in terms of Matsubara frequencies, the propagator corresponds to the scalar field $\phi(X) = \phi(x_0, \mathbf{x})$ can be written as

$$\Delta_T(X - Y) = \langle \phi(X)\phi(Y) \rangle = T \sum_{n=-\infty}^{+\infty} \int \frac{d^3k}{(2\pi)^2} \frac{e^{i\omega_n \tau} e^{-i\mathbf{k}\cdot(\mathbf{x}-\mathbf{y})}}{\omega_n^2 + k^2 + m^2}. \tag{2.9}$$

It can clearly be seen that the propagator has a temperature dependence via the Matsubara frequencies. To obtain the Feynmann rules for evaluating diagrams, one can write the Lagrangian in Euclidean space by $\mathcal{L}_E = -\mathcal{L}_M(t \to -i\tau)$; w; where $\mathcal{L}_M$ is Lagrangian in Minkowski space. For example, in Euclidean space the Lagrangian for a scalar field can be written as

$$\mathcal{L}_E = \frac{1}{2}\left(\frac{\partial \Phi}{\partial \tau}\right)^2 + \frac{1}{2}(\nabla\Phi)^2 + V(\phi). \tag{2.10}$$

2.2 Real time formalism

The static properties of a thermally equilibrated system are quite well described within the framework of ITF. Even the time dependent quantities can also be obtained by a more cumbersome procedure of analytic continuation from imaginary to real-time. On the other hand, from the beginning, one can also start with real-time variables within the RTF. In fact, RTF is more suitable for a dynamical/non-equilibrium system such as QGP in HICs [109, 110], and provide a transparent separation of vacuum and medium/temperature dependent terms. This naturally arises from the propagator structure that has separate temperature dependent and vacuum terms.

The real-time description of Green's function is allowed by choosing a contour in the complex time plane including the real-time axis as shown in Fig.2.1. While constructing the contour path, the field variables must satisfy the boundary condition (KMS) of Eq.2.6. In the imaginary time formulation, the contour is from t to $t - i\beta$, i.e., along the imaginary axis in the complex time plane. In the real-time formulation, the contour is deformed in various manner one of which is shown in Fig.2.1. Let us discuss the contour in somewhat detail. We first start from a large initial time $t_i \to$ along path C_1 and then moves down along the vertical path

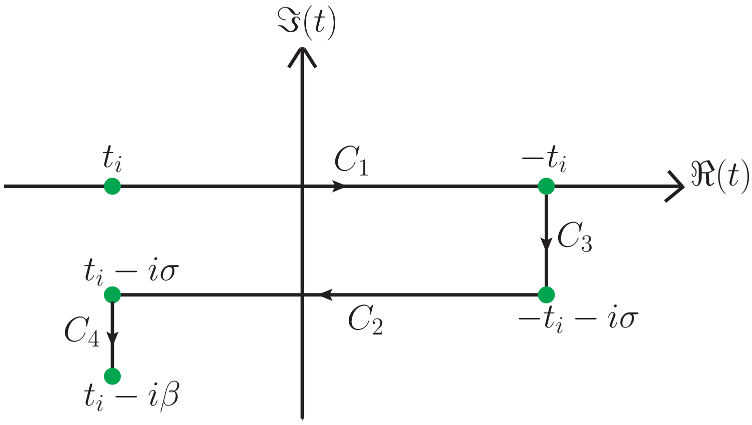

Figure 2.1: Keldysh-Schwinger contour in a complex plane [4] for $0 \leq \sigma \leq \beta$. Green dots define the boundries along parths C_1, C_2, C_3 and C_4. Figure adapted from [5].

C_3 where time becomes complex with $0 \leq \sigma \leq \beta$. After this point, one moves backward along the horizontal path C_3 and reaches a point at time $t_i - i\sigma$. Finally one moves along the second vertical path C_4 from time $t_i - i\sigma$ to $t_i - i\beta$. Taking $t_i \to -\infty$, one can span the entire real-time axis.

It has been argued that the contribution of vertical paths C_2 and C_4 can be neglected irrespective of choice of t_i [111, 112]. Therefore, one is left with the horizontal paths C_1, C_2 and the path integral can be decomposed accordingly. Thus for a two-point function, $\langle \Phi(X)\Phi(Y) \rangle$ the time arguments can either lie on C_1 or C_2 leading to a non-trivial structure of the propagator at finite temperature compared to $T = 0$ counterpart. RTF is suitable in describing a dynamical system, but the price one has to pay is a doubling of each field.

Generally, the Green's function for a spinor field $\psi(X)$ in the fundamental representation of $SU(N)$ group is defined as

$$i\mathcal{S}(X,Y)^{lm}_{\alpha\beta} = \langle \hat{T}(\psi^l_\alpha(X)\bar{\psi}^m_\beta(Y)) \rangle, \tag{2.11}$$

where $(\alpha, \beta) = 1, 2, 3, 4$ are spinor indices and $(l, m) = 1, 2, ..., N$ are color indices in the fundamental representation for $SU(N)$ group. Here, $\hat{T}$ is the time ordering operation along the contour defined as

$$\hat{T}(\mathcal{X}(X)\mathcal{Y}(Y)) = \mathcal{X}(X)\mathcal{Y}(Y)\theta(x_0 - y_0) \pm \mathcal{Y}(Y)\mathcal{X}(X)\theta(y_0 - x_0), \tag{2.12}$$

where $\theta(x_0 - y_0)$ is a step function which is 1 for $x_0 > y_0$ and 0; otherwise, plus sign stands for the bosonic operator, i.e., if $\mathcal{X}, \mathcal{Y}$ are vector field and the minus sign for the fermionic one. Similarly, for a vector field A^μ the contour Green's function is

$$i\mathcal{D}(X,Y)^{ab}_{\mu\nu} = \langle \hat{T}(A^a_\mu(X)A^b_\nu(Y))\rangle = \frac{Tr[\rho(t_i)\hat{T}A^a_\mu(X)A^b_\nu(Y)]}{Tr[\rho(t_i)]}, \tag{2.13}$$

where $(\mu,\nu) = 0,1,2,3$ are Lorentz indices and $(a,b) = 1,2,...,N^2$ are color indices in the adjoint representation for $SU(N)$ group. The trace here is summation over complete set of states i.e., $Tr[..] = \sum_n \langle n|..|n\rangle$. $\rho(t_i)$ is the density operator at the initial time t_i. Let us keep in mind that the time arguments x_0, y_0 are complex quantities. The positive and the negative value of the imaginary part locates them in the upper/lower branch of the contour. Therefore, depending on the locations of the time arguments, the four Green's function that one can define is as

$$i\mathcal{S}^>(X,Y)^{lm}_{\alpha\beta} = \langle \psi(X)^l_\alpha \bar{\psi}(Y)^m_\beta\rangle \qquad x_0 \in C_2, y_0 \in C_1, \tag{2.14}$$

$$i\mathcal{S}^<(X,Y)^{lm}_{\alpha\beta} = -\langle \bar{\psi}(Y)^m_\beta \psi(X)^l_\alpha\rangle \qquad x_0 \in C_1, y_0 \in C_2, \tag{2.15}$$

$$i\mathcal{S}^c(X,Y)^{lm}_{\alpha\beta} = \langle \hat{T}(\psi(X)^l_\alpha \bar{\psi}(Y)^m_\beta)\rangle \qquad x_0 \in C_1, y_0 \in C_1, \tag{2.16}$$

$$i\mathcal{S}^a(X,Y)^{lm}_{\alpha\beta} = \langle \hat{T}^\dagger(\psi(X)^l_\alpha)\bar{\psi}(Y)^m_\beta\rangle \qquad x_0 \in C_2, y_0 \in C_2, \tag{2.17}$$

for the fermionic fields. The ordering operator $\hat{T}^\dagger$ is the anti-time ordering operator defined as

$$\hat{T}^\dagger(\mathcal{X}(X)\mathcal{Y}(Y)) = \mathcal{X}(X)\mathcal{Y}(Y)\theta(y_0 - x_0) \pm \mathcal{Y}(Y)\mathcal{X}(X)\theta(x_0 - y_0), \tag{2.18}$$

where $\pm$ are for the bosonic and fermionic field. Similarly, for a vector field one can also define four Green's functions i.e., $i\mathcal{D}^>(X,Y), i\mathcal{D}^<(X,Y), i\mathcal{D}^c(X,Y)$ and $i\mathcal{D}^a(X,Y)$ where color and Lorentz indices are suppressed. These Green functions carry information about the microscopic interaction and statistical properties of the system under consideration.

The function $\mathcal{S}^c$ describes the particle propagation forward in time and anti-particle propagation backward in time. The function $\mathcal{S}^a$ is analogous to $\mathcal{S}^c$, but particles propagating backward in time and anti-particles propagating forward in time. In the zero density limit, the function $\mathcal{S}^c$ coincides with the usual Feynman propagator. The functions $\mathcal{S}^{>/<}$ plays the role of phase space densities of quasi particles and can be treated as a quantum analog of classical distribution functions. All these four components of the contour Green's function are not independent of each other but rather satisfy the relation

$$\mathcal{S} + \mathcal{S}^* = \mathcal{S}^> + \mathcal{S}^<. \tag{2.19}$$

The propagator thus is a 2×2 matrix corresponding to different components of the field having time coordinates on the upper or lower contour. Therefore, the propagator is written as

$$\mathcal{S} = \begin{pmatrix} \mathcal{S}_{11} & \mathcal{S}_{12} \\ \mathcal{S}_{21} & \mathcal{S}_{22} \end{pmatrix} = \begin{pmatrix} \mathcal{S}^c & \mathcal{S}^< \\ \mathcal{S}^> & \mathcal{S}^a \end{pmatrix}. \tag{2.20}$$

Here $1, 2$ corresponds to particles in the upper or lower contour respectively, and the spinor/color indices are suppressed. To write an explicit form of the propagator, one has to choose a value for the parameter σ, e.g., the Keldysh-Schwinger path corresponds to $\sigma \to 0$. In Keldysh-Schwinger, the different components of the propagator in momentum space are given as [113]

$$i\mathcal{S}^>(K)^{lm}_{\alpha\beta} = \delta^{lm}\frac{i\pi \not{K}_{\alpha\beta}}{E_k}\left[\delta(k_0 - E_k)(\tilde{f}(\mathbf{k}) - 1) + \delta(k_0 + E_k)\tilde{f}'(-\mathbf{k})\right], \tag{2.21}$$

$$i\mathcal{S}^<(K)^{lm}_{\alpha\beta} = \delta^{lm}\frac{i\pi \not{K}_{\alpha\beta}}{E_k}\left[\delta(k_0 - E_k)(\tilde{f}\mathbf{k}) + \delta(k_0 + E_k)(\tilde{f}'(-\mathbf{k}) - 1)\right], \tag{2.22}$$

$$i\mathcal{S}^c(K)^{lm}_{\alpha\beta} = \frac{\delta^{lm}\not{K}_{\alpha\beta}}{K^2 + i\epsilon} - \frac{\delta^{lm}\not{K}_{\alpha\beta} i\pi}{E_k}\left[\delta(k_0 - E_k)\tilde{f}(\mathbf{k}) + \delta(k_0 + E_k)\tilde{f}'(\text{-}\mathbf{k})\right], \tag{2.23}$$

$$i\mathcal{S}^a(K)^{lm}_{\alpha\beta} = -\frac{\delta^{lm}\not{K}_{\alpha\beta}}{K^2 - i\epsilon} - \frac{\delta^{lm}\not{K}_{\alpha\beta} i\pi}{E_k}\left[\delta(k_0 - E_k)\tilde{f}(\mathbf{k}) + \delta(k_0 + E_k)\tilde{f}'(\text{-}\mathbf{k})\right], \tag{2.24}$$

where $\tilde{f}(\mathbf{k})$ and $\tilde{f}'(\text{-}\mathbf{k})$ are the quark and anti-quark distribution function which are unpolarised with respect to spin and color. For a thermal equilibrium system these distribution functions are Fermi-Dirac distribution functions.

The Green's function defined in Eqs.(2.21- 2.24) have poor analyticity properties. This is due to the presence of the delta function. Indeed, in a statistical system, we are more interested in physical Green's functions, i.e., the usual advanced/retarded Green's function with poles below/above of the real axis. The physical Green's functions, i.e., retarded ($\mathcal{S}_R$), advance ($\mathcal{S}_R$) and symmetric ($\mathcal{S}_F$) are defined as

$$i\mathcal{S}_R(X,Y)^{lm} = \theta(x_0 - y_0)\langle\{\psi^l(X), \bar{\psi}^m(Y)\}\rangle, \tag{2.25}$$

$$i\mathcal{S}_A(X,Y)^{lm} = -\theta(y_0 - x_0)\langle\{\psi^l(X), \bar{\psi}^m(Y)\}\rangle, \tag{2.26}$$

$$i\mathcal{S}_F(X,Y)^{lm} = \theta(x_0 - y_0)\langle[\psi^l(X), \bar{\psi}^m(Y)]\rangle, \tag{2.27}$$

where $\{..\}$ stands for anti-commutation and $[..]$ stands for commutation relation. The physical Green's functions are also related to the contour Green's functions as [114]

$$\begin{aligned} \mathcal{S}_R(K)^{lm} &= (\mathcal{S}^>(X,Y) - \mathcal{S}^<(X,Y))\theta(x_0 - y_0) \\ &= \mathcal{S}^c(X,Y) - \mathcal{S}^<(X,Y) \\ &= \frac{\delta^{lm} \not{K}}{K^2 + i\epsilon}, \end{aligned} \tag{2.28}$$

$$\begin{aligned} \mathcal{S}_A(K)^{lm} &= -(\mathcal{S}^>(X,Y) - \mathcal{S}^<(X,Y))\theta(y_0 - x_0) \\ &= \mathcal{S}^c(X,Y) - \mathcal{S}^<(X,Y) \\ &= \frac{\delta^{lm} \not{K}}{K^2 - i\epsilon}. \end{aligned} \tag{2.29}$$

The retarded Green's function describes the propagation of both the particles and anti-particles forward in time while the advance Green's function describes the same but backward in time. A third Green's of this representation is the symmetric one that involves the single particle distribution function is given as

$$\mathcal{S}_F(K)^{lm} = \mathcal{S}^>(X,Y) + \mathcal{S}^<(X,Y)$$

$$= \frac{\delta^{lm}{}_1\pi \not{K}}{E_k}\left[\delta(k_0 - E_k)(2\tilde{f}(\mathbf{k}) - 1) + \delta(k_0 + E_k)(2\tilde{f}'(\text{-}\mathbf{k}))\right]. \quad (2.30)$$

Similar to Eq.2.19, the Green's function in Keldysh representation are not independent but related to each other the relation

$$\mathcal{S}_F(K) = \left(\frac{1}{2} - \tilde{f}(k_0)\right)[\mathcal{S}_R(K) - \mathcal{S}_A(K)], \quad (2.31)$$

where $\tilde{f}(k_0)$ is the distribution function of the fermions. Similarly, in the Keldysh-Schwinger formalism, the contour Green's function for gluons in the Feynman gauge is given as [113]

$$i\mathcal{D}^{>}(K)^{ab}_{\mu\nu} = \frac{i\pi}{E_k} g_{\mu\nu}\delta^{ab}(\delta(k_0 - E_k)(1 + f(\mathbf{k})) + \delta(k_0 + E_k)f(-\mathbf{k})), \quad (2.32)$$

$$i\mathcal{D}^{<}(K)^{ab}_{\mu\nu} = \frac{i\pi}{E_k} g_{\mu\nu}\delta^{ab}(\delta(k_0 - E_k)f(\mathbf{k}) + \delta(k_0 + E_k)(1 + (-\mathbf{k}))), \quad (2.33)$$

$$i\mathcal{D}^{c}(K)^{ab}_{\mu\nu} = -g^{\mu\nu}\delta^{ab}\left[\frac{1}{K^2 + i\epsilon} - \frac{i\pi}{E_k}(\delta(k_0 - E_k)f(\mathbf{k}) + \delta(k_0 + E_k)f(-\mathbf{k}))\right], \quad (2.34)$$

$$i\mathcal{D}^{a}(K)^{ab}_{\mu\nu} = g^{\mu\nu}\delta^{ab}\left[\frac{1}{K^2 - i\epsilon} + \frac{i\pi}{E_k}(\delta(k_0 - E_k)f(\mathbf{k}) + \delta(k_0 + E_k)f(-\mathbf{k}))\right]. \quad (2.35)$$

Here $f(\mathbf{k})$ is gluon distribution function which is assumed to be unpolarised with respect to spin and color. For a thermally equilibrated system $f(\mathbf{k})$ is Bose-Einstein distribution function. Green's functions $\mathcal{D}^{a/c}(K)^{ab}_{\mu\nu}$ satisfies the equation

$$K^2\mathcal{D}^{a/c}(K)^{ab}_{\mu\nu} = \mp\delta^{ab}g_{\mu\nu}, \quad (2.36)$$

while the other two Green's functions satisfies

$$K^2\mathcal{D}^{>/<}(K)^{ab}_{\mu\nu} = 0. \quad (2.37)$$

2.3 Hard thermal loop (HTL) approximation

Before coming to the computational/technical details of Feynmann diagram evaluations, let us discuss *hard thermal loops* (HTL) that determines the dispersion laws of the (quasi)particle excitations in the plasma at leading order in coupling [115, 116, 117]. In gauge theories at finite temperature, the usual notion of loop expansion order in terms of coupling constant g is lost so that even at leading order computations the higher order contributions arising from the loops known as hard thermal loops become relevant. In order to include higher order contributions one need to resum the infinite sets of diagram into effective propagator and vertices. This may be even more evident in high temperature scalar field theory with quartic coupling which is massless at tree level and develops mass $m_s \sim gT$ via tadpole diagram. This mass generation replaces the bare propagator $1/K^2$ by effective propagator $1/(K^2 + m_s^2)$ [117]. It ought to be mentioned that HTLs are gauge invariant even when they arise from N-point functions.

The loop corrections that needed to be resummed are of order g^2T^2/P^2 times the corresponding tree level contribution. So when external momentum P is hardm∼T, the loop contribution is of order g^2 and can be ignored. On the other hand, when P is soft$\sim gT$, the loop corrections are of order 1 and the hard thermal loops are as important as tree level contribution. Therefore, to evaluate any physical quantity one must resummed propagator involving HTLs whenever the external lines are soft. For QED at finite temperature, the resummed photon propagator in the Coulomb gauge and plasma frame is given as [100]

$$D_{\mu\nu}(K) = -\frac{\delta_{\mu 0}\delta_{\nu 0}}{k^2 + \Pi_L(K)} + \frac{\delta_{ij} - \hat{k}_i\hat{k}_j}{k^2 - \omega^2 + \Pi_T(K)}. \tag{2.38}$$

Here, Π_L/Π_T are longitudinal/transversal component of photon self-energy that arises from HTLs. For resummed gluon propagator in a magnetized thermal medium see Eq.4.24 and for the case of Polyakov loop background see Eq.6.33. Similarly, the resummed fermion propagator is given as

$$\mathcal{S}(K) = \frac{1}{\not{K} + m + \Sigma(P)}, \tag{2.39}$$

where $\Sigma(P)$ is electron self energy within the HTL approximation.

2.4 Self energies in thermal field theory

In order to discuss the applications of ITF and RTF, here we aim to provide the computational techniques in somewhat detail. We mainly focus on HTL contribution to the photon and electron self energy in both ITF and RTF.Besides somewhat detail discussion on HTL self energies, it is also relevant for the thesis that involves evaluation of Feynmann diagrams/self energies in a magnetic field background (see chapter3, chapter4) and with Polyakov-loop (see chapter6).

2.4.1 Photon self energy in ITF

As already discussed, in ITF, similar to momentum space one can perform calculations in frequency space and do sum over so called Matsubara frequencies. Finally,

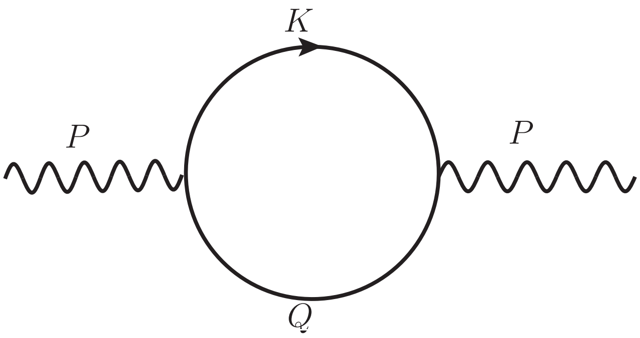

Figure 2.2: One loop photon self energy.

for a time dependent quantity, the analytic continuation is required. Here, we evaluate photon self energy diagram of Fig.2.2 in the Euclidean space where any four vector $P_\mu = (p_4 = -\omega, \mathbf{p})$; ω being Matsubara frequency. In the Feynman gauge, the photon polarisation is written as

$$\Pi_{\mu\nu}(p_0 = i\omega, \mathbf{p}) = -g^2 \int \frac{d^4K}{(2\pi)^4} Tr[\gamma_\mu \mathcal{S}(K)\gamma_\nu \mathcal{S}(Q)], \tag{2.40}$$

where $Q = P - K$ and $\mathcal{S}$ is electron propagator in the Euclidean space which is given as

$$\mathcal{S}(K) = \frac{m - \not{K}}{\omega_n^2 + |\mathbf{k}|^2 + m^2} = (m - \not{K})\tilde{\Delta}(\omega_n), \tag{2.41}$$

As discussed earlier, Euclidean space self-energy $\Pi(i\omega, \mathbf{p})$ is defined only for the discrete Matsubara frequencies. In order to obtain real time self energy, one need to perform an analytical continuation by replacing $i\omega \rightarrow p_0 + i\epsilon$ after summing over Matsubara frequencies. In the fermion propagator Eq.(2.41), $\omega_n = (2n+1)\pi T$ is the Matsubara frequency of the electron of four-momentum K. Since we are working in the high temperature limit, i.e., $T \gg m$, the mass term can be ignored to rewrite Eq.(2.40) as

$$\Pi_{\mu\nu}(p_0 = i\omega, \mathbf{p}) = -g^2 \int \frac{d^4K}{(2\pi)^4} Tr[\gamma_\mu \not{K} \gamma_\nu \not{Q}] \tilde{\Delta}(\omega_n, \mathbf{k}) \tilde{\Delta}(\omega_n - \omega, \mathbf{q}). \tag{2.42}$$

In the ITF, the energy integration is replaced by the frequency summation so the integration in Eq.(2.42) becomes

$$\int \frac{d^4K}{(2\pi)^4} = T \sum_n \frac{d\mathbf{k}}{(2\pi)^3}, \tag{2.43}$$

where summation is over fermionic Matsubara frequencies. In the view of HTL approximation, we also neglect the external momentum compared to loop momentum in the numerator of expression Eq.(2.42). Performing the trace over Dirac space to obtain

$$\Pi_{\mu\nu}(p_0 = i\omega, \mathbf{p}) = -4g^2 T \sum_n \int \frac{d\mathbf{k}}{(2\pi)^3} (2K_\mu K_\nu - K^2 g_{\mu\nu}) \tilde{\Delta}(\omega_n, \mathbf{k}) \tilde{\Delta}(\omega_n - \omega, \mathbf{q}). \tag{2.44}$$

The resummed photon propagator requires Π_L and Π_T components of self-energy. Here we only evaluate Π_L, Π_T can also be obtained in a similar manner. Therefore, with $\mu = 0, \nu = 0$, the longitudinal component of the self-energy can be written as

$$\Pi_L = 4g^2 T \sum_n \int \frac{d\mathbf{k}}{(2\pi)^3} (\tilde{\Delta}(\omega_n - \omega, \mathbf{q}) - 2k^2 \tilde{\Delta}(\omega_n, \mathbf{k}) \tilde{\Delta}(\omega_n - \omega, \mathbf{q})), \tag{2.45}$$

which we write as $\Pi_L = \delta\Pi_L^1 - \delta\Pi_L^2$. As may be noted in Eq.(2.45), there are two terms that involve two different kinds of Matsubara frequency summation. In the first term, the frequency sum is

$$
\begin{aligned}
T\sum_n \tilde{\Delta}(\omega_n-\omega,\mathbf{q}) &= T\sum_n \frac{1}{2E_q}\left[\frac{1}{E_q+i(\omega-\omega_n)}-\frac{1}{E_q-i(\omega-\omega_n)}\right] \\
&= \frac{1}{2E_K}\bigg(1-\tilde{f}(E_k)-\tilde{f}(E_q)\bigg), \qquad (2.46)
\end{aligned}
$$

where $\tilde{f}(E)$ is the Fermi-Dirac distribution function, $E_k = |\mathbf{k}|$ and $E_q = |\mathbf{p}-\mathbf{k}|$. In the limit of soft external photo, i.e., HTL approximation $1-\tilde{f}(E_K)-\tilde{f}(E_q) \approx 1-2\tilde{f}(E_k)$. On the other hand, the second term involves the frequecy sum including the productuct of two propagators. With simple simplification, this product can be written as

$$
\begin{aligned}
T\sum_n \tilde{\Delta}(\omega_n,\mathbf{k})\tilde{\Delta}(\omega_n-\omega,\mathbf{q}) &= \frac{T}{4E_kE_q}\left[\frac{1}{(E_k+i\omega_n)(E_q+i(\omega-\omega_n))}\right. \\
&+ \frac{1}{(E_k-i\omega_n)(E_q+i(\omega-\omega_n))} \\
&+ \frac{1}{(E_k+i\omega_n)(E_q-i(\omega-\omega_n))} \\
&+ \left.\frac{1}{(E_k-i\omega_n)(E_q-i(\omega-\omega_n))}\right], \qquad (2.47)
\end{aligned}
$$

and after performing summation over Matsubara frequencies one can get

$$
\begin{aligned}
T\sum_n \tilde{\Delta}(\omega_n,\mathbf{k})\tilde{\Delta}(\omega_n-\omega,\mathbf{q}) = \frac{1}{4E_qE_k}&\left[\frac{\tilde{f}(E_k)-\tilde{f}(E_q)}{i\omega+E_k-E_q}+\frac{\tilde{f}(E_k)-\tilde{f}(E_q)}{E_k-E_q-i\omega}\right. \\
&\left.+\frac{1-\tilde{f}(E_k)-\tilde{f}(E_q)}{E_k+E_q-i\omega}+\frac{1-\tilde{f}(E_k)-\tilde{f}(E_q)}{E_k+E_q+i\omega}\right]. \qquad (2.48)
\end{aligned}
$$

Now let us examine these two frequency summed terms in somewhat detail. In the third and fourth term of Eq.(2.48), the term independent of the distribution function is the vacuum term and the divergence in these terms are renormalized by using the standard methods of renormalization in the vacuum field theory. Further, we shall drop the vacuum term in order to consider the medium contribution. Keeping HTL approximation, It is convenient to write $E_q = E_k - |\mathbf{p}|\cos\theta$ where

θ is the angle between $\mathbf{p}$ and $\mathbf{k}$ and the distribution function $\tilde{f}(E_q)$ as

$$\tilde{f}(E_q) = \tilde{f}(E_k - p\cos\theta) = \tilde{f}(E_k) - |\mathbf{p}|\cos\theta \frac{\partial \tilde{f}(E_k)}{\partial k}. \tag{2.49}$$

In Eq.(2.46), the leading order contribution $\sim T^2$ comes from the term proportional to the distribution function so that

$$\delta\Pi_L^1 = -\frac{2g^2}{\pi^2}\int k\tilde{f}(k)dk, \tag{2.50}$$

where

$$\int k\tilde{f}(k)dk = \frac{\pi^2 T^2}{12}. \tag{2.51}$$

Another leading contribution in Π_L arises from $\delta\Pi_L^2$, which comes from the first and the second term involving the difference of distribution functions. Further, we also simplify the denominators of these terms as $i\omega \pm E_k \mp E_q \approx i\omega \pm |\mathbf{p}|\cos\theta$ to acquire

$$\delta\Pi_L^2 = \frac{8g^2}{(2\pi)^3}\int \frac{k^2 d\mathbf{k}}{4E_k E_q (2\pi)^3} p\cos\theta \frac{\partial \tilde{f}(E_k)}{\partial k}\left[\frac{1}{i\omega + p\cos\theta} - \frac{1}{i\omega - p\cos\theta}\right]. \tag{2.52}$$

In Eq.(2.52), $d\mathbf{k} = dk d\phi d\cos\theta$. Here, integrand is independent of ϕ so $\int d\phi = 2\pi$ also the angular integration and the momentum integration are well separated and can be integrated separately. After performing momentum integration, Eq.(2.52) can be written as

$$\delta\Pi_L^2 = -\frac{g^2T^2}{12}\int d(\cos\theta)\left[\frac{p\cos\theta}{i\omega + p\cos\theta} - \frac{p\cos\theta}{i\omega - p\cos\theta}\right]. \tag{2.53}$$

We further simplify the integration by writing

$$\frac{p\cos\theta}{i\omega + p\cos\theta} - \frac{p\cos\theta}{i\omega - p\cos\theta} = 2 - \frac{i\omega}{i\omega - p\cos\theta} - \frac{i\omega}{i\omega + p\cos\theta}, \tag{2.54}$$

and performing the angular integration the final expression of$\delta\Pi_L^2$ can be written as

$$\delta\Pi_L^2 = \frac{g^2T^2}{3}\left[1 + \frac{i\omega}{2p}\log\frac{i\omega + p}{i\omega - p}\right], \tag{2.55}$$

so the longitudinal component of self energy becomes

$$\Pi_L = \frac{g^2T^2}{6}\left[1 + \frac{i\omega}{p}\log\frac{i\omega + p}{i\omega - p}\right]. \tag{2.56}$$

Let us now move to RTF and discuss the retarded self-energy of photon. In the RTF, similar to retarded Green's function, the retarded self-energy can be written in terms of $\Pi_{11}^{\mu\nu}$ and $\Pi_{12}^{\mu\nu}$ components of self energy[118]

$$\Pi_R^{\mu\nu}(p_0, \mathbf{p}) = \Pi_{11}^{\mu\nu}(p_0, \mathbf{p}) - \Pi_{12}^{\mu\nu}(p_0, \mathbf{p}). \tag{2.57}$$

To evaluate the 11 and 12 components of self-energy, one follows the standard way of writing polarization tensor using the same components of propagator as in Eq.2.20.

$$\Pi_R^{\mu\nu}(p_0, \mathbf{p}) = -ig^2\int\frac{d^4K}{(2\pi)^4}\Big(Tr[\gamma^\mu S_{11}(Q)\gamma^\nu S_{11}(K) - \gamma^\mu S_{21}(Q)\gamma^\nu S_{12}(Q)]\Big). \tag{2.58}$$

Similar to ITF, only the longitudinal i.e., time-like component of self energy calculation will be presented here. Writing the fermion propagator $\mathcal{S}_{ij}(K) = \not{K}\Delta_{ij}(K)$, the trace over Dirac space $Tr[\gamma^\mu \not{Q}\gamma^\nu \not{K}] = 4[K^\mu Q^\nu + Q^\mu K^\nu - (K\cdot Q)g^{\mu\nu}]$, for $\mu = 0, \nu = 0$ the trace is $Tr[\gamma^0\not{Q}\gamma^0\not{K}] = 4[k_0q_0 + \mathbf{kq}]$, the longitudinal component of retarded self energy becomes

$$\Pi_R^L = -4ig^2\int\frac{d^4K}{(2\pi)^4}(q_0k_0 + \mathbf{q}\cdot\mathbf{k})(\Delta_{11}(Q)\Delta_{11}(K) - \Delta_{21}(Q)\Delta_{12}(K)), \tag{2.59}$$

where

$$\Delta_{11}(K) = \frac{1}{K^2 + i\epsilon} + 2\pi i\tilde{f}(k_0)\delta(K^2), \tag{2.60}$$

and

$$\Delta_{12}(K) = 2\pi i\tilde{f}(k_0)\delta(K^2). \tag{2.61}$$

Here, $\tilde{f}(k_0)$ is the fermion distribution function. In terms of advanced/retarded and symmetric propagators, Eq.(2.59) becomes

$$\Pi_R^L = -2ig^2\int\frac{d^4K}{(2\pi)^4}(q_0k_0 + \mathbf{q}\cdot\mathbf{k})(\Delta_F(Q)\Delta_R(K) + \Delta_A(Q)\Delta_F(K)). \tag{2.62}$$

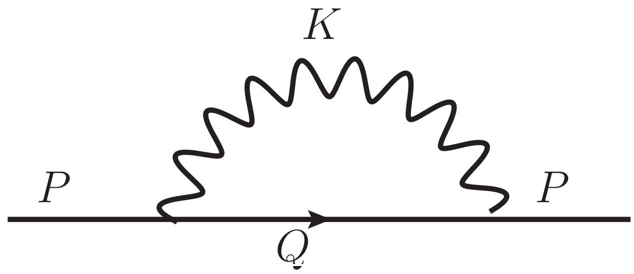

Figure 2.3: One loop electron self energy.

Now Replacing K by Q in the first term and using $\Delta_R(-Q) = \Delta_A(Q)$, the above expression can be simplified further on

$$\Pi_R^L = -8\pi g^2 \int \frac{d^4K}{(2\pi)^4}(q_0k_0 + \mathbf{q}\cdot\mathbf{k})(1-2\tilde{f}(k_0))\frac{\delta(K^2)}{Q^2 - isgn(q_0)\epsilon}. \quad (2.63)$$

So far this expression is exact. Within the HTL approximation, the final expression for the longitudinal component of the self-energy becomes

$$\Pi_R^L = -\frac{g^2T^2}{3}\left[1 - \frac{p_0}{2p}\ln\left(\frac{p_0+p+i\epsilon}{p_0-p+i\epsilon}\right)\right]. \quad (2.64)$$

Similarly, the transverse part of the self energy can be given as

$$\Pi_R^T = \frac{g^2T^2p_0^2}{6p^2}\left[1 - \left(1 - \frac{p^2}{p_0^2}\right)\frac{p_0}{2p}\ln\left(\frac{p_0+p+i\epsilon}{p_0-p+i\epsilon}\right)\right]. \quad (2.65)$$

For gluon self energy in the strong field within the framework of RTF see appendixA.1.

2.4.2 Electron self energy ITF

Electron self energy diagram is given in Fig.2.3. In order to evaluate the electron self energy we take HTL approximation.

In the Feynman gauge, the electron self energy in the Euclidean space is given as

$$\Sigma(P) = g^2 \int \frac{d^4K}{(2\pi)^4}[\gamma_\mu \not{Q} \gamma_\mu]\Delta(K)\tilde{\Delta}(\omega - \omega_n), \quad (2.66)$$

where $\Delta(K) = K^{-2} = (\omega_n^2 + \mathbf{k}^2)$ with $\omega_n = 2n\pi T$ as bosonic Matsubara frequency and $Q = P - K$. Writing $\gamma_\mu\gamma_\mu = 2$ and taking HTL approximation i.e., neglect P with respect to K in the numerator, we get

$$\Sigma(P) = -2g^2 T \sum_n \int \frac{d\mathbf{k}}{(2\pi)^3} \not{K} \Delta(K) \tilde{\Delta}(\omega - \omega_n), \tag{2.67}$$

where summation is over bosonic Matsubara frequencies. In the Euclidean space $\not{K} = \gamma_4 k_4 + \gamma \cdot \mathbf{k}$ with $k_4 = -\omega_n$. As can be seen in Eq.(2.67) and the definition of $\not{K}$, there are two types of frequency sums, one of which is

$$\begin{aligned} T\sum_n \Delta(K)\tilde{\Delta}(\omega - \omega_n) &= -\frac{1}{4E_k E_q}\Bigg[\left(\frac{1}{i\omega - E_k - E_q} - \frac{1}{i\omega + E_k + E_q}\right) \\ &\times \left(1 + f(E_k) - \tilde{f}(E_q)\right) + \left(\frac{1}{i\omega + E_k - E_q}\right. \\ &- \left.\frac{1}{i\omega - E_k + E_q}\right)\left(f(E_k) + \tilde{f}(E_q)\right)\Bigg], \end{aligned} \tag{2.68}$$

and the another one is

$$\begin{aligned} T\sum_n \omega_n \Delta(K)\tilde{\Delta}(\omega - \omega_n) &= -\frac{i}{4E_k}\Bigg[\left(\frac{1}{i\omega - E_k - E_q} + \frac{1}{i\omega + E_k + E_q}\right) \\ &\times \left(1 + f(E_k) - \tilde{f}(E_q)\right) - \left(\frac{1}{i\omega + E_k - E_q}\right. \\ &+ \left.\frac{1}{i\omega - E_k + E_q}\right)\left(f(E_k) + \tilde{f}(E_q)\right)\Bigg]. \end{aligned} \tag{2.69}$$

At finite temperature, the dominant contribution to the electron self-energy comes from the term that involves the sum of two distribution functions in Eqs.(2.68) and (2.69). Simplifying the denominators of these terms same as we did for the photon self-energy and performing momentum integration, the electron self-energy becomes

$$\Sigma(P) = \frac{g^2 T^2}{8} \int \frac{d\Omega}{4\pi} \frac{\hat{\not{K}}}{-i\omega + p\cos\theta}. \tag{2.70}$$

In the RTF, one can use the similar relation relating contour and retarded propagator even for the self energy (see Eq.2.57). For the case of magnetic field, quark self energy in the RTF is evaluated in chapter4.

2.5 In a magnetic field background

In HICs, the magnetic field is produced in the initial stage by the current of fast moving positively charged nuclei [119, 3, 120, 121, 122, 123]. In vacuum, the magnetic field decays very rapidly, however in a medium due to finite conductivity, the magnetic field satisfies the diffusion equation (see Eq.1.8) and can remain reasonably strong throughout QGP life-time [67, 68]. Therefore, one may expect its effects in the QGP properties, e.g., elliptic and directed flow. Though, so far, it has not been possible to know the exact magnitude of the magnetic field in the thermalized QGP medium due to poor understanding of electrical conductivity. Further, apart from HIC, magnetic field effects on particle dynamics are appreciable among various systems including the early universe and quasirelativistic materials such as graphene in condensed matter [124, 125]. In the following, we shall attempt to derive the propagator of a charged fermion in the presence of a constant magnetic field so that the inherent dynamics of the fermion in such a background field become explicit. Indeed, this is relevant to thesis in chapters 3, 4 and 5.

To start with, we consider the magnetic field $\mathbf{B}$ to be directed along the z-azis i.e., $\mathbf{B} = B\hat{z}$ and choose the electromagnetic vector potential in the Landau gauge, i.e., $A_\mu(\mathbf{x}) = (0, 0, Bx, 0)$. In an external magnetic field, Dirac equation for a fermion of mass m and charge e is given as

$$(i\partial\!\!\!/ + eA\!\!\!/ - m)\psi = 0, \tag{2.71}$$

where $\partial\!\!\!/ = \gamma^\mu\partial_\mu$ and $A\!\!\!/ = \gamma^\mu A_\mu$. The gamma matrices are represented as

$$\gamma^0 = \begin{pmatrix} \sigma^3 & 0 \\ 0 & -\sigma^3 \end{pmatrix}, \ \gamma^1 = \begin{pmatrix} i\sigma^1 & 0 \\ 0 & -i\sigma^1 \end{pmatrix}, \tag{2.72}$$

$$\gamma^2 = \begin{pmatrix} i\sigma^2 & 0 \\ 0 & -i\sigma^2 \end{pmatrix}, \ \gamma^3 = \begin{pmatrix} 0 & i\mathbb{1} \\ i\mathbb{1} & 0 \end{pmatrix}. \tag{2.73}$$

The fermion field operator can be expanded in terms of particle and anti-particle creation and annihilation operator as

$$\psi(\mathbf{x}) = \sum_{n,r} \frac{1}{2\pi} \int d\mathbf{p} \Big(a_r(n,\mathbf{p}) u_r(n,x,\mathbf{p}) + b_r^\dagger(n,-\mathbf{p}) v_r(n,x,-\mathbf{p}) \Big) e^{i\mathbf{p}\cdot\mathbf{x}}, \quad (2.74)$$

where $\mathbf{p} = (p_y, p_z)$. In Eq.(2.74), summation is over Landau levels denoted by $n = 0,1,2,..\infty$ and $r = \pm 1$ represents the spin state (up/down) of the particle. The particle annihilation operator a_r and anti-particle creation operation $b_r^\dagger$, respectively, satify the following anti-commutation relation

$$\{a_r(n,\mathbf{p}), a_s^\dagger(l,\mathbf{p}')\} = \delta_{rs}\delta_{nl}\delta(\mathbf{p}-\mathbf{p}') = \{b_r(n,\mathbf{p}), b_s^\dagger(l,\mathbf{p}')\}. \quad (2.75)$$

In Eq.(2.74), $u_r(n,x,\mathbf{p})$ and $v_r(n,x,-\mathbf{p})$ are particle and antiparticle spinors whose explicit form is obtained by solving Eq.2.71 and for a particle of mass m and charge e are written as

$$u_{+1}(n,x,\mathbf{p}) = \frac{1}{\sqrt{2E_n(E_n+m)}} \begin{pmatrix} (E_n+m)[\Theta(e)\mathcal{I}_n + \Theta(-e)\mathcal{I}_{n-1}] \\ 0 \\ p_z[\Theta(e)\mathcal{I}_n - \Theta(-e)\mathcal{I}_{n-1}] \\ -i\sqrt{2n|e|B}[\Theta(e)\mathcal{I}_n + \Theta(-e)\mathcal{I}_{n-1}] \end{pmatrix}, \quad (2.76)$$

$$u_{-1}(n,x,\mathbf{p}) = \frac{1}{\sqrt{2E_n(E_n+m)}} \begin{pmatrix} 0 \\ (E_n+m)[\Theta(-e)\mathcal{I}_n + \Theta(e)\mathcal{I}_{n-1}] \\ i\sqrt{2n|e|B}[\Theta(e)\mathcal{I}_n - \Theta(-e)\mathcal{I}_{n-1}] \\ -p_z[\Theta(e)\mathcal{I}_n - \Theta(-e)\mathcal{I}_{n-1}] \end{pmatrix}, \quad (2.77)$$

$$v_{+1}(n,x,-\mathbf{p}) = \frac{1}{\sqrt{2E_n(E_n+m)}} \begin{pmatrix} \sqrt{2n|e|B}[\Theta(e)\mathcal{I}_n - \Theta(-e)\mathcal{I}_{n-1}] \\ ip_z[\Theta(e)\mathcal{I}_{n-1} + \Theta(-e)\mathcal{I}_n] \\ 0 \\ i(E_n+m)[\Theta(e)\mathcal{I}_{n-1} + \Theta(-e)\mathcal{I}_n] \end{pmatrix}, \quad (2.78)$$

$$v_{-1}(n,x,-\mathbf{p}) = \frac{1}{\sqrt{2E_n(E_n+m)}} \begin{pmatrix} ip_z[\Theta(e)\mathcal{I}_n + \Theta(-e)\mathcal{I}_{n-1}] \\ \sqrt{2n|e|B}[\Theta(e)\mathcal{I}_{n-1} - \Theta(-e)\mathcal{I}_n] \\ -i(E_n+m)[\Theta(e)\mathcal{I}_n + \Theta(-e)\mathcal{I}_{n-1}] \\ 0 \end{pmatrix}. \tag{2.79}$$

In the above equations, $E_n = \sqrt{m^2 + p_z^2 + 2n|eB|}$ is the energy of the particle in the n^{th} Landau level. It ought to be mentioned here that LLL either acquire only positive energy states describing particles for $eB < 0$ or negative energy states associated with antiparticles for $eB > 0$. However, in contrast, the higher Landau levels acquire both negative as well as positive energy states describing antiparticles/particles for a given magnetic field. Further, the spinors u_r and v_r are normalised as

$$\int dx u_r^\dagger(n,x,\mathbf{p}) u_s(l,x,\mathbf{p}) = \delta_{rs}\delta_{rs} = \int dx v_r^\dagger(n,x,\mathbf{p}) v_s(l,x,\mathbf{p}). \tag{2.80}$$

For $n \geq 0$, in terms of the magnetic field and particle momentum $\mathcal{I}_n$ in spinors are given as

$$\mathcal{I}_n(\xi) = c_n \exp\left(-\frac{\xi^2}{2}\right) H_n(\xi), \tag{2.81}$$

where $\xi = |eB|(x - p_y/|eB|)$ and $\mathcal{I}_{-1} = 0$. Here H_n is n^{th} order Hermite Polynomial and the normalisation constant c_n is

$$c_n = \left(\frac{\sqrt{|eB|}}{n!2^n\sqrt{\pi}}\right)^{\frac{1}{2}}. \tag{2.82}$$

The function $\mathcal{I}_n$ also satisfy the orthogonal relation $\int d\xi \mathcal{I}_n(\xi)\mathcal{I}_l(\xi) = \sqrt{|eB|}\delta_{nl}$ ensuring the proper normalisation of spinors.

Having the field operator in terms of spinor, one can now write the propagator in a magnetic field background for a charged particle of mass m as

$$i\mathcal{S}_{\alpha\beta}(X,Y) = \langle \hat{T}\psi_\alpha(X)\bar{\psi}_\beta(Y)\rangle, \tag{2.83}$$

where $\hat{T}$ stands for the time-ordered product defined as

$$\hat{T}A(X)B(Y) = \theta(x_0 - y_0)A(X)B(Y) - \theta(y_0 - x_0)B(Y)A(X). \tag{2.84}$$

In terms of spinor product, the fermion propagator in the magnetic field background can be simplified as

$$\begin{aligned} i\mathcal{S}_{\alpha\beta}(X,Y) &= \theta(x_0 - y_0)\sum_n \int d\mathbf{p}\left[e^{-iE_n(x_0-y_0)}e^{i\mathbf{p}\cdot\mathbf{x}}\mathcal{P}_u(\mathbf{x},n,\mathbf{p})\right] \\ &- \theta(y_0 - x_0)\sum_n \int d\mathbf{p}\left[e^{iE_n(x_0-y_0)}e^{i\mathbf{p}\cdot\mathbf{x}}\mathcal{P}_v(\mathbf{x},n,\mathbf{p})\right], \end{aligned} \tag{2.85}$$

where the spinor product $\mathcal{P}_u$ is

$$\begin{aligned} \mathcal{P}_u(\mathbf{x},n,\mathbf{p}) &= \sum_r u_r(\mathbf{x},n,\mathbf{p})\bar{u}_r(\mathbf{x},n,\mathbf{p}) \\ &= \begin{pmatrix} \epsilon^+\mathcal{I}_n\mathcal{I}'_n & 0 & -p_z\mathcal{I}_n\mathcal{I}'_n & -\mathcal{B}\mathcal{I}_n\mathcal{I}'_{n-1} \\ 0 & \epsilon^+\mathcal{I}_{n-1}\mathcal{I}'_{n-1} & \mathcal{B}\mathcal{I}_{n-1}\mathcal{I}'_n & p_z\mathcal{I}_{n-1}\mathcal{I}'_{n-1} \\ p_z\mathcal{I}_n\mathcal{I}'_n & \mathcal{B}\mathcal{I}_n\mathcal{I}'_{n-1} & \epsilon^-\mathcal{I}_n\mathcal{I}'_n & 0 \\ -\mathcal{B}\mathcal{I}_{n-1}\mathcal{I}'_n & -p_z\mathcal{I}_{n-1}\mathcal{I}'_{n-1} & 0 & \epsilon^-\mathcal{I}_{n-1}\mathcal{I}'_{n-1} \end{pmatrix} \end{aligned} \tag{2.86}$$

and

$$\begin{aligned} \mathcal{P}_v(\mathbf{x},n,\mathbf{p}) &= \sum_r v_r(\mathbf{x},n,-\mathbf{p})\bar{v}_r(\mathbf{x},n,-\mathbf{p}) \\ &= \begin{pmatrix} -\epsilon^-\mathcal{I}_n\mathcal{I}'_n & 0 & p_z\mathcal{I}_n\mathcal{I}'_n & \mathcal{B}\mathcal{I}_n\mathcal{I}'_{n-1} \\ 0 & -\epsilon^-\mathcal{I}_{n-1}\mathcal{I}'_{n-1} & -\mathcal{B}\mathcal{I}_{n-1}\mathcal{I}'_n & -p_z\mathcal{I}_{n-1}\mathcal{I}'_{n-1} \\ -p_z\mathcal{I}_n\mathcal{I}'_n & -\mathcal{B}\mathcal{I}_n\mathcal{I}'_{n-1} & -\epsilon^+\mathcal{I}_n\mathcal{I}'_n & 0 \\ \mathcal{B}\mathcal{I}_{n-1}\mathcal{I}'_n & p_z\mathcal{I}_{n-1}\mathcal{I}'_{n-1} & 0 & -\epsilon^+\mathcal{I}_{n-1}\mathcal{I}'_{n-1} \end{pmatrix} \end{aligned} \tag{2.87}$$

In the above Eqs. $\epsilon^+ = E_n + m$, $\epsilon^- = m - E_n$, $\mathcal{B} = i\sqrt{2n|eB|}$ and $\mathcal{I}'_n = \mathcal{I}_n(\xi = y - p_y/|eB|)$. Now using the following integral representation of the step function, i.e.,

$$\theta(\tau) = i\int_{-\infty}^{\infty}\frac{d\omega}{2\pi}\frac{e^{-i\tau\omega}}{\omega - i\epsilon}, \tag{2.88}$$

where ϵ is infetimally small parameter and substituting $\omega + E_n = p_0$ in the first term of Eq.(2.85) and $\omega + E_n = -p_0$ in the second term of the same equation, the right hand side of Eq.(2.85) can be written as

$$\theta(x_0-y_0)e^{-iE_n(x_0-y_0)}e^{i\mathbf{p}\cdot\mathbf{x}}\mathcal{P}_u(\mathbf{x},n,\mathbf{p}) - \theta(y_0-x_0)e^{iE_n(x_0-y_0)}e^{i\mathbf{p}\cdot\mathbf{x}}\mathcal{P}_v(\mathbf{x},n,\mathbf{p})$$
$$= \frac{i}{2\pi}\int dp_0 e^{-ip_0(x_0-y_0)}\left[\frac{\mathcal{P}_u(\mathbf{x},n,\mathbf{p})}{p_0-E_n+i\epsilon}+\frac{\mathcal{P}_v(\mathbf{x},n,\mathbf{p})}{p_0+E_n-i\epsilon}\right]. \quad (2.89)$$

Further, using the identity $\mathcal{P}_u(\mathbf{x},n,\mathbf{p})|_{E_n=p_0} = -\mathcal{P}_v(\mathbf{x},n,\mathbf{p})|_{E_n=-p_0}$, the fermion propagator can be written with a proper pole structure as

$$\mathcal{S}(X,Y) = \frac{1}{(2\pi)^3}\int d\mathbf{p}dp_0 e^{i\mathbf{p}\cdot(\mathbf{x}-\mathbf{y})-ip_0(x_0-y_0)}\frac{\tilde{\mathcal{S}}(\mathbf{x},n,\mathbf{p})}{p_0^2-E_n^2+i\epsilon}, \quad (2.90)$$

where

$$\tilde{\mathcal{S}}(\mathbf{x},n,\mathbf{p}) = \begin{pmatrix} p_0^+\mathcal{I}_n\mathcal{I}'_n & 0 & -p_z\mathcal{I}_n\mathcal{I}'_n & -\mathcal{B}\mathcal{I}_n\mathcal{I}'_{n-1} \\ 0 & p_0^+\mathcal{I}_{n-1}\mathcal{I}'_{n-1} & \mathcal{B}\mathcal{I}_{n-1}\mathcal{I}'_n & p_z\mathcal{I}_{n-1}\mathcal{I}'_{n-1} \\ p_z\mathcal{I}_n\mathcal{I}'_n & \mathcal{B}\mathcal{I}_n\mathcal{I}'_{n-1} & -p_0^-\mathcal{I}_n\mathcal{I}'_n & 0 \\ -\mathcal{B}\mathcal{I}_{n-1}\mathcal{I}'_n & -p_z\mathcal{I}_{n-1}\mathcal{I}'_{n-1} & 0 & -p_0^-\mathcal{I}_{n-1}\mathcal{I}'_{n-1} \end{pmatrix}. \quad (2.91)$$

Here $p_0^+ = p_0 + m$ and $p_0^- = p_0 - m$. Further, one can also write the fermion propagator in terms of the Dirac matrices. In order to do this, we introduce the projection operators $\mathcal{P}_\pm = (1 \pm i\gamma_1\gamma_2)/2$ that aligns the spin of the particle along the direction/opposite of the magnetic field. These operators satisfies the general properties of a projection operator i.e., $\mathcal{P}_\pm\mathcal{P}_\pm = \mathcal{P}_\pm$ and $\mathcal{P}_\pm\mathcal{P}_\mp = 0$. Finally, with these projection operators, the propagator as defined in Eq.(2.91) can be simplified to

$$\tilde{\mathcal{S}}(\mathbf{x},n,\mathbf{p}) = [(\gamma\cdot\mathbf{p})_\parallel + m](\mathcal{P}_+\mathcal{I}_n\mathcal{I}'_n + \mathcal{P}_-\mathcal{I}_{n-1}\mathcal{I}'_{n-1}) + \mathcal{B}(\mathcal{P}_+\mathcal{I}_n\mathcal{I}'_n - \mathcal{P}_-\mathcal{I}_{n-1}\mathcal{I}'_{n-1}), \quad (2.92)$$

where $(\gamma\cdot\mathbf{p})_\parallel = \gamma_0 p_0 - \gamma_3 p_z$. In Eq.(2.92), it can be seen that in the lowest Landau level, i.e., $n = 0$ particle spin aligned opposite to the magnetic field do not contribute in the propagator. In other words, one can say that in the LLL particles are directed along the magnetic field direction only. In order to further simplify Eq.4.2, let us consider the y component of the momentum, so we write

$$\begin{aligned}\mathcal{I}_{n,n'} &= \int dp_y e^{ip_y(y-y')}\mathcal{I}_n\mathcal{I}_{n'} \\ &= \int dp_y e^{ip_y(y-y')}\frac{\sqrt{|eB|}}{n!2^n\sqrt{\pi}}\int dp_y e^{ip_y(y-y')}e^{-(\xi^2+\xi'^2)/2}H_n(\xi)H_n(\xi'). \end{aligned} \tag{2.93}$$

Substituting for ξ and ξ', one gets

$$\mathcal{I}_{n,n'} = \frac{\sqrt{|eB|}}{n!2^n\sqrt{\pi}}e^{|eB|(x^2+x'^2)/2}\int dp_y e^{-(p_y^2/|eB|-p_y((x+x')+i(y-y')))}H_n(\xi)H_n(\xi'). \tag{2.94}$$

For further simplification, it is convenient to do change of variable from p_y to a dimensionless variable $u = p_y/\sqrt{|eB|} - \sqrt{|eB|}/2(x+x'+i(y-y'))$ to obtain

$$\mathcal{I}_{n,n'} = \frac{|eB|}{n!2^n\sqrt{\pi}}e^{-|eB|z_\perp^2/2}e^{i\sqrt{|eB|}/2(y-y')(x+x')}\int du e^{-u^2}H_n(u+a)H_n(u+b), \tag{2.95}$$

where $z_\perp^2 = (x-x')^2+(y-y')^2$, $a = \sqrt{|eB|}/2(x-x'-i(y-y'))$ and $b = -\sqrt{|eB|}/2(x-x'+i(y-y'))$. Finally, using the relation $\int du e^{-u^2}H_n(u+a)H_n(u+b) = 2^n n! L_n(-2ab)$, we get

$$\mathcal{I}_{n,n'} = |eB|e^{-|eB|z_\perp^2/4}e^{i\sqrt{|eB|}/2(y-y')(x+x')}L_n\left(\frac{|eB|z_\perp^2}{2}\right), \tag{2.96}$$

where L_n is generalized Leguerre Polynomials given as

$$L_n(x) = \frac{1}{n!}\frac{d^n}{dx^n}(x^2e^{-x}). \tag{2.97}$$

Similary, in order to perform p_y integration, other terms can also be simplified such as

$$\mathcal{I}_{n-1,n'} = \int dp_y e^{ip_y(y-y')}\mathcal{I}_{n-1}\mathcal{I}'_n. \tag{2.98}$$

With variable change similar to the previous case one arrives

$$\int du e^{-u^2}H_{n-1}(u+a)H_n(u+b) = \frac{2^{n-1}n!\sqrt{\pi}}{a}\Big[L_n(-2ab)-L_{n-1}(-2ab)\Big]. \tag{2.99}$$

So the final form of $\mathcal{I}_{n-1,n'}$ becomes

$$\mathcal{I}_{n-1,n'} = \frac{\sqrt{2n|eB|}}{r_\perp^2} e^{-|eB|z_\perp^2/4(x-x'+i(y-y'))} e^{i\Phi(X,Y)} \left[L_n\left(\frac{|eB|z_\perp^2}{2}\right) - L_{n-1}\left(\frac{|eB|z_\perp^2}{2}\right)\right], \tag{2.100}$$

where $\Phi(X,Y) = |eB|/2(x+x')(y-y')$. Similarly

$$\mathcal{I}_{n,n-1} = -\frac{2n|eB|}{z_\perp^2} e^{-|eB|z_\perp^2/4} e^{i\Phi(X,Y)} \left[L_n\left(\frac{|eB|z_\perp^2}{2}\right) - L_{n-1}\left(\frac{|eB|z_\perp^2}{2}\right)\right]. \tag{2.101}$$

Therefore, the final form of the propagator the propagator $\mathcal{S}(X,Y)$ becomes

$$\mathcal{S}(X,Y) = e^{i\Phi(X,Y)}\mathcal{S}(X-Y). \tag{2.102}$$

Note here that $\Phi(X,Y)$ is not translationally invariant that makes $\mathcal{S}(X,Y)$ translationally non-invariant. This origin of translational invariance is the directionality of the magnetic field. Further, the translational invariant part is given as

$$\begin{aligned} \mathcal{S}(X-Y) \quad = \quad & \frac{\exp\left(\frac{\beta \mathbf{r}_\perp^2}{4}\right)}{(2\pi)^3} \int dp_\parallel \frac{1}{p_\parallel^2 - m^2 - 2n|eB| + i\epsilon} \Bigg[[(\gamma\cdot\mathbf{p})_\parallel + m] \\ & \left(\mathcal{P}_+ L_n\left(\frac{\beta\mathbf{r}_\perp^2}{2}\right) + \mathcal{P}_- L_n\left(\frac{\beta\mathbf{r}_\perp^2}{2}\right)\right) + 2n|eB|\Bigg(\mathcal{P}_+ L_n\left(\frac{\beta\mathbf{r}_\perp^2}{2}\right) \\ & -\mathcal{P}_- L_n\left(\frac{\beta\mathbf{r}_\perp^2}{2}\right)\Bigg)\Bigg], \end{aligned} \tag{2.103}$$

where $p_\parallel^2 = p_0^2 - p_z^2$ and $\mathbf{r}_\perp^2 = (\mathbf{x}-\mathbf{y})^2$. It is well known that the in the presence of magnetic field dimensional reduction from $D \to D-2$ takes place e.g., 3+1 $\to$ 1+1 and 2+1 $\to$ 0+1 which is also apparent in propagator structure given in Eq.2.103. The reason is that the motion of charged particles is restricted along the directions perpendicular to the magnetic field. Indeed, in a $3+1$ and $2+1$ space-time dimensions, the presence of a strong magnetic field dubbed as catalyst for the chiral symmetry breaking that lead to fermion mass generation [126, 127, 128]. In the catalysis mechanism, the LLL plays a very crucial role quite similar to the Fermi surface in BardeenCooperSchrieffer (BCS) theory [126]. Further, In general, it is convenient to write the propagator in the momentum space which can be obtained by using the Fourier transformation as

$$\mathcal{S}(P) = \frac{1}{(2\pi)^2} \int d\mathbf{r}_\perp \mathcal{S}(X,Y) e^{i(\mathbf{p}\cdot\mathbf{r})_\perp}. \tag{2.104}$$

This is discussed in chapter3 within the framework of ITF. For the real-time description of quark resummed propagator with a constant magnetic field backgrouns see chapter4. In the next chapter, we discuss the magnetized thermal medium modification on quarkonium potential and its thermal decay width.

CHAPTER 3

Quarkonia in a magnetized medium

Bound states of heavy quark and its antiquark (charmonium for $c/\bar{c}$ and bottomonium for $b/\bar{b}$) plays a very crucial role in the study of high energy nuclear collisions by allowing to probe the properties of the medium in a controlled manner. This vital role is mainly because of the larger mass of quarkonia compared to the inherent QCD scale (Λ_{QCD}). Indeed, the large mass allows a non-relativistic discription within the framework of potential model that can also be extended to incorporate medium effects on quarkonium properties. Moreover, the suppression of different quarkonium states in a thermalized QGP medium signals the temperature of the medium. Further, the magnetic field in HICs can also affect the quarkonium properties. In this regard, apart from temperature, we shall explore the magnetic field effects on the quarkonia potential and their thermal decay width in a thermalized QGP medium in this chapter.

Initially, it was thought that the strong magnetic field produced in high energy nuclear collisions decays very fast [129]. However, later, it has been argued that in a medium with finite electric conductivity, a reasonably strong magnetic field can sustain even in the QGP medium [130, 131]. The reason is that the magnetic field does not decay rapidly due to the induced currents in the medium, and it satisfies a diffusion equation. Indeed, it is shown that while the magnetic field initially decreases quite fast, at later times matter effects become more important that significantly reduces the decay rate of the magnetic field [130, 131]. This reduction in the decay rate effectively makes the external magnetic field a slowly varying function of time during the entire QGP lifetime. Simultaneously, heavy quark-antiquark pairs also develop into physical resonances over a formation time $t_{form} \sim 1/E_{bind}$, e.g., the $c\bar{c}$ pairs form resonances at $t_{c\bar{c}} \sim 0.3$ fm. Therefore, it is reasonable to assume that the heavy quark-antiquark pair is influenced by the magnetic field. As regards to the effects more directly, various studies have considered the possible influence of an external magnetic field on the static quark-antiquark potential [132, 133] and the screening masses [134]. So far, different studies have been carried out on the effects of magnetic field for static properties of quarkonia [135, 81, 136, 137, 132, 138, 139, 140] and of open heavy flavors [141, 142, 143, 144, 145]. The effect of the magnetic field on quarkonium production has been discussed in Refs. [141, 137]. Further, the influence of strong magnetic field on the evolution of J/ψ and the magnetic conversion of η_c into J/ψ has been discussed in Refs. [81, 146].

In order to add magnetic field contribution, we describe the medium effects on both the long and short-range quarkonia potential in the static limit by combining the generalized Gauss law and the dielectric permittivity of the magnetized thermal QCD medium. Once the vacuum parameter of the potential is fixed, the real/imaginary parts of the in-medium potential ($\Re V(r)/\Im V(r)$) is estimated by using the real/imaginary part of the permittivity. Further, the magnetic field contribution in the in-medium permittivity comes only from the quark loop in the gluon self-energy. Furthermore, the heavy quark mass (m_Q) is the dominant scale, i.e., $m_Q \gg \sqrt{eB} \gg T$ so a nonrelativistic potential can still describe the heavy quark. Since we consider the limit $\sqrt{eB} \gg T$ so only LLL effects are important.

This chapter is structured as follows. In Sec. 3.1, we first discuss the gluon self-energy using the imaginary time formalism and then calculate the Debye mass by taking the static limit of self-energy. Sec. 3.2 discusses the heavy quark complex potential in the presence of a magnetic field and describes the variation of the real and imaginary parts of the potential for various values of the magnetic field and temperatures. In Sec. 3.3, the effect of the magnetic field on decay width for both bottomonium and charmonium ground states are discussed. Finally, we conclude the chapter in Sec. 3.4.

3.1 Gluon self-energy in LLL approximation of the magnetic field

A critical property of the strongly interacting medium is the Debye screening of the color charges. This screening in the thermal medium, gets contribution from both the quark and the gluon loops; however, in the presence of a magnetic field, the contribution arises from the quark loop only. Further, in the strong field limit, i.e., $eB \gg T^2$, the gluonic contribution which is proportional to T^2 in the Debye screening mass is negligible compared to the quark loop contribution that is proportional to eB. In this regard, below we estimate the magnetic field contribution of the Debye mass in the LLL approximation using the ITF of field theory. In the ITF, a Euclidean four vector is represented as $b_\mu = (b_4, \mathbf{b})$. The parallel ($\|$) and the perpendicular ($\perp$) component of the four vector with respect to the magnetic field are given as

$$b^\mu_\| = (b_4, 0, 0, b_3); \quad b^\mu_\perp = (0, b_1, b_2, 0),$$

and the corresponding dot products are defined as

$$(a \cdot b)_\| = a_4 b_4 + a_3 b_3; \quad (a \cdot b)_\perp = a_1 b_1 + a_2 b_2.$$

Now, let us consider a charged particle of charge q_f and mass m_f is moving in a constant magnetic field (B) which directed along the $\hat{\mathbf{z}}$-direction, i.e., $\mathbf{B} = B\hat{\mathbf{z}}$. In this scenario, the propagator of the charged fermion which is a function of both the transverse and longitudinal component of the momentum is written as [147, 148]

$$\mathcal{S}(Y, Y') = \Phi(Y, Y') \int \frac{d^4K}{(2\pi)^4} e^{-iK\cdot(Y-Y')} \mathcal{S}(K), \tag{3.1}$$

where $\Phi(Y, Y')$ is the phase factor and can be gauged away. The form of the propagator in the position space is given in Eq.(2.103) and $S(K)$ is the Fourier transform in the momentum space. In the Euclidean space, the propagator ($\mathcal{S}(K)$) in the Landau level representation takes the form

$$S(K) = -ie^{-\frac{K_\perp^2}{|q_f B|}} \sum_{l=0}^{\infty} \frac{(-1)^l D_l(K)}{k_\parallel^2 + m_f^2 + 2l|q_f B|}, \tag{3.2}$$

where the sum is over the Landau levels ($l = 0, 1, 2,....$), and

$$\begin{aligned} D_l(K) &= (m_f - \not{k}_\parallel)\Bigg((1 + i\gamma_1\gamma_2)L_l\left(\frac{2k_\perp^2}{|q_f B|}\right) - (1 - i\gamma_1\gamma_2)L_{l-1}\left(\frac{2k_\perp^2}{|q_f B|}\right) \\ &+ 4\not{k}_\perp L_{l-1}^1\left(\frac{2k_\perp^2}{|q_f B|}\right)\Bigg), \end{aligned} \tag{3.3}$$

with $k_\parallel$ and $k_\perp$ as the parallel and the perpendicular component of the four vector K_μ as defined in Eq.(3.1). Here, $k_4 = -ik_0$ and γ_1, γ_2 are the Dirac matrices. The energy of a charged fermion in a Landau level l is given by

$$E_l^2(k_z) = k_z^2 + m_f^2 + 2l|q_f B|, \tag{3.4}$$

which can be obtained from Eq. (3.2) by equating the denominator of the propagator to zero. In the presence of a very strong magnetic field, i.e., $q_f B \gg T^2$ the higher Landau levels ($l \gg 1$) are at infinity as compared to LLL [149, 150]; therefore the dominant contribution comes from LLL. This further lead to dimensional reduction from (3+1)-dimension to (1+1)-dimension that can be seen in the propagator given in Eq. (3.5). Moreover, the dimensional reduction restricts the motion of charged particles perpendicular to the magnetic field. Using the relations $L_n(x) = L_n^0(x)$ and $L_{-1}^\alpha(x) = 0$, the fermion propagator in LLL approximation becomes

$$\mathcal{S}(K) = ie^{-\frac{k_\perp^2}{|q_f B|}}\left(\frac{\not{k}_\parallel - m_f}{k_\parallel^2 + m_f^2}\right)(1 + i\gamma_1\gamma_2). \tag{3.5}$$

Here, the factor $(1 + i\gamma_1\gamma_2)$ is the spin projection operator, which represents the spin polarization of fermion in the LLL. [151]. For the positive/negative charged particles the spin orientation is parallel/antiparallel to the magnetic field direction.

In order to obtain the Debye mass we first calculate the gluon polarization tensor correspond the diagram is shown in Fig. 3.1. As mentioned earlier, since

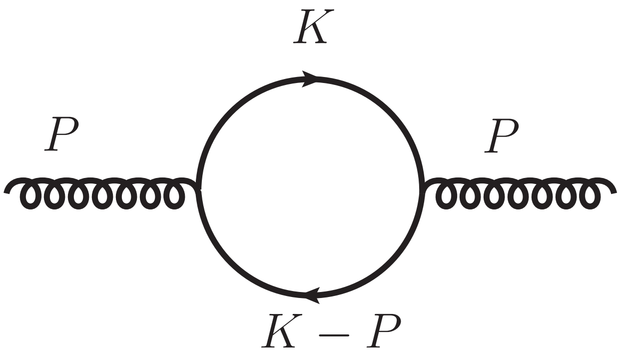

Figure 3.1: Gluon self-energy in the presence of strong magnetic field

.

the gluons do not interact with the magnetic field their contribution remains same as that of $B = 0$ case. Thus, the quarks loop contribution to the gluon self-energy in the presence of a magnetic fiel can be written as

$$\delta\Pi_{\mu\nu}(P, B) = g^2 \int \frac{d^4K}{(2\pi)^4} Tr[\gamma_\mu t^a \mathcal{S}(K)\gamma_\nu t^b \mathcal{S}(Q)], \tag{3.6}$$

where $S(K)$ is fermion propagator as defined in Eq. (3.5) and $Q = K - P$. The dimensional reduction separates the parallel and the perpendicular component dependent term in the propagator, so the self-energy can also be written separately in terms of the parallel and the perpendicular components. Therefore, the perpendicular part of the self energy in Eq. (3.6) is

$$\begin{aligned} \mathcal{I}_\perp &= \frac{1}{(2\pi)^2} \int_{-\infty}^{\infty} dk_x \int_{-\infty}^{\infty} dk_y \exp\left(\frac{-k_x^2 - q_x^2}{|q_f B|}\right) \exp\left(\frac{-k_y^2 - q_y^2}{|q_f B|}\right) \\ &= \sum_f \frac{\pi |q_f B|}{2(2\pi)^2} \exp\left(\frac{-p_\perp^2}{2 q_f B}\right), \end{aligned} \tag{3.7}$$

and Eq. (3.6) becomes

$$\delta\Pi_{\mu\nu}(P, B) = \frac{g^2 \mathcal{I}_\perp}{2} \int \frac{d^2k_\parallel}{(2\pi)^2} \frac{Tr[\gamma_\mu (\not{k}_\parallel - m_f)\mathcal{P}_+ \gamma_\nu ((\not{k} - \not{p})_\parallel - m_f)\mathcal{P}_+]}{(k_\parallel^2 + m_f^2)((k-p)_\parallel^2 + m_f^2)}, \tag{3.8}$$

where $\mathcal{P}_+ = 1 + i\gamma_1\gamma_2$. The Debye mass is obtained from the temporal component of the self energy which can be written as

$$\delta\Pi_{44}(P,B) = \frac{g^2\mathcal{I}_\perp T}{2}\int\frac{dk_z}{(2\pi)}\sum_n\frac{8\omega_n^2 - 8k_z^2 - 8m_f^2 - 8\omega_n\omega + 8k_zp_z}{(\omega_n^2 + E_{k_z}^2)((\omega-\omega_n)^2 + E_{q_z}^2)}, \tag{3.9}$$

where $\omega_n = (2n+1)\pi T$ is fermionic Matsubara frequency, ω is bosonic Matsubara frequency, $E_{k_z}^2 = k_z^2 + m_f^2$ and $E_{q_z}^2 = q_z^2 + m_f^2$. For massless fermion ($m_f = 0$), Eq.(3.9) reduces to

$$\delta\Pi_{44}(P,B) = 4g^2\mathcal{I}_\perp T\int\frac{dk_z}{(2\pi)}\sum_n\Big(\tilde{\Delta}(\omega_n) - (2k_z^2 + \omega_n\omega - k_zp_z)\tilde{\Delta}(\omega_n)\tilde{\Delta}(\omega-\omega_n)\Big), \tag{3.10}$$

where $\tilde{\Delta}(\omega_n) = [\omega_n^2 + k_z^2]^{-2}$, $\tilde{\Delta}(\omega-\omega_n) = [(\omega-\omega_n)^2 + q_z^2]^{-2}$. Furthermore, in order to calculate the Debye screening mass one need to take the static limit of temporal component of self-energy, Π_{44} *viz.* $m_D^2 = -\Pi_{44}(\omega = 0,\ \mathbf{p}\to 0)$. After taking the static limit Eq. (3.10) becomes

$$\delta\Pi_{44}(B)|_{(\omega=0,\mathbf{p}=0)} = 4g^2\mathcal{I}_\perp\int\frac{dk_z}{(2\pi)}T\sum_n\Big(\tilde{\Delta}(\omega_n) - 2k_z^2(\tilde{\Delta}(\omega_n))^2\Big). \tag{3.11}$$

Let us note that the temperature contribution to the self energy comes from the Matsubara frequencies. On the other hand the magnetic field ontribution comes from the transverse component of the propagator. Further, performing the sum over Matsubara frequency as given in Eqs.(2.46) and(2.48) we get

$$\delta m_D^2 = 4g^2\beta\mathcal{I}_\perp\int\frac{dk_z}{(2\pi)}\tilde{f}(E_{k_z})(1-\tilde{f}(E_{k_z})). \tag{3.12}$$

Replacing the transverse part of the self-energy by Eq.(3.7), the quark loop contribution to the Debye screening mass in a magnetic field background becomes

$$\delta m_D^2 = \sum_f\frac{|q_fB|g^2}{\pi T}\int_0^\infty\frac{dk_z}{2\pi}\tilde{f}(E_{k_z})(1-\tilde{f}(E_{k_z})). \tag{3.13}$$

To get the total Debye mass in the thermal medium with a background magnetic field, one also need to consider the gluon contributions to the screening mass.

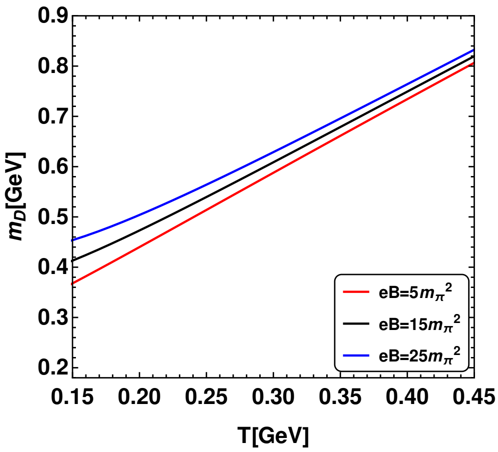

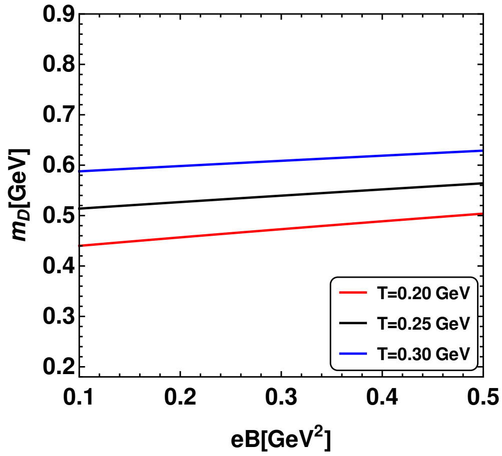

Figure 3.2: Debye mass m_D as a function of temperature and magnetic field.

Taking this into account, the final form of the Debye mass becomes

$$m_D^2 = \frac{4\pi\alpha_s(T)T^2N_c}{3} + \sum_f \frac{|q_fB|g^2}{\pi T}\int_0^\infty \frac{dk_z}{2\pi}\tilde{f}(E_{k_z})(1-\tilde{f}(E_{k_z})). \tag{3.14}$$

For massless fermions, $\int_0^\infty dk_z\tilde{f}(E_{k_z})(1-\tilde{f}(E_{k_z}) = T/2$. Therefore, Eq. (3.14) reduces to

$$m_D^2 = \frac{4\pi\alpha_s(T)T^2N_c}{3} + \sum_f \frac{|q_f|B\alpha_s(T)}{\pi}. \tag{3.15}$$

where $\alpha_s(T)$ is the running coupling constant which for one loop is given as [152]

$$\alpha_s(T) = \frac{g_s^2(T)}{4\pi} = \frac{6\pi}{(33-2N_f)\ln\left(\frac{2\pi T}{\Lambda_{\overline{\text{MS}}}}\right)}. \tag{3.16}$$

Here for $N_f = 3$ the quantity $\Lambda_{\overline{\text{MS}}} = 0.176$ GeV. Fig.(3.2) shows the variation of the Debye mass as given in Eq.(3.15) as a function of magnetic field and temperature for $m_f = 0$. From Fig. 3.2, it is clear that for a given value of the magnetic field with an increase in temperature, the Debye mass increases. Indeed, the effect of the magnetic field is more substantial at a lower temperature and becomes weaker at a higher temperature. At high temperature, with an increase in the magnetic field, the Debye mass does not increase much because, at large temperatures, the gluon contribution starts dominating the quark one. In the right side of Fig.(3.2), the variation of Debye mass with the magnetic field for various values of temperature is shown. It may be observed that the Debye mass increases with an increase in the magnetic field. The observed increase of screening mass as a function of the magnetic field is in qualitative agreement with lattice QCD computation [134]. Suppression of quarkonium state in a medium depends on the Debye screening. From Fig.(3.2), one can anticipate that quarkonia potential will get a finite contribution from the magnetic field in a magnetized thermal QGP medium.

3.2 In-medium heavy quark potential in magnetic field

The simplest form of the confining potential for a $Q\bar{Q}$ pair as a function of distance r is given as

$$V(r) = -\frac{\alpha_s}{r} + \sigma r, \tag{3.17}$$

where α_s as coupling constant and σ is the string tension. The medium effects in the quarkonia can be incorporated using the Debye-Hückle theory, which was proposed in Ref. [153]. Another way of including the medium effects is via the medium permittivity by combing the Gauss law and the Debye-Hückle theory which was originally proposed in Ref.[79]. Let us first discuss this in detail for a vanishing magnetic field. Consider that a test charged particle is placed at the origin, and an auxiliary vector field due to this at a distance $\mathbf{r}$ is as $\mathbf{E} = qr^{b-1}\hat{\mathbf{r}}$, where b is a parameter that can have any value. The corresponding potential of the auxiliary field can be defined by using the relation -$\nabla V(r) = \mathbf{E}(r)$. Therefore, the Gauss law can be defined as [79, 153]

$$\nabla \cdot \left(\frac{\mathbf{E}}{r^{b+1}}\right) = 4\pi q \delta(r). \tag{3.18}$$

choosing the appropriate values of b and q, one can obtain the Coulomb and string part of the potential. For $b = -1, q = \alpha(= \alpha_s C_F = \frac{g_s^2 C_F}{4\pi}; C_F = 4/3)$, Eq. (3.18) reduces to the Coulomb potential and for $b = 1, q = \sigma$, one can obtain the linearly rising (string part) potential, where σ is the string tension and α_s

is the QCD running coupling. As per the Debye-Hückle framework, the medium gets polarized and leads to a change of the source term on the right hand side of Eq. (3.18) from $\delta(r)$ to $\delta(r) + \langle\rho(r)\rangle$ so that

$$\nabla \cdot \left(\frac{\mathbf{E}}{r^{b+1}} \right) = 4\pi q(\delta(r) + \langle\rho(r)\rangle). \tag{3.19}$$

Here $\langle\rho(r)\rangle$ is the induced charged density which can be written in the Boltzmann's distribution as the difference of the particle and antiparticle charge deviation i.e.,

$$\langle\rho(r)\rangle = n_0(e^{-\beta V(r)} - 1) - n_0(e^{\beta V(r)} - 1), \tag{3.20}$$

where $\beta = 1/T$ and n_0 is the charge density in the absence of test charge. At high temperatures and weak in medium potential the charge density can be approximated as $\langle\rho(r)\rangle = -2q\beta n_0 V(r)$. Plugging this back in Eq.(3.19) and using the relation $\nabla V(r) = -\mathbf{E}(r)$, the differential equation for the potential becomes

$$-\frac{1}{r^{b+1}}\nabla^2 V(r) + \frac{1+b}{r^{b+2}}\nabla V(r) + 8\pi q n_0 \beta V(r) = 4\pi q \delta(r). \tag{3.21}$$

For $b = -1, q = \alpha$, the im-medium Coulombic part of the potential is given by

$$-\nabla^2 V_C(r) + 8\pi\alpha_s n_0 \beta V_C(r) = 4\pi\alpha_s \delta(r). \tag{3.22}$$

Similar, in the linear response approximation, for $b = 1, q = \sigma$ the string part of the in-medium potential is given by

$$-\frac{1}{r^2}\frac{d^2 V_s(r)}{dr^2} + 8\pi\sigma n_0 \beta V_s(r) = 4\pi\sigma\delta(r). \tag{3.23}$$

Let us note here that for Coulomb and string part of the potential, same charge density n_0 appears.

In the present approach, the medium effects, i.e., the effect of finite temperature and magnetic field can be incorporated by modifying the vacuum potential with dielectric permittivity as in Ref. [78]. The in-medium permittivity $\epsilon(\vec{p}, m_D)$ can be written as

$$\epsilon^{-1}(\mathbf{p}, m_D) = -\lim_{\omega\to 0} p^2 D^{00}(\omega, p) \ . \tag{3.24}$$

where D^{00} is the gluon resummed propagator calculated from the longitudinal component Π_L or (Π_{44}) of the gluon self-energy. In a magnetized thermal medium, the gluon propagator has contributions from the gluon as well as quark. The magnetic field contribution in the resummed propagator comes from the quark loop. We evaluate each contribution in the following way.

3.2.1 Gluon loop contribution to Π_L

As the gluonic contribution does not depend upon the magnetic field, the temperature dependent longitudinal part of the gluon self-energy can be written as [154]

$$\delta\Pi_L(\omega,p)_g = m_{Dg}^2\left[1-\frac{\omega}{2p}\ln\left(\frac{\omega+p}{\omega-p}\right)+i\pi\frac{\omega}{2p}\theta(p^2-\omega^2)\right], \tag{3.25}$$

where $m_{Dg}^2 = \frac{1}{3}g^2T^2N_c$ with N_c the number of colors and $\theta(p^2-\omega^2)$ is the step function. In Eq.(3.25), the imaginary part is related to the Landau damping, which corresponds to the emission and absorption of particle in the medium.

3.2.2 Quark loop contribution to Π_L

This contribution arises from the quark loop in the gluon self-energy. From Eq. (3.9), we can get the longitudinal component of the self energy $\delta\Pi_L(\omega,p) \equiv \delta\Pi_{44}(\omega,p)$ after summing over fermionic Matsubara frequencies. To estimate the quark contribution to the resummed gluon propagator, one needs the imaginary part of the longitudinal component of the self-energy $(\Im\delta\Pi_{44})$ which can be obtained by using the identity

$$\Im\delta\Pi_L(\omega,p)_f = \frac{1}{2i}\lim_{\eta\to 0}\left[\delta\Pi_L(\omega+i\eta,p)-\delta\Pi_L(\omega-i\eta,p)\right], \tag{3.26}$$

along with the expression

$$\frac{1}{2i}\left(\frac{1}{\omega+\sum_j E_j+i\eta}-\frac{1}{\omega+\sum_j E_j-i\eta}\right) = -\pi\delta(\omega+\sum_j E_j). \tag{3.27}$$

Using Eqs. (2.46) and 2.47 for the fermionic Matsubara frequency in Eq. (3.9), the imaginary part of the longitudinal component of self energy i.e., $\delta\Pi_L$ becomes

$$\delta\Im\Pi_L(\omega,p)_f = \pi 4 g^2 I_\perp \int \frac{dk_z}{2\pi}\left(\frac{2k_z^2 - k_z p_z - 2m_f^2}{4E_{q_z}E_{k_z}}\right)\Big[(-\tilde{f}(E_{k_z}) + \tilde{f}(E_{q_z}-\omega)) \\ \times\delta(\omega + E_{k_z} - E_{q_z}) + (\tilde{f}(E_{k_z}) - \tilde{f}(E_{q_z}))\delta(\omega - E_{k_z} + E_{q_z}) + (1-\tilde{f}(E_{k_z}) \\ -\tilde{f}(E_{q_z}))\delta(E_{k_z} + E_{q_z}) + (1-\tilde{f}(E_{k_z}) - \tilde{f}(E_{q_z}))\delta(E_{k_z} + E_{q_z} + \omega)\Big] \tag{3.28}$$

In the static limit, i.e., $\omega \to 0$, the third and fourth terms of Eq.3.28 vanishes; therefore, Eq.3.28 reduces to

$$\delta\Im\Pi_L(P)_f|_{\omega\to 0} = 4\pi\omega g^2 \int \frac{dk_z}{2\pi}\left(\frac{-2k_z^2 + k_z p_z + 2m_f^2}{4E_{q_z}E_{k_z}}\right)\frac{\partial f(E_{q_z})}{\partial E_{q_z}}\delta(E_{k_z} - E_{q_z}). \tag{3.29}$$

Further, the integral can be solved by using the properties of the Dirac delta function as

$$\delta(f(x)) = \sum_n \frac{\delta(x - x_n)}{|\frac{\partial f(x)}{\partial x}|_{x=x_n}}, \tag{3.30}$$

where x_n are the zeros of the function $f(x)$ which for the delta function in Eq. (3.28) are

$$k_{z0} = \frac{4p_z(p_z^2-\omega^2) \pm \sqrt{16p_z^2(p_z^2-\omega^2)^2 - 16(p_z^2-\omega^2)((p_z^2-\omega^2)^2 - 4m^2\omega^2)}}{8(p_z^2-\omega^2)}. \tag{3.31}$$

In the limit, $k_{z0} = p_z/2$; thus, the final form of $\delta\Im\Pi_{Lf}$ can be written as

$$\Im\delta\Pi_L(P) = \frac{\omega\beta g^2 m_f^2 I_\perp}{p_z E}(\tilde{f}(E) - \tilde{f}^2(E)), \tag{3.32}$$

where $E = \sqrt{m_f^2 + p_z^2/4}$.

3.2.3 Medium permittivity and potentials

The in-medium permittivity is a complex quantity in which the imaginary part comes from the imaginary part of the resummed gluon propagator which can be obtained by uing the relation [155]

$$\Im D^{\mu\nu}(P) = -\pi(1+e^{-\beta\omega})\xi^{\mu\nu}, \tag{3.33}$$

where $\xi^{\mu\nu}$ depends on the real and the imaginary part of the longitudinal self-energy. Here, we focus only on $D_L \equiv D^{00}$ so we write ξ^{00} as

$$\xi^{00}(P) = \frac{1}{\pi}\frac{e^{\beta\omega}}{e^{\beta\omega}-1}\rho_L(\omega, P). \tag{3.34}$$

Here ρ_L is the longitudinal part of spectral function which describes the quasiparticles with finite width. In Breight-Wigner form it is written as

$$\rho_L(P) = \frac{\Im\Pi_L}{(P^2-\Re\Pi_L)^2+\Im\Pi_L{}^2}. \tag{3.35}$$

Taking both the quark and gluon contributions into account, the real and the imaginary parts of self-energy can be written as

$$\Re\Pi_L(\omega, p) = \Re\Pi_L(\omega, p)_g + \Re\Pi_L(\omega, p)_f, \tag{3.36}$$

$$\Im\Pi_L(\omega, p) = \Im\Pi_L(\omega, p)_g + \Im\Pi_L(\omega, p)_f. \tag{3.37}$$

Here, $\Re\Pi_L$ is the real part of the longitudinal component of self-energy, which in the static limit is equal to the square of the Debye screening mass (m_D^2). Using the static limit expression for the real and the imaginary parts of the self-energy, the longitudinal gluon propagator (D^{00}) can be written as

$$D^{00}(p) = \frac{-1}{p^2+m_D^2} + \frac{i\pi T m_{Dg}^2}{p(p^2+m_D^2)^2} - \frac{i|q_fB|m_f^2\alpha_s}{2(p^2+m_D^2)^2 p_z E_{p_z}\cosh^2(\frac{\beta E_{p_z}}{2})}. \tag{3.38}$$

Note that due to the specific direction of the magnetic field the contribution of the fermion field loop makes the propagator anisotropic. However, in the limit of vanishing light quark mass the propagator remains isotropic with the effect of magnetic field showing only in the Debye mass. Thus, the dielectric permittivity can be calculated from Eq. (3.24) which in the limit of massless fermions, it becomes

$$\epsilon^{-1}(\mathbf{p}, m_D) = \frac{p^2}{p^2 + m_D^2} - i\pi T \frac{p m_{Dg}^2}{(p^2 + m_D^2)^2}. \tag{3.39}$$

From the above equation it is clear that the permittivity is isotropic in the vanishing light quark mass limit. As discussed earlier, for an effective description of quarkonium in terms of a potential at finite temperature, the mass of heavy quark , m_Q should be much larger than Λ_{QCD} as well as $m_Q \gg T$. For the magnetic field considered here, m_Q is still the largest scale ($m_Q \gg \sqrt{eB}$) i.e., the ratio, $m_Q^2/eB \simeq 3 - 15$ for the range of magnetic field $eB = 5 - 25\ m_\pi^2$, so that the quarkonium properties can still be described within the potential model framework.

Now, with the permittivity as written in Eq.(3.39), the medium effects on the quarkonia complex potential are incorporated by parametrizing the vacuum potential as

$$V(\mathbf{p}) = \frac{V(\mathbf{p})_0}{\epsilon(\mathbf{p}, m_D)}. \tag{3.40}$$

Here $V(\mathbf{p})_0$ is the vacuum potential. In the momentum space, the Coulomb part of the potential with medium effects can be written as [156]

$$k^2 V_C(\vec{p}) = 4\pi \frac{\alpha}{\epsilon(\vec{p}, m_D)}. \tag{3.41}$$

The Fourier transformation of Eq. (3.41) in coordinate space gives

$$-\nabla^2 V_C(r) + m_D^2 V_C(r) = \alpha(4\pi\delta(r) - iT m_{Dg}^2 h(m_D r)), \tag{3.42}$$

where $h(y) = 2\int_0^\infty dx \frac{x}{(x^2+1)} \frac{\sin(yx)}{yx}$. Comparing Eqs.(3.42) and (3.22), we get $n_0 = \frac{m_D^2 T}{4\pi\alpha}$. Unlike Coulomb potential, Gauss law does not does not allow a simple straightforward Fourier transform. Instead, by motivating from Eqs.(3.22) and (3.23), one can assume the validity of the linear approximation and take the similar charge density for the string potential as well [79]. Thus, the in-medium string potential can be obtained from the differential equation

$$-\frac{1}{r^2}\frac{d^2 V_S(r)}{dr^2} + \mu^4 V_S(r) = \sigma(4\pi\delta(r) - iT m_{Dg}^2 h(m_D r)), \tag{3.43}$$

where $\mu = (\frac{m_{Dg}^2 \sigma}{\alpha})^{1/4}$. Using the boundary conditions $m_D \to 0$, $\Re V_C(r) = -\frac{\alpha}{r}$ and $r \to 0$, $\Im V_C(r) = 0$ [73], one can obtain both the real and imaginary part of the Coulomb potential as

$$\Re V_C(r,T,B) = -\alpha \frac{e^{-m_D r}}{r} - \alpha m_D, \tag{3.44}$$

and

$$\Im V_C(r,T,B) = -2\alpha T g(m_D r), \tag{3.45}$$

where $g(y) = \int_0^\infty dx \frac{x}{(x^2+1)^2}\left(1 - \frac{\sin(yx)}{yx}\right)$. Thus, the magnetic field dependence of the potential arises from the field dependent Debye mass. Similarly, for the string part of the potential we use the following boundary conditions $\mu \to 0, \Re V_S(r) = \sigma r$, $r \to 0, \Im V_S(r) = 0$ and $r \to \infty, \frac{d\Im V_S(r)}{dr} = 0$. After using the boundary conditions we get both the real and imaginary parts of string potential as

$$\Re V_S(r,T,B) = -\frac{\Gamma(\frac{1}{4})}{2^{\frac{3}{4}}\sqrt{\pi}}\frac{\sigma}{\mu} D_{-\frac{1}{2}}(\sqrt{2}\mu r) + \frac{\Gamma(\frac{1}{4})}{2\Gamma(\frac{3}{4})}\frac{\sigma}{\mu}, \tag{3.46}$$

where $D_\nu(x)$ is the parabolic cylinder function, and

$$\Im V_S(r,T,B) = -\frac{\sigma m_{Dg}^2 T}{\mu}\phi(\mu r), \tag{3.47}$$

where

$$\begin{aligned}\phi(\mu r) &= D_{-\frac{1}{2}}(\sqrt{2}\mu r)\int_0^r dx \Re D_{-\frac{1}{2}}(i\sqrt{2}\mu x)x^2 g(m_D x) + \Re D_{-\frac{1}{2}}(i\sqrt{2}\mu r) \\ &\times \int_r^\infty dx D_{-\frac{1}{2}}(\sqrt{2}\mu x)x^2 g(m_D x) - D_{-\frac{1}{2}}(0)\int_0^\infty dx D_{-\frac{1}{2}}(\sqrt{2}\mu x)x^2 g(m_D x),\end{aligned} \tag{3.48}$$

The total real part of the potential after combining both the Coulombic and string parts in a magnetized medium can be written as

$$\begin{aligned}\Re V(r,T,B) &= \Re V_C(r,T,B) + \Re V_S(r,T,B) \\ &= -\alpha\frac{e^{-m_D r}}{r} - \alpha m_D - \frac{\Gamma(\frac{1}{4})}{2^{\frac{3}{4}}\sqrt{\pi}}\frac{\sigma}{\mu}D_{-\frac{1}{2}}(\sqrt{2}\mu r) + \frac{\Gamma(\frac{1}{4})}{2\Gamma(\frac{3}{4})}\frac{\sigma}{\mu}.\end{aligned} \tag{3.49}$$

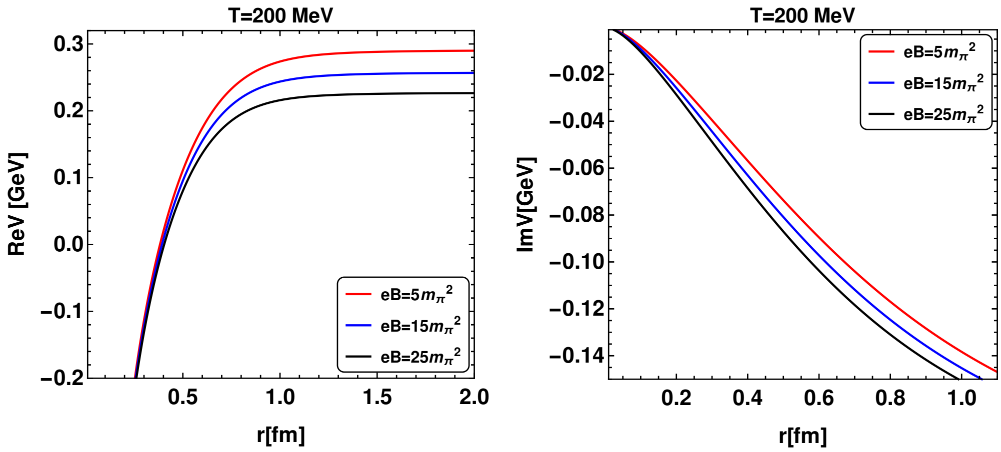

Figure 3.3: Real and imaginary parts of the potential as a function of separation r of $Q\bar{Q}$ pair for $eB = 5, 10, 15m_\pi^2$.

Similarly, the total imaginary part of the potential becomes

$$\begin{aligned} \Im V(r,T,B) &= \Im V_C(r,T,B) + \Im V_S(r,T,B) \\ &= -2\alpha T g(m_D r) - \frac{\sigma m_{Dg}^2 T}{\mu}\phi(\mu r), \end{aligned} \tag{3.50}$$

Let us note that In the framework of Debye-Hückel theory, the Coulomb and string terms were modified with different screening scales m_D and μ, respectively. Both the real as well as the imaginary parts of the potential gets significant contribution from the magnetic field as can be seen in Fig.(3.3). The left side of Fig.3.3 shows the variation of the real part of the potential with the separation distance (r) between the Q$\bar{Q}$ pair for different values of magnetic field ($eB = 5m_\pi^2,\ 15m_\pi^2,\ 25m_\pi^2$) at $T = 200$ MeV. Here, we use the value of the string tension, $\sigma = 0.174$ GeV^2 from Ref. [79] . We find that the screening increases with the increase in magnetic field. The screening is more at a higher temperature because at higher temperatures the quarkonium state is loosely bound as compared to the lower temperatures and gets easily dissociated. Alternatively, we can say that with the increase in temperature the gluonic contribution becomes more which results in more screening. Further, the right side of Fig.3.3 shows the variation of the imaginary part of the potential with the separation distance (r) for various values of magnetic field ($eB = 5m_\pi^2,\ 15m_\pi^2,\ 25m_\pi^2$) at temperatures $T = 200$ MeV. We find that the imaginary part of the potential increases in magnitude with the increase in magnetic field and hence it contributes more to the Landau damping induced thermal width obtained from the imaginary part of the potential. The increase in the magnitude of the imaginary part of the potential is more at a higher temperature for a given r.

3.3 Decay Width

The decay width (Γ) can be calculated from the imaginary part of the potential. The following formula gives a good approximation to the decay width of $Q\bar{Q}$ states [78, 157, 158]

$$\Gamma = -\int d^3\mathbf{r}\,|\psi(\mathbf{r})|^2\,\Im V(\mathbf{r}, T, B), \tag{3.51}$$

where $\psi(\mathbf{r})$ is the Coulombic wave function for the ground state and is given by

$$\psi(\mathbf{r}) = \frac{1}{\sqrt{\pi a_0^3}} e^{-r/a_0}, \tag{3.52}$$

where $a_0 = 2/(m_Q\alpha)$ is the Bohr radius of the heavy quarkonium system. We use the Coulomb-like wave functions to determine the width since the leading contribution to the potential for the deeply bound quarkonium states in a plasma is Coulombic. After substituting the expression for the imaginary part of the potential as given in Eq. (3.50), in Eq. (3.51) we estimate numerically the decay width for finite T and B. In the left of Fig. 3.4, we show the variation of the decay width for the ground states of charmonium and bottomonium at $T = 200$ MeV. Here we take charmonium and bottomonium masses as $m_c = 1.275$ GeV and $m_b = 4.66$ GeV respectively from Ref. [159]. As may be noted in Fig.(3.4), the thermal width increases with the increase in the magnetic field. The Υ width is much smaller than the J/ψ because the bottomonium states are smaller in size and larger in masses than the charmonium states and hence get dissociated at higher temperatures. The width at a higher temperature is more for both J/ψ and Υ. Alternatively, we can say that Γ increases with the increase in the magnetic field,

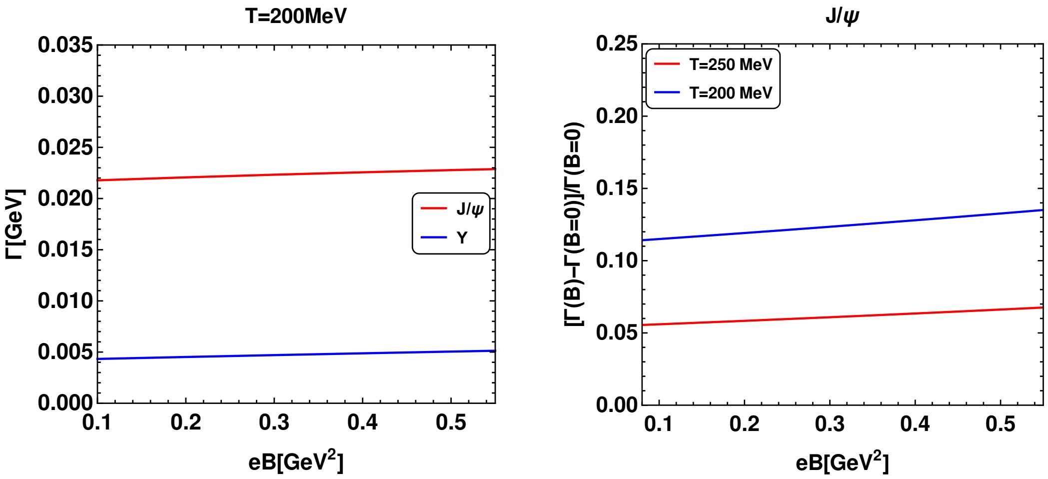

Figure 3.4: Decay width of J/ψ and Υ as a function of magnetic field at $T = 200$ MeV.

which results in the early dissociation of quarkonium states.

In the right side of Figure. 3.4, we have plotted the variation of the ratio of the decay width $[\Gamma(B = 0) - \Gamma(B = 0)/\Gamma(B = 0)]$ with magnetic field at $T = 200$ and $T = 250$ for J/ψ. From the figure it is clear that the change in decay width for $T = 200$ MeV is about 11% for $eB \simeq 5m_\pi^2$ to as large as 14% for $eB \simeq 25m_\pi^2$. For $T = 250$, the change is from 5% to 7% in the same range of magnetic field. The magnetic field effects become weaker at a high temperature as compared to a low temperature. Also, we are considering the strong field LLL approximation, i.e., $eB \gg T^2$. This approximation may not hold good at a high temperature.

3.4 Summary

The magnetic field effect on the heavy quark complex potential is discussed in the LLL approximation of the strong field limit. The LLL approximation is reasonable as quarkonia are produced during the initial stages of collision when the magnetic field is very high. Further, the higher Landau levels are at infinity as compared to LLL, and the dimensional reduction takes place. As discussed, in the QGP medium, this situation can arise at finite electrical conductivity. In order to incorporate the medium effects in the quarkonia potential, the gluon self-energy and the Debye screening mass in a magnetized thermal medium are estimated using the ITF and Schwinger propagator. It is found that the Debye mass increases with an increase in the magnetic field. However, at sufficiently high temperatures, the magnetic field dependence of the screening mass is somewhat weak. Further, the in-medium permittivity is estimated using the resummed gluon propagator that gets contributions from quark as well as gluon loops. The magnetic field brings an anisotropic contribution to the gluon propagator which, however, vanishes in the massless quark limit. Therefore, the potential remains isotropic even in the presence of the magnetic field.

The heavy quark complex potential is obtained by bringing together the generalized Gauss law with the characterization of in-medium effects, i.e., finite temperature and magnetic field, through the dielectric permittivity. Because of the heavy quark mass (m_Q), the requirement $m_Q \gg T$ and $m_Q \gg \sqrt{eB}$ is satisfied for the range of magnetic field $eB = 5 - 25\ m_\pi^2$. The real part of the potential decreases with an increase in the magnetic field and becomes more screened. The screening also increases with the increase in temperature. Since the $Q\bar{Q}$ potential is effectively more screened in the presence of a magnetic field, which results in the earlier dissociation of quarkonium states in a strongly magnetized hot QGP medium. The imaginary part of the potential increases in magnitude with the increase in magnetic field and temperature. As a result, the quarkonium states (J/ψ and Υ) get more broadened with the increase in the magnetic field and results in the earlier dissociation of quarkonium states in the presence of the magnetic field. The width for Υ is much smaller than the J/ψ because bottomonium states are tighter than the charmonium state and hence get dissociated at a higher temperature. The change in decay width from (11-14)% at $T = 200$ MeV and from (5- 7)% at $T = 250$, for the magnetic field ranging from (5-25) m_π^2. The magnetic field effects become very low at a high temperature; this may be because the LLL approximation, i.e., $eB \gg T^2$, may not be a good approximation at a high temperature. Combining both the effects of screening and the broadening due to damping, one can expect a lesser binding of a $Q\bar{Q}$ pair in a strongly magnetized hot QGP medium. To continue the HQ description in a magnetized thermal medium, we discuss the magnetic field contribution to the collisional energy loss within the weak coupling and strong field limit.

CHAPTER 4

Collisional energy loss of HQ

It is well known that a high energy particle created in the initial stages of the heavy ion collision loses its energy in the medium by interacting with the medium partons. This leads to the phenomena of jet quenching, which as anticipated many years ago, is one of the prominent probes of QGP [160, 161, 162, 163]. Generally, there are two types of processes that contribute to the energy loss namely; radiative process [164, 165, 166] and collisional process[88, 89, 90]. Experimental results for quenching of heavy flavors[167] were suggestive of including both radiative as well as collisional energy loss that has been discussed in Ref.[89, 168]. In this chapter, we focus our attention to the collisional energy loss of HQ in the background of a constant magnetic field which is relevant for the HICs [168, 169, 170, 171, 172].

The initial dynamics of the system of deconfined matter plays a pivotal role in deciding the longevity of the magnetic field in the HICs. It can be hypothesized that the magnetic field can induce an amount of electrical conductivity which becomes adequate enough for the decaying magnetic field to persist [130, 68, 173, 174]. This in turn can induce a current which opposes the rate of decrease of the magnetic field as per Lenz's Law [175, 176, 129]. Therefore, it is imperative that the external magnetic field persists long enough so that it can impart crucial effects on various properties of the medium. It is instructive to investigate the effect of this field on the space-time evolution of the medium. In this regard, some studies are trying to see this effect by reconstructing Hydrodynamic evolution in presence of magnetic field, i.e. Magneto hydrodynamics [177, 178, 131].

In the case of QGP, a more realistic approach of estimation of the magnetic field and its relaxation time must include the medium effects i.e., electrical conductivity (σ) of the medium. The phenomenological models that are used to describe QGP evolution show that the strongly interaction system in HICs is thermalised just after the collision ($\tau \sim 0.5$fm) where magnetic field is near its maximum value [179, 68]. Further, in a conducting medium, magnetic field satisfies a diffusion equation with diffusion coefficient $(\sigma\mu)^{-1}$, where μ is the magnetic permeability. With this one finds that the time scale over which magnetic field remain reasonably strong over a length scale L is $\tau = L^2\sigma/4$ [67]. For the electrical conductivity $\sigma \simeq 0.04$T from Ref.[180] at $T = 200$ MeV, the electrical conductivity $\sigma = 8$MeV. This leads to the relaxation time $\tau \sim 1$ fm for a system size of the order of 10 fm. Moreover, this also suggest that the magnetic field is a slowly varying function of time and can remain reasonably strong for a longer period of time compared to the case of without a medium. For higher temperatures σ will be higher [70] increasing the value of τ. Further, it is shown in Ref.[68] in an expanding medium the magnetic field remain somewhat constant for a longer time.

Consequently, it is of utmost importance to explore to what extent the magnetic field inside QGP affects different observables of the deconfined matter. To this end, surveying the in-medium properties of heavy quarks [141, 142, 143] and quarkonia have become quite relevant in the context of magnetic field [181, 182, 81, 135, 136, 137, 132, 138, 140, 183, 184, 185, 186]. However, since the HQs are moving in real time inside the QGP, understanding and estimating the dynamical properties of HQs are also necessary. In this context, transport coefficients like drag and diffusion of HQ have been estimated in presence of a strong external magnetic field in some of the recent literatures [144, 187]. AdS/CFT has also been employed to have an estimation of the drag force of HQ[188]. Most of the calculations with strong magnetic field have been performed using perturbative QCD (pQCD) techniques in Leading Order (LO) of the strong coupling α_s in the limit $M \gg \sqrt{eB}$ so that the motion of the HQ is not directly affected by the external magnetic field. Nonetheless, the light quarks/anti-quarks are affected by the magnetic field with the gluons remaining unaffected. The thermally equilibrated light quarks are Landau quantized. The magnetic field also affects the gluon self energy through the quark loop. Further they also affect the HQ light thermal parton scattering cross-sections.

This chapter intends to estimate the HQ collisional energy loss ($-dE/dx$) in the low coupling regime and strong magnetic field. Specifically we will consider the hierarchy in the scales i.e., $\sqrt{\alpha_s eB} \ll T \ll \sqrt{eB}$ and $\sqrt{eB} \ll M$. To do so, we first discuss the resummed gluon propagator in the strong magnetic field background in the RTF. As also discussed in chapter3, in the LLL approximation, only quark loop contributes to the resummed gluon propagator in the limit $eB \gg T^2$. This resummed propagator is used to estimate the collisional energy loss. In this hierarchy of scales, two types of processes (t-channel scatterings) that contribute to the scatterings of HQ with the light thermal partons affecting the HQ energy loss. As we shall see, the collisional energy loss increases with the magnetic field and for a given magnetic field, the field dependent contribution to the collisional energy loss could be similar in magnitude to the collisional energy loss in the absence of magnetic field.

This chapter is organized as follows. In Sec.4.1, we standardize the mathematical notations used for the real-time formalism which will also be used in chapter5. Further, in the real-time formalism of thermal field theory, we discuss the fermion propagator in Sec.4.2 and resummed gluon propagator in Sec.4.2.1 in the LLL approximation . In Sec.6.1, we discuss the formalism to calculate HQ energy loss i.e., $-dE/dx$ with descriptions of both the cases; (a) when HQ is interacting with light quarks (Sec.4.3.1) and (b) HQ scattering with the thermal gluons (Sec.4.3.2). Results for energy loss are presented in Sec.7.3 with the relevant plots and the possible explanation. In Sec.7.4, the results/outcome are summarized.

4.1 Set-up

For the present investigation, we assume here that the magnetic field is constant and is along the $\hat{z}$ direction i.e., $\vec{B} = B\hat{z}$. In the subsequent subsection, we shall discuss the quark propagator in the real-time formalism of thermal field theory and in the presence of such a magnetic field. For this purpose we use the following notation. The notations $\|$ and $\perp$ represents the components parallel and perpendicular to the magnetic field of the corresponding quantities. For the metric tensor, we use

$$g^{\parallel}_{\mu\nu} = (1, 0, 0, -1) \qquad g^{\perp}_{\mu\nu} = (0, -1, -1, 0). \tag{4.1}$$

The parallel (i.e., $a^{\parallel}_{\mu} = g^{\parallel}_{\mu\nu} a^{\nu}$) and perpendicular (i.e., $a^{\perp}_{\mu} = g^{\perp}_{\mu\nu} a^{\nu}$) components of a four-vector a_μ are represented as

$$a^{\parallel}_{\mu} = (a_0, 0, 0, -a_3) \qquad a^{\perp}_{\mu} = (0, -a_1, -a_2, 0). \tag{4.2}$$

The four-vector product ($a^\mu b_\mu = a \cdot b$) can be written as

$$a \cdot b = a_{\parallel} \cdot b_{\parallel} - a_{\perp} \cdot b_{\perp}. \tag{4.3}$$

Similarly, both the components of square of a four-vector is

$$a^2_{\parallel} = a^2_0 - a^2_3 \qquad a^2_{\perp} = a^2_1 + a^2_2. \tag{4.4}$$

4.2 Fermion propagator in LLL in RTF

The retarded and advanced propagators (S_R, S_A) of a free quark of electric charge q_f and mass m in the presence of magnetic field B can be given as [189]

$$S_{R/A}(K) = \sum_{n=0}^{\infty} \left[\frac{i\Xi_n(K)}{K^2 - m^2} \right]_{k_0 \to k_0 \pm i\epsilon}, \tag{4.5}$$

where the retarded (R)/advanced (A) corresponds to $+i\epsilon / -i\epsilon$. The sum is over all the Landau levels (LLs) that is represented by n. Four momentum squared $K^2 = k_0^2 - k_z^2 - 2n|q_f B|$. All LLs except the lowest ($n = 0$) are doubly degenerate. The numerator of Eq.(4.5) has the Dirac structure of form [189]

$$\Xi_n(K) = (\not{k}_{\parallel} + m)[\mathcal{P}_+ \Theta_n(\zeta) + \mathcal{P}_- \Theta_{n-1}(\zeta)] + \not{k}_{\perp} \Phi_{n-1}(\zeta), \tag{4.6}$$

where $\zeta = 2\frac{k_\perp^2}{|q_f B|}$ and

$$\Theta_l(\zeta) = 2e^{-\frac{\zeta}{2}}(-1)^l L_l(\zeta), \tag{4.7}$$

$$\Phi_l(\zeta) = 4e^{-\frac{\zeta}{2}}(-1)^{l-1}L_{l-1}^1(\zeta). \tag{4.8}$$

$L_l(\zeta)$ and $L_l^1(\zeta)$ are associated Laguerre Polynomials. In Eq.(4.5), the projection operator ($\mathcal{P}_\pm$) that projects the spin in the direction of magnetic field is defined as $\mathcal{P}_\pm = (1 \pm sgn(q_f B)i\gamma^1\gamma^2)/2$. Note here that the projection operator depends on the electric charge of the quark as the spin magnetic moment depends on the charge of the quark. In the limit $\sqrt{eB} \gg T, m$, only LLL is relevant and the dynamics of light quark is governed by the magnetic field. In this approximation (LLL) the associated Laguerre Polynomials $L_{-1}(\zeta) = 0$ and $L_0(\zeta) = 1$, so that Eq.(4.5) reduces to

$$S_{R/A}(K) = i\exp\left(-\frac{k_\perp^2}{|q_f B|}\right)\frac{2(\not{k}_\parallel + m)\mathcal{P}_+}{k_\parallel^2 - m^2 \pm i\epsilon k_0}. \tag{4.9}$$

As already mentioned in Eq.(4.26), Feynman propagator can be obtained by using the relation

$$\begin{aligned} S_F(K) &= \left(\frac{1}{2} - \tilde{f}(k_0)\right)\Big[S_R(K) - S_A(K)\Big] \\ &\equiv \left(\frac{1}{2} - \tilde{f}(k_0)\right)\rho_F(K), \end{aligned} \tag{4.10}$$

where $\tilde{f}(k_0)$ is Fermi-Dirac distribution function and $\rho_F(K)$ is quark spectral density. From Eq.(4.9), it is clear that in the limit $k_\perp^2 \ll q_f B$, the motion of a quark is restricted in the transverse directions and allowed only in the direction parallel to the magnetic field. It can also be observed that as earlier for the infrared limit, i.e., $m^2, T^2, k_\perp^2, k_0^2 \ll eB$, the dimensional reduction from 3+1-dimension to 1+1-dimension takes place. This dimensional reduction in the LLL approximation suggests that the pairing dynamics of quarks occur in 1+1 dimension, and spontaneous chiral symmetry breaking occurs even at weak interaction between quarks in 3+1 dimension [190].

4.2.1 Resummed gluon propagator in LLL

Next we consider the resummed retarded/advanced gluon propagator in the presence of magnetic field within the LLL approximation. The resummed propagator is obtained by inserting the self energy corrections in the bare propagator and can be written as

$$D^{R/A}_{\mu\nu}(K) = [(D^{R/A}_{\mu\nu}(K))^{-1}_0 + \Pi^{R/A}(K)_{\mu\nu}]^{-1}, \tag{4.11}$$

where the bare gluon propagator $(D^{R/A}_{\mu\nu}(K))_0$ in covariant gauge is given as

$$(D^{R/A}_{\mu\nu}(K))_0 = -\frac{P_{\mu\nu}(K)}{(k_0 \pm i\epsilon)^2 - k^2} + \xi \frac{K_\mu K_\nu}{((k_0 \pm i\epsilon)^2 - k^2)^2}. \tag{4.12}$$

In Eq.(4.12), the projection operator ($P_{\mu\nu}(K)$ is defined as

$$P_{\mu\nu}(K) = -g_{\mu\nu} + \frac{K_\mu K_\nu}{(k_0 \pm i\epsilon)^2 - k^2}, \tag{4.13}$$

and ξ is the gauge parameter. The retarded/advanced resummed gluon propagator depends on the retarded/advanced gluon self energy that, in general, can get contribution from both the gluon loop and the quark loop. The magnetic field does not affect the contribution from the gluon loop. However, the magnetic field modifies the quark loop contribution. The leading contribution from the gluon loop to the self energy at finite temperature T is proportional to g^2T^2 while we shall see that the leading contribution from the quark loop at finite T, B is proportional to $g^2|q_fB|$ as given in Eq.(A.12). Since we work in the limit $eB \gg T^2, m^2$, we shall drop the gluon loop contribution and keep quark loop contribution in the retarded/advanced gluon self energies. Taking the magnetic field in the the $\hat{z}$ direction, the most general form of gluon self energy at finite T and B can be written in terms of seven independent tensors as

$$\Pi^{R/A}_{\mu\nu}(K) = \sum_{j=\|,\perp,T,L} \Pi^{R/A}(K)_j P^j_{\mu\nu}(K) + \Pi_P \frac{K_\mu K_\nu}{K^2} + \Pi_n n_\mu n_\nu + \Pi_b b_\mu b_\nu, \tag{4.14}$$

where $L, T, \|, \perp$ respectively are for longitudinal, transverse, parallel and perpendicular components of the gluon self energy. The four-vectors $n^\mu = (1, \mathbf{0})$ and $b^\mu = (0, 0, 0, -1)$, break Lorentz and rotational symmetry due to thermal medium and the magnetic field respectively. Further, the projection operators are transverse to the momentum i.e., $P_\mu P^{\mu\nu}_j = 0$. It turns out that only the four projection tensors contribute to the retarded/advanced self energies in the leading order.

Explicitly these projection operators are given as

$$P^T_{\mu\nu}(K) = -g_{\mu\nu} + \frac{k_0}{k^2}\Big[K_\mu n_\nu + n_\mu K_\nu\Big] - \frac{1}{k^2}\Big[K_\mu K_\nu + K^2 n_\mu n_\nu\Big], \tag{4.15}$$

$$P^L_{\mu\nu}(K) = -\frac{k_0}{k^2}\Big[K_\mu n_\nu + n_\mu K_\nu\Big] + \frac{1}{k^2}\Big[\frac{k_0^2}{K^2}K_\mu K_\nu + K^2 n_\mu n_\nu\Big], \tag{4.16}$$

$$P^{\parallel}_{\mu\nu}(k) = -g^{\parallel}_{\mu\nu} + \frac{k^{\parallel}_\mu k^{\parallel}_\nu}{k^2_{\parallel}}, \tag{4.17}$$

$$P^{\perp}_{\mu\nu}(k) = -g^{\perp}_{\mu\nu} + \frac{k^{\perp}_\mu k^{\perp}_\nu}{k^2_{\perp}}. \tag{4.18}$$

The parallel and perpendicular components of self energy comes from the quark loop while the longitudinal and transverse components are from the gluon loop. Taking contribution from both quark and gluon loop the resummed retarded gluon propagator is given as [191]

$$\begin{aligned} D^R_{\mu\nu}(K) &= -\frac{1}{\Delta(K)}\Big[(K^2 - \Pi^{\parallel}_R(K) - \Pi^L_R(K))P^T_{\mu\nu}(K) + (K^2 - \Pi^{\parallel}_R(K) - \Pi^L_R(K)) \\ &\times P^L_{\mu\nu}(K) + \Pi^{\parallel}_R(K)P^{\parallel}_{\mu\nu}(K) + D_\perp(K)P^{\perp}_{\mu\nu}(K)\Big] + \xi\frac{K_\mu K_\nu}{(K^2)^2}, \end{aligned} \tag{4.19}$$

where

$$\begin{aligned} \Delta(K) &= (K^2 - \Pi^T_R(K))(K^2 - \Pi^L_R(K)) - \Pi^{\parallel}_R(K)\Big[K^2 - a\Pi^T_R(K)\frac{K^2}{k^2_{\parallel}} \\ &- \Pi^L_R(K)(1-a)\frac{k_0^2}{k^2_{\parallel}}\Big], \end{aligned} \tag{4.20}$$

and

$$\begin{aligned} D_\perp(K) &= \frac{1}{K^2 - \Pi^T_R(K) - \Pi^L_R(K)}\Big[\Pi_{\parallel}(K)(\Pi^L_R(K) - \Pi^T_R(K))(1-a)\frac{k_0^2}{k^2_{\parallel}} \\ &+ \Pi^{\perp}_R(K)(K^2 - \Pi^L_R(K) - \Pi^{\parallel}_R(K))\Big], \end{aligned} \tag{4.21}$$

and $a = k_3^2/k^2$. In the LLL approximation for the propagator as in Eq.(4.9) lead to $\Pi_\perp = 0$. This is due to the fact that there is no current in the transverse direction in LLL approximation. As already mentioned, the gluon loop contribution to the gluon self energy is of the order of $\alpha_s T^2$ which can be dropped with respect to the quark loop contribution which is of the order of $\alpha_s eB$. In this approximation, the resummed retarded gluon propagator becomes

$$D^R_{\mu\nu}(K) = -\frac{1}{\Delta}[(K^2 - \Pi^{\parallel}_R)(P^T_{\mu\nu} + P^L_{\mu\nu}) + \Pi^{\parallel}_R P^{\parallel}_{\mu\nu} + D_\perp(K)P^{\perp}_{\mu\nu}] + \xi\frac{K_\mu K_\nu}{(K^2)^2}, \quad (4.22)$$

where

$$P^L_{\mu\nu} + P^T_{\mu\nu} = -g_{\mu\nu} + \frac{q_\mu q_\nu}{q^2}. \quad (4.23)$$

Since $D_\perp(K) \sim \alpha_s^2 eBT^2 \ll \Pi_\parallel \sim \alpha_s eB$, the third term in Eq.(4.22) may be dropped. Further as may be observed from Eq.(4.20) $\Delta \approx K^2(K^2 - \Pi_\parallel(K))$ with similar argument. Thus Eq.(4.22), taking appropriate $i\epsilon$ factors into account, can be approximated as

$$D^R_{\mu\nu}(K) = -\frac{P_{\mu\nu}(K)}{(k_0 + i\epsilon)^2 - k^2} - \frac{\Pi^{\parallel}_R(k_0 + i\epsilon, \mathbf{k})P^{\parallel}_{\mu\nu}(K)}{K^2(K^2 - \Pi^{\parallel}_R(k_0 + i\epsilon, \mathbf{k}))} + \xi\frac{K_\mu K_\nu}{((k_0 + i\epsilon)^2 - k^2)^2}. \quad (4.24)$$

Similarly, the resummed advanced and Feynman gluon propagators can be written as

$$D^A_{\mu\nu}(K) = -\frac{P_{\mu\nu}(K)}{(k_0 - i\epsilon)^2 - k^2} - \frac{\Pi^{\parallel}_A(k_0 - i\epsilon, \mathbf{k})P^{\parallel}_{\mu\nu}(K)}{K^2(K^2 - \Pi^{\parallel}_A(k_0 - i\epsilon, \mathbf{k}))} + \xi\frac{K_\mu K_\nu}{((k_0 - i\epsilon)^2 - k^2)^2}, \quad (4.25)$$

$$D^F_{\mu\nu}(K) = (1 + 2f(k_0))\Big[D^R_{\mu\nu}(K) - D^A_{\mu\nu}(K)\Big]. \quad (4.26)$$

We shall use Eqs.(4.24), (4.25) and (4.26) to estimate the HQ energy loss.

4.3 Formalism

Consider a HQ of mass M, moving in a magnetized thermal medium of light quarks/anti-quarks and gluons, with momentum $\mathbf{p}$ and energy $E = \sqrt{\mathbf{p}^2 + M^2}$.

The rate of energy loss of a heavy fermion moving with velocity $\mathbf{v}$ in a thermal medium has been considered earlier in Ref. [88, 89] for QED plasma and for QGP in Ref. [90]. In general the energy loss of the heavy fermion is given by

$$-\frac{dE}{dx}=\frac{1}{v}\int_{M}^{\infty}dE'(E-E')\frac{d\Gamma}{dE'}, \tag{4.27}$$

where Γ is the interaction rate of heavy fermion with the medium particles. For the collisional energy loss, we confine our attention to $2\to 2$ processes only as has been considered earlier [90] . For large momentum of HQ, however, the energy loss by radiative processes will also be important. In general, for the case of HQ moving in a QGP medium of light partons there can be two types of scatterings namely the Coulomb scattering i.e., $Qq\to Qq$ and Compton scattering i.e., $Qg\to Qg$. As mentioned, we shall consider the limit $M\gg\sqrt{eB}\gg T$ so that HQ is not directly affected by the magnetic field and the light quarks are populated only in LLL. In the following sections we shall calculate the interaction rate and subsequently estimate the energy loss of the HQ.

4.3.1 Energy loss due to scattering with light quark: $Qq\to Qq$

The interaction rate Γ of the HQ is related to imaginary part of its retarded self energy in the medium [118]

$$\Gamma(E)=-\frac{1}{2E}(1-\tilde{f}(E))Tr\Big[(\not{P}+M)\Im\Sigma_R(P)\Big], \tag{4.28}$$

where $\tilde{f}(E)$ is Fermi-Dirac distribution function and $\Sigma_R(P)$ is the retarded self energy of HQ as shown in Fig.(4.1). In this figure, the bold solid line refers to HQ while the curly line corresponds to gluon. The black blob here shows the gluon resummed propagator in the presence of a magnetic field background. Let us note, in the LLL, the contribution to the resummed gluon propagator comes from the quark loop only.

In the RTF, similar to the retarded propagator as in Eq.(2.28), the retarded

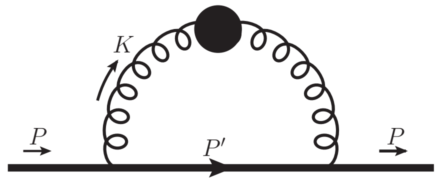

Figure 4.1: Feynman diagram for heavy quark self energy. The black blob here shows the gluon resummed propagator in the presence of a magnetic field background.

self energy can be written in terms of 11 and 12 components of self energy as

$$\Sigma_R(P) = \Sigma_{11}(P) - \Sigma_{12}(P). \tag{4.29}$$

Using the propagators for quark and gluon in the Keldysh basis the retarded self energy of HQ can be written as

$$\Sigma_R(P) = ig^2(t_a t_b)\int \frac{d^4K}{(2\pi)^4}\Big[D^{\mu\nu}_{11}(K)\gamma_\nu S_{11}(P')\gamma_\mu - D^{\mu\nu}_{12}(K)\gamma_\nu S_{12}(P')\gamma_\mu\Big]. \tag{4.30}$$

The HQ propagators are $S_{11}(K) = (\not{K}+M)\Delta_{11}(K)$ and $S_{12}(K) = (\not{K}+M)\Delta_{12}(K)$ where $\Delta_{11}(K)$ and $\Delta_{12}(K)$ are given as

$$\Delta_{11}(K) = \frac{1}{K^2 - M^2 + i\epsilon} + 2\pi i\tilde{f}(k_0)\delta(K^2 - M^2), \tag{4.31}$$

and

$$\Delta_{12}(K) = 2\pi i\tilde{f}(k_0)\delta(K^2 - M^2). \tag{4.32}$$

Here, $\tilde{f}(k_0)$ is the fermion distribution function of the HQ. With these simplifications, Eq.(4.30) becomes

$$\begin{aligned}\Sigma_R(P) &= ig^2(t_a t_b)\int \frac{d^4K}{(2\pi)^4}\Big[D^{\mu\nu}_{11}(K)\gamma_\nu(\not{P}' + M)\gamma_\mu\Delta_{11}(P') \\ &- D^{\mu\nu}_{12}(K)\gamma_\nu(\not{P}' + M)\gamma_\mu\Delta_{12}(P')\gamma_\mu\Big].\end{aligned} \tag{4.33}$$

It is easier for the evaluation of the retarded self energy to convert the Keldysh propagators to the RA basis using the relations similar to as given in Eqs.(2.28) and (2.29) for the propagators $D^{\mu\nu}_{ab}$ and Δ_{ab}. Let us note that in Eq.(4.33), the propagators $D^{\mu\nu}_{11}$ and $D^{\mu\nu}_{12}$ are resummed gluon propagators and S_{11}, S_{12} for the HQ and hence the corresponding Δ_{11}, Δ_{12} are bare propagators. Eq.(4.33) for the retarded self energy then can be rewritten as

$$\begin{aligned}\Sigma_R(P) &= \frac{ig^2(t_at_b)}{8}\int\frac{d^4K}{(2\pi)^4}\Big[D^{\mu\nu}_F(K)\lambda_{\mu\nu}\Delta_R(P') + D^{\mu\nu}_A(K)\lambda_{\mu\nu}\Delta_R(P') \\ &+ D^{\mu\nu}_R(K)\lambda_{\mu\nu}\Delta_F(P') + D^{\mu\nu}_R(K)\lambda_{\mu\nu}\Delta_A(P')\Big],\end{aligned} \tag{4.34}$$

where $\lambda_{\mu\nu} = \gamma_\mu(\not{P}'+M)\gamma_\nu$. The leading contribution to the self energy comes from the gluon propagator arising in the soft momentum transfer limit i.e., $|\mathbf{k}| \sim g\sqrt{eB}$. In the limit $E \gg \sqrt{eB} \gg T \gg |\mathbf{k}|$, out of the four terms in Eq.(4.34) only the first term becomes dominant. This is because $D^{\mu\nu}_F$ involves gluonic distribution function. Thus Eq.(4.34) reduces to

$$\begin{aligned}\Sigma_R(P) &= \frac{ig^2(t_at_b)}{8}\int\frac{d^4K}{(2\pi)^4}\Big[D^{00}_F\gamma_0(\not{P}'+M)\gamma_0 + 2D^{0i}_F\gamma_0(\not{P}'+M)\gamma_i + D^{ij}_F\gamma_i(\not{P}' \\ &+ M)\gamma_j\Big]\Delta_R(P').\end{aligned} \tag{4.35}$$

Using Eqs.(4.24),(4.25) and (4.26) in the Eqs.(4.28) and (4.34), the interaction rate of HQ can be given as

$$\begin{aligned}\Gamma(E) &= \frac{g^2}{8E}(1-\tilde{f}(E))\int\frac{d^4K}{(2\pi)^4}(1+2f(k_0))Tr\Big[(\not{P}+M)\gamma_0(\not{P}'+M)\gamma_0P^{00}_{\parallel} \\ &+ 2(\not{P}+M)\gamma_0(\not{P}'+M)\gamma_iP^{0j}_{\parallel} + (\not{P}+M)\gamma_i(\not{P}'+M)\gamma_jP^{ij}_{\parallel}\Big]\rho_L \\ &\times \Im(\Delta_R(P')),\end{aligned} \tag{4.36}$$

where

$$\rho_L = \frac{2\Im\Pi^{\parallel}_R(K)}{(K^2-\Re\Pi^{\parallel}_R(K))^2 + (\Im\Pi^{\parallel}_R(K))^2}. \tag{4.37}$$

In the above equation, $\Im\Pi^R_{\parallel}(K)$ and $\Re\Pi^R_{\parallel}(K)$ respectively are the imaginary and the real parts of retarded gluon self energy as defined in Eqs.(A.12) and (A.13). Further, let us note that the imaginary part in the retarded self energy of HQ comes from the propagator $\Delta_R(P')$ which can be written as

$$\Im(\Delta(P')) = -\frac{\pi}{2E'}\bigg(\delta(E-k_0-E')+\delta(E-k_0+E')\bigg). \tag{4.38}$$

The second delta function in Eq.(4.38) does not contribution due to kinematic reasons ($k_0 \ll M$). Therefore, we drop this term and continue with the first delta function. Thus, the interaction rate becomes

$$\begin{aligned}
\Gamma(E) &= -\frac{g^2}{8E}(1-\tilde{f}(E))\int\frac{d^4K}{(2\pi)^4}(1+2f(k_0))\bigg[(4EE'+4p^2-4\mathbf{p}\cdot\mathbf{k}+4M^2)k_z^2 \\
&+ 8(E(\mathbf{p'}\cdot\mathbf{k})+E'(\mathbf{p}\cdot\mathbf{k'}))k_0+4(\mathbf{p}\cdot(\mathbf{p}-\mathbf{k})+EE'-M^2)k_0^2\bigg] \\
&\times \frac{\rho_L\pi}{2E'k_\parallel^2}\delta(E-k_0-E').
\end{aligned} \tag{4.39}$$

Since we are working in the limit where $|\mathbf{k}| \sim g\sqrt{eB} \ll T$ so in this limit $E \gg |\mathbf{k}|$ and one can write $E' = \sqrt{(\mathbf{p}'^2+m^2)} \equiv E - \mathbf{v}\cdot\mathbf{k}$. The delta function in the above equation can be simplified as $\delta(E-k_0+E') \sim \delta(k_0-\mathbf{v}\cdot\mathbf{k})$. Further, we assume that HQ moves parallel to the magnetic field. The integration over azimuthal angle in Eq.(4.39) can be done trivially and the integration over the polar angle can be done by using the energy delta function. The energy loss is thus obtained as

$$\begin{aligned}
-\frac{dE}{dx}\bigg|_{Qq\to Qq} &= -\frac{g^2}{2E}(1-\tilde{f}(E))\int_0^\infty\frac{kdk}{(2\pi)^2}\int_{-kv}^{kv}\frac{k_0dk_0}{2\pi}(1+2f(k_0))\bigg[4(2E^2 \\
&- 2Ek_0)k_0^2k_0-4v^2(2E^2-Ek^2)k_0+4v^2(2E^2-2M^22Ek_0)k_0^2\bigg] \\
&\times \frac{\rho_L\pi}{2Ek_0^2(v^2-1)}.
\end{aligned} \tag{4.40}$$

In the above equation we have used $1/E \approx 1/E'$ as the momentum of the gluon is soft. The magnetic field dependence in the energy loss for $Qq \to Qq$ scattering comes through ρ_L as defined in Eq.(4.37) which depends on the real and the imaginary parts of retarded self energy of gluon.

4.3.2 HQ gluon Scattering: $Qg \to Qg$

The other contribution to the HQ energy loss comes from the scattering of the gluons off the the HQ i.e., $Q(P) + g(K) \to Q(P') + g(K')$ as shown in Fig.(4.2). The interaction rate for HQ and gluon scattering is given as

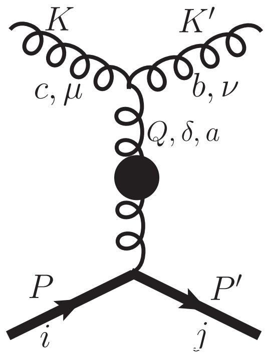

Figure 4.2: Feynman diagram for heavy quark and gluon scattering. In the strong magnetic field limit the contribution to the resummed gluon propagator comes from the quark loop only.

$$\begin{aligned}\Gamma(E) &= \frac{1}{2E}\int\frac{d\mathbf{p}'}{(2\pi)^3 2E'}\int\frac{d\mathbf{k}}{(2\pi)^3 2k}f(k)\int\frac{d\mathbf{k}'}{(2\pi)^3 2k'}(1+f(k')) \\ &\times \ (2\pi)^4\delta^4(P+K-P'-K')|\bar{\mathcal{M}}|^2, \end{aligned} \tag{4.41}$$

where $|\bar{\mathcal{M}}|^2$ is the matrix element squared averaged over initial spin and color degrees of freedom and summed over final spin and color for the $Qg \to Qg$ scattering and $f(k)$ is the gluonic thermal distribution function. Generally, there are three types of processes i.e., through s, t and u channels that can contribute to the total scattering amplitude for this process. However, we are considering the strong magnetic field limit (LLL approximation) i.e., $M \gg \sqrt{eB} \gg T$ and assume that the effect of the magnetic field on HQ is suppressed due to its large mass so that the s and the u channels, where HQ propagator arises, does not give any additional contribution arising from the magnetic field. Therefore, the only contribution to Eq.(4.41) comes from the t-channel scattering as shown in Fig.(4.2). Let us note that as mentioned earlier the resummed gluon propagator has thermal contribution ($\sim \alpha_s T^2$) from gluon loop and the magnetic field contribution

($\sim \alpha_s eB$) from quark loop in the gluon self energy. In LLL approximation, the thermal contributions are negligible as compared with that of the magnetic field. Consequently, we shall use the resummed gluon propagator as given in Eq.(4.24). The $t-$channel scattering amplitude can be written as

$$\mathcal{M} = -ig^2 f_{acb} t^a_{ji} [\bar{u}_j(P')\gamma^\alpha u_i(P)] D^R_{\delta\alpha}(Q) C^{\delta\mu\nu}(Q,K,-K')\epsilon_\mu(K)\epsilon^*_\nu(K'), \quad (4.42)$$

where $Q = P - P' = K' - K$ is four-momentum vector for the exchanged gluon and we have kept explicitly the color indices as in Fig.(4.2). The resulting matrix element squared can be written after performing the color and spin sum over the final state and averaging over the initial state as

$$\begin{aligned}
|\bar{\mathcal{M}}|^2 &= \frac{1}{4} g^4 C_F Tr[(\not{P}' + M)\gamma^\alpha(\not{P} + M)\gamma^{\alpha'}] D^R_{\delta\alpha}(Q) D^R_{\delta'\alpha'}(Q) C^{\delta\mu\nu}(Q,K,K') \\
&\times C^{\delta'\mu'\nu'}(Q,K,K') \sum \epsilon_\mu(K)\epsilon_{\mu'}(K) \sum \epsilon_\nu(K')\epsilon_{\nu'}(K') \\
&= \frac{1}{4} g^4 C_F Tr[(\not{P}' + M)\gamma^\alpha(\not{P} + M)\gamma^{\alpha'}] D^R_{\delta\alpha}(Q) D^R_{\delta'\alpha'}(Q) \\
&\times C^{\delta\mu\nu}(Q,K,-K') C^{\delta'}_{\mu\nu}(Q,K,-K'), \qquad (4.43)
\end{aligned}$$

where $C_F = 1/2$ is the color factor and $C^{\mu\nu\alpha}(P,Q,R) = (P-Q)^\alpha g^{\mu\nu} + (Q-R)^\mu g^{\nu\alpha} + (R-P)^\nu g^{\mu\alpha}$. To further simplify Eq.(4.43), we will use the transversality condition $\epsilon(K)\cdot K = \epsilon(K')\cdot K' = 0$ for the gluons to obtain

$$\begin{aligned}
C^{\delta\mu\nu}(Q,K,-K') &= -2g^{\delta\mu}K^\nu + g^{\mu\nu}(K+K')^\delta - 2g^{\nu\delta}K'^\mu \\
C^{\delta'}_{\mu\nu}(Q,K,-K') &= -2g^{\delta'}_\mu K_\nu + g_{\mu\nu}(K+K')^{\delta'} - 2g^{\delta'}_\nu K'_\mu, \qquad (4.44)
\end{aligned}$$

so that,

$$C^{\delta\mu\nu}(Q,K,-K') C^{\delta'}_{\mu\nu}(Q,K,-K') = 4(K^\delta K'^{\delta'} + K'^\delta K^{\delta'}). \qquad (4.45)$$

The product of propagators that appear in Eq.(4.43) can be simplified to

$$\begin{aligned}
D^R_{\delta\alpha}(Q) D^R_{\delta'\alpha'}(Q) &= \frac{g_{\delta\alpha} g_{\delta'\alpha'}}{Q^4} - \frac{\Pi^{\parallel}_R(Q) g_{\delta\alpha} P^{\parallel}_{\delta'\alpha'} + \Pi^{\parallel}_R(Q) g_{\delta'\alpha'} P^{\parallel}_{\delta\alpha}}{Q^4(Q^2 - \Pi^{\parallel}_R(Q))} \\
&+ \frac{(\Pi^{\parallel}_R(Q))^2 P^{\parallel}_{\delta\alpha} P^{\parallel}_{\delta'\alpha'}}{Q^4(Q^2 - \Pi^{\parallel}_R(Q))^2}. \qquad (4.46)
\end{aligned}$$

The first term in Eq.(4.46) corresponds to the vacuum contribution. Since we are interested in the medium contribution (i.e., T and B), we will not consider this term. The medium dependent term that appears in Eq.(4.43) can be written in compact manner as

$$(D^R_{\delta\alpha}(q)D^R_{\delta'\alpha'}(q))(C^{\delta\mu\nu}(K,K')C^{\delta'}_{\mu\nu}(K,K')) = \mathcal{A}_{\alpha\alpha'} + \mathcal{B}_{\alpha\alpha'} + \mathcal{C}_{\alpha\alpha'}, \tag{4.47}$$

where

$$\mathcal{A}_{\alpha\alpha'} = -\frac{4\Pi^{\|}_R(q)}{q^4(q^2-\Pi^{\|}_R(q))}(K^\delta K'^{\delta'} + K'^\delta K^{\delta'})g_{\delta\alpha}P^{\|}_{\delta'\alpha'}, \tag{4.48}$$

$$\mathcal{B}_{\alpha\alpha'} = -\frac{4\Pi^{\|}_R(q)}{q^4(q^2-\Pi^{\|}_R(q))}(K^\delta K'^{\delta'} + K'^\delta K^{\delta'})g_{\delta'\alpha'}P^{\|}_{\delta\alpha}, \tag{4.49}$$

$$\mathcal{C}_{\alpha\alpha'} = \frac{4(\Pi^{\|}_R(q))^2}{q^4(q^2-\Pi^{\|}_R(q))^2}(K^\delta K'^{\delta'} + K'^\delta K^{\delta'})P^{\|}_{\delta\alpha}.P^{\|}_{\delta'\alpha'} \tag{4.50}$$

So Eq.(4.43), can be written as

$$|\bar{\mathcal{M}}|^2 = \frac{1}{4}\times\frac{1}{2}g^4(\mathcal{T}_1^{\alpha\alpha'} + \mathcal{T}_2^{\alpha\alpha'})(\mathcal{A}_{\alpha\alpha'} + \mathcal{B}_{\alpha\alpha'} + \mathcal{C}_{\alpha\alpha'}), \tag{4.51}$$

where $\mathcal{T}_1^{\alpha\alpha'} = Tr[\not{P}'\gamma^\alpha\not{P}\gamma^{\alpha'}]$ and $\mathcal{T}_2^{\alpha\alpha'} = M^2Tr[\gamma^\alpha\gamma^{\alpha'}]$ are traces over Dirac space. Six tensor contracted terms of Eq.(4.51) are simplified in appendix(A.2). Further simplification leads to the final form of scattering amplitude as

$$\begin{aligned}
|\bar{\mathcal{M}}|^2 = {} & 4g^4\frac{(\Pi^{\|}_R(Q))^2}{Q^4(Q^2-\Pi^{\|}_R(Q))^2}[(P.P_{\|}.K)(P'.P_{\|}.K') + (P.P_{\|}.K')(K.P_{\|}.P') \\
& -(P.P')(K.P_{\|}.K')] - \frac{4g^4\Pi^{\|}_R(Q)}{Q^4(Q^2-\Pi^{\|}_R(Q))}[(P.K)(P'.P_{\|}.K') + (P.K') \\
& \times(K.P_{\|}.P') + (K.P')(P.P_{\|}.K') + (P'.K')(P.P_{\|}.K) - (P.P')(K.P_{\|}.K')] \\
& -4g^4M^2\left[\frac{2\Pi^{\|}_R(Q)}{Q^4(Q^2-\Pi^{\|}_R(Q))}(K.P_{\|}.K') + \frac{(\Pi^{\|}_R(Q))^2}{Q^4(Q^2-\Pi^{\|}_R(Q))^2}(K.P_{\|}.K')\right],
\end{aligned} \tag{4.52}$$

where the tensor product is

$$P.P_{\parallel}.K \;\; = \;\; P_\mu P_{\parallel}^{\mu\nu} K_\nu = \frac{(P.q_{\parallel})(K.q_{\parallel})}{q_{\parallel}^2} - (P.k_{\parallel}). \tag{4.53}$$

The expression for the retarded self energy $\Pi_R^{\parallel}$ is given explicitly in appendix (**??**). This completely defines the matrix element squared.

Energy loss of HQ due to thermal gluons

The contribution of $t-$channel Compton scattering i.e, $Qg \rightarrow Qg$, to the HQ energy loss can be obtained by using Eq.(4.27) and the interaction rate (Γ) as given in Eq.(4.41). Hence, one can write [88]

$$\begin{aligned} -\frac{dE}{dx}\bigg|_{Qg\rightarrow Qg} &= \frac{1}{2vE}\int \frac{d\mathbf{p}'}{(2\pi)^3 2E'}\int \frac{d\mathbf{k}}{(2\pi)^3 2k} f(k_0)\int \frac{d\mathbf{k}'}{(2\pi)^3 2k'}(1+f({k'}_0)) \\ &\times \;\; (2\pi)^4\delta^4(P+K-P'-K')(E-E')|\bar{\mathcal{M}}|^2. \end{aligned} \tag{4.54}$$

The energy and momentum transfer in each scattering are, $\omega = E - E' = |\mathbf{k}'| - |\mathbf{k}|$ and $\mathbf{q} = \mathbf{p} - \mathbf{p}' = \mathbf{k}' - \mathbf{k}$. A comment regarding the use of resummed gluon propagator may be relevant here. The hard contributions to the energy loss ($|\mathbf{q}| \sim T$) can be obtained by using the bare gluon propagator for the $Qg \rightarrow Qg$ scatterings since the self energy corrections are negligible at leading order (LO). We confine our attention here for the soft momentum transfer in the range $g\sqrt{eB} \leq |\mathbf{q}| \ll T \ll \sqrt{eB}$. This requires the resummation of the gluon propagator in the LLL approximation as we have used here. The $|\mathbf{p}'|$ integration in Eq.(4.54) can be performed with the help of momentum delta function. In the soft momentum transfer limit the energy $E' \approx E - \mathbf{v}\cdot\mathbf{q}$ so that the energy delta function reduces to $\delta(\omega - \mathbf{v}.\mathbf{q})$. With these simplifications, Eq.(4.54) becomes

$$-\frac{dE}{dx}\bigg|_{Qg\rightarrow Qg} = \frac{(2\pi)}{16vE^2}\int \frac{d\mathbf{k}}{(2\pi)^3 k} f(k)\int \frac{d\mathbf{k}'\omega}{(2\pi)^3 k'}(1+f(k'))\delta(\omega - \mathbf{v}\cdot\mathbf{q})|\bar{\mathcal{M}}|^2 \tag{4.55}$$

Now, the simplification of the above 6-dimensional integration requires a proper choice of the co-ordinate system which should also be compatible with the terms appearing in the matrix element squared. For this purpose, we choose the direction of the momentum of the incoming HQ along the $\hat{z}$-axis which is also the direction of the magnetic field. We denote the angle made by $\mathbf{k}$ and $\mathbf{k}'$ with the $\hat{z}$-axis as θ_k and $\theta_{k'}$ respectively. Further, the azimuthal angles made by the two momenta of the incoming and outgoing gluon are ϕ_k and $\phi k'$ respectively. Therefore, the energy loss can be written as

$$\begin{aligned} -\frac{dE}{dx}\bigg|_{Qg\to Qg} &= \frac{1}{(2\pi)^5 16vE^2}\int kdkf(k)\int k'dk'(1+f(k'))\int_{-1}^{1}dx\int_{-1}^{1}dy\int_0^{2\pi}d\phi_k \\ &\times \int_0^{2\pi}d\phi_{k'}|\bar{\mathcal{M}}|^2\omega\delta(\omega - vk'y + vkx), \end{aligned} \tag{4.56}$$

where, $x = \cos\theta_k$ and $y = \cos\theta_{k'}$. Now, we introduce a new integration variable ω which will take care of one of the angular integrations x or y.

$$\int_0^{\infty} d\omega\delta[\omega - k(1-vx)] = 1 \tag{4.57}$$

Using these two δ-functions, we perform x and y angular integrations by writing the δ-functions as $\delta[\omega - k(1-vx)] = \frac{1}{vk}\delta(x - \frac{k-\omega}{vk})$ and $\delta(\omega - vk'y + vkx) = \frac{1}{vk'}\delta(y - \frac{\omega + vkx}{vk'})$. So, the final expression of the energy loss becomes:

$$\begin{aligned} -\frac{dE}{dx}\bigg|_{Qg\to Qg} &= \frac{1}{(2\pi)^5 16vE^2}\int_0^{\infty}\omega d\omega\int_{\frac{\omega}{1+v}}^{\frac{\omega}{1-v}}f(k)dk\int(1+f(k'))dk'\int_0^{2\pi}d\phi_k \\ &\times \int_0^{2\pi}d\phi_{k'}|\bar{\mathcal{M}}|^2. \end{aligned} \tag{4.58}$$

The explicit form of the four-vector product and the tensor contractions in the matrix element squared are elaborately given in the appendix(A.2).

4.4 Results and discussion

The two scatterings that contribute to the HQ energy loss are $Qq \to Qq$ evaluated in Eq.4.40 and t channel $Qg \to Qg$ evaluated in Eq.4.58. As mentioned earlier, we have confined our attention to the case where the typical momentum transfer from light partons to HQ is soft i.e., $g\sqrt{eB} \leq |\mathbf{k}| \ll T \ll M$. Therefore, the resummed gluon propagator is used in the evaluation of the matrix element squared for these two processes. For simplicity, let us take the HQ momentum $\vec{p} = (0, 0, p_z)$ and magnetic field $\vec{B} = B\hat{z}$. For the numerical purpose we take HQ as the charm quark with mass $M = 1.2$ GeV, temperature $T = 0.25$ GeV and magnetic field $eB = 0.1$ GeV^2 ($\sim 5m_\pi^2$) so that the condition $eB \gg T^2$ is satisfied. Since $eB \gg T^2$, only LLL will be populated by the light quarks. We also take finite mass (m_f) of light quarks in the gluon self energy diagram. The energy loss contributions using Eqs.(4.58) and (4.40) has been plotted in Fig.(4.3). In the left of Fig.(4.3), the variation of the energy loss with the contributions from both the scattering processes as a function of velocity of HQ is shown. We have taken here $m_f = 10$ MeV for the light quark mass and number of flavors $n_f = 2$. At low velocity the collisional energy loss is very small $\sim 10^{-6}$ GeV^2, however with increase is HQ velocity the energy loss increases. While both the scattering processes contribute to the energy loss, it is observed numerically that the $Qg \to Qg$ gives the dominant contribution to the energy loss for a given value of velocity of the HQ essentially due to larger color factor compared to the Coulomb scattering.

This behavior is similar to the case of vanishing magnetic field. It ought to be mentioned here that in the presence of magnetic field the energy loss is of similar order as compared to the case of vanishing magnetic field as estimated in Ref.[90]. Indeed, the asymptotic value for the energy loss ($v \to 1$) of Ref.[90] is given by

$$\frac{dE}{dx} = \frac{4\pi}{33 - 2n_f} m_D^2, \tag{4.59}$$

with $m_D^2 = 4\pi\left(1 + \frac{n_f}{6}\right)\alpha_s T^2$ which with the parameters $\alpha_s = 0.3, n_f = 2$ and $T = 0.25$ GeV turns out to be 0.15 GeV^2.

This may be compared with the magnetic field contribution given by the red curve in the left panel of Fig.(4.3) which reaches to the value 0.1 GeV^2 in the same limit. Further, it may be relevant to note that in the limit of vanishing light quark mass i.e., $m_f = 0$, the magnetic field contribution to the gluon self energy vanishes as $\Pi_\parallel^R$ is proportional to m_f^2. This will lead to vanishing of the magnetic field dependent contribution to the energy loss. This is similar to the vanishing of magnetic field contribution for the dilepton production [149] in the same limit.

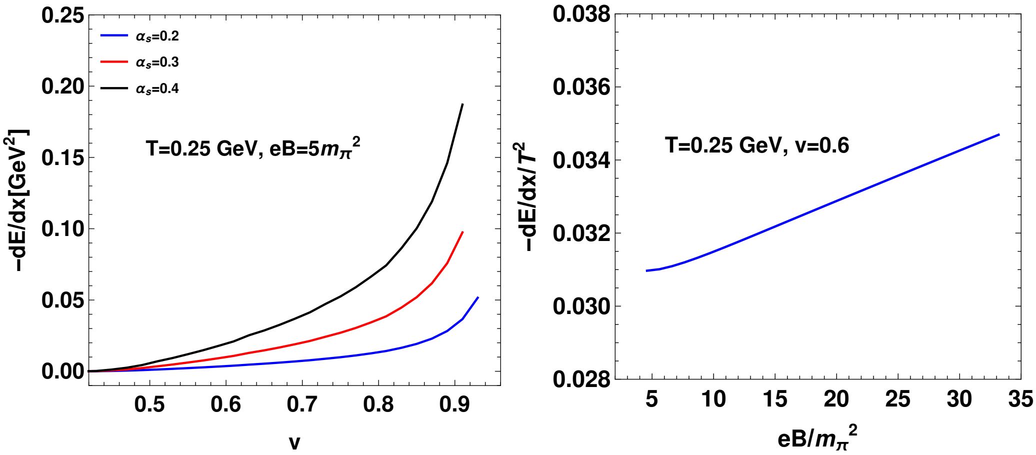

Figure 4.3: Collisional energy loss as a function of HQ velocity **v** and magnetic field $m_f = 10$ MeV, flavor $n_f = 2$.

In the right side of Fig.(4.3), the energy loss scaled with T^2 as a function of magnetic field scaled by pion mass square i.e., eB/m_π^2, where m_π is pion mass is displayed. We have taken here $T = 0.25$ GeV and the magnitude of the heavy quark velocity $v = 0.6$. As may be observed in the figure the energy loss increases with the increase in the magnetic field. Numerically, it is seen that $Qg \to Qg$ contribution is not affected too much with the magnetic field. For this process, the magnetic field dependence arises from the resummed gluon propagator with the field dependent contribution of the quark loop. This quark loop contribution increases with the magnetic field leading to a mild decrease of the energy loss due to this process as quark loop contribution lies in the retarded propagator. On the other hand, for the Coulomb scattering process i.e., $Qq \to Qq$ the contribution increase with increase in the magnetic field. This can be understood as follows; The energy loss is proportional to ρ_L that depends on real and imaginary parts of retarded self energies and related to the spectral function. The spectral function increases with increase in the magnetic field. This increase of ρ_L with the magnetic field was also observed in Ref.[149]. It turns out that this increase is significant and the contribution becomes similar order as the $Qg \to Qg$ for larger magnetic field leading to increase of the total energy loss with magnetic field as observed in Fig.(4.3).

4.5 Summary

The effect of the magnetic field on the HQ collisional energy loss in a thermalized QGP medium is discussed in this chapter. The analysis is done for the case of strong field limit i.e., $\sqrt{eB} \gg T$ so that the light quarks are populated only in the LLL. On the other hand, the heavy quark mass M is much larger than the strength of the magnetic field (i.e., $M \gg \sqrt{eB}$), so that heavy quark is not Landau quantized. The effect of the magnetic field manifests through resummed retarded/advanced gluon propagator through quarks loop. Since the gluon loop contribution to the gluon self energy is proportional to $\alpha_s T^2$ and the quark loop contribution is proportional to $\alpha_s eB$, in the limit $\sqrt{eB} \gg T$ the gluon loop contribution in the gluon resummed propagator is not taken into account. For the scattering of HQ with the thermalized light partons we have considered the soft momentum transfer limit i.e., $g\sqrt{eB} \leq |\mathbf{k}| \ll T \ll \sqrt{eB}$. With $M \gg \sqrt{eB}$ and the in the LLL approximation the relevant scattering processes are Coulomb scattering i.e., $Qq \to Qq$ and t-channel Compton scattering $Qg \to Qg$. The u and the s channels of the Compton scatterings are not affected by the magnetic field. For a given magnitude of the heavy quark velocity, the Compton scattering process is dominant over the Coulomb scattering process for the range of the magnetic field considered here.

It is observed that of the two processes, the Coulomb scattering process is more sensitive to the magnetic field as its contribution to the energy loss is proportional to the spectral function which increases with increase in the magnetic field. This leads to a net increase in the energy loss with increase in the magnetic field. It turns out that in this strong field limit, the magnetic field dependent collisional energy loss for $eB = 5m_\pi^2$ is comparable to the same in the vanishing field limit and therefore could be important for the jet quenching phenomena in HICs. However, In a realistic situation in HIC up to what extent the magnetic field can affect the collisional energy loss will also depend on the medium response to the magnetic field and require further investigations. In the vacuum, the magnetic field decreases very rapidly however, in a system with finite electrical conductivity, magnetic field satisfies diffusion equation and the relaxation time of the external magnetic field depends on the electrical conductivity of the system. In a system with larger conductivity magnetic field can sustain and resonably be strong for a longer period of time. However, it ought to be mentioned that this requires a proper estimation of the electrical conductivity of the medium as well as solutions of magneto hydrodynamic equations which needs further investigations. Furthermore, for smaller values of magnetic field one must include the effect of higher Landau levels. For the large momentum of heavy quark, the radiative contribution to the energy loss may also be relevant and could be affected by the magnetic field. This apart, for a moderate value of magnetic field $eB \sim T^2$ the contributions arising from the higher Landau levels could also be important for the energy loss and hence jet quenching. In this case, one must take the contribution of gluon loops in the gluon self energy for the resummed gluon propagator as well as the contribution from the s and u channels of Compton scattering. We continue the HQ description in a magnetized thermal medium in the next chapter. In this chapter, we discussed high momentum HQ dynamics, i.e., energy loss; however, in the next chapter we shall mainly focus on low momentum processes, i.e., diffusion of HQ.

CHAPTER 5

HQ momentum broadening in a magnetized medium

It is believed that intense magnetic field has been created in the initial stages of non-central Heavy Ion Collisions (HICs) [120, 3, 121, 123, 192, 193]. The created field is estimated to be in the order of $eB \sim m_\pi^2$ at Relativistic Heavy-Ion Collider (RHIC) and a few tens of pion mass square, $eB \sim 15m_\pi^2$ at the Large Hadron Collider (LHC). The intense magnetic field may affect various aspects of the physics of the deconfined hot nuclear matter created in HIC termed as Quark-Gluon Plasma (QGP). One of the major uncertainty of the magnetic field is its lifetime in hot nuclear matter. In vacuum, the magnetic field decays very rapidly. However, in a medium of charged particles, it can be sustained for a longer time due to the finite electrical conductivity (σ) of the medium [173, 174, 175, 176, 129]. As discussed in the previous chapter, for electrical conductivity $\sigma \approx 0.04T$ [180], at temperature $T = 200$ MeV the electrical conductivity $\sigma = 8$ MeV. Therefore, for $L = 10$ fm, the time over which the magnetic field remains reasonably strong is $\tau = 1$ fm. For higher temperatures, σ will be higher, leading to larger relaxation time. The investigations on various characteristics of the hot nuclear matter in the presence of the magnetic field have gained attention in recent years [194, 195, 196, 197, 198]. The study of the QGP in the magnetic field background opens up new avenues to explore physics in different directions such as Chiral Magnetic Effect (CME) [120, 199], charge-dependent elliptic flow [200, 201, 202], magnetic catalysis [190], various transport coefficients of QGP in the magnetic field [203, 204, 198], photon-dilepton production [149, 130, 205], in medium properties of quarkonia [184, 186] and their suppression [181, 182], transport coefficients of heavy quarks (HQs) in the magnetic field [206, 144, 187], etc.

To understand the properties of the QGP, one needs external probes such as highly energetic particles created at a very early stage of HICs. HQs serve as an effective probe to describe the properties of hot QCD medium created in the collision experiments, as they do not constitute the bulk medium, owing to their large mass compared to the temperature scale. The HQ traverses through the QGP medium as a nonthermal degree of freedom and gets random kicks from the thermal partons (light quarks/anti-quarks and gluons) in the bulk medium. Thus, the HQ dynamics could be explored within the scope of the Brownian motion [97, 207, 100, 208, 209, 210], and their transport parameters, the drag and the diffusion coefficients, have been estimated in the QGP medium [211, 212, 213, 214, 84, 85, 215]. The HQ production and dynamics in the nuclear matter and the associated experimental observables have been well explored in several works [216, 217, 218, 219, 220, 93, 221, 222, 223, 224]. The HQ evolution and momentum broadening in terms of momentum diffusion in thermal QGP are explained in Ref. [100]. There are some recent investigations on the HQ momentum diffusion coefficients in a strongly magnetized QGP medium in the weak coupling regime in the static limit of the HQ [144, 187].

It turns out that in the static limit, there are two diffusion coefficients of HQ in a magnetic field background, one in the direction of the magnetic field and the other to the perpendicular to the field. This, in turn, generates a magnetic field induced anisotropy in the momentum diffusion. It would be interesting to investigate the nature of the anisotropy in the momentum diffusion of HQ beyond the static limit.

In this chapter, we estimate the anisotropic diffusion coefficients of HQ moving with finite velocity $\mathbf{v}$. To estimate the same, we consider the strong field limit with the soft momentum transfer i.e., we shall be interested in the regime

$|\mathbf{q}| \leq g\sqrt{eB} \ll T \ll \sqrt{eB} \ll M$ and use the resummed gluon propagator at finite temperature and magnetic field. In chapter 4, we discussed the collisional energy loss of the HQ using a similar technique, which might throw some insights in the directions of jet quenching. The present calculation is more related to the momentum broadening of HQ depending upon the relative orientation of the magnetic field and the velocity of the HQ. We follow an approach similar to the Refs.[100, 225]. The HQ dynamics are described by the Langevin equations for two different cases, *viz*, the HQ moving parallel, and perpendicular to the magnetic field.

This chapter is organized as follows. In Sec.6.1, the Langevin formalism for HQ diffusion for both the cases, *i.e.*, HQ moving parallel and perpendicular to the magnetic field is discussed. In subsections.5.1.1 and 5.1.2, we discuss the qluon and light quarks/antiquarks contribution to the diffusion coefficients. Further in Sec.7.3, we discuss the results and finally, in Sec7.4, we summarise the implications and future possibilities of this chapter.

5.1 Langevin dynamics of HQ in a magnetized medium

Considering the strong magnetic field limit with $M \gg \sqrt{eB} \gg T$ which indicate that the light quarks/antiquarks occupy the Lowest Landau Level (LLL) while thermal gluons are unaffected by the field. As $M \gg \sqrt{eB}$, the HQ motion is not Landau quantized. In order to estimate the thermal gluons and thermal light quark/antiquark contributions to the HQ transport coefficients for the non-static case, *i.e.*, HQ is moving with velocity $\mathbf{v}$ in the medium, we consider two cases: first when HQ is moving along the direction of the magnetic field ($\mathbf{v} \parallel \mathbf{B}$) and second the HQ moves transverse to the magnetic field ($\mathbf{v} \perp \mathbf{B}$). Here, we denote the momentum diffusion (κ) coefficients by three indices. The superscript denotes the HQ velocity with respect to the magnetic field. Of the two indices which are given as subscripts of the diffusion coefficient, the first index describes the momentum diffusion relative to the direction of the velocity of the HQ while the second index corresponds to the momentum diffusion relative to the direction to the magnetic field e.g., $\kappa_{LL}^{\|}$ represents the diffusion coefficient parallel to both the magntic field and velocity for HQ moving along the magnetic field direction. Below we explain this in detail.

5.1.0.1 Case I: $\mathbf{v} \parallel \mathbf{B}$

The magnetic field $\mathbf{B}$, and the HQ velocity $\mathbf{v}$, are considered to be in the same direction as depicted in Fig. 5.1.

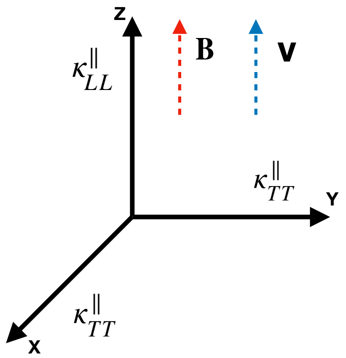

Figure 5.1: Anisotropic momentum diffusion coefficients for HQ moving parallel to the magnetic field

The general structure of HQ momentum diffusion tensor in this case can be decomposed as follows,

$$\kappa^{ij} = R^{ij}\kappa_{TT}^{\|} + Q^{ij}\kappa_{LL}^{\|}, \tag{5.1}$$

where $R^{ij} = \left(\delta^{ij} - \frac{p^i p^j}{p^2}\right)$ and $Q^{ij} = \frac{p^i p^j}{p^2}$ are the transverse and longitudinal projection operators orthogonal to each other, *i.e.*, $R^{ij}Q_{ij} = 0$. Here, $\kappa_{TT}^{\|}$ and $\kappa_{LL}^{\|}$ are the two diffusion coefficients, transverse and longitudinal to the direction of HQ motion (which is the same direction of $\mathbf{B}$). The symbol $\|$ denotes that the HQ motion is parallel to the direction of the magnetic field. The broadening of the variance of HQ momentum distribution can be described by the macroscopic equation of motion as follows [100],

$$
\begin{aligned}
&\frac{d}{dt}\langle p\rangle = -\eta_D^{\|}(p)p,\\
&\frac{1}{2}\frac{d}{dt}\langle(\Delta p_T)^2\rangle = \kappa_{TT}^{\|}(p),\\
&\frac{d}{dt}\langle(\Delta p_L)^2\rangle = \kappa_{LL}^{\|}(p),
\end{aligned}
\tag{5.2}
$$

where the coefficient $\eta_D^{\|}$ measures the average momentum loss. The variance of the HQ momentum distribution transverse and parallel to the direction of the motion can be respectively defined as $\langle(\Delta p_T)^2\rangle \equiv \langle p_T^2\rangle$ and $\langle(\Delta p_L)^2\rangle \equiv (p_L - \langle p_L\rangle)^2$. The factor $\frac{1}{2}$ in the transverse momentum broadening is due to two perpendicular directions. The HQ transport coefficients $\eta_D^{\|}$, $\kappa_{LL}^{\|}$ and $\kappa_{TT}^{\|}$ can be obtained from the kinetic theory by considering the proper collisional scattering matrix element squared and have the following form for the momentum loss,

$$
\frac{d}{dt}\langle p\rangle = \frac{1}{2v}\int_{k,q}|\bar{\mathcal{M}}|^2\omega\Big[f(k)\Big(1\pm f(k+\omega)\Big) - f(k+\omega)\Big(1\pm f(k)\Big)\Big],
\tag{5.3}
$$

where $v = p/E$ is the velocity of HQ, and f is the distribution of thermal particles in the magnetized QGP, $|\bar{\mathcal{M}}|$ is the HQ-thermal particle scattering matrix element, and ω is the transferred energy due to the scattering process. We can write similar expressions for the rate of transverse and longitudinal momentum broadening which are $\kappa_{TT}^{\|}(\mathbf{v})$ and $\kappa_{LL}^{\|}(\mathbf{v})$, *i.e.*,

$$
\kappa_{TT}^{\|}(\mathbf{v}) = \int_{k,q}|\bar{\mathcal{M}}|^2 q_T^2\Big[f(k)\Big(1\pm f(k+\omega)\Big)\Big],
\tag{5.4}
$$

$$
\kappa_{LL}^{\|}(\mathbf{v}) = \int_{k,q}|\bar{\mathcal{M}}|^2 q_z^2\Big[f(k)\Big(1\pm f(k+\omega)\Big)\Big].
\tag{5.5}
$$

The notation $\int_{k,q}$ denotes the relevant phase space integration over $\mathbf{k}$ and $\mathbf{q}$ with proper dimensions.

5.1.0.2 Case II: $\mathbf{v} \perp \mathbf{B}$

When the HQ motion is moving transverse to the direction of the magnetic field, say, $\mathbf{v} = (v_x, 0, 0)$ and $\mathbf{B} = B\hat{z}$, the momentum broadening can be characterized by three diffusion coefficients. Defining $\mathbf{b} = (0, 0, 1)$ to project the direction of

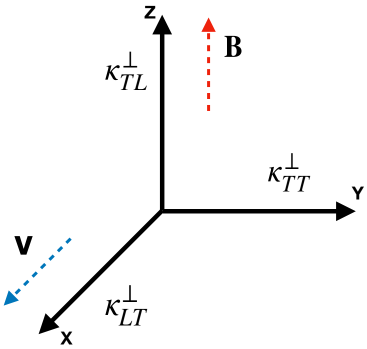

Figure 5.2: HQ is moving in the **x**-axis in the presence of the strong magnetic field $\mathbf{B} = B\hat{z}$.

magnetic field, the diffusion tensor can be decomposed as follows,

$$\kappa^{ij} = P^{ij}\kappa^{\perp}_{TL} + Q^{ij}\kappa^{\perp}_{LT} + R^{ij}\kappa^{\perp}_{TT}, \tag{5.6}$$

in which the projection operators takes the forms,

$$P^{ij} = \frac{b^i b^j}{b^2}, \qquad Q^{ij} = \frac{p^i p^j}{p^2}, \qquad R^{ij} = \left(\delta^{ij} - \frac{p^i p^j}{p^2} - \frac{b^i b^j}{b^2}\right), \tag{5.7}$$

such that the operators are orthogonal to each other. Note that the same decomposition is valid for the HQ motion along **y**-axis. In this case, the Langevin equations take the forms as,

$$\begin{aligned} &\frac{d}{dt}\langle p\rangle = -\eta^{\perp}_{D}(p)p, && \frac{d}{dt}\langle(\Delta p_z)^2\rangle = \kappa^{\perp}_{TL}(p), \\ &\frac{d}{dt}\langle(\Delta p_x)^2\rangle = \kappa^{\perp}_{LT}(p), && \frac{d}{dt}\langle(\Delta p_y)^2\rangle = \kappa^{\perp}_{TT}(p). \end{aligned} \tag{5.8}$$

The component $\kappa^{\perp}_{TL}$ denotes the diffusion coefficient in the direction transverse to the HQ motion and longitudinal to the direction of the magnetic field, *i.e.*, along **z**-axis. Similarly, $\kappa^{\perp}_{LT}$ and $\kappa^{\perp}_{TT}$ respectively define the components of the diffusion coefficient longitudinal to the HQ motion and transverse to the magnetic field (along **x**-axis), and in the direction transverse to both HQ motion and magnetic field (along **y**-axis). The diffusion coefficients are estimated from the following expressions [100, 225],

$$\kappa^{\perp}_{TL}(\mathbf{v}) = \int_{k,q} |\bar{\mathcal{M}}|^2 q_z^2 \Big[f(k)\Big(1 \pm f(k+\omega)\Big)\Big], \tag{5.9}$$

$$\kappa^{\perp}_{LT}(\mathbf{v}) = \int_{k,q} |\bar{\mathcal{M}}|^2 q_x^2 \Big[f(k)\Big(1 \pm f(k+\omega)\Big)\Big], \tag{5.10}$$

$$\kappa^{\perp}_{TT}(\mathbf{v}) = \int_{k,q} |\bar{\mathcal{M}}|^2 q_y^2 \Big[f(k)\Big(1 \pm f(k+\omega)\Big)\Big]. \tag{5.11}$$

In the following sections, we discuss the interaction of HQ with the thermal gluon and the light quark/antiquark in detail while considering the thermal particle kinematics in the magnetic field for each case.

5.1.1 Gluonic contribution to HQ diffusion

Gluonic contribution to the diffusion coefficient comes via the Compton scattering, *i.e.*, $Q(P) + g(K) \rightarrow Q(P^{'}) + g(K^{'})$, where g stands for gluon. Generally, at leading order in the coupling, there are three channels, s, t and u that contribute to Compton scattering. In the limit $M \gg \sqrt{eB} \gg T$, the leading order contribution to the diffusion coefficient in the magnetic field background arises from the t-channel scattering process. This is because the contribution from the s and the u-channels of the Compton scattering is negligible in the presence of magnetic field due the hierarchy in the scales considered here, *i.e.*, in the regime $M \gg \sqrt{eB}$, the HQ propagators in s and u channels are not affected by the magnetic field. In the t-channel scattering, the effect of the magnetic field comes through the resummed gluon propagator. For HQ at rest, *i.e.*, the static limit of HQ, the matrix elements for the t-channel scattering is well investigated in the Ref. [144] using the Debye mass screened gluon propagator. In contrast, here we use the resummed retarded gluon propagator and also consider the finite velocity $\mathbf{v}$ of the HQ. In this case, the color-averaged t-channel scattering amplitude is given in Eq.4.52,

$$\begin{aligned} |\bar{\mathcal{M}}|^2 &= \frac{4g^4(\Pi_R^{\|}(Q))^2}{Q^4(Q^2-\Pi_R^{\|}(Q))^2}\Big(\mathcal{A}-M^2(K.P_{\|}.K')\Big) \\ &- \frac{4g^4\Pi_R^{\|}(Q)\mathcal{B}}{Q^4(Q^2-\Pi_R^{\|}(Q))}\Big(\mathcal{B}-2M^2(K.P_{\|}.K')\Big), \end{aligned} \tag{5.12}$$

$$\mathcal{A} = (P.P_{\|}.K)(P'.P_{\|}.K') + (P.P_{\|}.K')(K.P_{\|}.P') + (P.P')(K.P_{\|}.K'), \tag{5.13}$$

$$\begin{aligned} \mathcal{B} &= (P.K)(P'.P_{\|}.K') + (P.K')(K.P_{\|}.P') + (K.P')(P'.K') + (P.P_{\|}.K) \\ &- 2(P.P')(K.P_{\|}.K'), \end{aligned} \tag{5.14}$$

with

$$P.P_{\|}.K = P_\mu P_{\|}^{\mu\nu} K_\nu = \frac{(P.q_{\|})(K.q_{\|})}{q_{\|}^2} - P.k_{\|}, \tag{5.15}$$

where $Q = K' - K = P - P'$, is the four momentum vector for the exchange gluon and $q_{\|}^2 = \omega^2 - q_z^2$. For the estimation of the diffusion and the drag coefficients, we restrict the energy transfer to be small, which can be done by assuming $\omega = \mathbf{v}\cdot\mathbf{q}$, where $\mathbf{q}$ is the three momentum transfer.

Now, let us first consider the case in which HQ moves along the direction of the magnetic field as shown in Fig.(5.1). Assuming that $\mathbf{v} = (0, 0, v\hat{\mathbf{z}})$ is the velocity of the HQ, initial and final gluon momenta $\mathbf{k}$ and $\mathbf{k}'$ make the angles respectively θ_k, ϕ_k and $\theta_{k'}, \phi_{k'}$ with the $\hat{\mathbf{z}}$ and the $\hat{\mathbf{x}}$-axis. The gluonic contribution to diffusion coefficient along the direction of the magnetic field then takes the form [100],

$$\begin{aligned} \kappa_{LL:Qg}^{\|} &= \frac{1}{16E^2}\int \frac{d\mathbf{k}}{(2\pi)^3|\mathbf{k}|}\frac{d\mathbf{k}'}{(2\pi)^3|\mathbf{k}'|}\frac{d\mathbf{p}'}{(2\pi)^3} q_z^2 |\bar{\mathcal{M}}|^2 f(|\mathbf{k}|) \\ &\times\ (1+f(|\mathbf{k}'|))(2\pi)^5\delta^4(P+K-P'-K'), \end{aligned} \tag{5.16}$$

where $f(k)$ is Bose-Einstein distribution function and $q_z = k'_z - k_z$ with $k_z =$

$k\cos\theta_k$ and $k'_z = k'\cos\theta_{k'}$ is the z-component of the exchange gluon momentum. From now onwards, we shall use the notations $k = |\mathbf{k}|$ and $k' = |\mathbf{k}'|$. After performing $\mathbf{p'}$ integration by using the three momenta Dirac delta function, Eq.(5.16) reduces to

$$\kappa^{\parallel}_{LL;Qg} = \frac{1}{16E^2(2\pi)^5}\int \frac{d\mathbf{k}}{k}\frac{d\mathbf{k}'}{k'} q_z^2|\bar{\mathcal{M}}|^2 f(k)(1+f(k'))\delta(E+k-E'-k'). \quad (5.17)$$

Further, for small momentum transfer, we can write $E - E' = \mathbf{v}\cdot\mathbf{q}$ and from the energy conservation we have the energy of the exchanged gluon as $\omega = |\mathbf{k}'| - |\mathbf{k}|$. Hence, the delta function in the above equation can be simplified to

$$\delta(\omega - \mathbf{v}\cdot\mathbf{q}) = \frac{1}{vk'}\delta\bigg(\cos\theta_{k'} - \frac{k\cos\theta_k}{k'} - \frac{\omega}{vk'}\bigg). \quad (5.18)$$

The energy delta function of Eq.(5.18) can be used to perform the angular integration (θ_k) in Eq.(5.17). To perform the other angular integration ($\theta_{k'}$ integration), we introduce another delta function $\int d\omega\delta(\omega - k + \mathbf{v}\cdot\mathbf{k}) = 1$ which can be simplified as

$$\delta(\omega - k + \mathbf{v}\cdot\mathbf{k}) = \frac{1}{vk}\delta\bigg(\cos\theta_k - \frac{\omega - k}{vk}\bigg). \quad (5.19)$$

Note that the second delta function, as given by Eq.(5.19), introduces one more integration variable in Eq.(5.17), which is the energy transfer to the HQ. Employing Eqs.(5.18) and (5.19) for performing the polar angular integrations, and integrating over both the azimuthal angles from 0 to 2π, $\kappa^{\parallel}_{LL}$ takes the form as follows,

$$\begin{aligned}\kappa^{\parallel}_{LL;Qg} &= \frac{1}{16E^2(2\pi)^5 v^2}\int d\omega \int_{\frac{\omega}{1-v}}^{\frac{\omega}{1+v}} dk \int dk' q_z^2 \int d\phi_k \int d\phi_{k'} |\bar{\mathcal{M}}|^2 f(k) \\ &\times (1+f(k')), \end{aligned} \quad (5.20)$$

and can be solved numerically. Similarly, the other component of the diffusion coefficient perpendicular to the plane containing the magnetic, *i.e.*, $\kappa^{\parallel}_{TT}$ can be described as follows,

$$\kappa^{\parallel}_{TT;Qg} = \frac{1}{16E^2(2\pi)^5 v^2}\int d\omega \int_{\frac{\omega}{1-v}}^{\frac{\omega}{1+v}} dk \int dk' q_\perp^2 \int d\phi_k \int d\phi_{k'} |\bar{\mathcal{M}}|^2 f(k)$$
$$\times \quad (1+f(k')), , \tag{5.21}$$

where $\mathbf{q}_\perp = \mathbf{k}'_\perp - \mathbf{k}_\perp$ is the transverse momentum of exchange gluon and lies in the xy plane as shown in Fig.(5.1). The square of transverse momentum can be defined as,

$$q_\perp^2 = k^2\sin^2\theta_k + k'^2\sin^2\theta_{k'} - 2kk'\sin\theta_k\sin\theta_{k'}\cos(\phi_k - \phi_{k'}). \tag{5.22}$$

Now, let us consider the other case where HQ moves perpendicular to the magnetic field, as shown in Fig.(5.2). Without loosing generality, we choose the HQ motion along the $\mathbf{x}$-axis so that the HQ velocity takes the form $\mathbf{v} = (v\hat{\mathbf{x}}, 0, 0)$. As mentioned earlier, in this case, there are three diffusion coefficients, $\kappa^{\perp}_{LT}, \kappa^{\perp}_{TL}$, and $\kappa^{\perp}_{TT}$. Similar to Eq.(5.17), the gluonic contribution to the diffusion coefficient $\kappa^{\perp}_{LT;Qg}$ takes the form,

$$\kappa^{\perp}_{LT;Qg} = \frac{1}{16E^2(2\pi)^5}\int \frac{d\mathbf{k}}{k}\frac{d\mathbf{k}'}{k'} q_x^2 |\bar{\mathcal{M}}|^2 f(k)(1+f(k'))\delta(E+k-E'-k'). \tag{5.23}$$

Instead of introducing the energy delta function identity (see before Eq.(5.19)) as in the case of $\mathbf{v} \parallel \mathbf{B}$, here it is convenient to introduce the momentum delta function $\int d\mathbf{q}\delta^3(\mathbf{q}+\mathbf{k}-\mathbf{k}') = 1$ identity so that Eq.(5.23) reduces to

$$\kappa^{\perp}_{LT;Qg} = \frac{1}{16E^2(2\pi)^5}\int \frac{d\mathbf{k}}{k}\frac{d\mathbf{q}}{k'} q_x^2 |\bar{\mathcal{M}}|^2 f(k)(1+f(k'))\delta(E+k-E'-k'). \tag{5.24}$$

Again, in the small momentum transfer limit, one can write $k - k' = k - |\mathbf{k} - \mathbf{q}| = -\mathbf{q}\cdot\hat{\mathbf{k}}$ and with $E - E' = \mathbf{v}\cdot\mathbf{q}$ (energy conservation), the energy delta function in Eq.(5.24) can be written as,

$$\delta(E - E' + k - k') = \delta(\mathbf{v}\cdot\mathbf{q} - \mathbf{q}\cdot\hat{\mathbf{k}}). \tag{5.25}$$

Taking θ_q, θ_k and ϕ_q, ϕ_k as polar angles and azimuthal angles of exchanged gluon and initial gluon, one can write

$$\mathbf{q}\cdot\hat{\mathbf{k}} = q(\sin\theta_k\sin\theta_q\cos(\phi_k-\phi_q)+\cos\theta_q\cos\theta_k), \tag{5.26}$$

and

$$\mathbf{v}\cdot\mathbf{q} = vq\sin\theta_q\cos\phi_q. \tag{5.27}$$

Using Eqs.(5.26) and (5.27), the energy delta function in Eq.(5.24) can be simplified to the following form,

$$\delta(\mathbf{v}\cdot\mathbf{q}-\mathbf{q}\cdot\hat{\mathbf{k}}) = \frac{1}{q\sin\theta_q\sin\theta_k}\delta\Bigg(\cos(\phi_k-\phi_q)+\cot\theta_q\cot\theta_k - v\frac{\cos\phi_q}{\sin\theta_k}\Bigg). \tag{5.28}$$

To perform the angular integration over azimuthal angle of $\mathbf{k}$ (ϕ_k integration) in Eq.(5.24), one can further simplify the delta function of Eq.(5.28) as,

$$\delta\Bigg(\cos(\phi_k-\phi_q)+\cot\theta_q\cot\theta_k - \frac{v\cos\phi_q}{\sin\theta_k}\Bigg) = \frac{\delta(\phi_k-\phi_k^0)}{|\sin(\phi_k^0-\phi_q)|}, \tag{5.29}$$

where,

$$\phi_k^0 = \phi_q + \cos^{-1}\Bigg(\frac{v\cos\phi_q}{\sin\theta_k} - \cot\theta_q\cot\theta_k\Bigg). \tag{5.30}$$

Eq.(5.30) sets the integration limit for θ_k integration, which can be obtained by solving the above equation by imposing the condition $|\cos(\phi_k^0-\phi_q)| \leq 1$. With these simplifications, Eq.(5.24) takes the following form,

$$\begin{aligned}\kappa^{\perp}_{LT;Qg} &= \frac{1}{16E^2(2\pi)^5}\int_0^\infty kdk\int_0^\infty \frac{qdq}{k'}\int_0^\pi \sin\theta_q d\theta_q\int_0^{2\pi}\\ &\times\ d\phi_q\int d(\cos\theta_k)q_x^2|\bar{\mathcal{M}}|^2 f(k)(1+f(k')).\end{aligned} \tag{5.31}$$

Similar to Eq.(5.31), the other two components of the diffusion coefficient in the yz-plane can be described as,

$$\begin{aligned}\kappa^{\perp}_{TL;Qg} &= \frac{1}{16E^2(2\pi)^5}\int_0^\infty kdk\int_0^\infty \frac{qdq}{k'}\int_0^\pi \sin\theta_q d\theta_q\int_0^{2\pi}\\ &\times\ d\phi_q\int d(\cos\theta_k)q_z^2|\bar{\mathcal{M}}|^2 f(k)(1+f(k')),\end{aligned} \tag{5.32}$$

where q_z is the magnitude of the exchange gluon momentum along the $\hat{z}$ direction and

$$\begin{aligned}\kappa^{\perp}_{TT;Qg} &= \frac{1}{16E^2(2\pi)^5}\int_0^{\infty} kdk\int_0^{\infty}\frac{qdq}{k'}\int_0^{\pi}\sin\theta_q d\theta_q\int_0^{2\pi} \\ &\times\ d\phi_q\int d(\cos\theta_k)q_y^2|\bar{\mathcal{M}}|^2 f(k)(1+f(k')),\end{aligned} \tag{5.33}$$

with q_y as the magnitude of the exchange gluon momentum along the $\hat{y}$ axis.

5.1.2 Light quark contribution to HQ diffusion

The other contribution to the diffusion coefficients in the LLL approximation arises from the Coulomb scattering, *i.e.*, scattering of HQ with that of LLL light thermal quarks. Let us first consider the case in which HQ moves in the direction of the magnetic field with velocity $\mathbf{v}$. Here, we use kinetic theory approach similar to Ref. [225] in which the momentum diffusion coefficient is related to energy loss per unit time that is given as

$$\frac{dE}{dt} = \Re\int d^4Q j^i_{ext}(Q)E^i_{ind}(Q). \tag{5.34}$$

Here $j^i_{ext}(Q) = q^a\mathbf{v}\delta(\omega-\mathbf{v}\cdot\mathbf{q})$ (with q^a as color charge) is external current and E^i_{ind} is induced color electric field. In the soft momentum transfer limit the diffusion coefficient is obtained by using $\kappa = -(2T/v^2)dE/dt$. In order to obtain the induced chromo-electric field, one can solve Maxwell equation

$$-iQ_\mu F^{\mu\nu}(Q) = j^\nu_{ind}(Q) + j^\nu_{ext}(Q), \tag{5.35}$$

where $j^\mu_{ind}(Q) = A_\nu(Q)\Pi^{\mu\nu}(Q)$ is induced current. Here $Pi_{\mu\nu}(Q)$ is gluon self energy in the presence of a constant magnetic field background and at leading order $F^{\mu\nu} = \partial_\mu A_\nu - \partial_\nu A_\mu$. Note here that in $F^{\mu\nu}$, the term containing coupling g is dropped for leading order contribution. Further Eq.5.35, can be simplified in order to obtain $E_i = iq_iA_0 - i\omega A_i$ as

$$(D^{-1})^{00}A_0 + (D^{-1})^{i0}A_i = -j^0_{ext}, \tag{5.36}$$

$$(D^{-1})^{0k}A_0 + (D^{-1})^{ik}A_i = -j^i_{ext}. \tag{5.37}$$

Above two equation can be solve to obtain A_0, A_i and hence E_i. Explicit form of A_0, A_i is given in appendixA.3. With $E_i = iq_iA_0 - i\omega A_i$ and Eq.5.34, the quark contribution to the diffusion coefficient $\kappa^{\|}_{LL;Qq}$ is given as

$$\kappa^{\|}_{LL;Qq} = \frac{g^2(N^2-1)}{2N}\Im\int\frac{d^4Q}{(2\pi)^4}\frac{2Tq_z^2}{\omega}\bigg(v_iA_i - A_0\bigg). \tag{5.38}$$

Similarly, the component transverse to the magnetic field can be written as

$$\kappa^{\|}_{LL;Qq} = \frac{g^2(N^2-1)}{2N}\Im\int\frac{d^4Q}{(2\pi)^4}\frac{2Tq_\perp^2}{\omega}\bigg(v_iA_i - A_0\bigg), \tag{5.39}$$

where $q_\perp^2 = q^2\sin^2\theta_q$. The inverse propagator in Eqs.5.36 and (5.37) are retarded propagator that is given by

$$D^R_{\mu\nu}(Q) = -\frac{P_{\mu\nu}(Q)}{(\omega+i\epsilon)^2-q^2} - \frac{\Pi^{\|}_R(\omega+i\epsilon,\mathbf{q})P^{\|}_{\mu\nu}(Q)}{Q^2(Q^2-\Pi^{\|}_R(\omega+i\epsilon,\mathbf{q}))} + \xi\frac{Q_\mu Q_\nu}{((\omega+i\epsilon)^2-q^2)^2}, \tag{5.40}$$

where $\Pi^{\|}_R$ is the retarded self energy of the gluon arising from the light quarks loop with light quarks in the LLL and ξ is the gauge parameter. The expression for $\Pi^{\|}_R$ is given in appendixA.1. $D^R_{0,ij}$ in Eq.(5.40) is the gluon propagator in vacuum. The longitudinal projection operator $P^{\|}_{\mu\nu}(Q)$ is defined as

$$P^{\|}_{\mu\nu}(Q) = -g^{\|}_{\mu\nu} + \frac{q^\mu_{\|}q^\nu_{\|}}{q^2_{\|}}, \tag{5.41}$$

and the other projection operator $P_{\mu\nu}(Q)$ takes the form as,

$$P_{\mu\nu}(Q) = -g_{\mu\nu} + \frac{Q_\mu Q_\nu}{(\omega\pm i\epsilon)^2-q^2}. \tag{5.42}$$

In Eq.(5.38), the imaginary contribution comes from the medium dependent term of the retarded propagator and can be described as,

$$\Im D^R_{ij}(Q) = -\frac{2\Im\Pi^{\|}_R}{(Q^2-\Re\Pi^{\|}_R)^2+(\Im\Pi^{\|}_R)^2}P^{\|}_{ij}(Q), \tag{5.43}$$

where $\Re\Pi^{\parallel}_{R}(Q)$ and $\Im\Pi^{\parallel}_{R}(Q)$ are the real and the imaginary parts of retarded self energy. Similar to the case of gluonic contribution, the angular integration in Eq.(5.38) can be performed by employing the energy delta function, and other integrations can be evaluated numerically.

Next, we consider the quark contribution to the diffusion coefficient for the case HQ moving perpendicular to the magnetic field. Similar to Eq.5.38, the other three diffusion coefficients are given as

$$\kappa^{\parallel}_{TL;Qq} = \frac{g^2(N^2-1)}{2N}\Im\int\frac{d^4Q}{(2\pi)^4}\frac{2Tq_z^2}{\omega}\bigg(v_iA_i - A_0\bigg), \tag{5.44}$$

$$\kappa^{\parallel}_{LT;Qq} = \frac{g^2(N^2-1)}{2N}\Im\int\frac{d^4Q}{(2\pi)^4}\frac{2Tq_x^2}{\omega}\bigg(v_iA_i - A_0\bigg), \tag{5.45}$$

$$\kappa^{\parallel}_{TT;Qq} = \frac{g^2(N^2-1)}{2N}\Im\int\frac{d^4Q}{(2\pi)^4}\frac{2Tq_y^2}{\omega}\bigg(v_iA_i - A_0\bigg). \tag{5.46}$$

An explicit form of term contributing to the diffusion coefficients is presented in appendixA.3 The total diffusion coefficients can be obtained by

$$\kappa^{\parallel}_{LL} = \kappa^{\parallel}_{LL;Qg} + \kappa^{\parallel}_{LL;Qq}, \tag{5.47}$$

$$\kappa^{\parallel}_{TT} = \kappa^{\parallel}_{TT;Qg} + \kappa^{\parallel}_{TT;Qq}, \tag{5.48}$$

$$\kappa^{\perp}_{LT} = \kappa^{\perp}_{LT;Qg} + \kappa^{\perp}_{LT;Qq}, \tag{5.49}$$

$$\kappa^{\perp}_{TL} = \kappa^{\perp}_{TL;Qg} + \kappa^{\perp}_{TL;Qq}, \tag{5.50}$$

$$\kappa^{\perp}_{TT} = \kappa^{\perp}_{TT;Qg} + \kappa^{\perp}_{TT;Qq}. \tag{5.51}$$

As we have observed that the diffusion coefficients are highly anisotropic with the inclusion of the magnetic field for the case of finite veclocity of HQ.

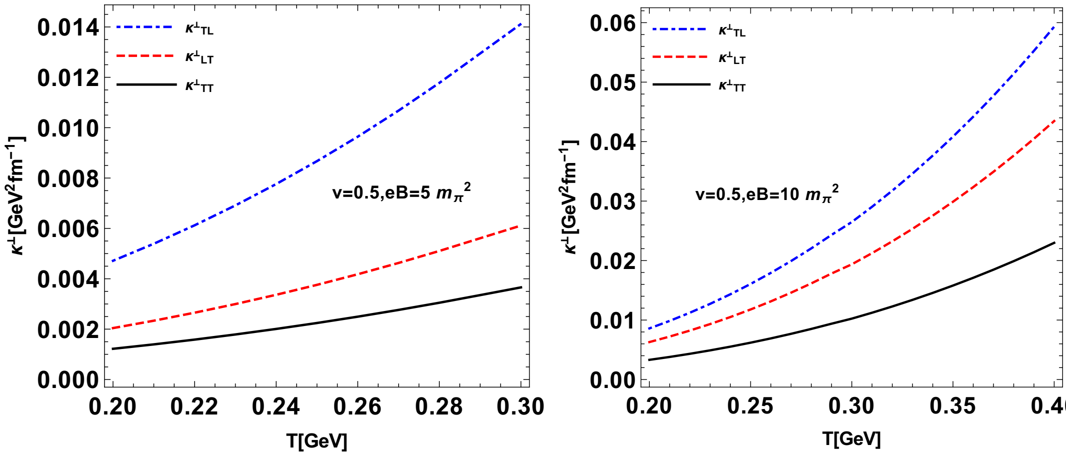

Figure 5.3: Diffusion coefficient ($\kappa^{\perp}$) for HQ moving along **x**-axis for $m = 20$ MeV, $eB = 5m_\pi^2, 10m_\pi^2$ and $v = 0.5$

5.2 Results and discussions

We discuss here the variation of different HQ anisotropic diffusion coefficient in a magnetized QGP medium as a function of HQ velocity and temperature. For the quantitative analysis, we consider QCD coupling constant $\alpha_s = 0.3$, HQ mass $M = 1.2$ GeV, light quark mass $m = 0.02$ GeV and quark flavor $N_f = 2$.

In Fig.(5.3), we have shown the variation of $\kappa^{\perp}$, *i.e.*, the momentum diffusion for the case of HQ moving perpendicular to the magnetic field as a function of temperature for $eB = 5m_\pi^2$ and $eB = 10m_\pi^2$, where m_π is pion mass. We have considered here HQ motion to be along **x**-axis. All three components of $\kappa^{\perp}$ increase with temperature and magnetic field. It is observed that the component of the coefficient $\kappa^{\perp}$ in the direction of the magnetic field (here, **z**-axis, *i.e.*, transverse to the direction of motion in this case) $\kappa^{\perp}_{TL}$ is dominant in comparison with diffusion along the transverse direction to the magnetic field and we have $\kappa^{\perp}_{TL} > \kappa^{\perp}_{LT} > \kappa^{\perp}_{TT}$.

In Fig.(5.4), the temperature dependence of $\kappa^{\parallel}$ is depicted for $v = 0.5$ at $eB = 5m_\pi^2$ and $eB = 10m_\pi^2$. Here, both the magnetic field and HQ velocity are along **z**-axis. We observe that the HQ momentum diffusion in the plane transverse to the magnetic field (xy plane) is larger than the diffusion along the magnetic field, *i.e.*, $\kappa^{\parallel}_{TT} \gg \kappa^{\parallel}_{LL}$ for all ranges of temperature considered here. For the case of

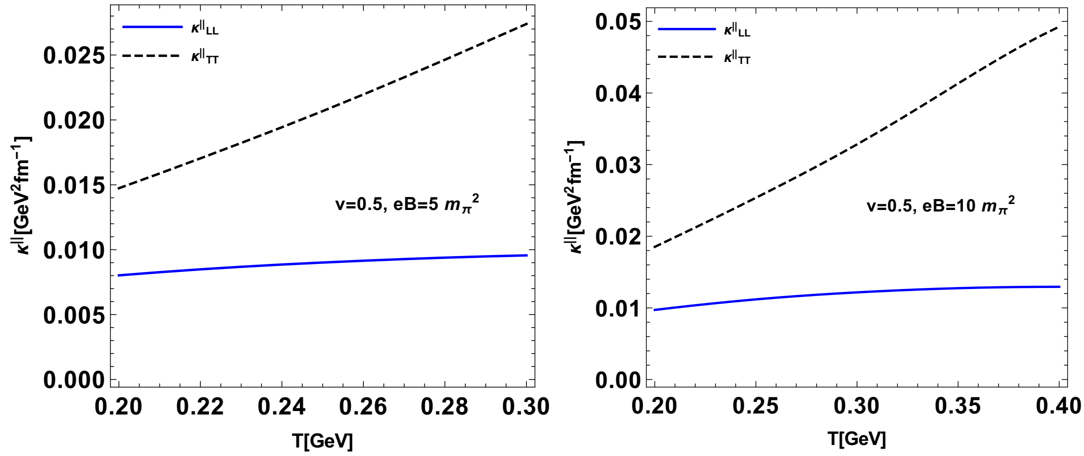

Figure 5.4: Diffusion coefficient ($\kappa^{\|}$) for HQ moving along $\mathbf{z}$-axis for $m = 20$ MeV, $eB = 5m_\pi^2, 10m_\pi^2$ and $v = 0.5$

the static limit of HQ ($\mathbf{v} = 0$), similar results have been obtained in Ref. [144, 187]. The component $\kappa^{\|}_{TT}$ has a strong dependence on temperature, on the other hand, $\kappa^{\|}_{LL}$ shows a weak dependence on the temperature. This behavior is in contrast with the case of $\kappa^{\perp}$ case where the diffusion along the magnetic field is dominant. Numerically it is observed that the Coulomb scattering terms dominate over the Compton scattering ones for the temperatures and the magnetic field considered here.

In the left of Fig.(5.5), the variation of $\kappa^{\perp}$ as a function of HQ velocity is shown. All three diffusion coefficients increase with an increase in the HQ velocity. However, $\kappa^{\perp}_{TT}$ has a very weak dependence on the HQ velocity. Out of three diffusion coefficients, $\kappa^{\perp}_{TL}$ is the dominant, *i.e.*, $\kappa^{\perp}_{TL} \gg \kappa^{\perp}_{LT}, \kappa^{\perp}_{TT}$ for all ranges of the HQ velocity. In the right of Fig.(5.5), diffusion coefficients, $\kappa^{\|}_{LL}$ and $\kappa^{\|}_{TT}$, are plotted as a function HQ velocity. Similar to the case of $v = 0$ (static limit) in Ref. [144], diffusion in the transverse direction is always larger than the diffusion along the longitudinal direction for all values of v. Apart from this, both $\kappa^{\|}_{TT}$ and $\kappa^{\|}_{LL}$ have a similar dependence on the HQ velocity.

The anisotropic HQ drag coefficients in the non-relativistic (NR) limit can be estimated by using the dissipation fluctuation theorem as,

$$\eta^{\|}_D = \frac{\kappa^{\|}}{2MT}, \tag{5.52}$$

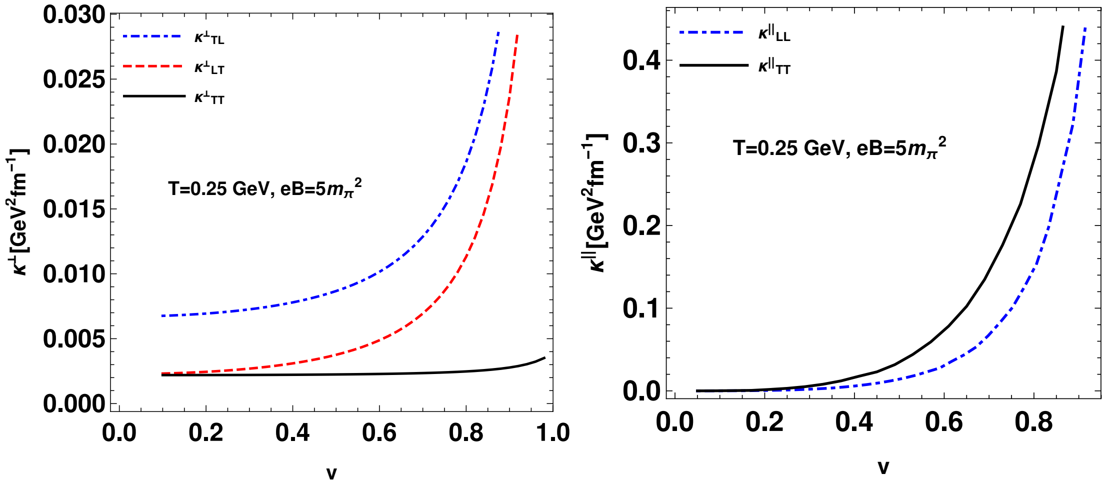

Figure 5.5: Diffusion coefficient ($\kappa^{\perp}, \kappa^{\|}$) as a function of HQ velocity for $eB = 5m_{\pi}^2$ and $T = 0.25$ GeV.

and

$$\eta_D^{\perp} = \frac{\kappa^{\perp}}{2MT}. \tag{5.53}$$

From Fig.(5.3), it can be observed that for the case of HQ moving perpendicular to the magnetic field, the drag parallel to $\mathbf{B}$ and perpendicular to $\mathbf{v}$ is the dominant one, *i.e.*, $\eta^{\perp}_{D;TL} > \eta^{\perp}_{D;LT}, \eta^{\perp}_{D;TT}$ for a given value of v. In this case, the HQ is dragged more in the direction of the magnetic field in comparison with the direction along its motion, and direction transverse to both the magnetic field and HQ motion. This anisotropic nature of drag forces to the HQ in the magnetized medium may generate an additional contribution to the flow coefficients, *i.e.*, directed flow and elliptic flow, of HQs. For the case of HQ moving parallel to the magnetic field, the drag perpendicular to the magnetic field is the dominant one, *i.e.*, $\eta^{\|}_{D;TT} > \eta^{\|}_{D;LL}$. This implies that HQ is more dragged in the plane perpendicular to the magnetic field (here, xy-plane) in the case of $\mathbf{v}\|\mathbf{B}$, which may generate anisotropic flow coefficients. The relative magnitudes of the drag and the diffusion coefficients quantify the anisotropic nature of the transport coefficients. With an increase in the magnetic field in the LLL approximation, the drag/diffusion coefficients increase in magnitude, while the relative trend of the coefficients still remains the same.

5.3 Summary

The anisotropic diffusion and drag coefficients of HQ beyond the static limit have been computed in a constant (along the $\mathbf{z}$-axis) magnetic field background, at leading order in the QCD coupling constant. In the medium, the HQ makes multiple collisions with the thermal partons, *i.e.*, light quarks and gluons, and the process is akin to the Brownian motion. The magnetic field is assumed to be strong such that the condition $\sqrt{eB} \gg T$ is satisfied, and the dynamics of light quarks are restricted in the LLL. Further, it is also assumed that $M \gg \sqrt{eB}$, so that HQ is not directly affected by the magnetic field due to its large mass. To study the diffusion of HQ, the momentum transfer in the collision of HQ and the thermal partons is assumed to be small.

It is observed that there can be total five momentum diffusion coefficients of HQ in the medium, depending on the orientation of its motion and magnetic field. In the case of the HQ motion along the direction of the magnetic field, $\mathbf{v} \parallel \mathbf{B}$, the coefficients $\kappa_{LL}^{\parallel}$ and $\kappa_{TT}^{\parallel}$ quantify the momentum diffusion along $\hat{z}$ direction and diffusion in the xy plane, *i.e.*, perpendicular to the plane containing magnetic field, respectively. Out of these two, diffusion along the direction of the magnetic field is smaller than the diffusion transverse to the direction of the magnetic field, *i.e.*,

$$\frac{\kappa_{LL}^{\parallel}}{\kappa_{TT}^{\parallel}} \ll 1. \tag{5.54}$$

In the strong field limit, the Coulomb scattering contribution to $\kappa^{\parallel}$ is observed to be dominant over the contribution arising from the Compton scattering of HQ and gluon.

Similarly, there are three diffusion coefficients for the case of HQ moving transverse to the direction of the magnetic field *i.e.*, $\mathbf{v} \perp \mathbf{B}$ denoted as $\kappa_{TL}^{\perp}, \kappa_{LT}^{\perp}, \kappa_{TT}^{\perp}$. In this case, diffusion in the direction transverse to velocity and parallel to $\mathbf{B}$ is dominant in comparison with other components and we observe,

$$\frac{\kappa_{TT}^{\perp}}{\kappa_{LT}^{\perp}}, \frac{\kappa_{LT}^{\perp}}{\kappa_{TL}^{\perp}}, \frac{\kappa_{TT}^{\perp}}{\kappa_{TL}^{\perp}} \ll 1. \tag{5.55}$$

The relative magnitudes of the diffusion coefficients suggest the anisotropic behavior of the momentum broadening. Further, in the non-relativistic limit, the drag coefficient can be estimated by using the *dissipation-fluctuation theorem*. Similar to the diffusion coefficients, there are five drag coefficients, and the relative magnitude of the drag coefficient suggests the anisotropic drag force on HQ. For HQ moving parallel to the magnetic field, our observation is qualitatively consistent with the results of Ref. [144] in the static limit, *i.e.*,

$$\frac{\eta^{\parallel}_{D;LL}}{\eta^{\parallel}_{D;TT}} \ll 1. \tag{5.56}$$

It seems that the outcome as in Eq.(5.56) is universal, *i.e.*, true in both the static and non-static limits. Similarly, for the case of HQ moving perpendicular to the magnetic field, the relative magnitudes of the drag coefficients satisfy,

$$\frac{\eta^{\perp}_{D;TT}}{\eta^{\perp}_{D;LT}}, \frac{\eta^{\perp}_{D;LT}}{\eta^{\perp}_{D;TL}}, \frac{\eta^{\perp}_{D;TT}}{\eta^{\perp}_{D;TL}} \ll 1, \tag{5.57}$$

and indicate the anisotropic drag force in different directions. The trend in Eq.(5.57) is in line with the results of the drag coefficient in an anisotropic QGP in Ref. [225]. The dependence of the magnetic field and HQ velocity on the momentum diffusion coefficients have been explored in the analysis.

We have investigated the anisotropic nature of the momentum diffusion and drag forces arising from the magnetic field considering the finite velocity of HQ. The anisotropic transport coefficients can be used as input parameters for the estimation of HQ flow coefficients in the magnetized medium. It may be noted that HQ directed flow v_1, is identified as a novel observable to probe the initial electromagnetic field produced in high energy collisions. The recent LHC measurement [193], along with the RHIC findings [192], on the D-meson flow coefficient v_1, give the indications of the strong electromagnetic field produced in high energy heavy-ion collisions. However, to compute the HQ directed flow, one needs to take into account the effect of electromagnetic field on HQ transport coefficients as well, which has been ignored in the previous calculations [145]. Heavy meson nuclear suppression factor and elliptic flow are the other experimentally measured observables that can be affected by the anisotropic HQ transport coefficient due to the presence of the electromagnetic field. The present investigation is limited to the strong field case of including LLL for the light quarks. For the case of the magnetic field of the order of the temperature *i.e.*, $eB \sim T^2$ higher Landau levels may give significant contributions to the transport coefficients. So far, we have been discussing the magnetic field effects on HQ. In next chapter, we shall investigate the non-perturbative effects originating from confinement and chiral symmetry breaking on HQ transport properties.

CHAPTER 6

Heavy quark diffusion in Polyakov loop medium

Experimental HIC programs at RHIC and LHC indicate the production of a liquid-like phase (QGP) of the matter, having a remarkably small value of shear viscosity to entropy density ratio, $\eta/s \approx 0.1$, where quarks and gluons govern the properties of the system [226, 227]. To characterize the properties of QGP, penetrating and well-calibrated probes are essential. In this context, the heavy quarks (HQs) [228, 224, 229, 218, 85, 84, 217], mainly charm and bottom, play a crucial role since they do not constitute the bulk part of the matter owing to their larger mass compared to the temperature created in heavy-ion collisions. Also, thermal production of heavy quarks is negligible, due to their large masses, in the QGP within the range of temperatures that can be achieved in RHIC and LHC colliding energies.

Heavy quarks are exclusively created in hard processes that can be handled by perturbative QCD calculations [230], and therefore, their initial distribution is theoretically known and can be verified by experiment. They interact with the plasma constituents, the light quarks, and the gluons, but their initial spectrum is too hard to come to equilibrium with the medium. Therefore, the high momentum heavy quarks spectrum carries the information of their interaction with the plasma particles during the expansion of the hot and dense fireball and on the plasma properties. Since the light quark, anti-quark, and gluons are thermalized, the heavy quark interaction with the light constituents leads to a Brownian motion, which can be treated with the framework of a Fokker Plank equation. Thus the interaction information of the heavy quark in QGP is contained in the drag and diffusion coefficients of the heavy quark. The resulting momentum distribution of the heavy mesons which depend upon the drag and diffusion coefficients get reflected in the nuclear modification factor (R_{AA}), which is measured experimentally.

Initially, pQCD predicted a small nuclear suppression factor [231, 232], R_{AA}, in nucleus-nucleus collisions in comparison with the proton-proton collisions. The first experiment data [233, 222, 223] on heavy quarks suggest a strong nuclear suppression factor that can not be explained within the pQCD framework. Several attempts [100, 209, 210, 234, 235, 221, 214, 236, 93, 237, 238, 239, 240, 241, 242, 243, 220, 244] have been made by different groups to study the heavy quarks interaction in QGP going beyond pQCD to include the nonperturbative effects. Quasi-particle models enjoy considerable success in describing heavy quark dynamics in QGP [235, 93].

In the present study, we are attempting to study heavy quark transport coefficient in QGP including the non-perturbative effects through a background gauge field (the Polyakov loop background) and chiral condensate. The Polyakov loop manifests itself in the transport coefficient in two ways. Firstly, through the Debye mass that enters in calculating the scatterings of the heavy quark off of light thermal partons. It also enters non-trivially on the statistical distribution of the light partons in a non-perturbative medium. Indeed, both the effects arising from the Polyakov loop and quark condensate are important near the transition temperature. The value of the normalized Polyakov loop is about half its asymptotic value at the critical temperature in different low energy effective models like Polyakov Nambu Jona Lasinio (PNJL) models [62, 245, 246], or Polyakov quark meson(PQM) [247, 248, 249, 250, 251, 252] models. Similarly, the chiral condensate remains significantly finite at temperatures around the critical temperature. Effects of Polyakov loop has been studied in various contexts such as dilepton and photon production [253], heavy quark energy loss [254]. Significant effects have been found by including these non-perturbative features. To estimate the quark masses and the Debye mass, we, therefore, need the value of the Polyakov loop as a function of temperature. We do so in two different approaches. One is phenomenological in the sense that we take Polyakov loop value as a function of temperature from PQM model. The other approach is to take the same from lattice QCD simulations.

This chapter is organized as follows, in Sec. 6.1 we discuss the Fokker-Plank framework for calculating drag and diffusion of heavy quarks by employing Boltzmann equation in soft momentum exchange between heavy quark and bulk medium [97]. Sec. 6.3 describes the non-perturbative effects (Polyakov loop and quark mass) on the Debye mass and light quark thermal mass. Such an effect can be important near the transition temperature where the light quark condensates could still be relevant. In Sec. 6.4, we discuss the relevant scattering amplitudes within the matrix model of semi-QGP. The drag and the diffusion coefficients are evaluated in Sec. (7.3) where the behavior of these transport coefficients as a function of temperature as well as momentum is also discussed. Finally, in Sec. (7.4), we summarise the results and present a possible outlook.

6.1 HQ diffusion in QGP: Fokker-Plank framework

The Brownian motion of HF particles in the bulk medium is described by the Fokker-Plank equation where the interactions of heavy quark with the bulk of light quarks and gluons are encoded in the transport coefficient. Assuming that HF quark of momentum $\boldsymbol{p}$ is traveling in a medium of light quark and gluon, the Boltzmann equation for phase-space distribution f_Q of heavy quark can be written as [97]

$$\left[\frac{\partial}{\partial t} + \frac{\boldsymbol{p}}{E_p}\frac{\partial}{\partial \boldsymbol{x}} + \boldsymbol{F}\frac{\partial}{\partial \boldsymbol{p}}\right] f_Q(\boldsymbol{p}, \boldsymbol{x}, t) = C[f_Q], \tag{6.1}$$

where $\boldsymbol{F}$ is the force due to external mean-field such as chromo electric or magnetic fields present in the initial stages of the heavy ion-collision , $E_p = \sqrt{m_Q^2 + \boldsymbol{p}^2}$ is the energy of heavy quark with mass m_Q and $C[f_Q]$ is the collision integral. Neglecting the mean-field effects, Eq[6.1] reduces to

$$\frac{\partial}{\partial t} f_Q(\boldsymbol{p}, t) = C[f_Q]. \tag{6.2}$$

On the right-hand side of Eq.[6.2], collision integral in terms of collision rate which change the momentum of HF quark from $\boldsymbol{p}$ to $\boldsymbol{p} - \boldsymbol{k}$ is written as

$$C[f_Q] = \int d^3k[w(\boldsymbol{p}+\boldsymbol{k}, \boldsymbol{k}) f_Q(\boldsymbol{p}+\boldsymbol{k}) - w(\boldsymbol{p}, \boldsymbol{k}) f_Q(\boldsymbol{p})], \tag{6.3}$$

where w is the transition rate of heavy quark colliding with heat bath particles of momentum $\boldsymbol{k}$. The first term in Eq.[6.3] is the gain term that describes the transition of HF quark from a state of momentum $\boldsymbol{p}+\boldsymbol{k}$ to momentum state $\boldsymbol{p}$ while the loss term (second term) represents the scattering out from the momentum state $\boldsymbol{p}$. Assuming the scatterings of HF quark with the bulk medium partons is dominated by small momentum transfer i.e., $|\boldsymbol{k}| \ll |\boldsymbol{p}|$, the distribution function of HQ and transition rate can be expanded up to second order with respect to $\boldsymbol{k}$ i.e.,

$$\begin{aligned} w(\boldsymbol{p}+\boldsymbol{k}, \boldsymbol{k}) f_Q(\boldsymbol{p}+\boldsymbol{k}) &\simeq w(\boldsymbol{p}, \boldsymbol{k}) f_Q(\boldsymbol{p}) + \boldsymbol{k}\frac{\partial}{\partial \boldsymbol{p}}[w(\boldsymbol{p}, \boldsymbol{k}) f_Q(\boldsymbol{p})] + \frac{1}{2} k_i k_j \\ &\times \frac{\partial^2}{\partial p_i \partial p_j}[w(\boldsymbol{p}, \boldsymbol{k}) f_Q(\boldsymbol{p})]. \end{aligned} \tag{6.4}$$

With this approximation the collision integral simplifies to

$$C[f_Q] = \int d^3k \left[k_j \frac{\partial}{\partial p_j} + \frac{1}{2} k_i k_j \frac{\partial^2}{\partial p_i \partial p_j} \right] w(\boldsymbol{p}, \boldsymbol{k}) f_Q(\boldsymbol{p}). \tag{6.5}$$

The function w can be expressed in terms of the cross-section for scattering processes in the heat bath. For, scattering of HQ with momentum $\boldsymbol{p}$ with the bulk medium-light thermal parton with momentum $\boldsymbol{q}$, one finds

$$w(\boldsymbol{p}, \boldsymbol{k}) = \gamma_l \int \frac{d^3q}{(2\pi)^3} f(q)_l |\boldsymbol{v}_{rel}| \frac{d\sigma}{d\Omega}(\boldsymbol{p}, \boldsymbol{q} \to \boldsymbol{p}-\boldsymbol{k}, \boldsymbol{q}+\boldsymbol{k}), \tag{6.6}$$

where $f(q)_l$ is Fermi-Dirac/or Bose-Einstein distribution function of light thermal partons and γ_l is degeneracy factor which is $\gamma_q = 6$ for quarks and $\gamma_g = 16$ for gluons. Boltzmann equation Eq.[6.2] can be approximated as Fokker-Plank equation

$$\frac{\partial}{\partial t} f_Q(\boldsymbol{p}, t) = \frac{\partial}{\partial p_i}\bigg(A_i(\boldsymbol{p}) f_Q(\boldsymbol{p}, t) + \frac{\partial}{\partial p_j} B_{ij}(\boldsymbol{p}) f_Q(\boldsymbol{p}, t)\bigg). \tag{6.7}$$

Here A_i and B_{ij} are drag and diffusion coefficient and are given as

$$A_i(\boldsymbol{p}) = \int d^3k w(\boldsymbol{p}, \boldsymbol{k}) k_i \tag{6.8}$$

$$B_{ij}(\boldsymbol{p}) = \frac{1}{2}\int d^3k w(\boldsymbol{p}, \boldsymbol{k}) k_i k_j. \tag{6.9}$$

For an isotropic heat bath at local thermal equilibrium one may define [255]

$$A_i(\boldsymbol{p}) = A(\boldsymbol{p}) p_i, \tag{6.10}$$

$$B_{ij}(\boldsymbol{p}) = B_0(\boldsymbol{p}) P_{ij}^{\parallel} + B_1(\boldsymbol{p}) P_{ij}^{\perp}, \tag{6.11}$$

where $P_{ij}^{\parallel}$ and $P_{ij}^{\perp}$ are longitudinal and transverse projection operators defined as

$$P_{ij}^{\parallel} = \frac{p_i p_j}{|\boldsymbol{p}|^2}\,, \qquad P_{ij}^{\perp} = \delta_{ij} - \frac{p_i p_j}{|\boldsymbol{p}|^2}. \tag{6.12}$$

For a process $lQ \rightarrow lQ$ (where l stands for light quarks and gluon) the drag and diffusion coefficients of HQ in the plasma of light quarks and gluons are given by the scalar integral of form

$$\begin{aligned} \langle X(\boldsymbol{p'})\rangle &= \frac{1}{2E_p}\int \frac{d^3q}{(2\pi)^3 2E_q}\int \frac{d^3p'}{(2\pi)^3 2E_{p'}}\int \frac{d^3q'}{(2\pi)^3 2E_{q'}} |\mathcal{M}|^2 \\ &\times (2\pi)^4 \delta^4(p + q - p' - q') f_l(q)(1 \pm f_l(q)) X(\boldsymbol{p'}), \end{aligned} \tag{6.13}$$

where $l = q, \bar{q}, g$. In the present study, we evaluate scattering amplitude for relevant $2 \rightarrow 2$ processes within the matrix model which make the matrix element squared color dependent. So in the presence of a background gauge field Eq.(6.13) becomes

$$\begin{aligned}\langle X(\boldsymbol{p'})\rangle &= \frac{1}{2E_p}\int\frac{d^3q}{(2\pi)^3 2E_q}\int\frac{d^3p'}{(2\pi)^3 2E_{p'}}\int\frac{d^3q'}{(2\pi)^3 2E_{q'}}\Bigg(\sum_{a,e}|\mathcal{M}_{qQ}|^2_{ab}f_a(q)(1\\ &- f_e(q')) + \sum_{e,f,g,h}|\mathcal{M}_{gQ}|^2_{efgh}f_{ef}(q)(1+f_{gh}(q'))\Bigg)(2\pi)^4\delta^4(p+q-p'-q')\\ &\times X(\boldsymbol{p'}), \end{aligned}\tag{6.14}$$

where a, e are color indices of incoming and outgoing light quark and ef, gh are color indices for incoming and outgoing gluon that interact with HQ, $|\mathcal{M}_{qQ}|^2_{ab}$ and $|\mathcal{M}_{gQ}|^2_{efgh}$ are matrix element squared respectively for the processes $q^aQ^c \to q^bQ^d$ and $g^{ef}Q^a \to g^{gh}Q^b$. In the notation as written in Eq.[6.14], the drag and diffusion coefficients are written as

$$A(\boldsymbol{p}) = \langle 1\rangle - \frac{\langle \boldsymbol{p}\cdot\boldsymbol{p'}\rangle}{|\boldsymbol{p}|^2} \tag{6.15}$$

$$B_0(\boldsymbol{p}) = \frac{1}{4}\Bigg(\langle|\boldsymbol{p'}|^2\rangle - \frac{\langle(\boldsymbol{p}\cdot\boldsymbol{p'})^2\rangle}{|\boldsymbol{p}|^2}\Bigg) \tag{6.16}$$

$$B_1(\boldsymbol{p}) = \frac{1}{2}\Bigg(\frac{\langle(\boldsymbol{p}\cdot\boldsymbol{p'})^2\rangle}{|\boldsymbol{p}|^2} - 2\langle\boldsymbol{p}\cdot\boldsymbol{p'}\rangle + |\boldsymbol{p}|^2\langle 1\rangle\Bigg). \tag{6.17}$$

In the presence of a non-trivial Polyakov loop background, apart from the matrix elements, the distribution functions also become color-dependent. We evaluate these scattering amplitudes within the matrix model of semi QGP, which we discuss in the next section.

6.2 Semi-QGP

At high temperature, the density of colored particles like quarks and gluon are large and can be calculated using perturbative QCD. However, at low temperature, colored particles are statistically suppressed and are measured by the small value of Polyakov loop e.g., at chiral cross-over temperature $T_c \sim 170$ MeV, $\phi = 0.2$[26] which is way smaller from its asymptotic value i.e., $\phi = 1$. Because of the suppression of colored particles, the region near chiral cross-over is termed as semi-QGP

[94]. Semi QGP is characterized by the Polyakov loop as defined in Eq.(6.20). The lagrangian of the matrix model is same as that of QCD [256]. In the mean-field approximation, we take the constant background field as $A_\mu^0 = \frac{1}{g}\delta_{\mu 0}Q^a$ with $Q^a = 2\pi q^a T$. Since A_0 is traceless so sum over Q's vanishes i.e., $\sum_a Q^a = 0$. For an $SU(3)$ group, $Q^a = (-Q^i, -Q^{i-1}, ..0, Q^{i-1}, Q^i)$, where $i = N/2$ if N is even and $(N-1)/2$ if N is odd. In the temporal direction, the Wilson line is written as

$$P = \mathcal{P} \exp\left(ig \int_0^\beta d\tau A_0(x_0, \boldsymbol{x})\right) \tag{6.18}$$

where $\mathcal{P}$ stands for the ordering of imaginary time and τ is imaginary time. Polyakov loop, which is the trace of Wilson line, in the constant background gauge field can be written as

$$\phi = \frac{1}{N}\sum_{a=1}^{N} \exp(i2\pi q^a). \tag{6.19}$$

For an $SU(3)$ group, where $q^a = (-q, 0, q)$ Eq.[6.19] is simplified to

$$\phi = \frac{1}{3}(1 + 2\cos(2\pi q)). \tag{6.20}$$

For the calculational purpose, we shall use double line notation which is quite useful in the matrix model of semi QGP. In the double line basis, quark carries one color index say $a = 1, 2, .., N$ and gluons carry double index say $ab = 1, 2, .., N^2$. For $SU(N)$ group such N^2 pairs lead to N^2 generators and the basis is over-complete by one generator. The over-complete basis is compensated by introducing the projection operator defined as [256, 257, 258]

$$\mathcal{P}^{ab}_{cd} = \mathcal{P}_{ba;cd} = \mathcal{P}^{ab;dc} = \delta^a_c \delta^b_d - \frac{1}{N}\delta^{ab}\delta_{cd} \tag{6.21}$$

hence the generator is given by

$$(t^{ab})_{cd} = \frac{1}{\sqrt{2}}\mathcal{P}^{ab}_{cd}. \tag{6.22}$$

The trace over two generators doesn't vanish but rather is again a projection operator i.e.,

$$Tr(t^{ab}t^{cd}) = \frac{1}{2}\mathcal{P}^{abcd}. \tag{6.23}$$

This is due to the presence of extra generator as compared to generators in an orthonormal basis. The structure constant of the group in the double line basis is given by

$$f^{ab,cd,ef} = \frac{i}{\sqrt{2}}(\delta^{ad}\delta^{cf}\delta^{eb} - \delta^{af}\delta^{cb}\delta^{ed}). \tag{6.24}$$

The background gauge field acts as an imaginary chemical potential for colored particles so the statistical distribution function of quark/anti-quark and the gluon are

$$f_a(E) = \frac{1}{e^{\beta(E-iQ_a)}+1}, \qquad \tilde{f}_a(E) = \frac{1}{e^{\beta(E+iQ_a)}+1}, \tag{6.25}$$

$$f_{ab}(E) = \frac{1}{e^{\beta(E-i(Q_a-Q_b))}-1}, \tag{6.26}$$

where the single and double indices are for quark/antiquark and gluon. For a background field and given Q^a these distribution functions are complex so are unphysical. Physical meaning comes when one integrates over all distributions of Q^a. Let us note that the quark distribution function involves only one color index because these are represented in fundamental representation. For gluons, the adjoint representation leads to two fundamental indices. For three colors, the color averaged statistical distribution function of the gluons becomes

$$\begin{aligned} f_g(E) &= \frac{1}{3^2}\sum_{a,b=1}^{3} f_{ab}(E) = \frac{1}{9}\Bigg(\frac{3}{e^{\beta E}-1} + \frac{e^{\beta E}(6\phi-2)-4}{1+e^{2\beta E}+e^{\beta E}(1-3\phi)} \\ &+ \frac{e^{\beta E}(9\phi^2-6\phi-1)-2}{1+e^{2\beta E}+e^{\beta E}(1+6\phi-9\phi^2)}\Bigg). \end{aligned} \tag{6.27}$$

A comment regarding the color dependent distribution function may be in order. Let us note that, for the color dependent gluon distribution functions, the diagonal ones i.e., $f_{11}(E)$, $f_{22}(E)$, $f_{33}(E)$ are real while the off diagonal ones i.e., $f_{ij}(E)$ and $f_{ji}(E)$ are complex conjugate of each other. When the color sum is performed the imaginary parts always cancel out leading to the sum to be real. This cancellation of imaginary parts also always occur for transport coefficients even with the color dependent masses and lead to the transport coefficient that are always real. The color averaged distribution functions of the quark/anti-quark is

$$f_{q/\bar{q}}(E) = \frac{1}{3}\sum_{a=1}^{3} f_a(E) = \frac{1}{3}\sum_{a=1}^{3} \tilde{f}_a(E) = \frac{\phi e^{-\beta E} + 2\phi e^{-2\beta E} + e^{-3\beta E}}{1 + 3\phi e^{-\beta E} + 3\phi e^{-2\beta E} + e^{-3\beta E}}. \quad (6.28)$$

Similar to color averaged distribution function $f_g(E)$ the color averaged distribution function of quark is real due to the cancellation of imaginary parts of $f_1(E)$ and $f_3(E)$. It may be noted that for pure gluon case, $\phi = 1$ in the confined phase and $\phi = 0$ in the deconfined phase. This leads to the gluon distribution function

$$f_g(E) = \frac{1}{e^{3\beta E} - 1}, \quad (6.29)$$

in the confined phase and

$$f_g(E) = \frac{1}{e^{\beta E} - 1}, \quad (6.30)$$

in the deconfined phase. In the presence of quarks, one does not have a rigorous order parameter for deconfinement, however in $\phi = 0$ case the color averaged quark/anti-quark distribution reduces to

$$f_{q/\bar{q}}(E) = \frac{1}{e^{3\beta E} + 1} \quad (6.31)$$

so that quark are suppressed statistically. In the perturbative limit i.e., $\phi = 1$ it becomes

$$f_{q/\bar{q}}(E) = \frac{1}{e^{\beta E} + 1}. \quad (6.32)$$

The color averaged distribution function of quark/anti-quark as given in Eq.(6.28) is exactly the same as that in PQM model within mean field approximation [252]. For the computation of Debye and thermal mass, we use double line notation [257, 258] which is more convenient here.

In the imaginary time formalism, similar to the case of no background field, the resummed gluon propagator in the presence of a static background gauge field is given as[259]

$$D\mu\nu; abcd(K) = P^L_{\mu\nu}\frac{k^2}{K^2}D^L_{abcd}(K) + P^T_{\mu\nu}D^T_{abcd}(K), \quad (6.33)$$

where $P^T_{\mu\nu} = g_{\mu i}\left(-g^{ij} - \frac{k^i k^j}{K^2}\right)g_{j\nu}$ and $P^L_{\mu\nu} = -g_{\mu\nu} + \frac{k_\mu k_\nu}{K^2} - P^T_{\mu\nu}$ are the longitudinal and the transverse projection operators. The longitudinal and the transverse gluon propagators are written as

$$D^L_{\mu\nu;abcd}(K) = \left(\frac{i}{K^2+F}\right)_{abcd}, \tag{6.34}$$

$$D^T_{\mu\nu;abcd}(K) = \left(\frac{i}{K^2-G}\right)_{abcd}, \tag{6.35}$$

where

$$F = 2M^2\left(1 - \frac{y}{2}\ln\left(\frac{y+1}{y-1}\right)\right), \tag{6.36}$$

$$G = M^2\left(y^2 + \frac{y(1-y^2)}{2}\ln\left(\frac{y+1}{y-1}\right)\right), \tag{6.37}$$

with $y = \frac{k_0}{|\boldsymbol{k}|}$ and $M^2 = (M^2)_{abcd}$ is the thermal mass of the gluon. For the drag and the diffusion of HQ studied here, the momentum transfer is small so only longitudinal propagator contributes to the squared matrix elements[255, 100].

6.3 Thermal and Debye masses in Polyakov loop background

In this section, we shall estimate the non-perturbative Debye screening mass and quark thermal mass in a nontrivial Polyakov loop background to be used in the estimation of the drag and diffusion coefficients using Eqs.(6.15) and (6.16). For the thermal masses of light quark and gluon, we also include the possible effects from a finite mass of the light quarks which can arise from a nonvanishing scalar quark- antiquark condensate. For the case of massless light quark, the thermal masses are discussed in Ref.[253, 254, 259, 256].

6.3.1 Quark loop contribution to Debye mass

Generally, Debye mass (m_D) is defined through the pole of effective propagator in the static limit i.e., $\omega = 0, \mathbf{p} \to 0$ and is related to the time-like component of gluon self-energy $\Pi_{44}(\omega = 0, \mathbf{p} \to 0)$ [5]. It turns out that, in the presence of a static background field, apart from the usual T^2 dependent term similar to as in perturbative HTL calculations, there is an additional T^3 dependent contribution to the gluon self energy. The later component arises because the background field induces a color current which couples to the gluon. While the T^2 dependent term in $\Pi_{\mu\nu}$ is transverse (i.e., $P^\mu \Pi^{\mu\nu}(P) = 0$), the T^3 dependent term is not and spoils the transversality relation which is required for the gauge invariance. Therefore, one needs an additional contribution which may be of non-perturbative origin to the gluon self energy to cancel such a term. Similar to Ref.[259], we assume that such a term exists and cancels this undesirable T^3 term. Under the assumptions taken here, it is clear that the pole (F) of the longitudinal propagator in Eq.(6.34) can be related to Π_{44} component of gluon self energy. Therefore, in the static limit, this term can be defined as Debye mass [256].

In this chapter, we shall focus only on the time like component of the gluon self energy with the assumption that T^3 dependent term is cancelled. For massless quarks, Debye mass has already been computed in Ref.[256]. We include here the effect of finite constituent quark mass in the quark loop contribution to the Debye mass. We work in the imaginary time formalism of thermal field theory for evaluating the corresponding diagrams. In this formalism, because of the boundary conditions of imaginary time, the energy of a fermion p_4 is an odd multiple of πT while that for a boson is an even multiple of πT. For calculating the Debye mass, we first evaluate the quark loop in the gluon self-energy for which the corresponding diagram is shown in Fig.(6.1), where the loop momentum four vector is written as $\tilde{K}^e_\mu = (K + \tilde{Q}_e)_\mu = (\omega_n + \tilde{Q}^e, \mathbf{k})$ with $\tilde{Q}_e = Q_e + \pi T$ In t'hooft double line notation, the polarization tensor can be written as

$$\begin{aligned}\Pi^q_{\mu\nu;b'baa'}(P,Q,m) &= g^2 N_f t^{aa'}_{ee'} t^{bb'}_{e'e} \int \frac{d^4K}{(2\pi)^4} Tr_D[\gamma_\mu(\tilde{\not{K}}_e - \tilde{\not{P}}_{bb'})\gamma_\nu \tilde{\not{K}}_e + m^2\gamma_\mu\gamma_\nu] \\ &\times \Delta(K)\Delta(P-K), \qquad (6.38)\end{aligned}$$

where $aa', bb'(e, e')$ are color indices of gluons (quark/antiquark), N_f is quark flavor number and $\Delta(K)^{-1} = (\omega_n + \tilde{Q}_e)^2 + \mathbf{k}^2 + m^2$ and

$$\Delta(P-K)^{-1} = (\omega - \omega_n + Q_{bb'} - \tilde{Q}_e)^2 + (\mathbf{p} - \mathbf{k})^2 + m^2 \qquad (6.39)$$

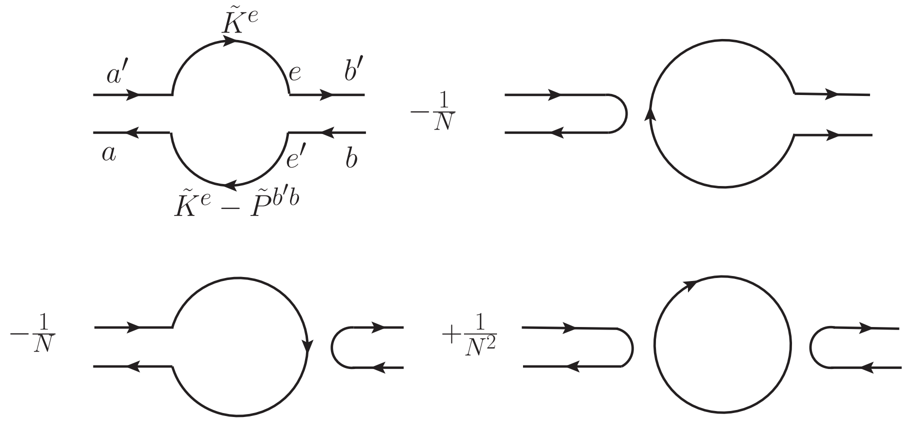

Figure 6.1: Quark loop of gluon self energy in double line notation.

with $Q_{bb'} = Q_b - Q_{b'}$, $E_k = \sqrt{\mathbf{k}^2 + m^2}$, $E_q = \sqrt{(\mathbf{p}-\mathbf{k})^2 + m^2}$, $\omega_n = (2n+1)\pi T$ and $P_4 = \omega$. Tr_D is trace in Dirac space and Q_i is the diagonal matrix in color space which is given as $Q_a = (-2\pi Tq, 0, 2\pi Tq)$ and q is related to the Polyakov loop expectation value as given in Eq.(6.20). Here, we take hard thermal loop (HTL) approximation and also assume that $m \ll T$. Thus, taking HTL limit and the trace over Dirac space, Eq.(6.38) reduces to

$$\begin{aligned} \Pi^q_{\mu\nu;b'baa'}(P,Q,m) &= g^2 N_f t^{aa'}_{ee'} t^{bb'}_{e'e} \int \frac{d^4K}{(2\pi)^4} [8(K+\tilde{Q}_e)_\mu (K+\tilde{Q}_e)_\nu - 4(K+\tilde{Q}_e)^2 \delta_{\mu\nu} \\ &- 4m^2 \delta_{\mu\nu}] \Delta(K)\Delta(P-K). \end{aligned} \tag{6.40}$$

As we are interested in calculating Debye mass for which we need time-like component (Π_{44}) of the gluon self-energy. So from here onwards, we shall proceed with this term. For this purpose, we write the integration in Eq.(6.40) as $\int \frac{d^4K}{(2\pi)^4} = T \sum\limits_{n=-\infty}^{\infty} \int \frac{d\mathbf{k}}{(2\pi)^3}$; $k_4 \equiv \omega_n = 2n\pi T$. Simplifying Eq.(6.40), we have

$$\begin{aligned} \Pi^q_{44;b'baa'}(P,Q,m) &= 4g^2 N_f t^{aa'}_{ee'} t^{bb'}_{e'e} \int \frac{d\mathbf{k}}{(2\pi)^3} T \sum_n [(-2k^2 - m^2)\Delta(K)\Delta(P-K) \\ &+ \Delta(P-K)]. \end{aligned} \tag{6.41}$$

The frequency sums in Eq.(6.41) over discrete Matsubara frequencies are somewhat involved but can be performed routinely leading to

$$\begin{aligned}
T\sum_{n=-\infty}^{\infty}\Delta(K)\Delta(P-K) &= \frac{1}{4E_kE_q}\Bigg(\frac{f(E_q+iQ2+i\omega)-f(E_k-iQ1)}{E_k-E_q+i(Q1+Q2+\omega)} \\
&+ \frac{1+f(E_k-iQ1)-f(E_q-iQ2-i\omega)}{E_k+E_q-i(Q1+Q2+\omega)} \\
&+ \frac{f(E_k+iQ1)-f(E_q-iQ2-i\omega)}{E_q-E_k+i(Q1+Q2+\omega)} \\
&+ \frac{1+f(E_k+iQ1)-f(E_q+iQ2+i\omega)}{E_k+E_q+i(Q1+Q2+\omega)}\Bigg), \quad (6.42)
\end{aligned}$$

$$T\sum_{n=-\infty}^{\infty}\Delta(P-K) = -\frac{1+f(E_q+iQ2+i\omega)+f(E_q-iQ2-i\omega)}{2E_q}, \quad (6.43)$$

where $Q2 = Q_{bb'}-\tilde{Q}_e$, $Q1 = \tilde{Q}_e$ and $f(E\pm iQ)$ is Bose-Einstein distribution function. In Eqs.(6.42) and (6.43), the term which is independent of distribution function is the vacuum contribution which can be dropped when one considers the medium dependent terms only. First and third term in Eq.(6.42) contribute to the T^3 dependent term. Such a term exists only in the presence of a background gauge field in the HTL approximations [256]. As mentioned earlier, this term spoils the transversality condition and we shall not consider this undesirable contribution. Furthermore, the T^2 dependent contributions are given by second and fourth term of Eq.(6.42) as well as by the medium dependent term in Eq.(6.43). In the static limit, the time like component of the gluon self-energy can be written as

$$\begin{aligned}
\Pi^q_{44;b'baa'}(Q,m)|_{(\omega=0,\vec{p}\to 0)} &= -4g^2N_ft^{aa'}_{ee'}t^{bb'}_{e'e}[2I_1(m,\tilde{Q}_e,Q_{bb'}-\tilde{Q}_e)+I_2(m,\tilde{Q}_e, \\
&\quad Q_{bb'}-\tilde{Q}_e)+I_3(m,Q_{bb'}-\tilde{Q}_e)], \quad (6.44)
\end{aligned}$$

where

$$\begin{aligned}
I_1(m,\tilde{Q}_e,Q_{bb'}-\tilde{Q}_e) &= \frac{T^2}{16\pi^2}\int\frac{x^4dx}{(x^2+y^2)^{\frac{3}{2}}}\Bigg(f(x,y,iq1)+f(x,y,-iq1) \\
&- f(x,y,iq2)-f(x,y,-iq2)\Bigg), \quad (6.45)
\end{aligned}$$

$$
\begin{aligned}
I_2(m,\tilde{Q}_e,Q_{bb'}-\tilde{Q}_e) &= \frac{m^2}{16\pi^2}\int\frac{x^2dx}{(x^2+y^2)^{\frac{3}{2}}}\Big(f(x,y,iq1)+f(x,y,-iq1)-f(x,y,iq2)\\
&- f(x,y,-iq2)\Big),
\end{aligned} \tag{6.46}
$$

$$
I_3(m,Q_{bb'}-\tilde{Q}_e) = \frac{T^2}{4\pi^2}\int\frac{x^2dx}{\sqrt{x^2+y^2}}\Big(f(x,y,iq2)+f(x,y,-iq2)\Big), \tag{6.47}
$$

where we have defined the dimensionless variables $x=\beta k$, $y=\beta m$ and $q1=\beta Q1$. Further, $f(x,y,iq)$'s are the Bose distribution functions in terms of these dimensionless variables as e.g.,

$$
f(x,y,iq) = \frac{1}{\exp(\sqrt{x^2+y^2}+iq)-1}. \tag{6.48}
$$

Also note that although distribution function is a complex quantity, the functions $I_1(m,\tilde{Q}_e,Q_{bb'}-\tilde{Q}_e), I_2(m,\tilde{Q}_e,Q_{bb'}-\tilde{Q}_e)$ and $I_3(m,Q_{bb'}-\tilde{Q}_e)$ are real functions. With further simplification, Π_{44} can be written as

$$
\begin{aligned}
\Pi^q_{44;b'baa'}(Q,m)|_{(\omega=0,\vec{p}\to 0)} &= -g^2N_f t^{aa'}_{e'e}t^{bb'}_{ee'}\frac{T^2}{4\pi^2}\Big[2(\mathfrak{D}(q1,y)-\mathfrak{D}(q2,y))+4\mathfrak{F}(q2,y)\\
&+ 2y^2\mathfrak{B}(Q2,y)\Big],
\end{aligned} \tag{6.49}
$$

where the dimensionless real functions $\mathfrak{D},\mathfrak{F}$ and $\mathfrak{B}$ are

$$
\mathfrak{D}(q,y) = \int\frac{x^4dx}{(x^2+y^2)^{\frac{3}{2}}}\Big(f(x,y,iq)+f(x,y,-iq)\Big), \tag{6.50}
$$

$$
\mathfrak{B}(q,y) = \int\frac{x^2dx}{(x^2+y^2)^{\frac{3}{2}}}\Big(f(x,y,iq)+f(x,y,-iq)\Big), \tag{6.51}
$$

$$
\mathfrak{F}(q,y) = \int\frac{x^2dx}{\sqrt{x^2+y^2}}\Big(f(x,y,iq)+f(x,y,-iq)\Big). \tag{6.52}
$$

In the limiting case of vanishing quark masses i.e. $y=0$, the function $\mathfrak{B}(q,y)$ do not contribute to Π^q_{44} as it is multiplied by a y^2 term while the functions $\mathfrak{D}(q,y=0)$ and $\mathfrak{F}(q,y=0)$ become equal and can be written in terms of Polylog functions $Li_2(z)$ as

$$\begin{aligned}\mathfrak{F}(q,y=0) &= \mathfrak{D}(q,y=0) = \int dx x\Big(f(x,y=0,iq)+f(x,y=0,-iq)\Big)\\ &\equiv Li_2(iq)+Li_2(-iq).\end{aligned} \tag{6.53}$$

The Polylog function $Li_2(z)$ can also be written in terms of Clausen functions $Cl_2(z)$ e.g.

$$Li_2(i2\pi q) = \frac{\pi^2}{6}(1-6q+6q^2)+iCl_2(2\pi q), \tag{6.54}$$

that has been used in Ref.[256]. In the present investigation, however, we will keep the effect of masses in Eqs(6.50), (6.51), (6.52) and integrate it numericaly to estimate the Debye mass. Generators appearing in the right side of Eq.(6.49) can be simplified by using projection operators, so that the product of two generators becomes

$$\begin{aligned}t^{aa'}_{e'e}t^{bb'}_{ee'} &= \frac{1}{2}\Bigg[\delta^{be}\delta^{b'e'}\delta^{a'e}\delta^{ae'} - \frac{1}{N}\Big(\delta^{bb'}\delta^{ee'}\delta^{a'e}\delta^{ae'}+\delta^{be}\delta^{b'e'}\delta^{aa'}\delta^{e'e}\Big)\\ &+ \frac{1}{N^2}\delta^{bb'}\delta^{ee'}\delta^{aa'}\delta^{e'e}\Bigg].\end{aligned} \tag{6.55}$$

Note that Π_{44} depends on the color of quark and gluon and has a, b, a', b' as free color indices. So we need to sum over other repeated color indices (i.e., e, e') which can be done by contracting color indices of Eq.(6.55) with that of Eq.(6.49). Using Eq.(6.55) along with Eq.(6.49) and summing over contracted color indices, gluon self energy can be written as

$$\begin{aligned}\Pi^q_{44;b'baa'}(Q,m)|_{(\omega=0,\vec{p}\to 0)} &= -g^2N_f\frac{T^2}{4\pi^2}\Bigg[\delta_{ab}\delta_{a'b'}\Big(\mathfrak{D}(\tilde{Q}_b,y)-\mathfrak{D}(\tilde{Q}_{b'},y)\\ &+ 2\mathfrak{F}(\tilde{Q}_{b'},y)+y^2\mathfrak{B}(\tilde{Q}_{b'},y)\Big) - \frac{1}{N}\Big(\mathfrak{D}(\tilde{Q}_{b'},y)\\ &+ \mathfrak{D}(\tilde{Q}_{a'},y)+\mathfrak{F}(\tilde{Q}_{b'},y)+\mathfrak{F}(\tilde{Q}_{a'},y)+2y^2\mathfrak{B}(\tilde{Q}_{a'},y)\\ &+ 2y^2\mathfrak{B}(\tilde{Q}_{b'},y)\Big)\delta_{aa'}\delta_{bb'}+\frac{1}{N^2}\sum_e\Big(\mathfrak{D}(\tilde{Q}_e,y)\\ &+ \mathfrak{F}(\tilde{Q}_e,y)+2y^2\mathfrak{B}(\tilde{Q}_e,y)\Big)\delta_{aa'}\delta_{bb'}\Bigg].\end{aligned} \tag{6.56}$$

6.3.2 Gluon contribution to Debye mass

For the sake of completeness, we recapitulate the results here. The Gluon loop contribution with tri-gluon vertex to the Debye mass is shown in Fig.(6.2). In

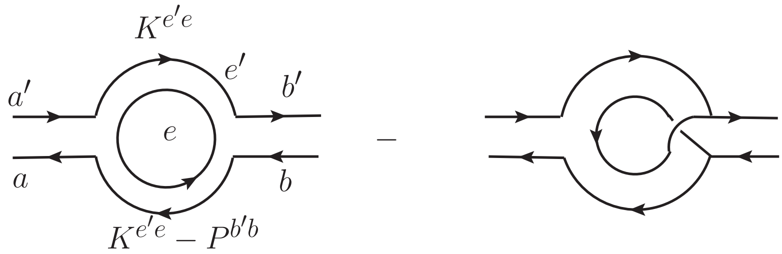

Figure 6.2: Gluon loop in gluon self energy in double line notation

the HTL approximation, the sum of gluon loop, four gluon vertex and ghost loop contribution to the gluon self energy can be written as

$$\begin{aligned}\Pi^{gl}_{\mu\nu;b'baa'}(P,Q) &= g^2 f^{(b'b,ee',gh)} f^{(aa',e'e,hg)} \int \frac{d^4K}{(2\pi)^4}[4K_{\mu e'e}K_{\nu e'e} - 2K^2_{e'e}\delta_{\mu\nu}]\Delta(K) \\ &\times \Delta(P-K). \end{aligned} \tag{6.57}$$

As explained earlier, the time like component of the self energy is needed for the Debye mass which can be written as

$$\begin{aligned}\Pi^{gl}_{44;b'baa'}(P,Q) &= g^2 f^{(b'b,ee',gh)} f^{(aa',e'e,hg)} \int \frac{d\mathbf{k}}{(2\pi)^3} \sum_n T[2\Delta(P-K) - 4k^2\Delta(K) \\ &\times \Delta(P-K)], \end{aligned} \tag{6.58}$$

where $\Delta(K)^{-1} = (\omega_n + Q_{e'e})^2$ and $\Delta(P-K)^{-1} = (\omega - \omega_n + Q_{b'b} - Q_{e'e})^2 + E_q^2$. Here $Q1 = Q_{e'e}$ and $Q2 = Q_{b'b} - Q_{e'e}$. Similar to quark loop, we shall not consider T^3 dependent term here and the summation over discrete Matsubara frequencies are same as in Eqs.(6.42) and (6.43). Using these summations and taking static limit, the T^2 dependent contribution to gluon self energy can be written as

$$\Pi^{gl}_{44;b'baa'}(Q)|_{(\omega=0,\vec{p}\to 0)} = -\frac{g^2T^2}{4\pi^2} f^{(b'b,ee',gh)} f^{(aa',e'e,hg)}[3\mathfrak{H}(Q_{b'b} - q_{e'e}) + \mathfrak{H}(Q_{e'e})], \tag{6.59}$$

where

$$\mathfrak{H}(Q) = \int x dx (f(x, iq) + f(x, -iq)) \equiv Li_2(iq) + Li_2(-iq). \tag{6.60}$$

Same as in the case of quark loop, for gluon loops, gluon self energy depends on the color of the gluon, and these color indices are free. Other repeated color indices can be summed by using Eq.(6.24) for structure constant. Thus Eq.(6.59) becomes

$$\begin{aligned}\Pi^{gl}_{44;b'baa'}(Q)|_{(\omega=0,\vec{p}\to 0)} &= \frac{g^2T^2}{8\pi^2}[4(\mathfrak{H}(Q_{ba}) + \mathfrak{H}(Q_{ab}))\delta^{b'b}\delta^{a'a} - 2(3\mathfrak{H}(Q_{be}) + \mathfrak{H}(Q_{b'e})) \\ &\times \delta^{a'b'}\delta^{ab}]. \end{aligned}\tag{6.61}$$

To get the total Debye mass we need to add both the contribution which are given in Eqs.(6.56) and (6.61). Taking both the contributions into account, Debye mass can be given as

$$(m_D^2)_{b'baa'} = -\Pi^q_{44;b'baa'}(m)|_{(\omega=0,\vec{p}\to 0)} - \Pi^{gl}_{44;b'baa'}(Q)|_{(\omega=0,\vec{p}\to 0)}, \tag{6.62}$$

leading to

$$\begin{aligned}(m_D^2)_{b'baa'} &= \frac{g^2T^2}{4\pi^2}\Bigg[N_f\Bigg(\delta_{ab}\delta_{a'b'}\Bigg(\mathfrak{D}(\tilde{Q}_b, y) - \mathfrak{D}(\tilde{Q}_{b'}, y) + 2\mathfrak{F}(\tilde{Q}_{b'}, y) + y^2\mathfrak{B}(\tilde{Q}_{b'}, y)\Bigg) \\ &- \frac{1}{N}\Bigg(\mathfrak{D}(\tilde{Q}_{b'}, y) + \mathfrak{D}(\tilde{Q}_{a'}, y) + \mathfrak{F}(\tilde{Q}_{b'}, y) + \mathfrak{F}(\tilde{Q}_{a'}, y) + 2y^2\mathfrak{B}(\tilde{Q}_{a'}, y) \\ &+ 2y^2\mathfrak{B}(\tilde{Q}_{b'}, y)\Bigg)\delta_{aa'}\delta_{bb'} + \frac{1}{N^2}\sum_e\Bigg(\mathfrak{D}(\tilde{Q}_e, y) + \mathfrak{F}(\tilde{Q}_e, y) \\ &+ 2y^2\mathfrak{B}(\tilde{Q}_e, y)\Bigg)\delta_{aa'}\delta_{bb'}\Bigg) + \Bigg(3\mathfrak{H}(Q_{be}) + \mathfrak{H}(Q_{b'e})\Bigg) \\ &\times \delta^{ab}\delta^{a'b'} - \Bigg(2(\mathfrak{H}(Q_{ba}) - \mathfrak{H}(Q_{ab}))\Bigg)\delta^{b'b}\delta^{a'a}\Bigg]. \end{aligned}\tag{6.63}$$

As Debye mass is color dependent and therefore, one need to sum the contributions from all the colors and then average over the number of colors to get the total

Debye mass i.e.,

$$\bar{m}_D^2 = \sum_{abcd} \frac{(m_D^2)_{abcd}}{N^4}. \tag{6.64}$$

In the large N limit (i.e., neglecting 1/N terms in Eq.(6.63)), the Debye mass is diagonal and its components can be written in the limit quark mass $m = 0$ as

$$(m_D^2)_1 = (m_D^2)_3 = \frac{g^2T^2}{6}(6 + N_f - 36q + (60 - 12N_f)q^2), \tag{6.65}$$

$$(m_D^2)_2 = \frac{g^2T^2}{6}(N_f + 6(1 - 2q)^2). \tag{6.66}$$

which is same as was derived in Ref.[256] It is easy to check that, in the limit $Q = 0$ and $m = 0$, the Debye mass as written in Eq.(6.63) reduces to its familiar HTL limit given as

$$(m_D^2)_{abcd} = \frac{g^2T^2}{3}\left(N_c + \frac{N_f}{2}\right)\mathcal{P}_{abcd}. \tag{6.67}$$

In our calculation for the heavy quark transport coefficients, however, we will use the color averaged Debye mass as given in Eq.(6.64).

6.3.3 Light Quark thermal mass

In the double line notation, the standard diagram of one loop quark self energy is shown in Fig.(6.3) where a and a' respectively are the color indices for incoming and outgoing quark. It is expected that similar to the gluon self energy, the quark self energy also depends on the colors of incoming and outgoing quark and in the presence of a background gauge field the same can be written as

$$\Sigma(P,Q,m)_{a'a} = g^2(t^{de})_{a'b}\mathcal{P}_{defg}(t^{fg})_{ba}\int \frac{d^4K}{(2\pi)^4}\frac{\gamma^\mu(m - \not{\tilde{K}}_b)\gamma_\mu}{(\tilde{P}_{a'} - \tilde{K}_b)^2(\tilde{K}_b^2 + m^2)}, \tag{6.68}$$

where g is coupling constant, $\tilde{K}_b = K + \tilde{Q}_b$ is quark momentum and $\tilde{P}_{a'} - \tilde{K}_b = P - K + \tilde{Q}_a - \tilde{Q}_b$ is gluon momentum. To solve the integration in Eq.(6.68), let us first write $\int \frac{d^4K}{(2\pi)^4} = \sum\limits_{n=-\infty}^{\infty} \int \frac{d\mathbf{k}}{(2\pi)^3}; k_4 \equiv \omega_n = 2n\pi T$ and perform Matsubara frequency sum. There are two types of terms where one need to perform

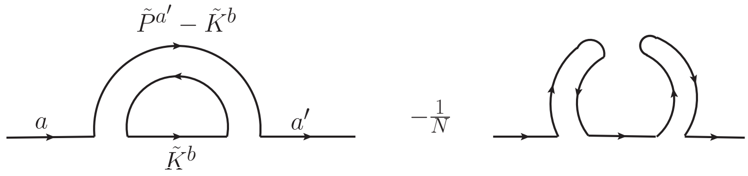

Figure 6.3: One loop quark self energy diagram in double line notation

frequency summation. One is similar to Eq.(6.42) with product of two propagators $\sum \Delta(K)\Delta(P-K)$ (arising from the term proportional to m) and another is $\sum \omega_n \Delta(K)\Delta(P-K)$ (arising from the $\not{\tilde{K}}_b$ term). The later one can be written as

$$
\begin{aligned}
T\sum_n \omega_n \Delta(K)\Delta(P-K) &= \frac{i}{4E_q}\Bigg(\frac{f(E_q+iQ2+i\omega)-f(E_k-iQ1)}{E_k-E_q-i(Q1+Q2+\omega)} \\
&+ \frac{1+f(E_k-iQ1)+f(E_q-iQ2-i\omega)}{E_k+E_q-i(Q1+Q2+\omega)} \\
&+ \frac{f(E_q-iQ2-i\omega)-f(E_k+iQ1)}{E_k-E_q+i(Q1+Q2+\omega)} \\
&+ \frac{1+f(E_q+iQ2+i\omega)+f(E_k+iQ1)}{E_k+E_q+i(Q1+Q2+\omega)}\Bigg). \qquad (6.69)
\end{aligned}
$$

We take HTL approximation and evaluate only T^2 dependent term in quark-self energy. We note here that, unlike gluon self energy, one does not get any extra term different in structure as compared to the usual perturbative HTL approximation for the quark self energy. The leading contribution arises from the terms having $E_q - E_k$ in the denominators of Matsubara frequency sums and in Eq.(6.69) comes from the first and the third terms. Simplifying Eq.(6.68) with Eqs.(6.42) and (6.69), quark self energy becomes

$$
\begin{aligned}
\Sigma(P,Q,m)_{a'a} &= g^2\mathcal{P}_{a'b,ba}\Bigg(m\int \frac{d\mathbf{k}}{(2\pi)^3}\frac{1}{4E_kE_q}\Bigg[\frac{f(E_q-iQ2)+f(E_q+iQ2)}{P_a.\hat{K}} \\
&- \frac{f(E_k+iQ1)+f(E_k-iQ1)}{P_a.\hat{K}}\Bigg] \\
&+ \int \frac{\not{\tilde{K}} d^3k}{E_k(2\pi)^3}\Bigg[\frac{f(E_k+iQ2)-f(E_q-i(Q1+\omega))}{P_a.\hat{K}}
\end{aligned}
$$

$$- \quad \frac{f(E_q+i(Q1+\omega))-f(E_k-iQ2)}{P_a.\hat{K}}\Bigg]\Bigg). \tag{6.70}$$

In the above equation, we have used HTL approximation so that $E_q - E_k \approx -\frac{\vec{P}.\vec{k}}{E_k}$, $f(E_k - iQ) \approx f(E_q - iQ)$ and $e^{\frac{i\omega}{T}} \simeq 1$. Here $Q1 = \tilde{Q}_b$, $Q2 = Q_{a'} - Q_b$ and $\hat{K} = (i, \hat{k})$. After simplifying Eq.(6.70) further, it can be written as

$$\begin{aligned}
\Sigma(P,Q,m)_{a'a} &= \frac{g^2T^2}{8\pi^2}\sum_{b=1}^{3}\mathcal{P}_{a'b,ba}\Bigg([\mathfrak{F}(q2,y)-\mathfrak{F}(q1,y)]\int\frac{d\Omega}{4\pi}\frac{\hat{\not{K}}}{P_a.\hat{K}}\\
&+ \frac{m}{T}(\mathfrak{J}(q2,y)-\mathfrak{J}(q1,y))\int\frac{d\Omega}{4\pi}\frac{1}{P_a.\hat{K}}\Bigg),
\end{aligned} \tag{6.71}$$

where as before, $y = \beta m$, $q1 = \beta Q1$; $\mathfrak{F}(q)$ is same as given in Eq.(6.52) and $\mathfrak{J}$ is given as

$$\mathfrak{J}(q,y) = \int\frac{x^2dx}{x^2+y^2}(f(x,y,-iq)+f(x,y,iq)). \tag{6.72}$$

It is easy to see that to estimate the quark thermal mass from its self energy, one need to sum over colors in Eq.(6.71) keeping a and a' open indices. After performing this color sum, quark self energy reduces to

$$\begin{aligned}
\Sigma(P,Q,m)_{a'a} &= \frac{g^2T^2}{8\pi^2}\delta_{a'a}\Bigg(\Bigg[\sum_{b=1}^{3}(\mathfrak{F}(q_{a'b},y)-\mathfrak{F}(\tilde{q}_b,y))-\frac{1}{3}(\mathfrak{F}(0,y)-\mathfrak{F}(\tilde{q}_a,y))\Bigg]\\
&\times \int\frac{d\Omega}{4\pi}\frac{\hat{\not{K}}}{P_a.\hat{K}}+\frac{m}{T}\Bigg[\sum_{b=1}^{3}(\mathfrak{J}(q_{a'b},y)-\mathfrak{J}(\tilde{q}_b,y))+\mathfrak{J}(0,y)-\mathfrak{J}(\tilde{q}_a,y)\Bigg]\\
&\times \int\frac{d\Omega}{4\pi}\frac{1}{P_a.\hat{K}}\Bigg).
\end{aligned} \tag{6.73}$$

In the HTL approximation, the effective fermion mass (thermal mass) can be written as [118]

$$4m_{th}^2 = Tr(\not{P}\Sigma(P)). \tag{6.74}$$

From Eqs.(6.74) and (6.73), the color dependent quark thermal mass a function of Polyakov loop parameter q can be written as

$$m_{a'}^2 = \frac{g^2T^2}{8\pi^2}\left(\sum_{b=1}^{3}(\mathfrak{F}(Q_{a'b},y)-\mathfrak{F}(\tilde{Q}_b,y))-\frac{1}{3}(\mathfrak{F}(0,y)-\mathfrak{F}(\tilde{Q}_{a'},y))\right). \tag{6.75}$$

In the limit of vanishing quark mass, using Eq.(6.53), it is easy to show that

$$m_a^2 = \frac{g^2T^2}{6}\left(1+\frac{3}{2}q_a+\frac{7}{2}q_a^2\right). \tag{6.76}$$

In the subsequent calculationS that follow, we however, keep the quark mass dependence as in Eq.(6.75). Similar to Eq.(6.64), one can define a color averaged quark thermal mass as

$$m_{th}^2 = \sum_{a=1}^{3}\frac{m_a^2}{3} \tag{6.77}$$

so the total quark mass becomes

$$m_q = m + m_{th}, \tag{6.78}$$

Thus the color averaged Debye mass for the gluons and color averaged thermal mass for quarks as given by Eqs.(6.64) and (6.77) depend upon the Polyakov loop parameter.

For the Polyakov loop parameter, we adopt here two approaches. Firstly, we estimate the same from a phenomenological 2 flavor PQM model [252, 247]. The salient features of the model and the parameters taken in the model is discussed in Appendix A. With this parameterization the critical temperature for the crossover transition $T_c \approx 176$ MeV. We also take the Polyakov loop parameter from lattice simulations as in Ref. [26]. The variation of the Polyakov loop with temperature (T) is shown on the left of Fig(6.4). Here, The red curve is from PQM model [252]. The blue curve is from the lattice results of Ref.[26]

Clearly, compared to the lattice simulations, the Polyakov loop parameter ϕ in PQM model shows a sharper rise and reaches its asymptotic value $\phi = 1$ at the temperature around 320 MeV. On the other hand, in the lattice simulations, this

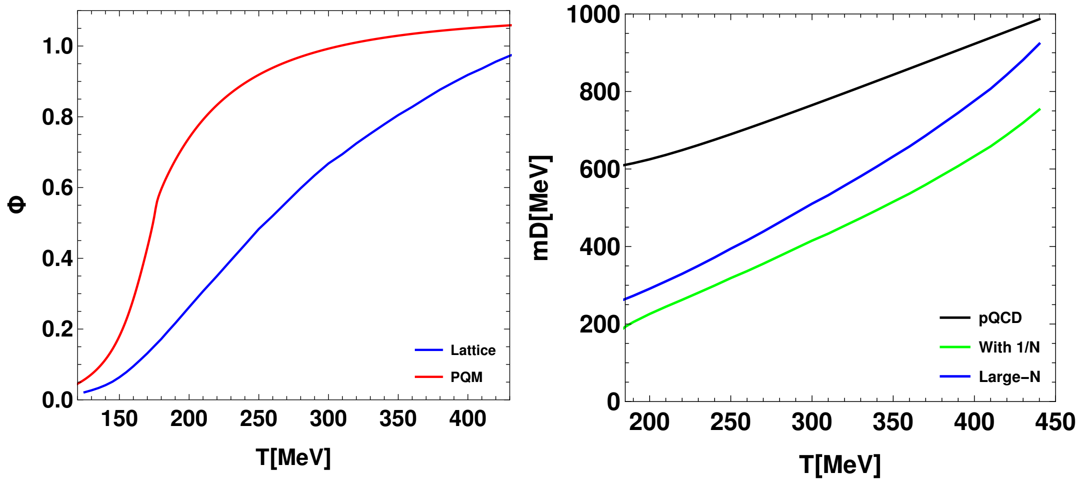

Figure 6.4: Polyakov loop and Debye mass as a function of temperature.

happens at a much higher temperature. This means that the non-perturbative effects are significant up to temperature as high as 400 MeV in lattice. However in PQM these effects are significant only temperatures upto around 320 MeV. In Fig(6.4), Debye mass as a function of temperature is shown. Here the black curve corresponds to the Debye mass in pQCD, while the blue and the green curves are in the presence of Polyakov loop. The blue curve corresponds to the large N limit (i.e., dropping 1/N terms in Eq.(6.56)). On the other hand, the Green curve corresponds to including the 1/N terms in Eq.(6.56). Clearly, the large N limit approaches the perturbative limit faster compared to the one including $1/N$ terms for the Debye mass.

For the light quarks, different contributions to the masses as a function of temperature (T) are shown in the left of Fig. (6.5). Here, the red and the blue curves correspond to quark thermal masses (m_{th}) as given in Eq.(6.77) evaluated in the HTL approximation in the presence of a background gauge field. The red curve corresponds to Polyakov loop value taken from PQM model while the blue curve corresponds to the same taken from lattice simulations. The HTL perturbative QCD thermal masse as in Ref. [5] is shown by the black curve. Clearly, with the lattice value of the Polyakov loop, thermal masses approach the perturbative results at a much higher temperature while with values taken from PQM, the perturbative limit reaches at a relatively lower temperature around 320 MeV. It

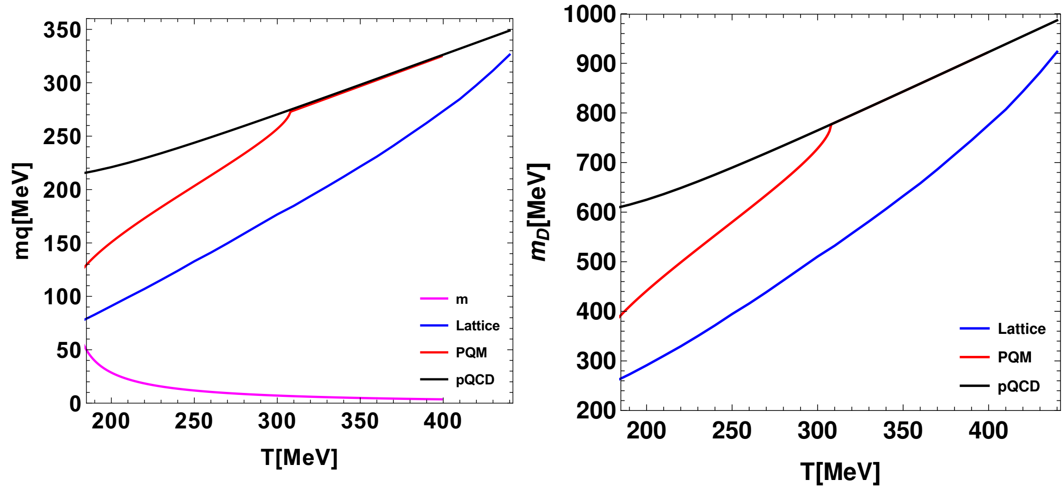

Figure 6.5: Quark and gluon thermal masses as a function of temperature.

ought to be mentioned that beyond 330 MeV ϕ value is larger than one in which case q becomes imaginary. We have taken here the real part of q for estimating the thermal masses. Beyond temperature 330 MeV the real part of q vanishes which leads to the perturbative limit. As compared to PQM model, the color averaged thermal mass is smaller for Polyakov loop expectation value taken from lattice simulation. This is because, with the smaller value of ϕ, statistical distribution functions are suppressed more. The magenta curve is the constituent quark mass estimated in PQM model. In the side of Fig.(6.5), shows the behavior of color averaged Debye mass in the large N limit of Eq(6.63). The red and the blue curves correspond to the masses with Polyakov loop value taken from PQM and lattice simulations respectively. Debye mass is smaller as compared to the perturbative QCD Debye mass and this suppression is more when ϕ is taken from the lattice simulations. The reason for this is the same as that for the case of quark thermal mass. In the estimation of the transport coefficients, we shall use the Debye mass and thermal masses of quarks as in Eq.(6.78). It is clear that the non-perturbative effects which are in the distribution function and the masses of quarks and gluons can significantly affect these transport coefficient as compared to the perturbative QCD.

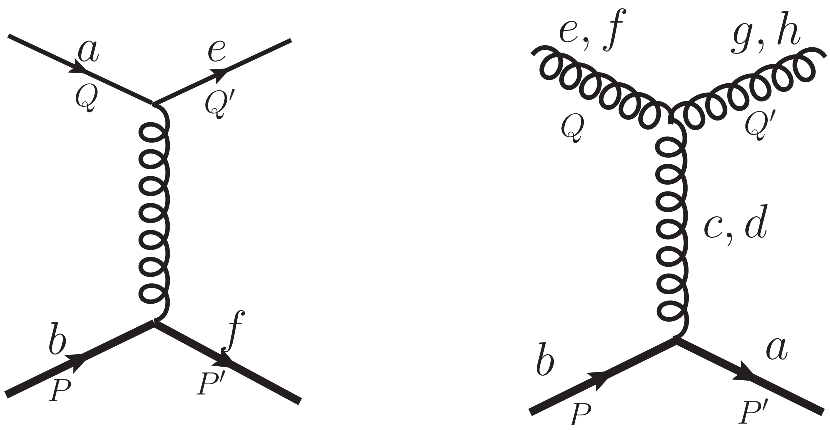

Figure 6.6: Coulomb scattering (left) of HQ (bold solid line) and light quark/antiquark (thin solid line). t-channel Compton scattering (right)

6.4 Scattering amplitudes

There are two types of scatterings that contribute to the drag and the diffusion coefficients namely Coulomb scattering i.e., scattering off of HQ from light quark and Compton scattering i.e., scattering off of gluon from HQ [97]. The dominant contribution for these scatterings arise from the gluon exchange in the t-channel which is infrared divergent [255, 100]. This is regularised by introducing the Debye screening [100, 97] which we have evaluated in the HTL limit in the background of Polyakov loop. In s and u channel, however, there is no such infrared divergences. Note that in the matrix model, m_D, in Eq.(6.63) is color dependent so the propagator is also color dependent. For N_f flavor of light quark, the spin averaged matrix element squared for Coulomb scattering as shown on the left side of Fig.(6.6), can be written as

$$|\mathcal{M}_C|^2 = \frac{16N_f g^4}{8N}\mathcal{P}\frac{((s-m^2-M^2)^2+(u-m^2-M^2)^2+2(M^2+m^2)t)}{(t+(m_D^2)_{mlcd})(t+(m_D^2)_{m'l'c'd'})}. \quad (6.79)$$

where $a, b(e, f)$ are color indices of initial (light,heavy) and final (light,heavy) quarks and $\mathcal{P} = \mathcal{P}^{cd}_{ae}\mathcal{P}^{ml}_{bf}\mathcal{P}^{c'd'}_{ea}\mathcal{P}^{m'l'}_{fb}$ is the product of the projection operators. For calculational simplifications, one can take the color averaged Debye mass as defined in Eq.(6.64) so that $(m_D^2)_{mlcd} \approx \bar{m}_D^2 \mathcal{P}_{mlcd}$. In this case, we get

$$\mathcal{P}_{ae}^{cd}\mathcal{P}_{bf}^{ml}\frac{1}{(t+(m_D^2)_{mlcd})} = \frac{1}{t+\bar{m}_D^2\mathcal{P}_{ae}^{fb}} - \frac{1}{N}\left(\frac{2}{t+\bar{m}_D^2} - \frac{1}{N}\frac{1}{t+\bar{m}_D^2}\right)\delta_{ae}\delta_{fb} \quad (6.80)$$

One can further simplify the expression in Eq.(6.79) by taking the leading order contribution in N. With this assumption, Eq. (6.79) reduces to

$$|\mathcal{M}_C|^2_{abef} = \frac{8g^4}{2N}\delta_a^f\delta_e^b\frac{((s-m^2-M^2)^2+(u-m^2-M^2)^2+2(M^2+m^2)t)}{(t+(\bar{m}_D^2)^2)^2} \quad (6.81)$$

where M is HQ mass. For the $q^aQ^b \to q^eQ^f$ scattering, the product of distribution function and matrix element squared that appears in Eq.(**??**) can be simplified by summing over color of initial and final light/heavy quarks. Note that for light quarks, the colors appearing in Eq.(6.81) has to be summed with the distribution function and can be written as

$$\delta_a^f\delta_e^b f(q)_e(1-f(q')_f) = N^2 f(q)_q(1-f(q')_q) \quad (6.82)$$

where $f(q)_q$ is the average distribution function of quark as defined in Eq.(6.28). Similarly for the t channel Compton scattering shown on the right side of Fig.(6.6), one can write

$$|\mathcal{M}_t|^2 = \frac{g^4}{4(N^2-1)}\mathcal{P}_{ba}^{ml}\mathcal{P}_{ab}^{l'm'}f^{cd,ef,gh}f^{d'c',fe,hg}\left(\frac{16(s-M^2)(M^2-u)}{(t+(m_D^2)_{mlcd})(t+(m_D^2)_{m'l'c'd'})}\right). \quad (6.83)$$

and can be simplified in a similar way as done for Coulomb scattering. Here $ef, b(gh, a)$ are the color indices for initial (final) gluon and quark. The scattering amplitude of u channel Compton scattering shown on the right side of Eq.(6.7) can be written as

$$|\mathcal{M}_u|^2 = \frac{8g^4}{8(N^2-1)}\mathcal{P}_{bc}^{gh}\mathcal{P}_{bc'}^{gh}\mathcal{P}_{ca}^{ef}\mathcal{P}_{c'a}^{ef}\left(\frac{M^4-us+M^2(3u+s)}{(u-M^2)^2}\right). \quad (6.84)$$

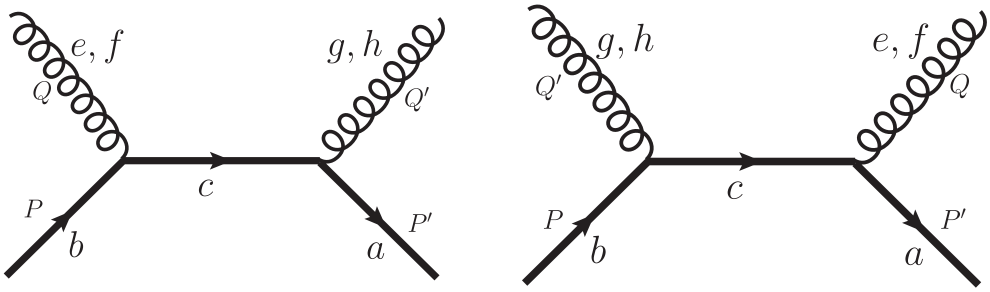

Figure 6.7: s-channel Compton scattering (left). u-channel Compton scattering (right)

Note here that the propagator has no color dependent term. Matrix element squared for s channel Compton scattering as shown on the left side of Fig.(6.7) is

$$|\mathcal{M}_s|^2 = \frac{8g^4}{8(N^2-1)}\mathcal{P}^{ef}_{bc}\mathcal{P}^{ef}_{bc'}\mathcal{P}^{gh}_{ca}\mathcal{P}^{gh}_{c'a}\left(\frac{M^4 - us + M^2(u+3s)}{(s-M^2)^2}\right). \tag{6.85}$$

There are interferences between different scatterings contributing to $g^{ef}Q^b \rightarrow g^{gh}Q^a$ that can be written as

$$\mathcal{M}_s{\mathcal{M}_u}^\dagger = \mathcal{M}_u{\mathcal{M}_s}^\dagger = \frac{g^4}{8(N^2-1)}\mathcal{P}^{ef}_{bc}\mathcal{P}^{gh}_{ca}\mathcal{P}^{gh}_{bc'}\mathcal{P}^{ef}_{c'a}\left(\frac{32M^4 - 8M^2t}{(s-M^2)(u-M^2)}\right). \tag{6.86}$$

$$\mathcal{M}_s{\mathcal{M}_t}^\dagger = \mathcal{M}^\dagger_s\mathcal{M}_t = \frac{g^4}{4\sqrt{2}(N^2-1)}\mathcal{P}_1\left(\frac{-8(M^4 - 2M^2s + us)}{(s-M^2)(t+(m_D^2)_{mlcd})}\right). \tag{6.87}$$

$$\mathcal{M}_u{\mathcal{M}_t}^\dagger = \mathcal{M}^\dagger_u\mathcal{M}_t = \frac{g^4}{4\sqrt{2}(N^2-1)}\mathcal{P}_2\left(\frac{8(4M^4 - M^2t)}{(u-M^2)((t+(m_D^2)_{mlcd}))}\right). \tag{6.88}$$

where $\mathcal{P}_1 = \mathcal{P}^{ef}_{bc}\mathcal{P}^{gh}_{ca}\mathcal{P}^{lm}_{ab}(if^{dc,fe,hg})$ and $\mathcal{P}_2 = \mathcal{P}^{gh}_{bc}\mathcal{P}^{ef}_{ca}\mathcal{P}^{lm}_{ab}(if^{dc,fe,hg})$. Total matrix element squared that contribute to Compton scattering i.e., $gQ \rightarrow gQ$ is $|\mathcal{M}_{Cm}|^2_{abefgh} = |\mathcal{M}_s|^2 + |\mathcal{M}_u|^2 + |\mathcal{M}_t|^2 + \mathcal{M}_u\mathcal{M}^\dagger_s + \mathcal{M}_s\mathcal{M}^\dagger_u + \mathcal{M}_t\mathcal{M}^\dagger_s + \mathcal{M}_s\mathcal{M}^\dagger_t + \mathcal{M}_u\mathcal{M}^\dagger_t + \mathcal{M}_t\mathcal{M}^\dagger_u$. These matrix elements are used in Eq.(**??**) to estimate the drag and the diffusion coefficient.

6.5 Results and discussions

With the thermal mass of the quarks and the Debye mass as computed in the background of a nontrivial Polyakov loop, we next numerically compute the drag and diffusion coefficients using Eq.(6.15). For the heavy quark elastic interaction with the light quarks and gluons, $qQ \to qQ$ and $gQ \to gQ$ scattering processes are considered where Q stands for heavy quark, q stands for light quarks and g stands for the gluon. In the case of massless light quark and gluon, the leading-order (LO) matrix elements for $qQ \to qQ$ and $gQ \to gQ$ scattering have been calculated in Ref. [260, 97]. These pQCD cross sections have to be supplemented by the value of the coupling constant and the Debye screening mass which is needed to shield the divergence associated with the t-channel diagrams to compute the heavy quark transport coefficients. For massive light quark and gluon, the calculation of the scattering matrix, $\mathcal{M}_{(q,g)+Q\to(q,g)+Q}$, is performed considering the leading-order (LO) diagram with massive quark and gluon propagators for $gQ \to gQ$ and a massive gluon propagator for $qQ \to qQ$ scatterings [236, 221]. Within the matrix model, the scattering amplitudes are summarised in Appendix(B). Similar to previous work [236, 221], massive gluon propagator for $qQ \to qQ$ and t-channel of $gQ \to gQ$ is used. We estimate the transport coefficients for the charm quark whose mass is taken as $m_C = 1.27$ GeV. Here we use the two loop running coupling constant given as [261]

$$\alpha_s = \frac{1}{4\pi}\left(\frac{1}{2\beta_0 \ln(\frac{\pi T}{\Lambda}) + \frac{\beta_1}{\beta_0}\ln(2\ln(\frac{\pi T}{\Lambda}))}\right) \tag{6.89}$$

where

$$\beta_0 = \frac{1}{16\pi^2}\left(11 - \frac{2N_f}{3}\right) \tag{6.90}$$

$$\beta_1 = \frac{1}{(16\pi^2)^2}\left(102 - \frac{38N_f}{3}\right) \tag{6.91}$$

with $\Lambda = 260$ MeV and $N_f = 2$.

We evaluate the drag and diffusion coefficients of heavy quark in QGP with Polyakov loop value from two different models. In one case the Polyakov loop value, hence the Debye mass and thermal masses, has been taken from PQM

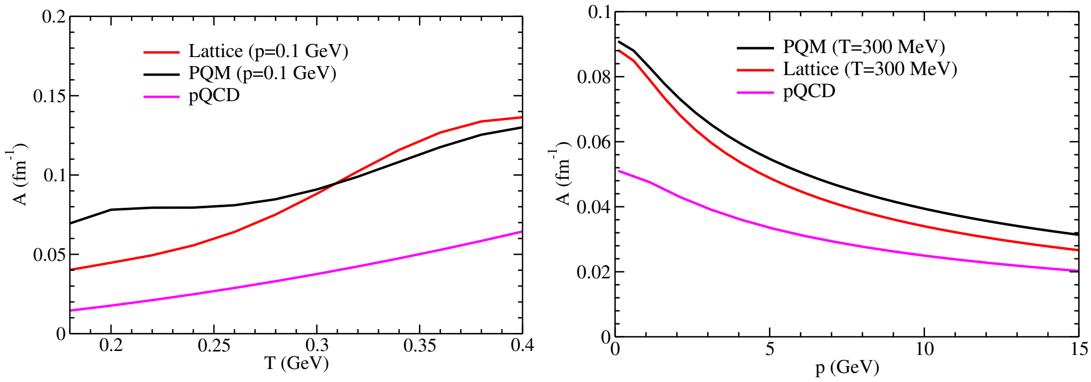

Figure 6.8: Variation of drag coefficients (A) with temperature (left) for momentum $p = 100$ MeV and with momentum (right) for temperature $T = 300$ MeV.

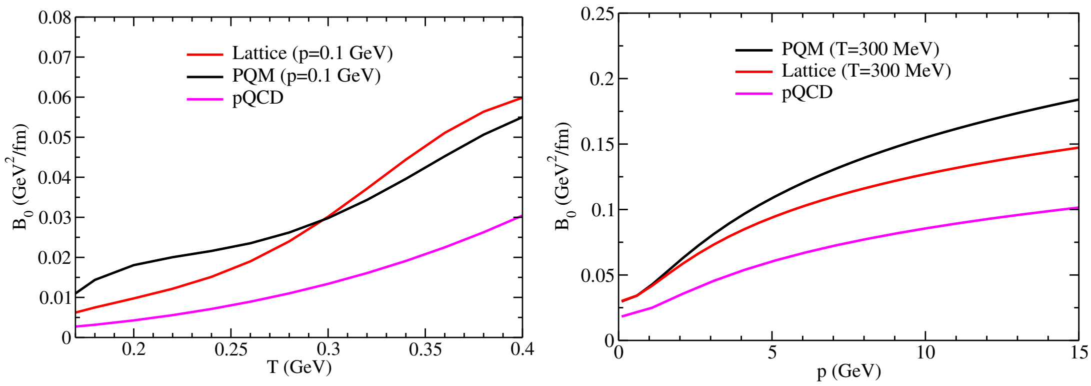

Figure 6.9: Variation of diffusion coefficients (B_0) with temperature (left) for momentum $p = 100$ MeV and with momentum (right) for temperature $T = 300$ MeV.

calculation as inputs to compute the heavy quark transport and we label it as PQM. In the other case, Polyakov loop value has been taken from the lattice simulatons and hence, we label it as lattice in the following discussions.

The temperature variation of the drag coefficient has been shown in the left side of Fig.(6.8) for charm quark interaction with light quarks and gluon for a given momentum (p=0.1 GeV) obtained for both PQM and lattice Polyakov loop values.

We obtain quite a mild temperature dependence of heavy quark drag coefficient for the case of PQM. However, with lattice, we obtained a quite stronger temperature dependence of heavy quark drag coefficient than the one with PQM.

We notice that the drag coefficient obtained with PQM input is larger at low temperature than the one obtained with lattice inputs whereas the trend is opposite at high temperature. This is mainly because of the interplay between the Debye mass and Polyakov loop value obtained within both the models. In the same plot, for comparison, we have also included results for the drag coefficient obtained within the standard LO pQCD calculations with a constant coupling ($\alpha_s = 0.2$) to display the non-perturbative effects arising from non-trivial Polyakov loop and chiral condensate on the HQ drag coefficient.

A smaller value of the Polyakov loop, as shown in Fig.(6.4), in case of lattice reduces the magnitude of the drag coefficients at low temperature. However, at high temperature, with smaller Debye mass, as shown in the right of Fig.(6.4), obtained with lattice input enhances the magnitude of heavy quark drag coefficients. Hence, at low temperature Polyakov loop value plays the dominant role (e.g., at T=180 MeV, the Polyakov loop value obtained within both the models differ by a factor about 2) whereas at high temperature the Debye mass plays the dominant role (e.g., T=300 MeV, the differences between the Polyakov loop value obtained within both cases reduced significantly) for the behavior of the drag coefficient.

We observed temperature dependence of heavy quark drag coefficient obtained with PQM Polyakov loop value is quite consistent with the results obtained with other quasi-particle models [235, 236] and T-matrix approach [210]. It is important to mention that the temperature dependence of the drag coefficient plays a significant role [235] to describe heavy quark R_{AA} and v_2 simultaneously, which is a challenge to almost all the models on heavy quark dynamics. A constant or weak temperature dependence of the drag coefficient is an essential ingredient to reproduce the heavy quarks R_{AA} and v_2 simultaneously, whereas in pQCD the drag coefficient increases with temperature.

The momentum variation of the drag coefficient has been shown in the right panel of Fig.(6.8) for charm quark interaction with light quarks and gluon obtained with PQM and lattice Polyakov loop value. We observe a strong momentum dependence of heavy quark drag coefficient as compared to the same estimated within pQCD [85, 221]. This is mainly due to the inclusion of non-perturbative effects through the Polyakov loop background. At T=300 MeV the drag obtained with the PQM Polyakov loop (at p=0.1 GeV) is marginally larger than the drag obtained

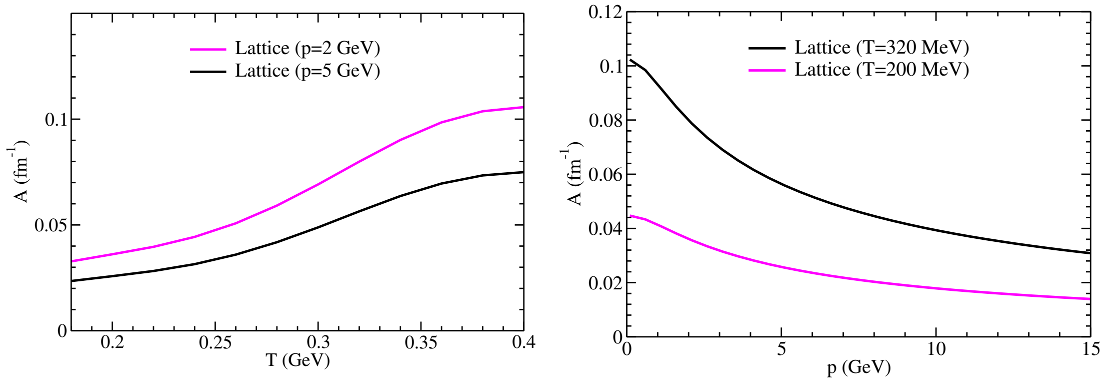

Figure 6.10: Variation of drag coefficients (A) with temperature (left) for different values of momentum and with momentum (right) for different values of temperature.

with lattice Polyakov value. Hence, the momentum variation of drag coefficients obtained with inputs from PQM is marginally larger than the one obtained with inputs from lattice simulation in the entire momentum range considered here.

In the left of Fig.(6.9) heavy quark diffusion coefficient B_0 has been displayed as a function of temperature obtained with input parameter from PQM and lattice. The diffusion coefficients increases with temperature for both the cases as it involves the square of the momentum transfer. In terms of magnitude the diffusion coefficient obtained within both the cases follow similar trend of drag coefficient due to the same reason (i.e., interplay between Debye mass and Polyakov loop value). In the same plot we have also included the diffusion coefficient obtained within the standard LO pQCD calculation for a constant coupling to highlight the non-perturbative features arising from non-trivial Polyakov loop and chiral condensate.

The momentum variation of the diffusion coefficient has been shown in the right side of Fig.(6.9) for charm quark interaction with light quarks and gluons for the same values of Polyakov loop. Similar to the drag coefficient, the diffusion coefficient also shows the same trend with PQM having larger value then that from the lattice as a function of momentum. Stronger suppression of distribution function at high momentum in lattice Polyakov loop than that of from PQM also play a marginal role in the momentum variation of heavy quark drag and diffusion coefficients obtained.

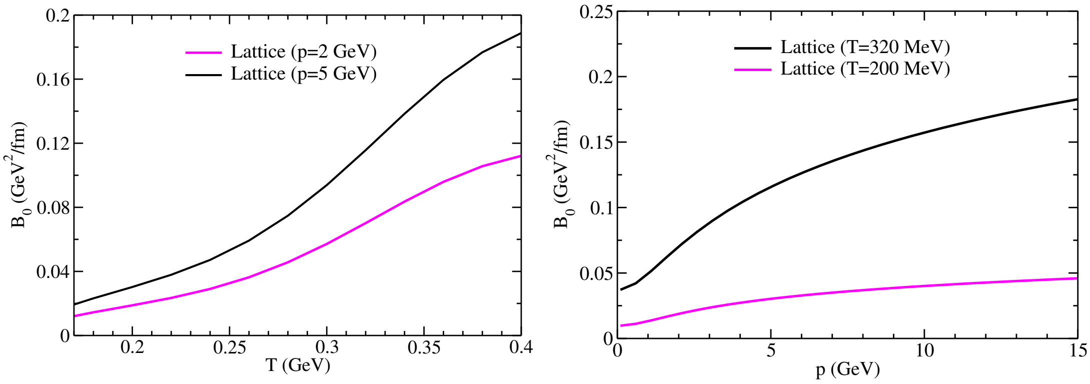

Figure 6.11: Variation of diffusion coefficients (B_0) with temperature for different values of the momentum(left) and with momentum (right) for different values of temperature.

To understand the temperature dependence of the transport coefficients, we plot the temperature variation of the drag coefficient in the left side of Fig. 6.10 at different momentum obtained with Polyakov loop value from lattice simulations. We obtain almost similar temperature dependence of heavy quark drag coefficient at both the momentum having larger magnitude at p=2 GeV than at p=5 GeV. In the left side of Fig. 6.11 we have depicted the temperature variation of diffusion coefficient at different momentum for the same values of Polyakov loop. As expected, the magnitude of the diffusion coefficient is large at p=5 GeV than p=2 GeV having similar temperature variation for both the momenta.

In the right side of Fig. 6.10 we have shown the variation of drag coefficient with momentum at different temperature obtained with the lattice inputs. We observe a larger magnitude of the drag coefficient at T=320 MeV than T=200 MeV but the momentum variation is similar at both temperature. Momentum variation of the diffusion coefficient has been depicted in the right side of Fig. 6.11 at difference temperature. At both the momenta the diffusion increase with temperature having larger magnitude at T=320 MeV than T=200 MeV.

It is worth mentioning here that, non-perturbative effects from a different perspective has been investigated recently in Ref. [262, 263, 264] and employed to calculate the transport coefficients [264]. The method here consisted of using T-matrix with an in-medium potential for the heavy quarks. This potential is constrained by the heavy quark free energy from the lattice data. The lattice heavy quark free energy is directly related to the Polyakov loop and hence is correlated with the strength of the confining potential. Therefore it is nice to see that the behavior of drag coefficient being rather flat with regards to temperature dependence whereas the diffusion coefficient having a strong temperature dependence as observed here was also observed in Ref.[264]. This consistency suggest of having a possible existence of model independent correlation between Polyakov loop and the heavy quark transport coefficients.

6.6 Summary

In this chapter, we have computed the heavy quark drag and diffusion coefficients in QGP including non-perturbative effects via a Polyakov loop background. In order to incorporate these effects we first calculate quark and gluon thermal masses also taking the quark constituent mass into account. We found that for temperatures below 300 MeV quark thermal mass and gluon Debye mass starts deviating from its perturbative value this effect significant for even higher temperatures when Polyakov values are taken from the lattice simulations. This decrease in the Debye mass of gluon and the thermal mass of light quarks is due to color suppression manifested in the quark and gluon distribution functions in the presence of a background Polyakov loop field. In the calculation of HQ diffusion coefficient the distribution function of the light quark and the Debye mass play complimentary roles. While the distribution function with Polyakov loop tend to decrease the HQ transport coefficient the Debye mass has the effect of increasing these transport coefficients. We have found a weak temperature dependence of the heavy quark drag coefficient with Polyakov loop value taken from PQM which is consistent with other models like T-matrix and quasi particle model which also take into account the non-perturbative effects in a different manner. This consistency suggests existence of possible model independent correlations between the results obtained with the Polyakov loop and other non-perturbative models and reaffirm the temperature and momentum dependence of heavy quark transport coefficients. In the present investigation, we have aconfined our attention to the elastic $2 \to 2$ processes within the matrix model. Inclusion of other effects arising from $2 \to 3$ processes, LPM effects are expected to be sub-dominant due to the large mass of the heavy quark[265] but, none the less, can be important at high parton density. In order to continue our discussion on HQ transport coefficient, in the next chapter we shall investigate the viscous correction (both shear and bulk) along with the inclusion of Polyakov loop.

CHAPTER 7

Heavy quark diffusion in a viscous medium

The aim of HIC experiments is to characterize the properties of deconfined state of matter. In order to do this, well-calibrated probes are required. In this regard, the transport properties of HQ; especially charm and bottom is considered as one of the promising probes. As already mentioned, the HQs interaction with the thermal partons in the QGP medium reflects in the transverse momentum (p_T) spectra of open heavy flavor (HF) meson such as D-meson for charm quark, and in the elliptic flow v_2 of open meson for a non-central collision[266, 267, 222, 233, 268, 269, 85].

HQs are useful especially in the sense that these are produced in the initial stages of the collisions during hard scatterings that governed by perturbative quantum chromodynamics (pQCD) mostly through gluon fusion[270, 271, 272]. Moreover, the thermal production (in medium) is suppressed due to the large mass, i.e., $M \gg T$. Therefore, once produced in the hard collisions, HQ propagates throughout the space-time evolution of the medium and interact with the light thermal partons of in bulk medium, consequently, this interaction modifies the spectra of HF hadrons. The HQ and bulk medium interaction is described by the scattering of HQ with the light thermal partons. At low momenta, the dominant contribution to the HQ and bulk particle scattering arises from the elastic scatterings and can be described by the diffusion akin to Brownian motion. Further, the thermalization process of HQ in the bulk medium is slowed down by its large mass. Therefore, the transport of non-equilibrated HQ in the thermalized medium yield valuable information throughout its propagation. In particular, the low momentum interaction of HQ with the bulk medium is characterized by the spatial diffusion coefficient.

Perturbative QCD based calculations for HQ transport coefficients namely the drag and the diffusion cannot explain the observed suppression and collective flow [168] so it is required to include the possible non-perturbative effects. There have been various efforts to incorporate non-perturbative effects using various phenomenological models such as T-matrix model[92, 263], quasi particle model[93, 236, 235], resonance model[95] for estimating the HQ transport coefficients. The most reliable results for the HQ spatial diffusion comes from the first principle lattice simulations[96, 273, 274]. Indeed, a smaller value of the spatial diffusion coefficient as compared to the perturbative QCD is predicted by the lattice simulations which is essential to explain observed R_{AA} and v_2. In Ref.[210], HQ transport coefficients (the drag and the momentum diffusion) are evaluated in the T-matrix approach including non-perturbative effects by employing the potential interaction of heavy-light quark extracted from lattice QCD simulations. A good agreement with the observed R_{AA} and collective flow v_2 of this calculation suggests existence of the strongly interacting nature of QGP. Recently, based on a Polyakov loop model, heavy quark drag and the diffusion coefficients have been computed for charm quark in Ref.[212]. The estimation of the drag coefficient here is observed being rather somewhat flat with temperature while diffusion coefficient exhibited a strong temperature dependence similar to the results obtained in Refs.[210, 92]. The consistency in the results suggest that there could be some model independent correlations between the results obtained within the Polyakov loop and other non-perturbative models from a different perspective.

On the other hand, it may also be mentioned here that QGP formed in HICs, behaves like almost an ideal fluid with a very small value for the ratio of shear viscosity to entropy density η/s. Evidence for such a small η/s is provided by the large elliptic flow data that requires $\eta/s \sim 0.08 - 0.2$[275, 276, 277, 278]. Viscous coefficients in the QGP as well as in the hadronic medium have been studied in Refs.[279, 280, 281]. In these studies it was found that the dominant contribution of dissipation in both the QGP and the hadronic medium arises from shear viscosity. However, bulk viscosity is equally important and may dominates near transition temperature i.e., $\xi/s \sim 1$[282] and can significantly affect hadrons p_T spectra and elliptic flow v_2[283]. Viscous corrections have also been studied for dilepton production in QGP[284, 285], photon production[286], damping rate of heavy quark[287], heavy quark radiative energy loss[288, 289, 290], event-plane correlations[291, 292] etc. Effect of shear and bulk viscosities on the HQ drag and diffusion coefficients have been studied in Ref.[214] using a fugacity model. In the present study, we intend to include the viscous corrections (both shear and bulk) along with a non-trivial Polyakov loop background that is used to describe the "semi QGP" within a matrix model. We find that in the perturbative limit our results are consistent with the previous results, however, with the inclusion of Polyakov loop (ϕ), at low temperature our results are different from that of Ref.[214]. In this work, we include the viscous corrections (both shear and bulk) in the single particle distribution functions of quark and gluon to estimate the viscous effects on the HQ transport coefficients. We estimate this using Fokker-Plank equation and use the matrix model of semi QGP to evaluate the relevant scattering amplitudes. The single particle distribution function (see Eqs.(**??**) and (**??**)) is modified using second moment ansatz. In Ref.[288] it was shown that viscous effects induce a larger energy loss of HQ. So one may expect that, viscous corrections may be important and significantly affect the transport properties of HQ in the bulk medium. However, we find that for small shear and bulk viscosities, the dissipative effects on the drag and the diffusion coefficients are somewhat weak.

We organize this chapter as follows. In section (7.1), an ansatz for the first order viscous correction on quark/gluon distribution is discussed. In section (7.2), we discuss the interaction of HQ with the light thermal parton and present matrix element squared for Coulomb and Compton scatterings within the matrix model. These matrix element squared are used to evaluate the drag and diffusion coefficients . In section (7.3) we discuss the viscous effects on HQ quark transport and present the numerical results for the drag and the diffusion coefficient for constant values of η/s and ξ/s. Finally, we summarize and give an outlook in section(7.4).

7.1 Viscous corrections in the distribution functions

In this section, we briefly describe the first order viscous corrections on the thermal distribution function of quarks and gluons. We start with the energy-momentum tensor of a non-ideal fluid which is given as[283]

$$T^{\mu\nu} = (\epsilon + P)u^{\mu}u^{\nu} + Pg^{\mu\nu} + \pi^{\mu\nu} + \Pi\nabla^{\mu\nu}, \tag{7.1}$$

where ϵ, P, u^{μ} are the energy density, pressure density and four-velocity of the fluid. For metric tensor, we use the convention $g^{\mu\nu} = diag(-1, +1, +1, +1)$ so that $u^{\mu}u_{\mu} = -1$ and the term $\nabla^{\mu\nu} = g^{\mu\nu} + u^{\mu}u^{\nu}$. The first two terms at the right hand side of Eq.(7.1) describes the energy-momentum tensor for an ideal fluid and the rest two terms are part of viscous corrections that summarizes the effect of shear and bulk viscosities respectively. The dissipative terms are constructed from the derivatives $\Delta^{\alpha} = \nabla^{\alpha\beta}\partial_{\beta}$ and $\nabla^{\mu\nu}$. In the first-order approximation, the symmetric tensor $\pi^{\mu\nu}$ satisfying the condition $u_{\mu}\pi^{\mu\nu} = 0$, in the local rest frame is given as

$$\pi^{\mu\nu} = -\eta\bigg(\Delta^{\mu}u^{\nu} + \Delta^{\nu}u^{\mu} - \frac{2}{3}\nabla^{\mu\nu}\Delta_{\alpha}u^{\alpha}\bigg) \tag{7.2}$$

and the bulk viscosity dependent term

$$\Pi = -\xi\Delta_{\alpha}u^{\alpha}. \tag{7.3}$$

Dissipative effects can be incorporated in the color dependent distribution functions $f_{a/ab}(E)$ which contains the ideal part as well as viscous corrections. For this purpose, we write $f_{a/ab}(E) = f^0_{a/ab}(E) + \delta f_{a/ab}(E)$ ($f^0_{a/ab}(E)$ is equilibrium distribution function of quark/antiquark and gluon) and use the second-moment ansatz as in Refs.[293, 294, 283], so that

$$\delta f(E)_{a/ab} = \frac{1}{T^3 s} f(E)^0_{a/ab}(1 + f(E)^0_{a/ab})p^{\mu}p^{\nu}\bigg(\frac{A}{2}\pi_{\mu\nu} + \frac{B}{5}\Pi\nabla_{\mu\nu}\bigg) \tag{7.4}$$

where A and B are constants. Constrain on $\delta f_{a/ab}$ comes from the continuity of stress-energy tensor across the freeze-out hypersurface [294] i.e.,

$$\delta T^{\mu\nu} = \int \frac{d^3k}{(2\pi)^3}\frac{k^\mu k^\nu}{E_k}\delta f_{a/ab}(E). \tag{7.5}$$

The choice of $\delta f_{a/ab}$ is not unique, as pointed out in Ref.[295], $\delta f_{a/ab}$ can have linearly increasing form with momentum and also quadratically increasing with momentum or anything in between linear to quadratic increasing behavior. However, we will continue with the form as in Ref.[294, 283]. In the local rest frame of the fluid i.e., $u_0 = 1, u_i = 0, \partial_\mu u_0 = 0$ and $\partial_\mu u_i \neq 0$, the deviation in distribution function can be written as [294, 283]

$$\delta f(E)_{a/ab} = \frac{1}{T^3 s} f(E)^0_{a/ab}(1 \mp f(E)^0_{a/ab}) p^\mu p^\nu \left(\frac{1}{2}\pi_{\mu\nu} + \frac{1}{5}\Pi\nabla_{\mu\nu}\right). \tag{7.6}$$

The first term of Eq.(7.6) i.e., the shear viscosity dependent term is

$$p^\mu p^\nu \pi_{\mu\nu} = -p^\mu p^\nu \eta\left(\Delta_\mu u_\nu + \Delta_\nu u_\mu - \frac{2}{3}\nabla_{\mu\nu}(\partial^\alpha + u^\alpha u^\beta \partial_\beta)u_\alpha\right). \tag{7.7}$$

One can use the normalization condition $u_\mu u^\mu = -1$ and differentiating this relation leads to $u^\mu \partial_\nu u_\nu = 0$. Using this and the relation $\Delta_\mu = \nabla_{\mu\nu}u^\nu$ one obtains

$$p^\mu p^\nu \pi_{\mu\nu} = -\eta\left(p^\mu p^\nu(\partial_\mu u_\nu + \partial_\nu u_\mu) + 2(p\cdot u)p^\nu u^\beta \partial_\beta u_\nu - \frac{2}{3}(p^2 - (p\cdot u)^2)\partial^\alpha u_\alpha\right). \tag{7.8}$$

Now, one can further use the relations $\partial_\mu u_\nu = (\tilde{g}_{\mu\nu} - u_\mu u_\nu)/\tau$ and $\partial^\alpha u_\alpha = 1/\tau$ [296], where τ is the proper time so that in the local rest frame of the fluid, Eq.(7.8) reduces to[288]

$$p^\mu p^\nu \pi_{\mu\nu} = \frac{2\eta}{\tau}\left(-p_z^2 + \frac{\mathbf{p}^2}{3}\right). \tag{7.9}$$

Similarly, the bulk viscosity dependent term can be written as

$$p^\mu p^\nu \nabla_{\mu\nu}\Pi = -\xi p^\mu p^\nu (g_{\mu\nu} + u_\mu u_\nu)\Delta_\alpha u^\alpha. \tag{7.10}$$

Using the same relations as for the case of shear viscosity, Eq.(7.10) can be written as

$$p^\mu p^\nu \nabla_{\mu\nu}\Pi = \frac{\xi}{\tau}\mathbf{p}^2. \tag{7.11}$$

Thus the distribution functions of quarks and gluons of Eq.(7.6) with the effect of shear and bulk viscosities can be written as

$$f(E)_a = f(E)_a^0 + \frac{f(E)_a^0(1-f(E)_a^0)}{T^3\tau}\left[\frac{\eta}{s}\left(-p_z^2+\frac{\mathbf{p}^2}{3}\right)+\frac{\xi}{s}\frac{\mathbf{p}^2}{5}\right] \tag{7.12}$$

$$f(E)_{ab} = f(E)_{ab}^0 + \frac{f(E)_{ab}^0(1+f(E)_{ab}^0)}{T^3\tau}\left[\frac{\eta}{s}\left(-p_z^2+\frac{\mathbf{p}^2}{3}\right)+\frac{\xi}{s}\frac{\mathbf{p}^2}{5}\right]. \tag{7.13}$$

In the present investigation, for evaluating drag and diffusion coefficients, we shall use Eqs.(7.12) and (7.13) for quark/antiquark and gluon distribution function in Eq.(6.14).

7.2 Scatterings amplitudes within matrix model

In this section, We shall discuss the scattering of HQ of mass M and energy $E=\sqrt{p^2+M^2}$ with the light thermal partons in the bulk medium and we shall also compute the scattering amplitude squared within the matrix model of semi QGP. To compute the drag and the diffusion coefficients of HQ transport we shall follow a similar approach to include screening effects as in Ref.[97, 100]. For the elastic collision, there are two types of scattering processes that contributes to the drag and the diffusion coefficient of HQ. One is Coulomb scattering i.e., scattering off of HQ with light quark and another is Compton scattering i.e., scattering off of HQ with gluons. In the following we present these in detail.

Coulomb scattering: The Feynman diagram for the Coulomb scattering of HQ and a light quark is shown on the left side of Fig.(6.6). Here a, c, b, d are the color indices of initial and final quarks. In the double line notation, the scattering amplitude for this process is

$$i\mathcal{M}_{qQ} = \frac{(ig)^2}{(t+(m_D^2)_{mljk})}(t^{jk})_{ab}(t^{ml})_{cd}[\bar{u}_b(q')\gamma^\mu u_a(q)][\bar{u}_d(p')\gamma_\mu u_c(p)], \tag{7.14}$$

where g is coupling constant, t is Mandelstam variable and m, l, j, k are the color indices of gluon propagator. In the limit of soft momentum transfer, only time-like component of the propagator contributes and the propagators simply become Debye screened propagator with $1/t \to 1/(t + m_D^2)$ [97, 100] where m_D^2 is color dependent Debye mass and can be given as

$$\begin{aligned}(m_D^2)_{abcd} &= \frac{g^2}{6}\Bigg[\delta_{ad}\delta_{bc}\Bigg(\sum_{e=1}^{3}\Big(\mathcal{D}(Q_{ae}) + \mathcal{D}(Q_{eb})\Big) - N_f(\tilde{\mathcal{D}}(Q_a) + \tilde{\mathcal{D}}(Q_b))\Bigg) \\ &- 2\delta_{ab}\delta_{cd}\Bigg(\mathcal{D}(Q_{ac}) - \frac{N_f}{N}\Big(\tilde{\mathcal{D}}(Q_a) + \tilde{\mathcal{D}}(Q_c)\Big) + \frac{N_f}{N^2}\sum_{e=1}^{3}\tilde{\mathcal{D}}(Q_e)\Bigg)\Bigg] \quad (7.15)\end{aligned}$$

where

$$\mathcal{D}(Q_a) = \frac{3}{\pi^2}\int_0^\infty dEE\Bigg(\frac{1}{e^{\beta(E+iQ_a)} - 1} + \frac{1}{e^{\beta(E-iQ_a)} - 1}\Bigg), \quad (7.16)$$

and $\tilde{\mathcal{D}}(Q_a) = \mathcal{D}(Q_a + \pi T)$. In the perturbative limit, Eq.(7.14) can be written as

$$i\mathcal{M}_{qQ} = -\frac{g^2}{t}(t^{jk})_{ab}(t^{jk})_{cd}[\bar{u}_b(q')\gamma^\mu u_a(q)][\bar{u}_d(p')\gamma_\mu u_c(p)], \quad (7.17)$$

and the product of projection operator with open color index a, b can be written as

$$\mathcal{P}^{jk}_{ab}\mathcal{P}^{jk}_{cd}\mathcal{P}^{j'k'}_{ba}\mathcal{P}^{j'k'}_{dc} = (N-1)\Bigg(1 - \frac{\delta_{ba}}{N}\Bigg). \quad (7.18)$$

However, for the computation of the drag and the diffusion coefficient, we shall use Eq.(7.14). Simplifying Eq.(7.14) for massless light quark and massive heavy quark by summing and averaging over final and initial spins, the scattering amplitude squared ($|\mathcal{M}_{qQ}|^2$) can be written as

$$|\mathcal{M}_{qQ}|^2 = \frac{g^4}{16N_c^2}\mathcal{P}^{jk}_{ab}\mathcal{P}^{ml}_{cd}\mathcal{P}^{j'k'}_{ba}\mathcal{P}^{m'l'}_{dc}\frac{(8(s-M^2)^2 + 8(u-M^2)^2 + 16M^2t)}{(t + (m_D^2)_{mljk})(t + (m_D^2)_{m'l'j'k'})} \quad (7.19)$$

Let us note here that the drag and the diffusion coefficient of HQ as defined in Eqs.(6.15) and (6.16) depends on the color of incoming and outgoing light quark i.e., Q^a and Q^b in the distribution functions; see Eq.(6.14). So to compute the color-averaged quantity, the color index a and b in Eq.(7.19) will be summed with the distribution function. With the distribution function as defined in Eq.(**??**), for Coulomb scattering the bracketed quantity in Eq.(6.14) becomes

$$\begin{aligned}\langle X(p')\rangle &= \frac{1}{2E_p}\sum_{abcd}\int\frac{d^3q}{2E_q(2\pi)^3}\frac{d^3p'}{2E_{p'}(2\pi)^3}\frac{d^3q'}{2E_{q'}(2\pi)^3}\sum_{jkj'k'}\sum_{mlm'l'}|\mathcal{M}_{qQ}|^2\\ &\times \quad (f_a^0(q)+\delta f_a(q))(1-f_b^0(q')-\delta f_b(q'))\langle X(p')\rangle \end{aligned} \tag{7.20}$$

Compton scattering: There are three types of scatterings (s, t and u channels) that contribute to the Compton scattering i.e., scattering off of a gluon from a quark. For s and u channel scatterings, the corresponding Feynman diagrams are shown in Fig.[6.7] and for the t channel scattering the relevant diagram is shown in right side of Fig.[6.6]. We shall evaluate the scattering amplitude for Compton scattering below.

s-channel: The relevant diagram for this channel is shown on the left side of Fig.[6.7] where $ef(gh), a(b)$ are color indices of incoming (outgoing) gluon and quark. In the double line notation, the scattering amplitude for the process is given as

$$i\mathcal{M}_s = i(ig)^2(t^{ef})_{ac}(t^{gh})_{cb}\left[\frac{\bar{u}_b(p')\not{\epsilon}(\not{p}+\not{q}+M)\not{\epsilon}u_a(p)}{s-M^2}\right]. \tag{7.21}$$

where s is Mandelstam variable and M is the mass of HQ. Note here that unlike Coulomb scattering there is no color dependence on the HQ propagator. This is because of the large mass of heavy quark. For massive quark and massless gluon the matrix element squared for s-channel Compton scattering can be written as

$$|\mathcal{M}_s|^2 = \frac{8g^4}{16N_c(N_c^2-1)}\mathcal{P}^{ef}_{ac}\mathcal{P}^{ef}_{ac'}\mathcal{P}^{gh}_{cb}\mathcal{P}^{gh}_{c'b}\left(\frac{M^2(M^2-u-3s)-us}{(s-M^2)^2}\right). \tag{7.22}$$

Note that the scattering amplitude depends on the color of quarks and gluons. For the evaluation of the transport coefficients one needs to perform a color sum. Same as in the case of Coulomb scattering, the color indices of incoming and outgoing gluon (ef, gh) in Eq.(7.22) will be summed with the distribution functions appearing in Eq.(6.14).

u channel: The corresponding Feynman diagram for u channel Compton scattering is illustrated at the right side of Fig.(6.7). Scattering amplitude that depends on the color of incoming and outgoing color particles can be written as

$$i\mathcal{M}_u = i(ig)^2(t^{ef})_{cb}(t^{gh})_{ac}\left[\frac{\bar{u}_b(p')\not\epsilon(\not p - \not q' + M)\not\epsilon u_a(p)}{u - M^2}\right]. \tag{7.23}$$

Simplifying Eq.(7.23) with the polarization sum of massless gluon and spin sum and average over heavy quark gives

$$|\mathcal{M}_u|^2 = \frac{8g^4}{16N_c(N_c^2-1)}\mathcal{P}^{gh}_{ac}\mathcal{P}^{gh}_{ac'}\mathcal{P}^{ef}_{cb}\mathcal{P}^{ef}_{c'b}\left(\frac{M^2(M^2-3u-s)-us}{(u-M^2)^2}\right). \tag{7.24}$$

In the Eq.(7.24), the product of projection operator can be simplified by summing over the color indices a, b and c. However, the color indices of initial and final gluon should be summed with the distribution function in Eq.(6.14). Keeping ef, gh as open indices, the product of the projection operators can be simplified to

$$\begin{aligned}
\mathcal{P}^{gh}_{ac}\mathcal{P}^{gh}_{ac'}\mathcal{P}^{ef}_{cb}\mathcal{P}^{ef}_{c'b} &= \delta_{eh} - \frac{1}{N_c}\Big(2\delta_{ef}\delta_{fh}\delta_{eh} + \delta_{gh}\delta_{eg}\delta_{eh}\Big) + \frac{1}{N_c^2}\Big(\delta_{ef} + \delta_{ef}\delta_{gf}\delta_{eh}\delta_{gh} \\
&+ \delta_{ef}\delta_{fh}\delta_{eg}\delta_{gh} + \delta_{eh}\delta_{fg}\delta_{ef}\delta_{gh} + \delta_{gh}\Big) - \frac{1}{N_c^3}\Big(\delta_{ef}\delta_{gh} \\
&+ \delta_{ef}\delta_{eh}\delta_{gh}\Big).
\end{aligned} \tag{7.25}$$

t channel: The relevant Feynman diagram for the t channel Compton scattering is shown on the right side of Fig.[6.6]. For the color dependent scattering amplitude one can write

$$i\mathcal{M}_t = (ig)^2(t^{ml})_{ab}f^{cd,ef,gh}\left[\frac{\epsilon_\mu(q)\epsilon^*_\nu(q')C^{\mu\alpha\nu}(q-q',-q,-q')\bar{u}_b(p')\gamma_\alpha u_a(p)}{(t+(m_D^2)_{mlcd})}\right], \tag{7.26}$$

where

$$C^{\mu\nu\rho}(k_1,k_2,k_3) = [(k_1-k_2)^\rho g^{\mu\nu} + (k_2-k_3)^\mu g^{\nu\rho} + (k_3-k_1)^\nu g^{\mu\rho}]. \tag{7.27}$$

In Eq.(7.26), $f^{cd,ef,gh}$ is structure constant as defined in Eq.(6.24) and $\epsilon_\mu(q), \epsilon^*_\nu(q')$ are the polarization vectors for incoming and outgoing gluon. The matrix element squared can be obtained by performing appropriate polarization sum for gluons and spin sum and average for heavy quark. Doing so, matrix element squared becomes

$$|\mathcal{M}_t|^2 = \frac{16g^4}{8N(N^2-1)}\mathcal{P}^{ml}_{ab}\mathcal{P}^{l'm'}_{ba}f^{cd,ef,gh}f^{d'c',fe,hg}\left(\frac{-(M^2-s)(M^2-u)}{(t+(m_D^2)_{mlcd})(t+(m_D^2)_{m'l'c'd'})}\right). \tag{7.28}$$

The corresponding interference terms among Compton scatterings are given in appendix(A). To that the total scattering amplitude of Compton scattering that enters in Eq.(6.14) for evaluation of the drag and the diffusion coefficients is $|\mathcal{M}_{gQ}|^2_{efgh} = |\mathcal{M}_s|^2 + |\mathcal{M}_u|^2 + |\mathcal{M}_t|^2 + |\mathcal{M}_s|^\dagger|\mathcal{M}_u| + |\mathcal{M}_u|^\dagger|\mathcal{M}|_s + |\mathcal{M}_s|^\dagger|\mathcal{M}_t| + |\mathcal{M}_t|^\dagger|\mathcal{M}|_s| + |\mathcal{M}_t|^\dagger|\mathcal{M}_u| + |\mathcal{M}_u|^\dagger|\mathcal{M}|_t$. For computational simplification, we shall use the leading order contribution in the Debye mass that appears in the t channel scatterings.

7.3 Results and discussions

With the scattering amplitude for the processes $lQ \to lQ$ (where l stands for light quark/antiquark and gluon and Q stands for HQ) as evaluated in the previous section, we numerically compute the drag and the diffusion coefficients using Eq.[6.14] and incorporate the dissipative effects in the quark/antiquark and gluon color distribution functions as defined in Eqs.(7.12) and (7.13).

For this purpose, we use charm quark mass $M = 1.27$ GeV and the two loop running coupling constant [261]

$$\alpha_s = \frac{1}{4\pi}\frac{1}{2\beta_0 \ln\frac{\pi T}{\Lambda} + \frac{\beta_1}{\beta_0}\ln(2\ln(\frac{\pi T}{\Lambda}))} \tag{7.29}$$

where

$$\beta_0 = \frac{1}{16\pi^2}\left(11 - \frac{2N_f}{3}\right) \tag{7.30}$$

$$\beta_1 = \frac{1}{(16\pi^2)^2}\left(102 - \frac{38N_f}{3}\right) \tag{7.31}$$

with $\Lambda = 260$ MeV and light quark flavor $N_f = 2$. We also evaluate the HQ transport coefficients in pQCD by evaluating scattering amplitude squared within

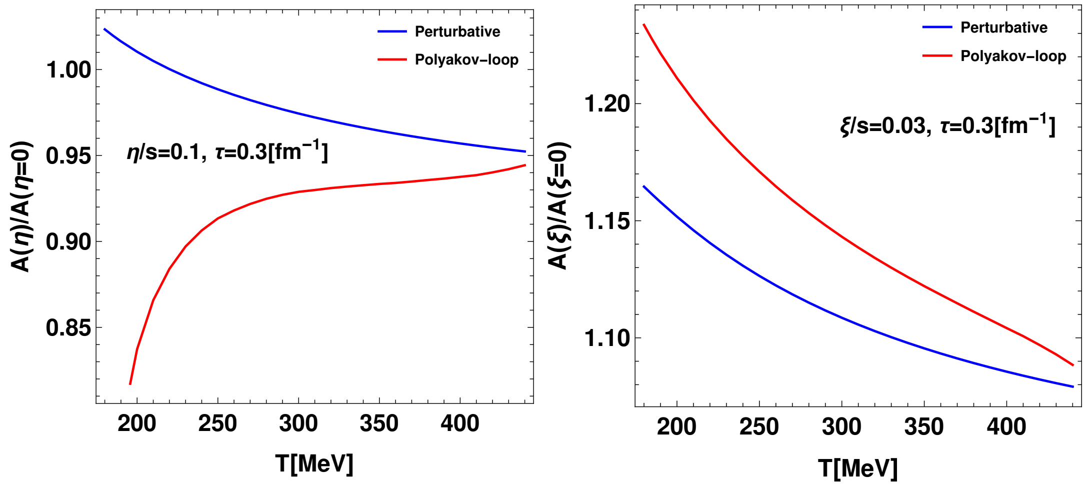

Figure 7.1: The ratiso $A(\eta)/A(\eta = 0)$ and $A(\xi)/A(\xi = 0)$ of drag coefficients as a function of temperature for $p = 1$ GeV, $\eta/s = 0.1, \xi/s = 0.03$ and $\tau = 0.3$ fm^{-1}.

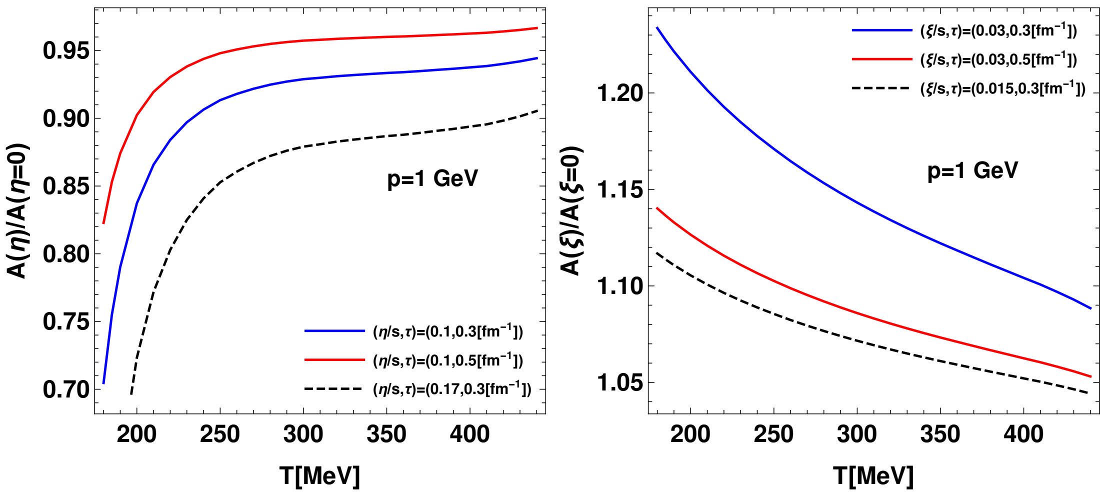

Figure 7.2: The ratio $A(\eta)/A(\eta = 0)$ and $A(\xi)/A(\xi = 0)$ as a function of temperature respectively for HQ momentum $p = 1$ GeV, $\xi/s = 0, \eta/s = 0.1, 0.17$ and $\xi/s = 0.03, 0.15, \eta/s = 0$ and $\tau = 0.3, 0.5$ fm^{-1}.

the pQCD framework.

In general, there are two factors that essentially affect the heavy quark transport properties. One is the Debye mass that appears in the evaluation of the matrix elements and the other is the Polyakov loop dependent distribution functions of quark/anti-quark and gluon. At low temperature, a lower value of the Debye mass increases the transport coefficients. On the other hand, the distribu-

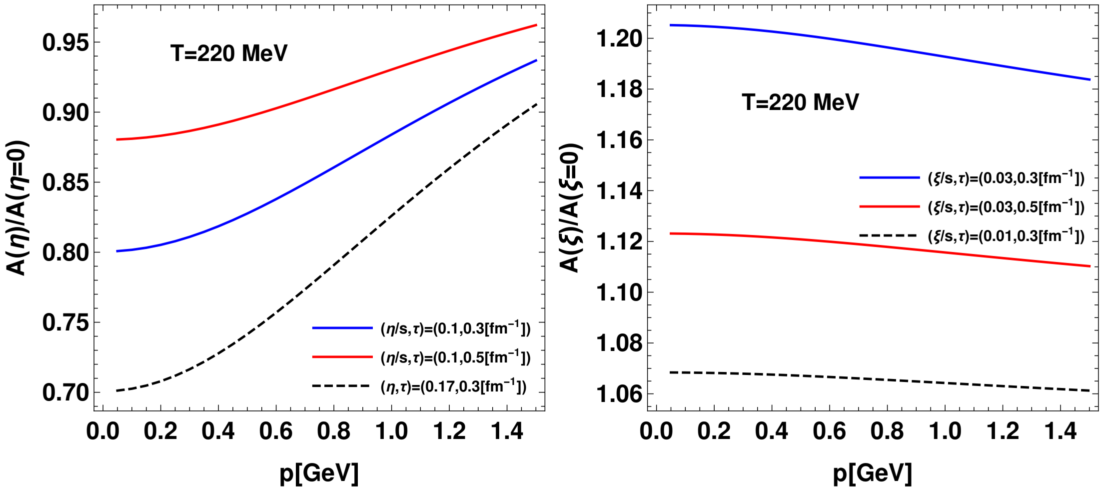

Figure 7.3: The ratios $A(\eta)/A(\eta = 0)$ and $A(\xi)/A(\xi = 0)$ of drag coefficients as a function of HQ momentum for $\eta/s = 0.1, 0.17$, $\xi/s = 0.01, 0.03$, $\tau = 0.5, 0.3$ and and $T = 220$.

tion function with the non-trivial ϕ tend to reduce it. These apart, a third factor that plays an important role here is the momentum dependence of departure $\delta f_{a/ab}$ in Eqs.(**??**) and (**??**) of the distribution function from the equilibrium distribution function. Now let us examine the results in somewhat detail. In Fig.(7.1), we show the dependence of the drag coefficient as a function of temperature. In the left panel, we have plotted the drag coefficient (Eq.(6.15)) for a constant value of η/s and $\xi/s = 0$ normalized to the drag coefficient for $\eta/s = 0, \xi/s = 0$ i.e., $A(\eta)/A(\eta = 0)$. In both the figures of Fig.(7.1), we have taken $\tau = 0.3$ fm^{-1} and the HQ momentum $p = 1$ GeV. The blue curve corresponds to the pQCD results and the red curve corresponds to the effect of the Polyakov loop within the matrix model. It is clear that at low temperature, for $\eta/s = 0.1$ and $\tau = 0.3$ fm^{-1}, the drag coefficient is small within the matrix model compared to pQCD. As the temperature increases the suppression in the drag coefficient decreases and approaches the perturbative value at high temperature beyond which it decreases similar to the perturbative results. This non-monotonic behavior is mainly because of the negative contribution from the momentum factor $(\mathbf{q}^2/3 - q_z^2)$ in $\delta f_{a/ab}$ and can be understood as follows. In the Polyakov loop background, a smaller value of the Debye mass at low temperature lead to more negative contribution due to the momentum factor in $\delta f_{a/ab}$ and hence smaller drag coefficient with finite η/s. Another reason for more suppression in the drag coefficient within the matrix model is due to the distribution function i.e., colored particles are suppressed due to small value of Polyakov loop compared to pQCD. In the right panel of Fig.(7.1), the temperature behavior of the normalized drag coefficient $(A(\xi)/A(\xi = 0))$ is shown for $\xi/s = 0.03$ and $\eta/s = 0$. It can be observed that with the inclusion of the bulk viscosity the drag coefficient is large compared to the $\xi/s = 0$ case. The drag coefficient within the matrix model is large compared to pQCD. This is because the ξ/s term in $\delta f_{a/ab}$ is always positive so the smaller value of the Debye mass within the matrix model enhances the drag coefficient.

The ratio $A(\eta)/A(\eta = 0)$ of the drag coefficient as defined in Eq.(6.15) is plotted as a function of temperature for HQ momentum $p = 1$ GeV in Fig.(7.2) for various value of η/s and τ to see the effect of both $(\eta/s, \tau)$ the quantities. Here the scattering amplitude squared for the relevant scatterings are evaluated within the matrix model. As anticipated from the effect of phase space (momentum dependent term in $\delta f_{a/ab}$), Polyakov loop dependent distribution functions of quark/anti-quark and gluon, and the Debye mass, with an increase in η/s the HQ drag coefficient decreases as shown by the black dashed and the blue curves on the left panel of Fig.(7.2). Here the blue line is for $\eta/s = 0.1$ and black dashed line for $\eta/s = 0.17$ with $\tau = 0.3$ fm^{-1}. With increase in the proper time the drag coefficient increases which is shown by the red and the blue curve of the same figure. This can be understood from $1/\tau$ factor in Eqs.[7.12] and [7.13]. It is also observed that, for small value of η/s and sufficiently large value of τ, the effect of η/s on the HQ drag coefficient is weak. On the right panel of Fig.(7.2), the effect of ξ/s and τ on the drag coefficient is shown. As expected, with an increase in ξ/s, the drag coefficient increases as shown by a dashed black and the blue curve i.e., $\xi/s = 0.015$ (dashed black lines) and $\xi/s = 0.03$ (blue lines) for $\tau = 0.3$ fm^{-1}. Same as earlier, with an increase in τ, the drag coefficient decreases.

Drag coefficient $A(\eta)$ normalized with $A(\eta = 0)$ as a function of HQ momentum p for $T = 220$ MeV is shown in Fig.(7.3). Here, we have also shown the results for HQ momenta $p \sim M$. The extrapolated results for higher momenta will not be reliable as we have not taken contribution from gluon radiation. As may be observed from the left panel of the same figure, for finite η/s, the drag coefficient increases with an increase in the HQ momentum. However, with an increase in η/s,

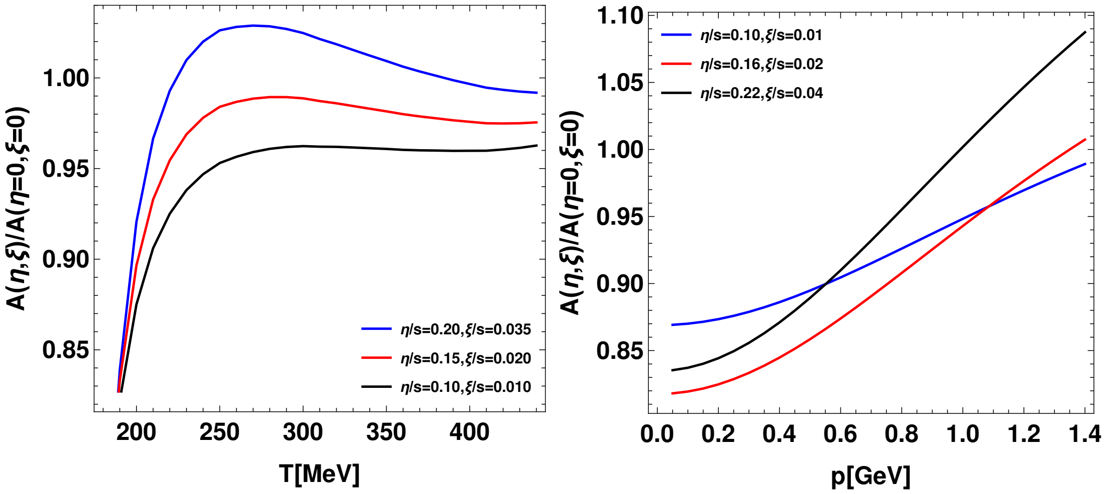

Figure 7.4: The ratio $A(\eta, \xi)/A(\eta = 0, \xi = 0)$ of drag coefficients as function of temperature and HQ momentum for $\eta/s = 0.1, 0.15, 0.2$, $\xi/s = 0.01, 0.035$ and and $\tau = 0.3$ fm^{-1}.

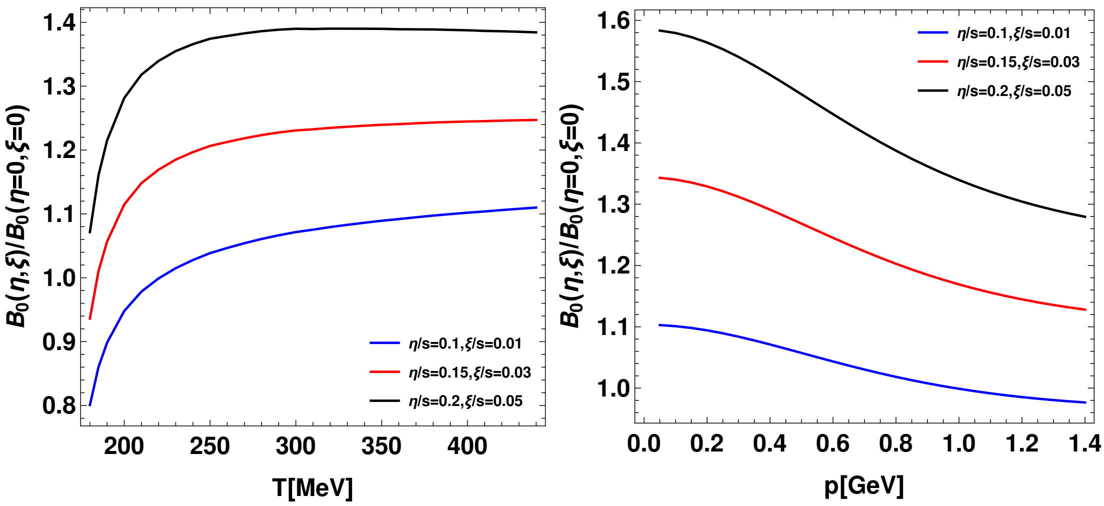

Figure 7.5: The ratio $B_0(\eta, \xi)/B_0(\eta = 0, \xi = 0)$ of diffusion coefficients as function of temperature and HQ momentum for $\eta/s = 0.1, 0.15, 0.2$, $\xi/s = 0.01, 0.03, 0.05$ and and $\tau = 0.3$ fm^{-1}.

the drag coefficient decreases as shown by the black dashed curve ($\eta/s = 0.17$) and the blue curve ($\eta/s = 0.1$). As earlier, this behavior can be explained by taking account of phase space suppression (momentum dependent term in $\delta f_{a/ab}$). Same as earlier, with an increase in τ, the drag coefficient decreases. On the right panel of the same figure, the effect of bulk viscosity on the HQ drag coefficient is shown.

Here, the drag coefficient decreases with an increases in the HQ momentum. Note that unlike η/s, with increase in ξ/s, the drag coefficient increases. Same as earlier, with an increases in τ the drag coefficient decreases.

On the left panel of Fig.(7.4), the effect of both the bulk viscosity (ξ/s) and the shear viscosity (η/s) for $\tau = 0.3$ fm^{-1} on the normalized drag coefficient ($A(\eta,\xi)/A(\eta = 0,\xi = 0)$) as a function of temperature is shown. At low temperature, shear viscosity dominates due to the phase space suppression so the drag coefficient decreases. At moderate temperature i.e., around 250 MeV, the bulk viscosity dominates so the drag coefficient increases, again at high temperature i.e., around 320 MeV, as seen earlier in Fig.(7.2), both η/s and ξ/s decreases the drag coefficient. As can be noted, for a smaller value of η/s and ξ/s e.g., $\eta/s = 0.1, \xi/s = 0.01$, the dependence of the drag coefficient on temperature is somewhat weak, however, the dependence is strong for a larger value of η/s and ξ/s. On the right panel of Fig.(7.4) the same ratio as a function of momentum is plotted. Similar to the case of temperature behavior, for smaller values of η/s and ξ/s the drag coefficient is somewhat weakly dependent on the HQ momentum (see blue curve; $\eta/s = 0.1, \xi/s = 0.01$), however, it strongly depends on the same for larger values η/s and ξ/s. Also note that at low momentum, for finite value of η/s and ξ/s, the drag coefficient is small and increases with an increase in the HQ momentum.

The ratio $B_0(\eta,\xi)/B_0(\eta = 0,\xi = 0)$ of diffusion coefficients as defined in Eq.(6.16) is plotted as a function of temperature and momentum in Fig.(7.5). On the left panel of Fig.(7.5), the black curve corresponds to $\eta/s = 0.2, \xi/s = 0.05$, the red curve corresponds to $\eta/s = 0.15, \xi/s = 0.03$ and the blue curve corresponds to $\eta/s = 0.1, \xi/s = 0.01$. Here, we have taken $\tau = 0.3$ fm^{-1} and the HQ momentum $p = 1$ GeV. It is observed that with an increase in $\eta/s, \xi/s$ and temperature, the diffusion coefficient increases. However, for smaller values of η/s and ξ/s e.g., $\eta/s = 0.1, \xi/s = 0.01$, the diffusion coefficient is not affected much. Note also that at low temperature for a smaller value of η/s and ξ/s e.g., blue curve, the diffusion coefficient is smaller as compared to the case of $\eta/s = 0, \xi/s = 0$. Similarly, as can be seen in the right panel of the same figure, with as increase in the HQ momentum the diffusion coefficient decreases. For the HQ momentum $p \ll M$, with an increase in η/s and ξ/s, the diffusion coefficient increases. In pQCD, the

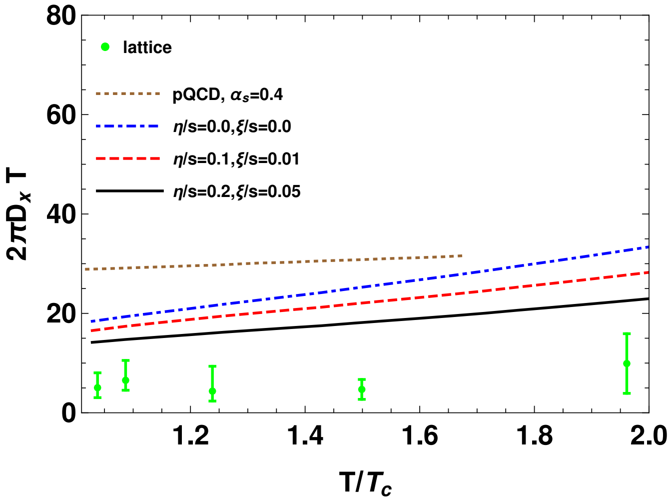

Figure 7.6: The spatial diffusion $2\pi D_x T$ as a function of temperature scaled by T_c for $\tau = 0.3$ fm^{-1},$\eta/s = 0.1, 0.2$ and $\xi/s = 0.01, 0.005$.

results for the drag and the diffusion coefficients for various values of $\eta/s, \xi/s, \tau$ as a function of temperature and momentum that are presented here are similar as pointed out in Ref.[214]. However, the differences are due to the effect of the Polyakov loop.

It may be noted that with the Fokker-Plank formalism, one can relate the momentum diffusion coefficient $B_0(p)$ as estimated here to the spatial diffusion coefficient D_x that appears e.g., in the Ficks diffusion law. The diffusion coefficient D_x is also estimated in the lattice QCD simulation. The two coefficients are related as [297]

$$D_x = \frac{T^2}{B_0(p \to 0)}. \tag{7.32}$$

In Fig.(7.6), we have plotted the quantity $2\pi D_x T$ from leading order (LO) pQCD along with the lattice simulations and within the matrix model for various values of η/s, ξ/s and $\tau = 0.3$ fm^{-1} as a function of T/T_c. The brown dotted line is LO pQCD result for constant coupling $\alpha_s = 0.4$. The blue (dashed dotted), red (dashed) and black (solid) lines are within the matrix model respectively for $\eta/s = 0, 0.1, 0.2$ and $\xi/s = 0, 0.01, 0.05$. The green dots are the lattice results from Ref. [96].

The main observation in this figure are the following. The spatial diffusion coefficient is smaller compared to the perturbative QCD estimate. Inclusion of the viscous effect makes the coefficient even smaller. However, even with the inclusion of viscous effects as well as Polyakov loop, the spatial diffusion coefficient is still larger being almost about three times the corresponding lattice estimate. This indicates that there could be other non-perturbative effects possibly the contribution of finite light quark mass and also the radiative corrections for the estimation of diffusion coefficients.

7.4 Summary

In this chapter, we have computed the corrections due to the effects of the shear and the bulk viscosities on the HQ drag and diffusion coefficients within the matrix model of semi QGP. To incorporate the viscous corrections we first write the distribution function of quark and gluon ($f_{a/cd} = f^0_{a/cd} + \delta f_{a/cd}$, where $f^0_{a/cd}$ is equilibrium distribution function and $\delta f_{a/cd}$ summarizes the effect of shear and bulk viscosities) as defined in Eqs.(**??**) and (**??**). We next calculate the color dependent scattering amplitudes of HQ from the light thermal partons in the bulk medium within the matrix model of semi QGP. Non-perturbative effects are included via the Polyakov loop in quark/antiquark and gluon distribution functions as well as in the Debye mass. In all the calculations, we have taken the constant values for the viscosity to entropy density ratio .e., without their temperature dependence. With a reasonable constant value of η/s for the temperature range we have considered, we find that the drag coefficient within the matrix model is small compared to that of perturbative QCD. Similarly, for a constant value of ξ/s, the drag coefficients is large within the matrix model compared the pQCD results. Furthermore, with an increase in temperature and momentum the drag coefficient increases, however, the diffusion coefficient increases with an increase in temperature and decreases with an increase in momentum. The spatial diffusion coefficient decreases with increase in the η/s and ξ/s. For a small value of η/s and ξ/s, both the drag and the diffusion coefficients have a weak dependence on temperature and momentum for all range of temperature and momentum considered here.

CHAPTER 8

Conclusion

Measurements related to heavy quark-antiquark bound state and the HQ open meson has been a promising tool to study the properties of the deconfined matter in the HICs. The in-medium modifications to the quarkonia binding are well described by the potential models, which is rigorously validated by the effective field theories. Here, we have attempted to incorporate the magnetized in-medium effects on both the Coulomb as well as the string part of the Cornell potential. In medium permittivity is used to include the impact of the medium on the vacuum Cornell potential. The jet quenching data suggestive of more energy loss of high/intermediate momentum heavy quark jet. In addition to the temperature, we estimate the contribution from the magnetic field in the strong-field limit. We found that in this limit, both thermal and magnetic field contributions are of a similar order. In the low momentum limit, the magnetic field gives rise to the anisotropic nature of the diffusion coefficient. These anisotropic drag/diffusion may be useful to estimate the directed and collective flow of the open mesons. In the low momentum regime, the large collectivity also requires the coupling to be large, i.e., non-perturbative effects. We employ these effects via the Polyakov loop and constituent mass of light quarks within the matrix model of semi-QGP.

The brief introduction of the topics considered in the present work is discussed in chapter1. After the short presentations of the introductory topics, we have discussed the in-medium quarkonia potential in a magnetized thermal QGP medium in chapter 2. For the magnetic field, we have considered the strong-field limit, i.e., LLL approximation. To incorporate the magnetic field and temperature effects on both the Coulomb as well as the string part of the Cornell potential, we have used the generalized Gauss law with the in-medium permittivity. We have found that both the real and the imaginary part of the potential gets modified. The imaginary part of the potential increases in magnitude with the increase in magnetic field and temperature. As a result, the width of the quarkonium states (J/ψ and Υ) get more broadened with the increase in the magnetic field and results in the earlier dissociation of quarkonium states in the presence of the magnetic field. The width for Υ is much smaller than the J/ψ because bottomonium states are tighter than the charmonium state. Thus the bottomonium states dissociate at a higher temperature. The change in decay width from (11-14)% at $T = 200$ MeV and from (5- 7)% at $T = 250$, for the magnetic field ranging from (5-25) m_π^2. For the magnetic field $\mathbf{B} \sim T^2$, one also needs to take higher LLs contribution in the quarkonia potential. In order to fully understand the suppression of quarkonia potential, one not only needs to know the quark-antiquark pair evolution but also the non-perturbative effects that so far have not been understood quite well. The real-time quarkonium dynamics is further simplified within the open quantum system framework that allows one to incorporate all the relevant time scales. So far, the implementation of non-perturbative effects within the open quantum system approach is not explored.

In chapter 4, we have estimated the effect of the magnetic field on the HQ collisional energy loss. Here, we have assumed the strong-field limit of the magnetic field, i.e., $eB \gg T^2$, so that only LLL is active. We have also considered the scale hierarchy $M \gg \sqrt{eB} \gg T \gg g\sqrt{eB}$ so that the HQ is not directly affected by the magnetic field. Thus, at leading order in the coupling, out of four scattering diagrams, only t-channel scatterings contribute to the collisional energy loss. For these scatterings of HQ with the thermalized light partons we have considered the soft momentum transfer limit i.e., $g\sqrt{eB} \leq |\mathbf{k}| \ll T \ll \sqrt{eB}$. With $M \gg \sqrt{eB}$. Out of these two t-channel scatterings, Coulomb scattering, i.e., $Qq \to Qq$, is more sensitive to the magnetic field because of its dependency on the spectral function which increases with the magnetic field. Furthermore, this finally leads to an increase in energy loss with the magnetic field. For the magnetic field $eB = 5m_\pi^2$, the energy loss with and without the magnetic field are quite similar. For the realistic situation for the magnetic field in the HIC, one also needs to take the contribution from the higher LLs. In addition to the magnetic field contributions, a systematic study of non-perturbative effects on HQ collisional energy loss is needed in order to understand the thermalization of HQ/jet quenching in the bulk medium.

In chapter 5, we have studied the anisotropic nature of the momentum diffusion coefficient of HQ in the presence of the magnetic field. Here again, we have considered the strong-field limit of the magnetic field along with the scale hierarchy $M \gg \sqrt{eB} \gg T \gg g\sqrt{eB}$. Similar to the collisional energy loss in chapter 4, here also, the HQ is not directly affected by the magnetic field, and only t-channel scatterings contribute to transport coefficients. Depending on the relative directions of the HQ velocity and the magnetic field, there are five diffusion coefficients. For the case HQ velocity to align along the magnetic field, there are two momentum diffusion coefficients. Out of these two, the diffusion in the transverse direction is larger than that of the longitudinal one, i.e., $\kappa_{TT}^{\parallel} \gg \kappa_{LL}^{\parallel}$. On the other hand, for the case of the HQ velocity to align perpendicular to the magnetic field, there are three momentum diffusion coefficients. Out of these three, the diffusion coefficient transverse to the HQ velocity and longitudinal to the magnetic field is the dominant one, i.e., $\kappa_{TL}^{\perp} \gg \kappa_{LT}^{\perp} \gg \kappa_{TT}^{\perp}$. The anisotropic nature of the diffusion coefficient signifies the anisotropy in the drag force. For the case where the magnetic field is of the order of temperature, i.e., $eB \sim T^2$, the contribution of higher LLs becomes significant and can not be ignored. One important question one can ask is up to what extent these anisotropic diffusion coefficients contribute to the directed as well as elliptic flow of HQ. In fact, the directed flow of heavy open mesons has been proposed as one of the potential observable to probe the magnetic field in HICs. So far, with the current understanding of HQ evolution in the medium, it has not been possible to quantify this effect.

In chapter 6, we have discussed the possible non-perturbative effects arising from confinement and chiral symmetry on HQ transport coefficients. The first one is summarised via the non-zero expectation value of the Polyakov loop while the later one is included via constituent quark mass. In order to incorporate these two effects, we first estimate quark/gluon thermal/Debye mass. It was found that temperatures below 300 MeV quark thermal mass and gluon Debye mass start deviating from its perturbative value; this effect significant for even higher temperatures when Polyakov values are taken from the lattice simulations. This decrease in the Debye mass of gluon and the thermal mass of light quarks is due to color suppression manifested in the quark and gluon distribution functions in the presence of a background Polyakov loop field. In the calculation of the HQ diffusion coefficient, the distribution function of the light quark and the Debye mass play complementary roles. While the distribution function with the Polyakov loop tends to decrease the HQ transport coefficient, the Debye mass has the effect of increasing these transport coefficients. We have found a weak temperature dependence of the heavy quark drag coefficient with Polyakov loop value taken from PQM, which is consistent with other models like the T-matrix and quasi-particle model that also take into account the non-perturbative effects in a different manner. This consistency suggests the existence of possible model-independent correlations between the results obtained with the Polyakov loop and other non-perturbative models and reaffirm the temperature and momentum dependence of heavy quark transport coefficients.

In chapter 7, we estimate viscous effects on HQ transport coefficients within the matrix model of semi-QGP. In order to do this we first write the distribution function of quark and gluon, i.e.,$f_{a/cd} = f^0_{a/cd} + \delta f_{a/cd}$, where $f^0_{a/cd}$ is equilibrium distribution function and $\delta f_{a/cd}$ summarizes the effect of shear and bulk viscosities. We next calculate the color-dependent scattering amplitudes of HQ from the light thermal partons in the bulk medium within the matrix model of semi QGP. Non-perturbative effects are included via the Polyakov loop in quark/antiquark and gluon distribution functions as well as in the Debye mass. With a reasonable constant value of η/s for the temperature range, we have considered, we find that the drag coefficient within the matrix model is small compared to that of perturbative QCD. Similarly, for a constant value of ξ/s, the drag coefficients are large within the matrix model compared to the pQCD results. Furthermore, with an increase in temperature and momentum, the drag coefficient increases; however, the diffusion coefficient increases with an increase in temperature and decreases with an increase in momentum. The spatial diffusion coefficient decreases with increase in the η/s and ξ/s. For a small value of η/s and ξ/s, both the drag and the diffusion coefficients have a weak dependence on temperature and momentum. Indeed, there are enough hints, both theoretically, and experimentally that appreciate the need of (strong coupling) non-perturbative effects on HQ transport coefficients. Experimentally, observable such as v_2 and R_{AA} of open heavy flavor meson require a large drag coefficient of HQ compared to perturbative QCD predictions. On the other hand, the radiative corrections in the non-perturbative regime are not understood quite well. Some of these questions will be explored in the near future as in continuation of the work presented in this thesis.

APPENDIX **A**

Appendix

A.1 Gluon self energy in a magnetic field background

In the RTF, the retarded self energy of gluon in the Keldysh basis can be written as

$$\Pi_R^{\mu\nu}(p_0, \mathbf{p}) = \Pi_{11}^{\mu\nu}(p_0, \mathbf{p}) + \Pi_{12}^{\mu\nu}(p_0, \mathbf{p}), \tag{A.1}$$

where $\Pi_{11}^{\mu\nu}$ and $\Pi_{12}^{\mu\nu}$ are 11 and 12 component of the gluon self energy. Both 11 and 22 components of self energy can be obtained by using the quark propagators to acquire

$$\Pi_R^{\mu\nu}(p_0, \mathbf{p}) \;\; = \;\; \Omega \int \frac{d^2k_\parallel}{(2\pi)^2}\Bigg(Tr[\gamma^\mu S_{11}(Q)\gamma^\nu S_{11}(K) - \gamma^\mu S_{21}(Q)\gamma^\nu S_{12}(Q)]\Bigg), \tag{A.2}$$

where

$$\Omega = \frac{-ig^2|q_fB|}{16\pi}\exp\Bigg(-\frac{p_\perp^2}{|2q_fB|}\Bigg). \tag{A.3}$$

In Eq.(A.2), the B dependent term (i.e., Ω) comes from the transverse part in the quark propagator. In the LLL, the dynamics in the transverse direction is restricted due to dimensional reduction from (3+1)-dimension to (1+1)-dimension. Therefore, the gauge invariant form of the gluon self energy in a magnetic field background can be written as

$$\Pi_R^{\mu\nu}(p_0, \mathbf{p}) = \Pi_R^{\parallel}(P)\Bigg(g_\parallel^{\mu\nu} - \frac{p_\parallel^\mu p_\parallel^\mu}{p_\parallel^2}\Bigg). \tag{A.4}$$

To estimate the energy loss, we need $\Pi^{\parallel}_R(P)$ which can be obtained from the relation $\Pi^{\parallel}_R(P) = -(p^2_{\parallel}/p^2_z)\Pi^{00}_R(p_0, \mathbf{p})$. Therefore, we focus only on the time-like component (Π^{00}_R) of retarded self energy. Taking the trace over Dirac matrices in Eq.(A.2), we get

$$\Pi^{00}_R(p_0, \mathbf{p}) \quad = \quad 8\Omega \int \frac{d^2k_{\parallel}}{(2\pi)^2}(\mathcal{K}\cdot\mathcal{Q})\Big(\Delta_{11}(Q)\Delta_{11}(K) - \Delta_{21}(Q)\Delta_{12}(K)\Big), \tag{A.5}$$

where Δ_{11} and Δ_{12} are defined in Eqs.(4.31) and (4.32) with $\mathcal{K}\cdot\mathcal{Q} = k_0q_0 + k_zq_z + m^2$. Similar to Δ_{11}, Δ_{21} can also be obtained from S_{21}. Eq.(A.5) can further be simplified by writing the propagators Δ_{ij} in terms of the retarded, advanced and symmetric propagators similar to the one defined in chapter2 to acquire

$$\Pi^{00}_R(p_0, \mathbf{p}) \quad = \quad 4\Omega \int \frac{d^2k_{\parallel}}{(2\pi)^2}(\mathcal{K}\cdot\mathcal{Q})\Big(\Delta_F(Q)\Delta_R(K) + \Delta_A(Q)\Delta_F(K)\Big). \tag{A.6}$$

Replacing $K \to -Q$ and using the relation $\Delta_R(-Q) = \Delta_A(Q)$, Eq.(A.6) becomes

$$\Pi^{00}_R(p_0, \mathbf{p}) \quad = \quad 2\pi|\Omega| \int \frac{d^2k_{\parallel}}{(2\pi)^2}(\mathcal{K}\cdot\mathcal{Q})(1-2\tilde{f}(k_0))\delta(k^2_{\parallel} - m^2_f)\frac{1}{q^2_{\parallel} - m^2_f - i\epsilon q_0} \tag{A.7}$$

The first term of Eq.(A.7) which is independent of the Fermi Dirac distribution function, is the vacuum contribution to the time-like component of the gluon self energy. The time-like component of the gluon self energy can be separated into the vacuum and the thermal parts to get

$$\Pi^{00}_R(p_0, \mathbf{p}) = \Pi^{00}_R(p_0, \mathbf{p})|_{vac} + \Pi^{00}_R(p_0, \mathbf{p})|_{th}, \tag{A.8}$$

where the vacuum term is given as [144]

$$\Pi^{00}_R(p_0, \mathbf{p})|_{vac} \quad = \quad \frac{2|\Omega|p^2_z}{p^2_{\parallel} + i\epsilon p_0}\left[1 - \frac{4m^2_f}{\sqrt{p^2_{\parallel}(4m^2_f - p^2_{\parallel})}}\arctan\left(\frac{p^2_{\parallel}}{\sqrt{p^2_{\parallel}(4m^2_f - p^2_{\parallel})}}\right)\right] \tag{A.9}$$

For the thermal contribution to the time-like component of the gluon self energy, the energy integral in Eq.(A.7) can be done by using the energy delta function to obtain

$$\Pi^{00}_R(p_0, \mathbf{p})|_{th} \quad = \quad -\frac{2\pi|\Omega|m^2_fp^2_z}{p^2_{\parallel}}\left(\mathcal{J}_0(P) + \frac{2p_z}{p^2_{\parallel}}\mathcal{J}_1(P)\right), \tag{A.10}$$

with

$$\mathcal{J}_a = \int_{-\infty}^{\infty}\frac{dk_z}{2\pi E}\tilde{f}(E)\frac{k^a_z}{(k_z - p_z/2)^2 - p^2_0/4 + p^2_0m^2_f/p^2_{\parallel} - ip_0\epsilon}, \tag{A.11}$$

where $a = 0, 1$. Using Eq.(A.10) and the relation $\Pi_R^{\parallel}(P) = -(p_{\parallel}^2/p_z^2)\Pi_R^{00}(p_0, \mathbf{p})$, the parallel component of the medium dependent gluon self energy can be written as

$$\Pi_R^{\parallel}(P) = 2\pi|\Omega|m_f^2\left[\mathcal{J}_0(P) + \frac{2p_z}{p_{\parallel}^2}\mathcal{J}_1(P)\right]. \tag{A.12}$$

Imaginary part of the gluon self energy: The imaginary part of the retarded self energy of the gluon can be obtained from the imaginary part of the 11 component of gluon self energy by using the relation [5]

$$\Im\Pi_R^{\mu\nu}(p_0, \mathbf{p}) = (1 - \tilde{f}(p_0))\Im\Pi_{11}^{\mu\nu}(p_0, \mathbf{p}), \tag{A.13}$$

where

$$\Pi_{11}^{\mu\nu}(p_0, \mathbf{p}) = ig^2t^at^b\int\frac{d^2k_\perp}{(2\pi)^2}e^{-\frac{k_\perp^2+q_\perp^2}{|q_fB|}}\int\frac{d^2k_\parallel}{(2\pi)^2}Tr[\gamma^\mu S_{11}(K)\gamma^\nu S_{11}(Q)]. \tag{A.14}$$

$S_{11}(P)$ in Eq.(A.14), is the 11 component of the quark propagator in RTF that can be obtained from the retarded, advanced and symmetric propagators obtained by inverting the relations given in Eqs.2.28, 2.29 and2.30. Using the Eqs.(4.9) and (4.10), the imaginary part of $\Pi_{11}^{\mu\nu}(P)$ can be written as

$$\begin{aligned}
\Im\Pi_{11}^{\mu\nu}(p_0, \mathbf{p}) &= \pi g^2t^at^b\Omega\int_{-\infty}^{\infty}\frac{dk_z}{2\pi}\frac{1}{4E_kE_q}\Bigg[\Big(1 - \tilde{f}(E_k) - \tilde{f}(E_q) + 2\tilde{f}(E_k)\tilde{f}(E_q)\Big)\\
&\times \Big(\mathcal{N}^{\mu\nu}(k_0 = E_k)\delta(p_0 - E_k - E_q) + \mathcal{N}^{\mu\nu}(k_0 = -E_k)\delta(p_0 + E_k + E_q)\Big)\\
&+ \Big(-\tilde{f}(E_k) - \tilde{f}(E_q) + 2\tilde{f}(E_k)\tilde{f}(E_q)\Big)\Big(\mathcal{N}^{\mu\nu}(k_0 = -E_k)\delta(p_0 - E_k + E_q)\\
&+ \mathcal{N}^{\mu\nu}(k_0 = E_k)\delta(p_0 + E_k - E_q)\Big)\Bigg],
\end{aligned} \tag{A.15}$$

where

$$\mathcal{N}^{\mu\nu} = Tr[\gamma^\mu\mathcal{S}_0(K)\gamma^\nu\mathcal{S}_0(Q)], \tag{A.16}$$

with

$$\mathcal{S}_0(K) = (\not{k}_{\parallel} + m_f)(1 + i\gamma^1\gamma^2). \tag{A.17}$$

The imaginary part of the retarded self energy i.e., $\Im\Pi_R^{\parallel}$ can be obtained from $\Im\Pi_R^{00}$ by using the general structure of the retarded self energy as given in Eq.(A.4). So only the time-like component of $\Im\Pi_{11}^{\mu\nu}$ i,e., $\Im\Pi_{11}^{00}$ is relevant which can be obtained from Eq.(A.15). The momentum integration in Eq.(A.15) can be done by using the energy delta functions. Let us first simplify the energy delta functions and re-write those in terms of k_z. By using the relation

$$\delta(f(x)) = \sum_n \frac{\delta(x-x_n)}{\left|\frac{\partial f(x)}{\partial x}\right|_{x=x_n}}, \tag{A.18}$$

one can write

$$\delta(p_0 - E_k - E_q) = \frac{\delta(k_z - k_z^0)E_{k_z^0}E_{q_z^0}}{k_z^0(E_{k_z^0}+E_{q_z^0})} + \frac{\delta(k_z - k_z^1)E_{k_z^1}E_{q_z^1}}{k_z^1(E_{k_z^1}+E_{q_z^1})}, \tag{A.19}$$

$$\delta(p_0 + E_k - E_q) = \frac{\delta(k_z - k_z^0)E_{k_z^0}E_{q_z^0}}{k_z^0(E_{k_z^0}-E_{q_z^0})} + \frac{\delta(k_z - k_z^1)E_{k_z^1}E_{q_z^1}}{k_z^1(E_{k_z^1}-E_{q_z^1})}, \tag{A.20}$$

where

$$k_z^0 = -\frac{p_z}{2} + \frac{1}{2|p_\parallel|}\sqrt{p_z^2p_\parallel^2 - 4p_0^2m_f^2 + p_\parallel^4}, \tag{A.21}$$

and

$$k_z^1 = -\frac{p_z}{2} - \frac{1}{2|p_\parallel|}\sqrt{p_z^2p_\parallel^2 - 4p_0^2m_f^2 + p_\parallel^4}. \tag{A.22}$$

With further simplification, the imaginary part of Π_{11}^{00} can be written as

$$\begin{aligned}
\Im\Pi_{11}^{00}(p_0,\mathbf{p}) &= g^2t^at^b\Omega\pi 2m_f^2\Bigg[\Bigg(\frac{1}{k_z^0(E_{k_z^0}+E_{q_z^0})} + \frac{1}{k_z^1(E_{k_z^1}+E_{q_z^1})}\Bigg) - (\tilde{f}(k_z^0)+\tilde{f}(q_z^0) \\
&- 2\tilde{f}(k_z^0)\tilde{f}(q_z^0))\Bigg(\frac{2E_{k_z^0}}{k_z^0p_z(2k_z^0+p_z)}\Bigg) - (\tilde{f}(k_z^1)+\tilde{f}(q_z^1) - 2\tilde{f}(k_z^1)\tilde{f}(q_z^1)) \\
&\times \Bigg(\frac{2E_{k_z^1}}{k_z^1p_z(2k_z^1+p_z)}\Bigg)\Bigg].
\end{aligned} \tag{A.23}$$

As mentioned earlier, Eq.(A.23) can be used to obtain $\Im\Pi_R^\parallel$.

A.2 $Qg \to Qg$ scattering

The contracted terms of Eq.(4.51) are

Term-1:

$$\begin{aligned}
\mathcal{T}_1^{\mu\nu}\mathcal{A}_{\mu\nu} &= -\frac{16\Pi_R^\parallel(q)}{q^4(q^2-\Pi_R^\parallel(q))}[P^\mu P'^\nu + P'^\mu P^\nu - (P.P')g^{\mu\nu}][K_\mu K'^\delta P_{\delta\nu}^\parallel + K'_\mu K^\delta P_{\delta\nu}^\parallel] \\
&= -\frac{16\Pi_R^\parallel(q)}{q^4(q^2-\Pi_R^\parallel(q))}[(P.K)(K'.P_\parallel.P') + (P.K')(K.P_\parallel.P') \\
&+ (K.P')(K'.P_\parallel.P) + (P'.K')(K.P_\parallel.P) - 2(P.P')(K'.P_\parallel.K)].
\end{aligned} \tag{A.24}$$

Term-2:

$$\begin{aligned}
\mathcal{T}_1^{\mu\nu}\mathcal{B}_{\mu\nu} &= -\frac{16\Pi_R^{\|}(q)}{q^4(q^2-\Pi_R^{\|}(q))}[P^\mu P'^\nu + P'^\mu P^\nu - (P.P')g^{\mu\nu}][K^\delta P^{\|}_{\delta\mu}K'_\nu \\
&+ K'^\delta P^{\|}_{\delta\mu}K_\nu] \\
&= -\frac{16\Pi_R^{\|}(q)}{q^4(q^2-\Pi_R^{\|}(q))}[(P'.K')(K.P_{\|}.P) + (K.P')(K'.P_{\|}.P) \\
&+ (P.K')(K.P_{\|}.P') + (P.K)(K'.P_{\|}.P') - 2(P.P')(K.P_{\|}.K')]. \qquad (A.25)
\end{aligned}$$

Term3:

$$\begin{aligned}
\mathcal{T}_1^{\mu\nu}\mathcal{C}_{\mu\nu} &= \frac{16(\Pi_R^{\|}(q))^2}{q^4(q^2-\Pi_R^{\|}(q))^2}[P^\mu P'^\nu + P'^\mu P^\nu - (P.P')g^{\mu\nu}][K^\delta P^{\|}_{\delta\mu}K'^{\delta'}P^{\|}_{\delta'\nu} \\
&+ K'^\delta P^{\|}_{\delta\mu}K^{\delta'}P^{\|}_{\delta'\nu}] \\
&= \frac{16(\Pi_R^{\|}(q))^2}{q^4(q^2-\Pi_R^{\|}(q))^2}[(K.P_{\|}.P)(K'.P_{\|}.P') + (K'.P_{\|}.P)(K.P_{\|}.P') \\
&+ (K.P_{\|}.P')(K'.P_{\|}.P) + (K'.P_{\|}.P')(K.P_{\|}.P) \\
&+ 2(P.P')(K.P_{\|}.K')]. \qquad (A.26)
\end{aligned}$$

Here, we make use of the identity:

$$g^{\mu\nu}P^{\|}_{\delta\mu}P^{\|}_{\delta'\nu} = -P^{\|}_{\delta\delta'}. \qquad (A.27)$$

Term-4:

$$\begin{aligned}
\mathcal{T}_2^{\mu\nu}\mathcal{A}_{\mu\nu} &= -\frac{16M^2\Pi_R^{\|}(q)}{q^4(q^2-\Pi_R^{\|}(q))}g^{\mu\nu}[K_\mu K'^\delta P^{\|}_{\delta\nu} + K'_\mu K^\delta P^{\|}_{\delta\nu}] \\
&= -\frac{32M^2\Pi_R^{\|}(q)}{q^4(q^2-\Pi_R^{\|}(q))}(K.P_{\|}.K'). \qquad (A.28)
\end{aligned}$$

Term-5:

$$\begin{aligned}
\mathcal{T}_2^{\mu\nu}\mathcal{B}_{\mu\nu} &= -\frac{16M^2\Pi_R^{\|}(q)}{q^4(q^2-\Pi^{\|}(q)_R)}g^{\mu\nu}[K^\delta P^{\|}_{\delta\mu}K'_\nu + K'^\delta P^{\|}_{\delta\mu}K_\nu] \\
&= -\frac{32M^2\Pi_{\|}(q)}{q^4(q^2-\Pi_{\|}(q))}(K.P_{\|}.K'). \qquad (A.29)
\end{aligned}$$

Term-6:

$$\begin{aligned}
\mathcal{T}_2^{\mu\nu}\mathcal{C}_{\mu\nu} &= \frac{16M^2(\Pi_R^{\parallel}(q))^2}{q^4(q^2-\Pi_R^{\parallel}(q))^2} g^{\mu\nu}[K^{\delta}P_{\delta\mu}^{\parallel}K'^{\delta'}P_{\delta'\nu}^{\parallel} + K'^{\delta}P_{\delta\mu}^{\parallel}K^{\delta'}P_{\delta'\nu}^{\parallel}] \\
&= -\frac{32M^2(\Pi_R^{\parallel}(q))^2}{q^4(q^2-\Pi_R^{\parallel}(q))^2}(K.P_{\parallel}.K'). \qquad (A.30)
\end{aligned}$$

A.2.1 Four vector product and tensor contractions

With the assumption that the HQ quark moves in the direction of the magnetic field, the four-vector products in the matrix element squared i.e., $|\bar{\mathcal{M}}|^2$ as given in Eq.(4.52) can be given as

$$\begin{aligned}
P.K &= Ek - \mathbf{p}.\mathbf{k} = Ek - pk\cos\theta_k = Ek - pkx \\
P.K' &= Ek' - \mathbf{p}\cdot\mathbf{k'} = Ek' - pk'y \\
P'.K &= E'k - (\mathbf{p}+\mathbf{k}-\mathbf{k'})\cdot\mathbf{k} = Ek - vkk'y + vk^2x - pkx - k^2 + \mathbf{k}\cdot\mathbf{k'} \\
P'.K' &= E'k' - (\mathbf{p}+\mathbf{k}-\mathbf{k'})\cdot\mathbf{k'} = Ek' - vk'^2y + vkk'x - pk'y + k'^2 - \mathbf{k}\cdot\mathbf{k'} \\
P.P' &= EE' - \mathbf{p}\cdot(\mathbf{p}-\mathbf{q}) = M^2. \qquad (A.31)
\end{aligned}$$

Here $\mathbf{k}.\mathbf{k'} = kk'[\sqrt{(1-x^2)(1-y^2)}(\cos\phi_k\cos\phi_{k'} + \sin\phi_k\sin\phi_{k'}) + xy]$ with $x = \cos\theta_k$ and $y = \cos\theta_{k'}$. The tensor contractions can be splitted into the four-vector dot products as

$$\begin{aligned}
P.P_{\parallel}.K &= \frac{(P.q_{\parallel})(K.q_{\parallel})}{q_{\parallel}^2} - P.K_{\parallel} \\
P.P_{\parallel}.K' &= \frac{(P.q_{\parallel})(K'.q_{\parallel})}{q_{\parallel}^2} - P.K'_{\parallel} \\
P'.P_{\parallel}.K &= \frac{(P'.q_{\parallel})(K.q_{\parallel})}{q_{\parallel}^2} - P'.K_{\parallel} \\
P'.P_{\parallel}.K' &= \frac{(P'.q_{\parallel})(K'.q_{\parallel})}{q_{\parallel}^2} - P'.K'_{\parallel} \\
K.P_{\parallel}.K' &= \frac{(K.q_{\parallel})(K'.q_{\parallel})}{q_{\parallel}^2} - K.K'_{\parallel} \qquad (A.32)
\end{aligned}$$

The dot products in Eq.A.32 can also be simplified by taking the same assumption for the heavy quark motion as

$$\begin{aligned}
P.q_{\parallel} &= E\omega - pq_z = E\omega - p(k'_z - k_z) = E\omega - pk'y + pkx, \\
K.q_{\parallel} &= \omega k - k_z q_z = \omega k - k_z(k'_z - k_z) = \omega k - kk'xy + k^2x^2, \\
K'.q_{\parallel} &= \omega k' - k'_z(k'_z - k_z) = \omega k' - k'^2y^2 + kk'xy, \\
P'.q_{\parallel} &= E'\omega - (p + k_z - k'_z)(k'_z - k_z) \\
&= E\omega - v\omega k'y + v\omega kx - pk'y + pkx + k^2x^2 + k'^2y^2 - 2kk'xy, \\
P.K_{\parallel} &= Ek - pk_z = Ek - pkx, \\
P.K'_{\parallel} &= Ek' - pk'y, \\
P'.K_{\parallel} &= E'k - (p_z + k_z - k'_z)k_z = Ek - vkk'y + vk^2x - pkx - k^2x^2 + kk'xy, \\
P'.K'_{\parallel} &= E'k' - (p + k_z - k'_z)k'_z = Ek' - vk'^2y + vkk'x - pk'y - kk'xy + k'^2y^2, \\
K.K'_{\parallel} &= kk' - k_z{k'}_z,
\end{aligned} \tag{A.33}$$

A.3 Solution of A_0 and A_i

Solving Eqs.5.36 and (5.37) to obtain

$$A_0 = \sum_{i,k} \mathcal{D}^{ik}\tilde{\Delta}^{ik}, \tag{A.34}$$

$$A_i = \sum_{k} \mathcal{D}^{0k}\tilde{\Delta}^{ik}, \tag{A.35}$$

where

$$\mathcal{D}^{ik} = -(D^{-1})^{0k} j^0_{ext} + (D^{-1})^{i0} j^k_{ext}, \quad \mathcal{D}^{0k} = (D^{-1})^{0k} j^0_{ext} - (D^{-1})^{00} j^k_{ext}, \tag{A.36}$$

$$\tilde{\Delta}^{ik} = \frac{1}{(D^{-1})^{00}(D^{-1})^{ik} - (D^{-1})^{i0}(D^{-1})^{0k}}. \tag{A.37}$$

Subtracting the bare terms, the explicit form of all the terms in A_0 is

$$\begin{aligned}
\mathcal{D}^{11}\tilde{\Delta}^{11} &= \frac{(D^{-1})^{10}v - (D^{-1})^{11}}{(D^{-1})^{11}(D^{-1})^{00} - (D^{-1})^{10}(D^{-1})^{01}} \\
&= \frac{q^2 - q_x^2}{\omega^2 q_x^2 - (Q^2 + q_x^2)(q^2 + q_z^2\Pi_{\parallel})} - \frac{q^2 - q_x^2}{\omega^2 q_x^2 - (Q^2 + q_x^2)(q^2)},
\end{aligned} \tag{A.38}$$

$$\begin{aligned}
\mathcal{D}^{12}\tilde{\Delta}^{12} &= \frac{(D^{-1})^{20}v - (D^{-1})^{21}}{(D^{-1})^{21}(D^{-1})^{00} - (D^{-1})^{20}(D^{-1})^{01}} \\
&= \frac{\omega v - q_x}{q_x(\omega^2 - q^2 - q_z^2\Pi_{\parallel})} - \frac{\omega v - q_x}{q_x(\omega^2 - q^2)},
\end{aligned} \tag{A.39}$$

$$\begin{aligned}\mathcal{D}^{13}\tilde{\Delta}^{13} &= \frac{(D^{-1})^{30}v - (D^{-1})^{31}}{(D^{-1})^{31}(D^{-1})^{00} - (D^{-1})^{30}(D^{-1})^{01}} \\ &= \frac{q_x - \omega v(1+\Pi_\parallel)}{q_x(\omega^2 - q^2 - q_\parallel^2\Pi_\parallel)} - \frac{q_x - \omega v}{q_x(\omega^2 - q^2)},\end{aligned} \tag{A.40}$$

$$\begin{aligned}\mathcal{D}^{21}\tilde{\Delta}^{21} &= -\frac{(D^{-1})^{12}}{(D^{-1})^{12}(D^{-1})^{00} - (D^{-1})^{10}(D^{-1})^{02}} \\ &= -\frac{1}{Q^2 - q_z^2\Pi_\parallel} - \frac{1}{Q^2},\end{aligned} \tag{A.41}$$

$$\begin{aligned}\mathcal{D}^{22}\tilde{\Delta}^{22} &= -\frac{(D^{-1})^{22}}{(D^{-1})^{22}(D^{-1})^{00} - (D^{-1})^{20}(D^{-1})^{02}} \\ &= \frac{Q^2 + q_y^2}{(Q^2+q_y^2)(q^2 + q_z^2\Pi_\parallel) - \omega^2 q_y^2} - \frac{Q^2 + q_y^2}{(Q^2+q_y^2)q^2 - \omega^2 q_y^2},\end{aligned} \tag{A.42}$$

$$\begin{aligned}\mathcal{D}^{23}\tilde{\Delta}^{23} &= -\frac{(D^{-1})^{32}}{(D^{-1})^{32}(D^{-1})^{00} - (D^{-1})^{30}(D^{-1})^{02}} \\ &= -\frac{1}{Q^2 + q_\parallel^2\Pi_\parallel} - \frac{1}{Q^2},\end{aligned} \tag{A.43}$$

$$\begin{aligned}\mathcal{D}^{31}\tilde{\Delta}^{31} &= -\frac{(D^{-1})^{13}}{(D^{-1})^{13}(D^{-1})^{00} - (D^{-1})^{10}(D^{-1})^{03}} \\ &= -\frac{1}{Q^2 + q_\parallel^2\Pi_\parallel} + \frac{1}{Q^2},\end{aligned} \tag{A.44}$$

$$\begin{aligned}\mathcal{D}^{32}\tilde{\Delta}^{32} &= -\frac{(D^{-1})^{23}}{(D^{-1})^{23}(D^{-1})^{00} - (D^{-1})^{20}(D^{-1})^{03}} \\ &= -\frac{1}{Q^2 + (\omega^2 - q_z^2)\Pi_\parallel} + \frac{1}{Q^2},\end{aligned} \tag{A.45}$$

$$\begin{aligned}\mathcal{D}^{33}\tilde{\Delta}^{33} &= -\frac{(D^{-1})^{33}}{(D^{-1})^{33}(D^{-1})^{00} - (D^{-1})^{30}(D^{-1})^{03}} \\ &= -\frac{\omega^2\Pi_\parallel + Q^2 + q_z^2}{(\omega^2\Pi_\parallel + Q^2 + q_z^2)(q^2 + q_z^2\Pi_\parallel) - \omega^2 q_z^2(1+\Pi_\parallel)^2} + \frac{Q^2 + q_z^2}{(Q^2+q_z^2)q^2 - \omega^2 q_z^2},\end{aligned} \tag{A.46}$$

A.4 Polyakov loop extended Quark Meson model

Polyakov loop extended quark meson model(PQM) captures two important features of quantum chromodynamics(QCD) - namely chiral symmetry breaking and its restoration at high temperature and/densities as well as the confinement - deconfinement transitions. Explicitly, the Lagrangian of the PQM model is given by[247, 248, 249, 250, 251]

$$\begin{aligned}\mathcal{L} &= \bar{\psi}\left(i\gamma^{\mu}D_{\mu} - m - g_{\sigma}(\sigma + i\gamma_5\tau\cdot\pi)\right)\psi + \frac{1}{2}\left[\partial_{\mu}\sigma\partial^{\mu}\sigma + \partial_{\mu}\pi\partial^{\mu}\pi\right] \\ &- U_{\chi}(\sigma,\pi) - U_P(\phi,\bar{\phi}).\end{aligned} \tag{A.47}$$

In the above, the first term is the kinetic and interaction term for the quark doublet $\psi = (u, d)$ interacting with the scalar (σ) and the isovector pseudoscalar pion (π) field. The scalar field σ and the pion field π together form a SU(2) isovector field. The quark field is also coupled to a spatially constant temporal gauge field A_0 through the covariant derivative $D_{\mu} = \partial_{\mu} - ieA_{\mu}$; $A_{\mu} = \delta_{\mu 0}A_{\mu}$.

The mesonic potential $U_{\chi}(\sigma,\pi)$ essentially describes the chiral symmetry breaking pattern in strong interaction and is given by

$$\boldsymbol{U_{\chi}(\sigma,\pi) = \frac{\lambda}{4}(\sigma^2 + \pi^2 - v^2) - c\sigma.} \tag{A.48}$$

The last term in the Lagrangian in Eq.(A.47) is responsible for including the physics of color confinement in terms of a potential energy for the expectation value of the Polyakov loop ϕ and $\bar{\phi}$ which are defined in terms of the Polyakov loop operator which is a Wilson loop in the temporal direction

$$\mathcal{P} = P\exp\left(i\int_0^{\beta} dx_0 A_0(x_0,\mathbf{x})\right). \tag{A.49}$$

In the Polyakov gauge A_0 is time independent and is in the Cartan subalgebra i.e. $A_0^a = A_0^3\lambda_3 + A_0^8\lambda_8$. One can perform the integration over the time variable trivially as path ordering becomes irrelevant so that $\mathcal{P}(\mathbf{x}) = \exp(\beta\mathbf{A_0})$. The Polyakov loop variable ϕ and its hermitian conjugate $\bar{\phi}$ are defined as

$$\phi(\mathbf{x}) = \frac{\mathbf{1}}{\mathbf{N_c}}\mathbf{Tr}\mathcal{P}(\mathbf{x}) \qquad \bar{\phi}(\mathbf{x}) = \frac{\mathbf{1}}{\mathbf{N_c}}\mathcal{P}^{\dagger}(\mathbf{x}). \tag{A.50}$$

In the limit of heavy quark mass, the confining phase is center symmetric and therefore $\langle\phi\rangle = 0$ while for deconfined phase $\langle\phi\rangle \neq 0$. Finite quark masses break this symmetry explicitly. The explicit form of the potential $U_p(\phi,\bar{\phi})$ is not known from first principle calculations. The common strategy is to choose a functional form of the potential that reproduces the pure gauge lattice simulation thermodynamic results. Several forms of this potential has been suggested in literature. We shall use here the following polynomial parameterization [247]

$$U_P(\phi,\bar{\phi}) = T^4\left[-\frac{b_2(T)}{2}\bar{\phi}\phi - \frac{b_3}{2}(\phi^3+\bar{\phi}^3) + \frac{b_4}{4}(\bar{\phi}\phi)^2\right], \tag{A.51}$$

with the temperature dependent coefficient b_2 given as

$$b_2(T) = a_0 + a_1(\frac{T_0}{T}) + a_2(\frac{T_0}{T})^2 + a_3(\frac{T_0}{T})^3. \tag{A.52}$$

The numerical values of the parameters are

$$\begin{aligned} &a_0 = 6.75, \quad a_1 = -1.95, \quad a_2 = 2.625, \quad a_3 = -7.44 \\ &b_3 = 0.75, \quad b_4 = 7.5. \end{aligned} \tag{A.53}$$

$$\tag{A.54}$$

The parameter T_0 corresponds to the transition temperature of Yang-Mills theory. However, for the full dynamical QCD, there is a flavor dependence on $T_0(N_f)$. For two flavors we take it to be $T_0(2) = 192$ MeV as in Ref.[247].

The Lagrangian in Eq.(A.47) is invariant under $SU(2)_L \times SU(2)_R$ transformation when the explicit symmetry breaking term $c\sigma$ vanishes in the potential U_χ in Eq.(A.48). The parameters of the potential U_χ are chosen such that the chiral symmetry is spontaneously broken in the vacuum. The expectation values of the meson fields in vacuum are $\langle\sigma\rangle = f_\pi$ and $\langle\pi\rangle = 0$. Here $f_\pi = 93$ MeV is the pion decay constant. The coefficient of the symmetry breaking linear term is decided from the partial conservation of axial vector current (PCAC) as $c = f_\pi m_\pi^2$, $m_\pi = 138$ MeV, being the pion mass. Then minimizing the potential one has $v^2 = f_\pi^2 - m_\pi^2/\lambda$. The quartic coupling for the meson, λ is determined from the mass of the sigma meson given as $m_\sigma^2 = m_\pi^2 + 2\lambda f_\pi^2$. In the present work we take $m_\sigma = 600$MeV which gives λ=19.7. The coupling g_σ is fixed here from the constituent quark mass in vacuum $M_q = g_q f_\pi$ which has to be about (1/3)rd of nucleon mass that leads to $g_\sigma = 3.3$ [298].

To calculate the bulk thermodynamical properties of the system we use a mean field approximation for the meson and the Polyakov fields while retaining the quantum and thermal fluctuations of the quark fields. The thermodynamic potential can then be written as

$$\Omega(T,\mu) = \Omega_{\bar{q}q} + U_\chi + U_P(\phi,\bar{\phi}). \tag{A.55}$$

The fermionic part of the thermodynamic potential is given as

$$\begin{aligned}\Omega_{\bar{q}q} &= -2N_f T \int \frac{d^3p}{(2\pi)^3}\Bigg[\ln\left(1+3(\phi+\bar{\phi}e^{-\beta\omega_-})e^{-\beta\omega_-}+e^{-3\beta\omega_-}\right) \\ &+ \ln\left(1+3(\phi+\bar{\phi}e^{-\beta\omega_+})e^{-\beta\omega_+}+e^{-3\beta\omega_+}\right) \qquad (A.56) \\ bigg], & \qquad (A.57)\end{aligned}$$

modulo a divergent vacuum part. In the above, $\omega_{\mp} = E_p \mp \mu$, with the single particle quark/anti-quark energy $E_p = \sqrt{\mathbf{p^2+M^2}}$. The constituent quark/anti-quark mass is defined to be

$$M^2 = g_\sigma^2(\sigma^2+\pi^{\mathbf{2}}). \qquad (A.58)$$

The divergent vacuum part arises from the negative energy states of the Dirac sea. Using standard renormalisation, it can be partly absorbed in the coupling λ and v^2. However, a logarithmic correction from the renormalisation scale remains which we neglect in the calculations that follow [298].

The mean fields are obtained by minimizing Ω with respect to σ, ϕ, $\bar{\phi}$, and π. Extremising the effective potential with respect to σ field leads to

$$\lambda(\sigma^2+\pi^{\mathbf{2}}-\mathbf{v^2})-\mathbf{c}+\mathbf{g}_\sigma\rho_{\mathbf{s}}=\mathbf{0}, \qquad (A.59)$$

where, the scalar density $\rho_s = -\langle\bar{\psi}\psi\rangle$ is given by

$$\rho_s = 6N_f g_\sigma \sigma \int \frac{d\mathbf{p}}{(2\pi)^3}\frac{1}{E_P}\left[f_-(\mathbf{p})+\mathbf{f}_+(\mathbf{p})\right]. \qquad (A.60)$$

In the above, $f_{\mp}(\mathbf{p})$ are the distribution functions for the quarks and anti quarks given as

$$f_-(\mathbf{p}) = \frac{\phi\mathbf{e}^{-\beta\omega_-}+\mathbf{2}\bar{\phi}\mathbf{e}^{-\mathbf{2}\beta\omega_-}+\mathbf{e}^{-\mathbf{3}\beta\omega_-}}{\mathbf{1}+\mathbf{3}\phi\mathbf{e}^{-\beta\omega_-}+\mathbf{3}\bar{\phi}\mathbf{e}^{-\mathbf{2}\beta\omega_-}+\mathbf{e}^{-\mathbf{3}\beta\omega_-}}, \qquad (A.61)$$

and,

$$f_+(\mathbf{p}) = \frac{\bar{\phi}\mathbf{e}^{-\beta\omega_+}+\mathbf{2}\phi\mathbf{e}^{-\mathbf{2}\beta\omega_+}+\mathbf{e}^{-\mathbf{3}\beta\omega_+}}{\mathbf{1}+\mathbf{3}\bar{\phi}\mathbf{e}^{-\beta\omega_+}+\mathbf{3}\phi\mathbf{e}^{-\mathbf{2}\beta\omega_+}+\mathbf{e}^{-\mathbf{3}\beta\omega_+}}, \qquad (A.62)$$

The condition $\frac{\partial\Omega}{\partial\phi}=0$ leads to

$$T^4\left[-\frac{b_2}{2}\bar{\phi}-\frac{b_3}{2}\phi^2+\frac{b_4}{2}\bar{\phi}\phi\bar{\phi}\right]+I_\phi=0, \qquad (A.63)$$

where ,

$$\begin{aligned}I_\phi &= \frac{\partial\Omega_{\bar{q}q}}{\partial\phi} = -6N_f T\int\frac{d\mathbf{p}}{(2\pi)^3}\Bigg[\frac{e^{-\beta\omega_-}}{1+3\phi e^{-\beta\omega_-}+3\bar{\phi}e^{-2\beta\omega_-}+e^{-3\beta\omega_-}} \\ &+ \frac{e^{-2\beta\omega_+}}{1+3\bar{\phi}e^{-\beta\omega_+}+3\phi e^{-2\beta\omega_+}+e^{-3\beta\omega_+}}\Bigg]. \qquad (A.64)\end{aligned}$$

Similarly, $\frac{\partial\Omega}{\partial\bar{\phi}} = 0$ leads to

$$T^4\left[-\frac{b_2}{2}\phi - \frac{b_3}{2}\bar{\phi}^2 + \frac{b_4}{2}\bar{\phi}\phi^2\right] + I_{\bar{\phi}} = 0, \tag{A.65}$$

with,

$$\begin{aligned} I_{\bar{\phi}} &= \frac{\partial\Omega_{\bar{q}q}}{\partial\bar{\phi}} = -6N_fT\int\frac{d\mathbf{p}}{(2\pi)^3}\left[\frac{e^{-2\beta\omega_-}}{1+3\phi e^{-\beta\omega_-}+3\bar{\phi}e^{-2\beta\omega_-}+e^{-3\beta\omega_-}}\right. \\ &+ \left.\frac{e^{-\beta\omega_+}}{1+3\phi e^{-\beta\omega_+}+3\bar{\phi}e^{-2\beta\omega_+}+e^{-3\beta\omega_+}}.\right]. \end{aligned} \tag{A.66}$$

By solving Eqs.(A.59),(A.63) and (A.65) self consistently one can get the values of constituent quark mass, Polyakov loop variable and the conjugate Polyakov loop variable as a function of temperature.

A.5 Feynman rules in double line notation

In this appendix, we shall discuss the relevant Feynman rules used in chapter6 and chapter7 for evaluating diagrams within the matrix model of semi-QGP. We write these rules in Euclidean space with the anti-commutation relation $\{\gamma_\mu,\gamma_\nu\} = 2\delta_{\mu\nu}$. Let us start with the Lagrangian of matrix model [256]

$$\mathcal{L} = \sum_f^{N_f}\bar{\psi}_f(\not{D}+m)\psi_f + \frac{1}{2}tr(F_{\mu\nu})^2. \tag{A.67}$$

Here N_f stands for flavor and quark ψ is represented in the fundamental representation of $SU(3)$ gauge group. In order to get background field fluctuation, we expands about the background static gauge field as $A_\mu = A^0_\mu + \delta A_\mu$; where δA_μ is represents the fluctuations and $SU(3)$ matrix $A^0_\mu = \frac{1}{g}\delta_{\mu 0}Q^a$ with $Q^a = 2\pi q^a T$. The covariant derivative $\not{D}_\mu = \partial_\mu - igA_\mu$ and field tensor

$$F_{\mu\nu} = \partial_\mu A_\nu - \partial_\nu A_\mu - ig[A_\mu, A_\nu]. \tag{A.68}$$

The gauge fixing and ghost terms for gauge parameter ξ are defined in terms of background field [256]

$$\mathcal{L}_{gauge} = \frac{1}{\xi}tr(D^0_\mu\delta A_\mu) - 2tr(\bar{\eta}D^0_\mu D_\mu\eta), \tag{A.69}$$

where $D^0_\mu = \partial_\mu - igA^0_\mu$ so that $D^0_\mu\psi^a(K) = -i\tilde{K}^a_\mu$ with $\tilde{K}^a_\mu = K_\mu + Q^a + \pi T$ and η denote ghost field. With these, the explicit form of color dependent quark

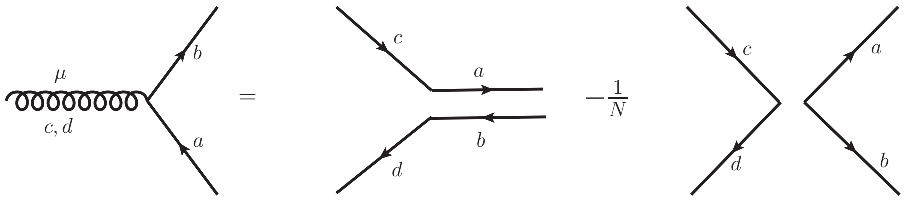

Figure A.1: Quark gluon vertex in double line notation

propagator can be written as

$$\langle \psi^a(K)\bar{\psi}^b(-K)\rangle = \frac{\delta_{ab}}{-i\not{K}+m}. \quad \text{(A.70)}$$

Similarly, for gluon and ghost, the color dependent propagator is

$$\langle \delta A^{ab}_\mu(K)\delta A^{cd}_\nu(-K)\rangle = \left(\delta_{\mu\nu} - (1-\xi)\frac{K^{ab}_\mu K^{cd}_\nu}{(K^{ab})^2}\right)\frac{\mathcal{P}^{ab,cd}}{(K^{ab})^2}, \quad \text{(A.71)}$$

$$\langle \eta^{ab}(K)\bar{\eta}^{cd}(-K)\rangle = \frac{\mathcal{P}^{ab,cd}}{(K^{ab})^2}, \quad \text{(A.72)}$$

where $K^{ab}_\mu = K_\mu + Q^a - Q^b$. For an $SU(N)$ gauge group

$$\mathcal{P}^{ab,cd} = \delta^a_d\delta^b_c - \frac{1}{N}\delta^{ab}\delta_{dc}. \quad \text{(A.73)}$$

It is worth mentioning here that for $K_a = k_0 + Q_a$ both color flow and particle momentum are in same direction. For the case when momentum and color flow are in opposite direction $K_a = k_0 - Q_a$. The vertices between the fluctuation δA_μ, ψ and ghost η are given as

$$\delta A^{ab}\psi^a\bar{\psi}^b = ig(t^{cd})_{ab}\gamma_\mu, \quad \text{(A.74)}$$

where t^{ab}_{cd} is generator of the group. In diagramatic notation the corresponding vertex is shown in Fig.A.1. Similarly, gluon ghost vertex can be written as

$$\delta A^{dc}\eta^{fe}\bar{\eta}^{ba}(K) = igf^{ab,cd,ef}K^{ab}_\mu. \quad \text{(A.75)}$$

In diagramatic representation this is shown in Fig.A.3. Further, the tripple gluon vertex can be written as

$$\delta A^\lambda_{fe}(R)\delta A^\nu_{dc}(Q)\delta A^\mu_{ba}(P) = -if^{ab,cd,ef}C^{\mu\nu\lambda}(P^{ab}, Q^{cd}, R^{ef}), \quad \text{(A.76)}$$

where with all lines going outward from the vertex and

$$C_{\mu\nu\lambda}(P^{ab}, Q^{cd}, R^{ef}) = (P^{ab}_\lambda - Q^{cd}_\lambda)\delta_{\mu\nu} + (Q^{cd}_\mu - R^{ef}_\mu)\delta_{\nu\lambda} + (R^{ef}_\nu - P^{ab}_\nu)\delta_{\lambda\mu}. \quad \text{(A.77)}$$

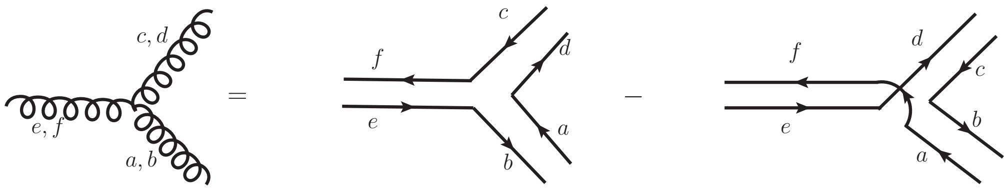

Figure A.2: Tripple gluon vertex in double line notation

.

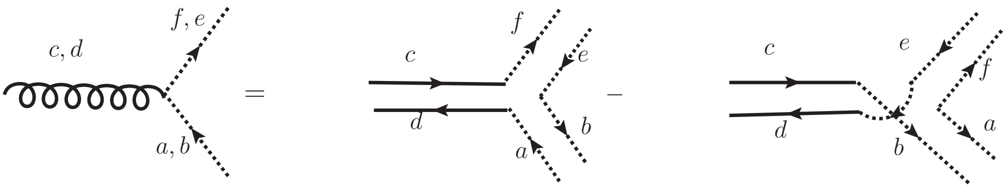

Figure A.3: Gluon ghost vertex in double line notation

.

In diagramatic representation this is shown in Fig.A.2. Finally, the four gluon vertex can be written as

$$\begin{aligned}\delta A^{\lambda}_{fe}(R)\delta A^{\nu}_{dc}(Q)\delta A^{\mu}_{ba}(P)A^{\sigma}_{gh}(S) &= -g^2\sum_{i,j=1}^{N}\Big[f^{ab,cd,ij}f^{ef,gh,ji}(\delta_{\mu\lambda}\delta_{\nu\sigma} \\ &- \delta_{\mu\sigma}\delta_{\nu\lambda}) + f^{ab,ef,ij}f^{gh,cd,ji}(\delta_{\mu\sigma}\delta_{\lambda\nu} \\ &- \delta_{\mu\nu}\delta_{\lambda\sigma}) + f^{ab,gh,ij}f^{cd,ef,ji}(\delta_{\mu\nu}\delta_{\sigma\lambda} \\ &- \delta_{\mu\lambda}\delta_{\sigma\nu})\Big]. \end{aligned} \tag{A.78}$$

References

[1] M. Aaboud *et al.*, "Determination of the strong coupling constant α_s from transverse energy–energy correlations in multijet events at $\sqrt{s} = 8$ TeV using the ATLAS detector," *Eur. Phys. J. C*, vol. 77, no. 12, p. 872, 2017.

[2] K. Fukushima and T. Hatsuda, "The phase diagram of dense QCD," *Rept. Prog. Phys.*, vol. 74, p. 014001, 2011.

[3] V. Skokov, A. Illarionov, and V. Toneev, "Estimate of the magnetic field strength in heavy-ion collisions," *Int. J. Mod. Phys. A*, vol. 24, pp. 5925–5932, 2009.

[4] L. V. Keldysh, "Diagram technique for nonequilibrium processes," *Zh. Eksp. Teor. Fiz.*, vol. 47, pp. 1515–1527, 1964, [Sov. Phys. JETP20,1018(1965)].

[5] M. L. Bellac, *Thermal Field Theory*, ser. Cambridge Monographs on Mathematical Physics. Cambridge University Press, 3 2011.

[6] K. G. Chetyrkin, B. A. Kniehl, and M. Steinhauser, "Strong coupling constant with flavor thresholds at four loops in the MS scheme," *Phys. Rev. Lett.*, vol. 79, pp. 2184–2187, 1997.

[7] G. Altarelli and J. Wells, *QCD: The Theory of Strong Interactions.* Cham: Springer International Publishing, 2017, pp. 27–96. [Online]. Available: https://doi.org/10.1007/978-3-319-51920-3_2

[8] R. Brock *et al.*, "Handbook of perturbative QCD: Version 1.0," *Rev. Mod. Phys.*, vol. 67, pp. 157–248, 1995.

[9] P. de Forcrand and D. Noth, "Precision lattice calculation of SU(2) 't Hooft loops," *Phys. Rev.*, vol. D72, p. 114501, 2005.

[10] K. Fukushima and V. Skokov, "Polyakov loop modeling for hot QCD," *Prog. Part. Nucl. Phys.*, vol. 96, pp. 154–199, 2017.

[11] J. Braun, H. Gies, and J. M. Pawlowski, "Quark Confinement from Color Confinement," *Phys. Lett.*, vol. B684, pp. 262–267, 2010.

[12] K. Fukushima, "Chiral effective model with the Polyakov loop," *Phys. Lett.*, vol. B591, pp. 277–284, 2004.

[13] P. N. Meisinger and M. C. Ogilvie, "Chiral symmetry restoration and Z(N) symmetry," *Phys. Lett. B*, vol. 379, pp. 163–168, 1996.

[14] C. Ratti, M. A. Thaler, and W. Weise, "Phases of QCD: Lattice thermodynamics and a field theoretical model," *Phys. Rev. D*, vol. 73, p. 014019, 2006.

[15] J. C. Collins and M. J. Perry, "Superdense Matter: Neutrons Or Asymptotically Free Quarks?" *Phys. Rev. Lett.*, vol. 34, p. 1353, 1975.

[16] H. Heiselberg and M. Hjorth-Jensen, "Phases of dense matter in neutron stars," *Phys. Rept.*, vol. 328, pp. 237–327, 2000.

[17] E. Annala, T. Gorda, A. Kurkela, J. Nttil, and A. Vuorinen, "Evidence for quark-matter cores in massive neutron stars," *Nature Phys.*, 2020.

[18] G. Endrdi, "QCD phase diagram: overview of recent lattice results," *J. Phys. Conf. Ser.*, vol. 503, p. 012009, 2014.

[19] F. Cuteri, O. Philipsen, and A. Sciarra, "QCD chiral phase transition from noninteger numbers of flavors," *Phys. Rev.*, vol. D97, no. 11, p. 114511, 2018.

[20] G. Endrodi, Z. Fodor, S. D. Katz, and K. K. Szabo, "The QCD phase diagram at nonzero quark density," *JHEP*, vol. 04, p. 001, 2011.

[21] O. Kaczmarek, F. Karsch, E. Laermann, C. Miao, S. Mukherjee, P. Petreczky, C. Schmidt, W. Soeldner, and W. Unger, "Phase boundary for the chiral transition in (2+1) -flavor QCD at small values of the chemical potential," *Phys. Rev.*, vol. D83, p. 014504, 2011.

[22] S. Borsanyi, G. Endrodi, Z. Fodor, A. Jakovac, S. D. Katz, S. Krieg, C. Ratti, and K. K. Szabo, "The QCD equation of state with dynamical quarks," *JHEP*, vol. 11, p. 077, 2010.

[23] S. Borsanyi, G. Endrodi, Z. Fodor, S. D. Katz, S. Krieg, C. Ratti, and K. K. Szabo, "QCD equation of state at nonzero chemical potential: continuum results with physical quark masses at order mu^2," *JHEP*, vol. 08, p. 053, 2012.

[24] C. DeTar and U. Heller, "QCD Thermodynamics from the Lattice," *Eur. Phys. J. A*, vol. 41, pp. 405–437, 2009.

[25] Y. Aoki, G. Endrodi, Z. Fodor, S. Katz, and K. Szabo, "The Order of the quantum chromodynamics transition predicted by the standard model of particle physics," *Nature*, vol. 443, pp. 675–678, 2006.

[26] A. Bazavov, N. Brambilla, H. T. Ding, P. Petreczky, H. P. Schadler, A. Vairo, and J. H. Weber, "Polyakov loop in 2+1 flavor QCD from low to high temperatures," *Phys. Rev.*, vol. D93, no. 11, p. 114502, 2016.

[27] K. Yamazaki and T. Matsui, "Quark-Hadron Phase Transition in the PNJL model for interacting quarks," *Nucl. Phys.*, vol. A913, pp. 19–50, 2013.

[28] A. Bazavov *et al.*, "The chiral and deconfinement aspects of the QCD transition," *Phys. Rev. D*, vol. 85, p. 054503, 2012.

[29] S. Borsanyi, Z. Fodor, C. Hoelbling, S. D. Katz, S. Krieg, C. Ratti, and K. K. Szabo, "Is there still any T_c mystery in lattice QCD? Results with physical masses in the continuum limit III," *JHEP*, vol. 09, p. 073, 2010.

[30] Y. Aoki, S. Borsanyi, S. Durr, Z. Fodor, S. D. Katz, S. Krieg, and K. K. Szabo, "The QCD transition temperature: results with physical masses in the continuum limit II." *JHEP*, vol. 06, p. 088, 2009.

[31] G. A. Contrera, A. G. Grunfeld, and D. B. Blaschke, "Phase diagrams in nonlocal Polyakov-Nambu-Jona-Lasinio models constrained by lattice QCD results," *Phys. Part. Nucl. Lett.*, vol. 11, pp. 342–351, 2014.

[32] G. Aarts, F. Attanasio, B. Jger, E. Seiler, D. Sexty, and I.-O. Stamatescu, "Insights into the heavy dense QCD phase diagram using Complex Langevin simulations," *PoS*, vol. LATTICE2015, p. 155, 2016.

[33] H.-T. Ding, F. Karsch, and S. Mukherjee, "Thermodynamics of strong-interaction matter from Lattice QCD," *Int. J. Mod. Phys.*, vol. E24, no. 10, p. 1530007, 2015.

[34] C. Ratti, "Lattice QCD: bulk and transport properties of QCD matter," *Nucl. Phys.*, vol. A956, pp. 51–58, 2016.

[35] S. Borsanyi, "Frontiers of finite temperature lattice QCD," *EPJ Web Conf.*, vol. 137, p. 01006, 2017.

[36] V. A. Goy, V. Bornyakov, D. Boyda, A. Molochkov, A. Nakamura, A. Nikolaev, and V. Zakharov, "Sign problem in finite density lattice QCD," *PTEP*, vol. 2017, no. 3, p. 031D01, 2017.

[37] P. Huovinen and P. Petreczky, "Equation of state at finite baryon density based on lattice QCD," *J. Phys. G*, vol. 38, p. 124103, 2011.

[38] S. Borsanyi, Z. Fodor, J. N. Guenther, R. Kara, S. D. Katz, P. Parotto, A. Pasztor, C. Ratti, and K. K. Szabo, "The QCD crossover at finite chemical potential from lattice simulations," 2 2020.

[39] K. Fukushima, "Phase diagram from PNJL models," *PoS*, vol. CPOD2009, p. 016, 2009.

[40] C. Sasaki, "The Phase Structure of Dense QCD from Chiral Models," *Acta Phys. Polon. Supp.*, vol. 3, pp. 659–668, 2010.

[41] M. Buballa, A. G. Grunfeld, A. E. Radzhabov, and D. Scheffler, "Aspects of the phase diagram in (P)NJL-like models," *Prog. Part. Nucl. Phys.*, vol. 62, pp. 365–370, 2009.

[42] W. Weise, C. Ratti, and S. Roessner, "Phases of QCD, Polyakov loop and quasiparticles," *Prog. Theor. Phys. Suppl.*, vol. 168, pp. 435–443, 2007.

[43] C. Ratti, M. A. Thaler, and W. Weise, "Phase diagram and thermodynamics of the PNJL model," 2006.

[44] K. Fukushima, "Phase diagram of hot and dense QCD constrained by the Statistical Model," *Phys. Lett.*, vol. B695, pp. 387–391, 2011.

[45] G. Y. Shao, M. Di Toro, V. Greco, M. Colonna, S. Plumari, B. Liu, and Y. X. Liu, "Phase diagrams in the Hadron-PNJL model," *Phys. Rev.*, vol. D84, p. 034028, 2011.

[46] K. Fukushima and C. Sasaki, "The phase diagram of nuclear and quark matter at high baryon density," *Prog. Part. Nucl. Phys.*, vol. 72, pp. 99–154, 2013.

[47] X. Luo and N. Xu, "Search for the QCD Critical Point with Fluctuations of Conserved Quantities in Relativistic Heavy-Ion Collisions at RHIC : An Overview," *Nucl. Sci. Tech.*, vol. 28, no. 8, p. 112, 2017.

[48] N. Yu, D. Zhang, and X. Luo, "Search for QCD critical point by transverse velocity dependence of anti-deuteron to deuteron ratio," *Chin. Phys. C*, vol. 44, no. 1, p. 014002, 2020.

[49] K. Rajagopal and F. Wilczek, "The Condensed matter physics of QCD," in *At the frontier of particle physics. Handbook of QCD. Vol. 1-3*, M. Shifman and B. Ioffe, Eds., 2000, pp. 2061–2151.

[50] M. G. Alford, A. Schmitt, K. Rajagopal, and T. Schfer, “Color superconductivity in dense quark matter,” *Rev. Mod. Phys.*, vol. 80, pp. 1455–1515, 2008.

[51] M. Huang, “QCD Phase Diagram at High Temperature and Density,” 2010.

[52] M. G. Alford, K. Rajagopal, and F. Wilczek, “Color flavor locking and chiral symmetry breaking in high density QCD,” *Nucl. Phys.*, vol. B537, pp. 443–458, 1999.

[53] M. Alford and S. Reddy, “Compact stars with color superconducting quark matter,” *Phys. Rev.*, vol. D67, p. 074024, 2003.

[54] J. A. Bowers and K. Rajagopal, “The Crystallography of color superconductivity,” *Phys. Rev.*, vol. D66, p. 065002, 2002.

[55] D. H. Rischke, “Debye screening and Meissner effect in a three flavor color superconductor,” *Phys. Rev.*, vol. D62, p. 054017, 2000.

[56] P. Amore, M. C. Birse, J. A. McGovern, and N. R. Walet, “Color superconductivity in finite systems,” *Phys. Rev.*, vol. D65, p. 074005, 2002.

[57] L. McLerran and R. D. Pisarski, “Phases of cold, dense quarks at large N(c),” *Nucl. Phys. A*, vol. 796, pp. 83–100, 2007.

[58] Y. Hidaka, L. D. McLerran, and R. D. Pisarski, “Baryons and the phase diagram for a large number of colors and flavors,” *Nucl. Phys. A*, vol. 808, pp. 117–123, 2008.

[59] L. McLerran, “Quarkyonic Matter and the Phase Diagram of QCD,” in *8th Workshop on Continuous Advances in QCD (CAQCD-08)*, 8 2008, pp. 125–134.

[60] L. McLerran and S. Reddy, “Quarkyonic Matter and Neutron Stars,” *Phys. Rev. Lett.*, vol. 122, no. 12, p. 122701, 2019.

[61] L. McLerran, K. Redlich, and C. Sasaki, “Quarkyonic Matter and Chiral Symmetry Breaking,” *Nucl. Phys. A*, vol. 824, pp. 86–100, 2009.

[62] K. Fukushima, “Phase diagrams in the three-flavor Nambu-Jona-Lasinio model with the Polyakov loop,” *Phys. Rev. D*, vol. 77, p. 114028, 2008, [Erratum: Phys.Rev.D 78, 039902 (2008)].

[63] R. Venugopalan, “The Color glass condensate: A Summary of key ideas and recent developments,” in *INFN Eloisatron Project 44th Workshop on QCD at Cosmic Energies: The Highest Energy Cosmic Rays and QCD Erice, Italy, August 29-September 5, 2004*, 2004.

[64] L. D. McLerran and R. Venugopalan, “Computing quark and gluon distribution functions for very large nuclei,” *Phys. Rev.*, vol. D49, pp. 2233–2241, 1994.

[65] E. Iancu, A. Leonidov, and L. D. McLerran, “Nonlinear gluon evolution in the color glass condensate. 1.” *Nucl. Phys.*, vol. A692, pp. 583–645, 2001.

[66] R. Venugopalan, “From Glasma to Quark Gluon Plasma in heavy ion collisions,” *J. Phys. G*, vol. 35, p. 104003, 2008.

[67] K. Tuchin, “Synchrotron radiation by fast fermions in heavy-ion collisions,” *Phys. Rev. C*, vol. 82, p. 034904, 2010, [Erratum: Phys.Rev.C 83, 039903 (2011)].

[68] ——, “Particle production in strong electromagnetic fields in relativistic heavy-ion collisions,” *Adv. High Energy Phys.*, vol. 2013, p. 490495, 2013.

[69] H.-T. Ding, A. Francis, O. Kaczmarek, F. Karsch, E. Laermann, and W. Soeldner, "Thermal dilepton rate and electrical conductivity: An analysis of vector current correlation functions in quenched lattice QCD," *Phys. Rev. D*, vol. 83, p. 034504, 2011.

[70] S. Gupta, "The Electrical conductivity and soft photon emissivity of the QCD plasma," *Phys. Lett.*, vol. B597, pp. 57–62, 2004.

[71] R. K. Mohapatra, P. Saumia, and A. M. Srivastava, "Enhancement of flow anisotropies due to magnetic field in relativistic heavy-ion collisions," *Mod. Phys. Lett. A*, vol. 26, pp. 2477–2486, 2011.

[72] T. Matsui and H. Satz, "J/ψ Suppression by Quark-Gluon Plasma Formation," *Phys. Lett.*, vol. B178, pp. 416–422, 1986.

[73] S. Digal, O. Kaczmarek, F. Karsch, and H. Satz, "Heavy quark interactions in finite temperature QCD," *Eur. Phys. J. C*, vol. 43, pp. 71–75, 2005.

[74] F. Karsch, M. Mehr, and H. Satz, "Color Screening and Deconfinement for Bound States of Heavy Quarks," *Z. Phys. C*, vol. 37, p. 617, 1988.

[75] E. Megias, E. Ruiz Arriola, and L. Salcedo, "Dimension two condensates and the Polyakov loop above the deconfinement phase transition," *JHEP*, vol. 01, p. 073, 2006.

[76] Y. Guo, L. Dong, J. Pan, and M. R. Moldes, "Modelling the non-perturbative contributions to the complex heavy-quark potential," *Phys. Rev. D*, vol. 100, no. 3, p. 036011, 2019.

[77] M. Strickland and D. Bazow, "Thermal Bottomonium Suppression at RHIC and LHC," *Nucl. Phys. A*, vol. 879, pp. 25–58, 2012.

[78] L. Thakur, U. Kakade, and B. K. Patra, "Dissociation of Quarkonium in a Complex Potential," *Phys. Rev.*, vol. D89, no. 9, p. 094020, 2014.

[79] Y. Burnier and A. Rothkopf, "A gauge invariant Debye mass and the complex heavy-quark potential," *Phys. Lett.*, vol. B753, pp. 232–236, 2016.

[80] D. Lafferty and A. Rothkopf, "Improved Gauss law model and in-medium heavy quarkonium at finite density and velocity," *Phys. Rev. D*, vol. 101, no. 5, p. 056010, 2020.

[81] K. Marasinghe and K. Tuchin, "Quarkonium dissociation in quark-gluon plasma via ionization in magnetic field," *Phys. Rev.*, vol. C84, p. 044908, 2011.

[82] K. Tuchin, "J/ψ dissociation in parity-odd bubbles," *Phys. Lett. B*, vol. 705, pp. 482–486, 2011.

[83] K. M. Burke *et al.*, "Extracting the jet transport coefficient from jet quenching in high-energy heavy-ion collisions," *Phys. Rev.*, vol. C90, no. 1, p. 014909, 2014.

[84] S. Cao *et al.*, "Toward the determination of heavy-quark transport coefficients in quark-gluon plasma," *Phys. Rev.*, vol. C99, no. 5, p. 054907, 2019.

[85] A. Beraudo *et al.*, "Extraction of Heavy-Flavor Transport Coefficients in QCD Matter," *Nucl. Phys.*, vol. A979, pp. 21–86, 2018.

[86] J. Bjorken, "Energy Loss of Energetic Partons in Quark - Gluon Plasma: Possible Extinction of High p(t) Jets in Hadron - Hadron Collisions," 8 1982.

[87] M. H. Thoma and M. Gyulassy, "Quark Damping and Energy Loss in the High Temperature QCD," *Nucl. Phys.*, vol. B351, pp. 491–506, 1991.

[88] E. Braaten and M. H. Thoma, “Energy loss of a heavy fermion in a hot plasma,” *Phys. Rev.*, vol. D44, pp. 1298–1310, 1991.

[89] S. Peigne and A. Peshier, “Collisional Energy Loss of a Fast Muon in a Hot QED Plasma,” *Phys. Rev.*, vol. D77, p. 014015, 2008.

[90] ——, “Collisional energy loss of a fast heavy quark in a quark-gluon plasma,” *Phys. Rev.*, vol. D77, p. 114017, 2008.

[91] P. Romatschke and M. Strickland, “Energy loss of a heavy fermion in an anisotropic QED plasma,” *Phys. Rev.*, vol. D69, p. 065005, 2004.

[92] M. Mannarelli and R. Rapp, “Hadronic modes and quark properties in the quark-gluon plasma,” *Phys. Rev.*, vol. C72, p. 064905, 2005.

[93] T. Song, H. Berrehrah, D. Cabrera, J. M. Torres-Rincon, L. Tolos, W. Cassing, and E. Bratkovskaya, “Tomography of the Quark-Gluon-Plasma by Charm Quarks,” *Phys. Rev.*, vol. C92, no. 1, p. 014910, 2015.

[94] R. D. Pisarski and V. V. Skokov, “Chiral matrix model of the semi-QGP in QCD,” *Phys. Rev.*, vol. D94, no. 3, p. 034015, 2016.

[95] H. van Hees and R. Rapp, “Thermalization of heavy quarks in the quark-gluon plasma,” *Phys. Rev.*, vol. C71, p. 034907, 2005.

[96] D. Banerjee, S. Datta, R. Gavai, and P. Majumdar, “Heavy Quark Momentum Diffusion Coefficient from Lattice QCD,” *Phys. Rev.*, vol. D85, p. 014510, 2012.

[97] B. Svetitsky, “Diffusion of charmed quarks in the quark-gluon plasma,” *Phys. Rev.*, vol. D37, pp. 2484–2491, 1988.

[98] J. Uphoff, O. Fochler, Z. Xu, and C. Greiner, “Elastic and radiative heavy quark interactions in ultra-relativistic heavy-ion collisions,” *J. Phys. G*, vol. 42, no. 11, p. 115106, 2015.

[99] P. B. Gossiaux, “Recent results on heavy quark quenching in ultrarelativistic heavy ion collisions: the impact of coherent gluon radiation,” *Nucl. Phys. A*, vol. 910-911, pp. 301–305, 2013.

[100] G. D. Moore and D. Teaney, “How much do heavy quarks thermalize in a heavy ion collision?” *Phys. Rev.*, vol. C71, p. 064904, 2005.

[101] N. P. Landsman and C. G. van Weert, “Real and Imaginary Time Field Theory at Finite Temperature and Density,” *Phys. Rept.*, vol. 145, p. 141, 1987.

[102] B. Bezzerides and D. F. DuBois, “Many-Body Theory for Quantum Kinetic Equations,” *Phys. Rev.*, vol. 168, pp. 233–248, 1968.

[103] S. Ichimaru and S. P. n. b. Ichimaru, *Plasma physics : an introduction to statistical physics of charged particles*. Menlo Park, Calif. : Benjamin/Cummings Pub. Co, 1986, based on: Purazuma no butsuri. Tokyo : Sangyo Tosho, 1981.

[104] K. Enqvist and K. J. Eskola, “Thermalization in the Early Universe,” *Mod. Phys. Lett.*, vol. A5, pp. 1919–1926, 1990.

[105] J. C. Mather *et al.*, “A Preliminary measurement of the Cosmic Microwave Background spectrum by the Cosmic Background Explorer (COBE) satellite,” *Astrophys. J. Lett.*, vol. 354, pp. L37–L40, 1990.

[106] T. Matsubara, "A New approach to quantum statistical mechanics," *Prog. Theor. Phys.*, vol. 14, pp. 351–378, 1955.

[107] J. S. Schwinger, "Brownian motion of a quantum oscillator," *J. Math. Phys.*, vol. 2, pp. 407–432, 1961.

[108] J. Ghiglieri, A. Kurkela, M. Strickland, and A. Vuorinen, "Perturbative Thermal QCD: Formalism and Applications," 2 2020.

[109] M. E. Carrington, D.-f. Hou, and M. H. Thoma, "Equilibrium and nonequilibrium hard thermal loop resummation in the real time formalism," *Eur. Phys. J. C*, vol. 7, pp. 347–354, 1999.

[110] U. Kraemmer and A. Rebhan, "Advances in perturbative thermal field theory," *Rept. Prog. Phys.*, vol. 67, p. 351, 2004.

[111] F. Gelis, "A New approach for the vertical part of the contour in thermal field theories," *Phys. Lett. B*, vol. 455, pp. 205–212, 1999.

[112] ——, "The Effect of the vertical part of the path on the real time Feynman rules in finite temperature field theory," *Z. Phys. C*, vol. 70, pp. 321–331, 1996.

[113] A. Czajka and S. Mrowczynski, "Ghosts in Keldysh-Schwinger Formalism," *Phys. Rev. D*, vol. 89, no. 8, p. 085035, 2014.

[114] S. Mrowczynski, B. Schenke, and M. Strickland, "Color instabilities in the quark–gluon plasma," *Phys. Rept.*, vol. 682, pp. 1–97, 2017.

[115] J. Frenkel and J. C. Taylor, "High Temperature Limit of Thermal QCD," *Nucl. Phys.*, vol. B334, pp. 199–216, 1990.

[116] E. Braaten and R. D. Pisarski, "Resummation and Gauge Invariance of the Gluon Damping Rate in Hot QCD," *Phys. Rev. Lett.*, vol. 64, p. 1338, 1990.

[117] ——, "Soft Amplitudes in Hot Gauge Theories: A General Analysis," *Nucl. Phys.*, vol. B337, pp. 569–634, 1990.

[118] M. H. Thoma, "New developments and applications of thermal field theory," 10 2000.

[119] J. Rafelski and B. Muller, "Magnetic Splitting of Quasimolecular Electronic States in Strong Fields," *Phys. Rev. Lett.*, vol. 36, p. 517, 1976.

[120] D. E. Kharzeev, L. D. McLerran, and H. J. Warringa, "The Effects of topological charge change in heavy ion collisions: 'Event by event P and CP violation'," *Nucl. Phys.*, vol. A803, pp. 227–253, 2008.

[121] V. Voronyuk, V. D. Toneev, W. Cassing, E. L. Bratkovskaya, V. P. Konchakovski, and S. A. Voloshin, "(Electro-)Magnetic field evolution in relativistic heavy-ion collisions," *Phys. Rev.*, vol. C83, p. 054911, 2011.

[122] A. Bzdak and V. Skokov, "Event-by-event fluctuations of magnetic and electric fields in heavy ion collisions," *Phys. Lett.*, vol. B710, pp. 171–174, 2012.

[123] W.-T. Deng and X.-G. Huang, "Event-by-event generation of electromagnetic fields in heavy-ion collisions," *Phys. Rev.*, vol. C85, p. 044907, 2012.

[124] K. S. Novoselov, A. K. Geim, S. V. Morozov, D. Jiang, Y. Zhang, S. V. Dubonos, I. V. Grigorieva, and A. A. Firsov, "Electric field effect in atomically thin carbon films," *Science*, vol. 306, no. 5696, pp. 666–669, 2004. [Online]. Available: https://science.sciencemag.org/content/306/5696/666

[125] Y. Zhang, Y.-W. Tan, H. L. Stormer, and P. Kim, "Experimental observation of the quantum Hall effect and and Berry's phase in graphene," *Nature*, vol. 438, pp. 201–204, 2005.

[126] V. P. Gusynin, V. A. Miransky, and I. A. Shovkovy, "Dynamical flavor symmetry breaking by a magnetic field in (2+1)-dimensions," *Phys. Rev.*, vol. D52, pp. 4718–4735, 1995.

[127] ——, "Catalysis of dynamical flavor symmetry breaking by a magnetic field in (2+1)-dimensions," *Phys. Rev. Lett.*, vol. 73, pp. 3499–3502, 1994, [Erratum: Phys. Rev. Lett.76,1005(1996)].

[128] ——, "Dimensional reduction and dynamical chiral symmetry breaking by a magnetic field in (3+1)-dimensions," *Phys. Lett.*, vol. B349, pp. 477–483, 1995.

[129] L. McLerran and V. Skokov, "Comments About the Electromagnetic Field in Heavy-Ion Collisions," *Nucl. Phys.*, vol. A929, pp. 184–190, 2014.

[130] K. Tuchin, "Photon decay in strong magnetic field in heavy-ion collisions," *Phys. Rev.*, vol. C83, p. 017901, 2011.

[131] A. Das, S. S. Dave, P. S. Saumia, and A. M. Srivastava, "Effects of magnetic field on plasma evolution in relativistic heavy-ion collisions," *Phys. Rev.*, vol. C96, no. 3, p. 034902, 2017.

[132] C. Bonati, M. D'Elia, and A. Rucci, "Heavy quarkonia in strong magnetic fields," *Phys. Rev.*, vol. D92, no. 5, p. 054014, 2015.

[133] C. Bonati, M. D'Elia, M. Mariti, M. Mesiti, F. Negro, A. Rucci, and F. Sanfilippo, "Magnetic field effects on the static quark potential at zero and finite temperature," *Phys. Rev.*, vol. D94, no. 9, p. 094007, 2016.

[134] ——, "Screening masses in strong external magnetic fields," *Phys. Rev.*, vol. D95, no. 7, p. 074515, 2017.

[135] J. Alford and M. Strickland, "Charmonia and Bottomonia in a Magnetic Field," *Phys. Rev.*, vol. D88, p. 105017, 2013.

[136] S. Cho, K. Hattori, S. H. Lee, K. Morita, and S. Ozaki, "QCD sum rules for magnetically induced mixing between η_c and J/ψ," *Phys. Rev. Lett.*, vol. 113, no. 17, p. 172301, 2014.

[137] X. Guo, S. Shi, N. Xu, Z. Xu, and P. Zhuang, "Magnetic Field Effect on Charmonium Production in High Energy Nuclear Collisions," *Phys. Lett.*, vol. B751, pp. 215–219, 2015.

[138] R. Rougemont, R. Critelli, and J. Noronha, "Anisotropic heavy quark potential in strongly-coupled $\mathcal{N} = 4$ SYM in a magnetic field," *Phys. Rev.*, vol. D91, no. 6, p. 066001, 2015.

[139] D. Dudal and T. G. Mertens, "Melting of charmonium in a magnetic field from an effective AdS/QCD model," *Phys. Rev.*, vol. D91, p. 086002, 2015.

[140] A. V. Sadofyev and Y. Yin, "The charmonium dissociation in an anomalous wind," *JHEP*, vol. 01, p. 052, 2016.

[141] C. S. Machado, F. S. Navarra, E. G. de Oliveira, J. Noronha, and M. Strickland, "Heavy quarkonium production in a strong magnetic field," *Phys. Rev.*, vol. D88, p. 034009, 2013.

[142] C. S. Machado, S. I. Finazzo, R. D. Matheus, and J. Noronha, "Modification of the B Meson Mass in a Magnetic Field from QCD Sum Rules," *Phys. Rev.*, vol. D89, no. 7, p. 074027, 2014.

[143] P. Gubler, K. Hattori, S. H. Lee, M. Oka, S. Ozaki, and K. Suzuki, "D mesons in a magnetic field," *Phys. Rev.*, vol. D93, no. 5, p. 054026, 2016.

[144] K. Fukushima, K. Hattori, H.-U. Yee, and Y. Yin, "Heavy Quark Diffusion in Strong Magnetic Fields at Weak Coupling and Implications for Elliptic Flow," *Phys. Rev. D*, vol. 93, no. 7, p. 074028, 2016.

[145] S. K. Das, S. Plumari, S. Chatterjee, J. Alam, F. Scardina, and V. Greco, "Directed Flow of Charm Quarks as a Witness of the Initial Strong Magnetic Field in Ultra-Relativistic Heavy Ion Collisions," *Phys. Lett.*, vol. B768, pp. 260–264, 2017.

[146] D.-L. Yang and B. Muller, "J/ψ Production by Magnetic Excitation of η_c," *J. Phys.*, vol. G39, p. 015007, 2012.

[147] J. S. Schwinger, "On gauge invariance and vacuum polarization," *Phys. Rev.*, vol. 82, pp. 664–679, 1951.

[148] A. Chodos, K. Everding, and D. A. Owen, "QED With a Chemical Potential: 1. The Case of a Constant Magnetic Field," *Phys. Rev. D*, vol. 42, pp. 2881–2892, 1990.

[149] A. Bandyopadhyay, C. A. Islam, and M. G. Mustafa, "Electromagnetic spectral properties and Debye screening of a strongly magnetized hot medium," *Phys. Rev. D*, vol. 94, no. 11, p. 114034, 2016.

[150] G. Calucci and R. Ragazzon, "Nonlogarithmic terms in the strong field dependence of the photon propagator," *J. Phys. A*, vol. 27, pp. 2161–2166, 1994.

[151] V. A. Miransky and I. A. Shovkovy, "Quantum field theory in a magnetic field: From quantum chromodynamics to graphene and Dirac semimetals," *Phys. Rept.*, vol. 576, pp. 1–209, 2015.

[152] N. Haque, A. Bandyopadhyay, J. O. Andersen, M. G. Mustafa, M. Strickland, and N. Su, "Three-loop HTLpt thermodynamics at finite temperature and chemical potential," *JHEP*, vol. 05, p. 027, 2014.

[153] V. V. Dixit, "Charge Screening and Space Dimension," *Mod. Phys. Lett.*, vol. A5, p. 227, 1990.

[154] Q. Chen and D.-f. Hou, "HTL resummation in the light cone gauge," *Chin. Phys.*, vol. C42, no. 4, p. 043102, 2018.

[155] H. A. Weldon, "Reformulation of finite temperature dilepton production," *Phys. Rev.*, vol. D42, pp. 2384–2387, 1990.

[156] J. D. Jackson, *Classical electrodynamics*, 3rd ed. New York, NY: Wiley, 1999. [Online]. Available: http://cdsweb.cern.ch/record/490457

[157] L. Thakur, N. Haque, and H. Mishra, "Heavy quarkonium moving in hot and dense deconfined nuclear matter," *Phys. Rev.*, vol. D95, no. 3, p. 036014, 2017.

[158] B. K. Patra, H. Khanchandani, and L. Thakur, "Velocity-induced Heavy Quarkonium Dissociation using the gauge-gravity correspondence," *Phys. Rev.*, vol. D92, no. 8, p. 085034, 2015.

[159] K. A. Olive *et al.*, “Review of Particle Physics,” *Chin. Phys.*, vol. C38, p. 090001, 2014.

[160] M. Xie, S.-Y. Wei, G.-Y. Qin, and H.-Z. Zhang, “Extracting jet transport coefficient via single hadron and dihadron productions in high-energy heavy-ion collisions,” *Eur. Phys. J.*, vol. C79, no. 7, p. 589, 2019.

[161] C. Han, D.-f. Hou, B.-f. Jiang, and J.-r. Li, “Jet energy loss in quark-gluon plasma: Kinetic theory with a Bhatnagar-Gross-Krook collisional kernel,” *Eur. Phys. J.*, vol. A53, no. 10, p. 205, 2017.

[162] F. Arleo, “Quenching of Hadron Spectra in Heavy Ion Collisions at the LHC,” *Phys. Rev. Lett.*, vol. 119, no. 6, p. 062302, 2017.

[163] S. Cao and X.-N. Wang, “Jet quenching and medium response in high-energy heavy-ion collisions: a review,” 2020.

[164] R. Abir, U. Jamil, M. G. Mustafa, and D. K. Srivastava, “Heavy quark energy loss and D-mesons in RHIC and LHC energies,” *Phys. Lett.*, vol. B715, pp. 183–189, 2012.

[165] M. Djordjevic and M. Gyulassy, “Heavy quark radiative energy loss in QCD matter,” *Nucl. Phys.*, vol. A733, pp. 265–298, 2004.

[166] M. Gyulassy, P. Levai, and I. Vitev, “Reaction operator approach to nonAbelian energy loss,” *Nucl. Phys.*, vol. B594, pp. 371–419, 2001.

[167] J. Bielcik, “Centrality dependence of heavy flavor production from single electron measurement in s(NN)**(1/2) = 200-GeV Au + Au collisions,” *Nucl. Phys.*, vol. A774, pp. 697–700, 2006.

[168] S. Wicks, W. Horowitz, M. Djordjevic, and M. Gyulassy, “Elastic, inelastic, and path length fluctuations in jet tomography,” *Nucl. Phys.*, vol. A784, pp. 426–442, 2007.

[169] M. Connors, C. Nattrass, R. Reed, and S. Salur, “Jet measurements in heavy ion physics,” *Rev. Mod. Phys.*, vol. 90, p. 025005, 2018.

[170] M. Rohrmoser, P.-B. Gossiaux, T. Gousset, and J. Aichelin, “Discrimination of effective radiative and collisional in-medium energy-loss models by their effects on angular jet structure,” *Acta Phys. Polon.*, vol. B49, p. 1325, 2018.

[171] T. Edmonds, Q. Li, and F. Wang, “Collisional broadening of angular correlations in a multiphase transport model,” *Nucl. Phys.*, vol. A966, pp. 124–134, 2017.

[172] G. Coci, F. Scardina, and V. Greco, “Heavy quark dynamics within a Boltzmann transport model: radiative vs collisional energy loss,” *J. Phys. Conf. Ser.*, vol. 832, no. 1, p. 012022, 2017.

[173] K. Fukushima, “Simulating net particle production and chiral magnetic current in a CP-odd domain,” *Phys. Rev.*, vol. D92, no. 5, p. 054009, 2015.

[174] K. A. Mamo and H.-U. Yee, “Thermalization of Quark-Gluon Plasma in Magnetic Field at Strong Coupling,” *Phys. Rev.*, vol. D92, no. 10, p. 105005, 2015.

[175] K. Tuchin, “Time and space dependence of the electromagnetic field in relativistic heavy-ion collisions,” *Phys. Rev.*, vol. C88, no. 2, p. 024911, 2013.

[176] ——, “Initial value problem for magnetic fields in heavy ion collisions,” *Phys. Rev.*, vol. C93, no. 1, p. 014905, 2016.

[177] U. Grsoy, D. Kharzeev, and K. Rajagopal, "Magnetohydrodynamics and charged currents in heavy ion collisions," *Nucl. Phys.*, vol. A931, pp. 986–991, 2014.

[178] G. Inghirami, L. Del Zanna, A. Beraudo, M. H. Moghaddam, F. Becattini, and M. Bleicher, "Numerical magneto-hydrodynamics for relativistic nuclear collisions," *Eur. Phys. J.*, vol. C76, no. 12, p. 659, 2016.

[179] P. F. Kolb and R. Rapp, "Transverse flow and hadrochemistry in Au+Au collisions at (S(NN))**(1/2) = 200-GeV," *Phys. Rev.*, vol. C67, p. 044903, 2003.

[180] Y. Yin, "Electrical conductivity of the quark-gluon plasma and soft photon spectrum in heavy-ion collisions," *Phys. Rev.*, vol. C90, no. 4, p. 044903, 2014.

[181] M. Hasan, B. Chatterjee, and B. K. Patra, "Heavy Quark Potential in a static and strong homogeneous magnetic field," *Eur. Phys. J.*, vol. C77, no. 11, p. 767, 2017.

[182] B. Singh, L. Thakur, and H. Mishra, "Heavy quark complex potential in a strongly magnetized hot QGP medium," *Phys. Rev.*, vol. D97, no. 9, p. 096011, 2018.

[183] N. Dutta and S. Mazumder, "Majorana flipping of quarkonium spin states in transient magnetic field," *Eur. Phys. J.*, vol. C78, no. 6, p. 525, 2018.

[184] A. Mishra, A. Jahan CS, S. Kesarwani, H. Raval, S. Kumar, and J. Meena, "Charmonium decay widths in magnetized matter," *Eur. Phys. J.*, vol. A55, no. 6, p. 99, 2019.

[185] J. C. S. Amal, N. Dhale, R. P. Sushruth, S. Kesarwani, and A. Mishra, "Charmonium states in strong magnetic fields," *Phys. Rev.*, vol. C98, no. 6, p. 065202, 2018.

[186] S. Reddy P., A. Jahan C. S., N. Dhale, A. Mishra, and J. Schaffner-Bielich, "D mesons in strongly magnetized asymmetric nuclear matter," *Phys. Rev.*, vol. C97, no. 6, p. 065208, 2018.

[187] M. Kurian, S. K. Das, and V. Chandra, "Heavy quark dynamics in a hot magnetized QCD medium," *Phys. Rev.*, vol. D100, no. 7, p. 074003, 2019.

[188] K. Rajagopal and A. V. Sadofyev, "Chiral drag force," *JHEP*, vol. 10, p. 018, 2015.

[189] K. Fukushima and Y. Hidaka, "Resummation for the Field-theoretical Derivation of the Negative Magnetoresistance," 6 2019.

[190] V. P. Gusynin, V. A. Miransky, and I. A. Shovkovy, "Dimensional reduction and catalysis of dynamical symmetry breaking by a magnetic field," *Nucl. Phys.*, vol. B462, pp. 249–290, 1996.

[191] K. Hattori and D. Satow, "Gluon spectrum in a quark-gluon plasma under strong magnetic fields," *Phys. Rev.*, vol. D97, no. 1, p. 014023, 2018.

[192] J. Adam *et al.*, "First Observation of the Directed Flow of D^0 and $\overline{D^0}$ in Au+Au Collisions at $\sqrt{s_{\mathrm{NN}}} = 200$ GeV," *Phys. Rev. Lett.*, vol. 123, no. 16, p. 162301, 2019.

[193] S. Acharya *et al.*, "Probing the effects of strong electromagnetic fields with charge-dependent directed flow in Pb-Pb collisions at the LHC," 2019.

[194] B. Karmakar, R. Ghosh, A. Bandyopadhyay, N. Haque, and M. G. Mustafa, "Anisotropic pressure of deconfined QCD matter in presence of strong magnetic field within one-loop approximation," *Phys. Rev.*, vol. D99, no. 9, p. 094002, 2019.

[195] B. Karmakar, N. Haque, and M. G. Mustafa, "Second-order quark number susceptibility of deconfined QCD matter in presence of magnetic field," 2020.

[196] A. Dash, S. Samanta, J. Dey, U. Gangopadhyaya, S. Ghosh, and V. Roy, "Anisotropic transport properties of Hadron Resonance Gas in magnetic field," 2020.

[197] K. Hattori, X.-G. Huang, D. H. Rischke, and D. Satow, "Bulk Viscosity of Quark-Gluon Plasma in Strong Magnetic Fields," *Phys. Rev.*, vol. D96, no. 9, p. 094009, 2017.

[198] M. Kurian and V. Chandra, "Effective description of hot QCD medium in strong magnetic field and longitudinal conductivity," *Phys. Rev.*, vol. D96, no. 11, p. 114026, 2017.

[199] K. Fukushima, D. E. Kharzeev, and H. J. Warringa, "The Chiral Magnetic Effect," *Phys. Rev.*, vol. D78, p. 074033, 2008.

[200] D. E. Kharzeev and H.-U. Yee, "Chiral Magnetic Wave," *Phys. Rev.*, vol. D83, p. 085007, 2011.

[201] Y. Burnier, D. E. Kharzeev, J. Liao, and H.-U. Yee, "Chiral magnetic wave at finite baryon density and the electric quadrupole moment of quark-gluon plasma in heavy ion collisions," *Phys. Rev. Lett.*, vol. 107, p. 052303, 2011.

[202] E. V. Gorbar, V. A. Miransky, and I. A. Shovkovy, "Normal ground state of dense relativistic matter in a magnetic field," *Phys. Rev.*, vol. D83, p. 085003, 2011.

[203] B. Feng, "Electric conductivity and Hall conductivity of the QGP in a magnetic field," *Phys. Rev.*, vol. D96, no. 3, p. 036009, 2017.

[204] K. Fukushima and Y. Hidaka, "Electric conductivity of hot and dense quark matter in a magnetic field with Landau level resummation via kinetic equations," *Phys. Rev. Lett.*, vol. 120, no. 16, p. 162301, 2018.

[205] S. Ghosh and V. Chandra, "Electromagnetic spectral function and dilepton rate in a hot magnetized QCD medium," *Phys. Rev.*, vol. D98, no. 7, p. 076006, 2018.

[206] S. I. Finazzo, R. Critelli, R. Rougemont, and J. Noronha, "Momentum transport in strongly coupled anisotropic plasmas in the presence of strong magnetic fields," *Phys. Rev.*, vol. D94, no. 5, p. 054020, 2016, [Erratum: Phys. Rev.D96,no.1,019903(2017)].

[207] M. Golam Mustafa, D. Pal, and D. Kumar Srivastava, "Propagation of charm quarks in equilibrating quark - gluon plasma," *Phys. Rev.*, vol. C57, pp. 889–898, 1998, [Erratum: Phys. Rev.C57,3499(1998)].

[208] S. Caron-Huot and G. D. Moore, "Heavy quark diffusion in perturbative QCD at next-to-leading order," *Phys. Rev. Lett.*, vol. 100, p. 052301, 2008.

[209] H. van Hees, V. Greco, and R. Rapp, "Heavy-quark probes of the quark-gluon plasma at RHIC," *Phys. Rev.*, vol. C73, p. 034913, 2006.

[210] H. van Hees, M. Mannarelli, V. Greco, and R. Rapp, "Nonperturbative heavy-quark diffusion in the quark-gluon plasma," *Phys. Rev. Lett.*, vol. 100, p. 192301, 2008.

[211] S. K. Das, F. Scardina, S. Plumari, and V. Greco, "Heavy-flavor in-medium momentum evolution: Langevin versus Boltzmann approach," *Phys. Rev.*, vol. C90, p. 044901, 2014.

[212] B. Singh, A. Abhishek, S. K. Das, and H. Mishra, "Heavy quark diffusion in a Polyakov loop plasma," *Phys. Rev.*, vol. D100, no. 11, p. 114019, 2019.

[213] B. Singh and H. Mishra, "Heavy quark transport in a viscous semi QGP," *Phys. Rev.*, vol. D101, no. 5, p. 054027, 2020.

[214] S. K. Das, V. Chandra, and J.-e. Alam, "Heavy-quark transport coefficients in a hot viscous quarkgluon plasma medium," *J. Phys.*, vol. G41, p. 015102, 2013.

[215] D. Giataganas and H. Soltanpanahi, "Heavy Quark Diffusion in Strongly Coupled Anisotropic Plasmas," *JHEP*, vol. 06, p. 047, 2014.

[216] W. M. Alberico, A. Beraudo, A. De Pace, A. Molinari, M. Monteno, M. Nardi, F. Prino, and M. Sitta, "Heavy flavors in *AA* collisions: production, transport and final spectra," *Eur. Phys. J.*, vol. C73, p. 2481, 2013.

[217] X. Dong and V. Greco, "Heavy quark production and properties of QuarkGluon Plasma," *Prog. Part. Nucl. Phys.*, vol. 104, pp. 97–141, 2019.

[218] G. Aarts *et al.*, "Heavy-flavor production and medium properties in high-energy nuclear collisions - What next?" *Eur. Phys. J.*, vol. A53, no. 5, p. 93, 2017.

[219] S. Cao, G.-Y. Qin, and S. A. Bass, "Heavy-quark dynamics and hadronization in ultra-relativistic heavy-ion collisions: Collisional versus radiative energy loss," *Phys. Rev.*, vol. C88, p. 044907, 2013.

[220] S. Plumari, V. Minissale, S. K. Das, G. Coci, and V. Greco, "Charmed Hadrons from Coalescence plus Fragmentation in relativistic nucleus-nucleus collisions at RHIC and LHC," *Eur. Phys. J.*, vol. C78, no. 4, p. 348, 2018.

[221] F. Scardina, S. K. Das, V. Minissale, S. Plumari, and V. Greco, "Estimating the charm quark diffusion coefficient and thermalization time from D meson spectra at energies available at the BNL Relativistic Heavy Ion Collider and the CERN Large Hadron Collider," *Phys. Rev.*, vol. C96, no. 4, p. 044905, 2017.

[222] A. Adare *et al.*, "Energy Loss and Flow of Heavy Quarks in Au+Au Collisions at s(NN)**(1/2) = 200-GeV," *Phys. Rev. Lett.*, vol. 98, p. 172301, 2007.

[223] S. S. Adler *et al.*, "Nuclear modification of electron spectra and implications for heavy quark energy loss in Au+Au collisions at s(NN)**(1/2) - 200-GeV," *Phys. Rev. Lett.*, vol. 96, p. 032301, 2006.

[224] A. Andronic *et al.*, "Heavy-flavour and quarkonium production in the LHC era: from protonproton to heavy-ion collisions," *Eur. Phys. J.*, vol. C76, no. 3, p. 107, 2016.

[225] P. Romatschke, "Momentum broadening in an anisotropic plasma," *Phys. Rev.*, vol. C75, p. 014901, 2007.

[226] E. V. Shuryak, "What RHIC experiments and theory tell us about properties of quark-gluon plasma?" *Nucl. Phys.*, vol. A750, pp. 64–83, 2005.

[227] B. V. Jacak and B. Muller, "The exploration of hot nuclear matter," *Science*, vol. 337, pp. 310–314, 2012.

[228] F. Prino and R. Rapp, "Open Heavy Flavor in QCD Matter and in Nuclear Collisions," *J. Phys.*, vol. G43, no. 9, p. 093002, 2016.

[229] V. Greco, "Heavy Flavor Production, Flow and Energy Loss," *Nucl. Phys.*, vol. A967, pp. 200–207, 2017.

[230] M. Cacciari, P. Nason, and R. Vogt, "QCD predictions for charm and bottom production at RHIC," *Phys. Rev. Lett.*, vol. 95, p. 122001, 2005.

[231] M. Djordjevic, M. Gyulassy, R. Vogt, and S. Wicks, "Influence of bottom quark jet quenching on single electron tomography of Au + Au," *Phys. Lett.*, vol. B632, pp. 81–86, 2006.

[232] N. Armesto, M. Cacciari, A. Dainese, C. A. Salgado, and U. A. Wiedemann, "How sensitive are high-p(T) electron spectra at RHIC to heavy quark energy loss?" *Phys. Lett.*, vol. B637, pp. 362–366, 2006.

[233] B. I. Abelev *et al.*, "Transverse momentum and centrality dependence of high-p_T non-photonic electron suppression in Au+Au collisions at $\sqrt{s_{NN}} = 200\,\mathrm{GeV}$," *Phys. Rev. Lett.*, vol. 98, p. 192301, 2007, [Erratum: Phys. Rev. Lett.106,159902(2011)].

[234] M. He, R. J. Fries, and R. Rapp, "Heavy-Quark Diffusion and Hadronization in Quark-Gluon Plasma," *Phys. Rev.*, vol. C86, p. 014903, 2012.

[235] S. K. Das, F. Scardina, S. Plumari, and V. Greco, "Toward a solution to the R_{AA} and v_2 puzzle for heavy quarks," *Phys. Lett.*, vol. B747, pp. 260–264, 2015.

[236] H. Berrehrah, E. Bratkovskaya, W. Cassing, P. B. Gossiaux, J. Aichelin, and M. Bleicher, "Collisional processes of on-shell and off-shell heavy quarks in vacuum and in the Quark-Gluon-Plasma," *Phys. Rev.*, vol. C89, no. 5, p. 054901, 2014.

[237] P. B. Gossiaux and J. Aichelin, "Towards an understanding of the RHIC single electron data," *Phys. Rev.*, vol. C78, p. 014904, 2008.

[238] W. M. Alberico, A. Beraudo, A. De Pace, A. Molinari, M. Monteno, M. Nardi, and F. Prino, "Heavy-flavour spectra in high energy nucleus-nucleus collisions," *Eur. Phys. J.*, vol. C71, p. 1666, 2011.

[239] T. Lang, H. van Hees, J. Steinheimer, G. Inghirami, and M. Bleicher, "Heavy quark transport in heavy ion collisions at energies available at the BNL Relativistic Heavy Ion Collider and at the CERN Large Hadron Collider within the UrQMD hybrid model," *Phys. Rev.*, vol. C93, no. 1, p. 014901, 2016.

[240] Y. Xu, J. E. Bernhard, S. A. Bass, M. Nahrgang, and S. Cao, "Data-driven analysis for the temperature and momentum dependence of the heavy-quark diffusion coefficient in relativistic heavy-ion collisions," *Phys. Rev.*, vol. C97, no. 1, p. 014907, 2018.

[241] S. Cao, T. Luo, G.-Y. Qin, and X.-N. Wang, "Linearized Boltzmann transport model for jet propagation in the quark-gluon plasma: Heavy quark evolution," *Phys. Rev.*, vol. C94, no. 1, p. 014909, 2016.

[242] C. A. G. Prado, J. Noronha-Hostler, R. Katz, A. A. P. Suaide, J. Noronha, M. G. Munhoz, and M. R. Cosentino, "Event-by-event correlations between soft hadrons and D^0 mesons in 5.02 TeV PbPb collisions at the CERN Large Hadron Collider," *Phys. Rev.*, vol. C96, no. 6, p. 064903, 2017.

[243] M. Nahrgang, J. Aichelin, S. Bass, P. B. Gossiaux, and K. Werner, "Elliptic and triangular flow of heavy flavor in heavy-ion collisions," *Phys. Rev.*, vol. C91, no. 1, p. 014904, 2015.

[244] S. K. Das, M. Ruggieri, S. Mazumder, V. Greco, and J.-e. Alam, "Heavy quark diffusion in the pre-equilibrium stage of heavy ion collisions," *J. Phys.*, vol. G42, no. 9, p. 095108, 2015.

[245] C. Ratti, S. Roessner, M. A. Thaler, and W. Weise, "Thermodynamics of the PNJL model," *Eur. Phys. J.*, vol. C49, pp. 213–217, 2007.

[246] P. Costa, C. A. de Sousa, M. C. Ruivo, and H. Hansen, "The QCD critical end point in the PNJL model," *EPL*, vol. 86, no. 3, p. 31001, 2009.

[247] B.-J. Schaefer, J. M. Pawlowski, and J. Wambach, "The Phase Structure of the Polyakov–Quark-Meson Model," *Phys. Rev.*, vol. D76, p. 074023, 2007.

[248] U. S. Gupta and V. K. Tiwari, "Revisiting the Phase Structure of the Polyakov-quark-meson Model in the presence of Vacuum Fermion Fluctuation," *Phys. Rev.*, vol. D85, p. 014010, 2012.

[249] B. W. Mintz, R. Stiele, R. O. Ramos, and J. Schaffner-Bielich, "Phase diagram and surface tension in the three-flavor Polyakov-quark-meson model," *Phys. Rev.*, vol. D87, no. 3, p. 036004, 2013.

[250] S. Carignano, M. Buballa, and W. Elkamhawy, "Consistent parameter fixing in the quark-meson model with vacuum fluctuations," *Phys. Rev.*, vol. D94, no. 3, p. 034023, 2016.

[251] H. Mishra and R. K. Mohapatra, "Z(3) metastable states in a Polyakov quark meson model," *Phys. Rev.*, vol. D95, no. 9, p. 094014, 2017.

[252] A. Abhishek, H. Mishra, and S. Ghosh, "Transport coefficients in the Polyakov quark meson coupling model: A relaxation time approximation," *Phys. Rev.*, vol. D97, no. 1, p. 014005, 2018.

[253] Y. Hidaka, S. Lin, R. D. Pisarski, and D. Satow, "Dilepton and photon production in the presence of a nontrivial Polyakov loop," *JHEP*, vol. 10, p. 005, 2015.

[254] S. Lin, R. D. Pisarski, and V. V. Skokov, "Collisional energy loss above the critical temperature in QCD," *Phys. Lett.*, vol. B730, pp. 236–242, 2014.

[255] R. Rapp and H. van Hees, "Heavy Quarks in the Quark-Gluon Plasma," in *Quark-gluon plasma 4*, 2010, pp. 111–206.

[256] Y. Hidaka and R. D. Pisarski, "Hard thermal loops, to quadratic order, in the background of a spatial 't Hooft loop," *Phys. Rev.*, vol. D80, p. 036004, 2009.

[257] G. 't Hooft, "A Planar Diagram Theory for Strong Interactions," *Nucl. Phys.*, vol. B72, p. 461, 1974.

[258] P. Cvitanovic, "Group theory for Feynman diagrams in non-Abelian gauge theories," *Phys. Rev.*, vol. D14, pp. 1536–1553, 1976.

[259] Y. Hidaka and R. D. Pisarski, "Small shear viscosity in the semi quark gluon plasma," *Phys. Rev.*, vol. D81, p. 076002, 2010.

[260] B. L. Combridge, "Associated Production of Heavy Flavor States in p p and anti-p p Interactions: Some QCD Estimates," *Nucl. Phys.*, vol. B151, pp. 429–456, 1979.

[261] W. E. Caswell, "Asymptotic Behavior of Nonabelian Gauge Theories to Two Loop Order," *Phys. Rev. Lett.*, vol. 33, p. 244, 1974.

[262] S. Y. F. Liu and R. Rapp, "Spectral and transport properties of quarkgluon plasma in a nonperturbative approach," *Eur. Phys. J.*, vol. A56, no. 2, p. 44, 2020.

[263] ——, "T-matrix Approach to Quark-Gluon Plasma," *Phys. Rev.*, vol. C97, no. 3, p. 034918, 2018.

[264] S. Y. F. Liu, M. He, and R. Rapp, "Probing the in-Medium QCD Force by Open Heavy-Flavor Observables," *Phys. Rev.*, vol. C99, no. 5, p. 055201, 2019.

[265] B.-W. Zhang, E. Wang, and X.-N. Wang, "Heavy quark energy loss in nuclear medium," *Phys. Rev. Lett.*, vol. 93, p. 072301, 2004.

[266] S. S. Adler *et al.*, "Elliptic flow of identified hadrons in Au+Au collisions at s(NN)**(1/2) = 200-GeV," *Phys. Rev. Lett.*, vol. 91, p. 182301, 2003.

[267] C. Adler *et al.*, "Azimuthal anisotropy and correlations in the hard scattering regime at RHIC," *Phys. Rev. Lett.*, vol. 90, p. 032301, 2003.

[268] M. Aaboud *et al.*, "Measurement of the suppression and azimuthal anisotropy of muons from heavy-flavor decays in Pb+Pb collisions at $\sqrt{s_{\mathrm{NN}}} = 2.76$ TeV with the ATLAS detector," *Phys. Rev.*, vol. C98, no. 4, p. 044905, 2018.

[269] X. Dong, "Recent Results on Heavy Quark Production in High Energy Nucleus Collisions," in *13th Conference on the Intersections of Particle and Nuclear Physics (CIPANP 2018) Palm Springs, California, USA, May 29-June 3, 2018*, 2018.

[270] H. Satz, *Extreme States of Matter in Strong Interaction Physics: An Introduction.* Cham: Springer, 2018, vol. 945.

[271] M. Cacciari, M. Greco, and P. Nason, "The P(T) spectrum in heavy flavor hadroproduction," *JHEP*, vol. 05, p. 007, 1998.

[272] M. Cacciari, S. Frixione, N. Houdeau, M. L. Mangano, P. Nason, and G. Ridolfi, "Theoretical predictions for charm and bottom production at the LHC," *JHEP*, vol. 10, p. 137, 2012.

[273] H. T. Ding, A. Francis, O. Kaczmarek, F. Karsch, H. Satz, and W. Soeldner, "Charmonium properties in hot quenched lattice QCD," *Phys. Rev.*, vol. D86, p. 014509, 2012.

[274] A. Francis, O. Kaczmarek, M. Laine, T. Neuhaus, and H. Ohno, "Nonperturbative estimate of the heavy quark momentum diffusion coefficient," *Phys. Rev.*, vol. D92, no. 11, p. 116003, 2015.

[275] Z. Qiu, C. Shen, and U. Heinz, "Hydrodynamic elliptic and triangular flow in Pb-Pb collisions at $\sqrt{s} = 2.76$ATeV," *Phys. Lett.*, vol. B707, pp. 151–155, 2012.

[276] P. Romatschke and U. Romatschke, "Viscosity Information from Relativistic Nuclear Collisions: How Perfect is the Fluid Observed at RHIC?" *Phys. Rev. Lett.*, vol. 99, p. 172301, 2007.

[277] R. S. Bhalerao, A. Jaiswal, and S. Pal, "Collective flow in event-by-event partonic transport plus hydrodynamics hybrid approach," *Phys. Rev.*, vol. C92, no. 1, p. 014903, 2015.

[278] B. Schenke, S. Jeon, and C. Gale, "Higher flow harmonics from (3+1)D event-by-event viscous hydrodynamics," *Phys. Rev.*, vol. C85, p. 024901, 2012.

[279] M. Prakash, M. Prakash, R. Venugopalan, and G. Welke, "Nonequilibrium properties of hadronic mixtures," *Phys. Rept.*, vol. 227, pp. 321–366, 1993.

[280] G. Baym, H. Monien, C. J. Pethick, and D. G. Ravenhall, "Transverse Interactions and Transport in Relativistic Quark - Gluon and Electromagnetic Plasmas," *Phys. Rev. Lett.*, vol. 64, pp. 1867–1870, 1990.

[281] P. B. Arnold, G. D. Moore, and L. G. Yaffe, "Transport coefficients in high temperature gauge theories. 2. Beyond leading log," *JHEP*, vol. 05, p. 051, 2003.

[282] D. Kharzeev and K. Tuchin, "Bulk viscosity of QCD matter near the critical temperature," *JHEP*, vol. 09, p. 093, 2008.

[283] K. Dusling and T. Schfer, "Bulk viscosity, particle spectra and flow in heavy-ion collisions," *Phys. Rev.*, vol. C85, p. 044909, 2012.

[284] G. Vujanovic, C. Young, B. Schenke, R. Rapp, S. Jeon, and C. Gale, "Dilepton emission in high-energy heavy-ion collisions with viscous hydrodynamics," *Phys. Rev.*, vol. C89, no. 3, p. 034904, 2014.

[285] J. R. Bhatt, H. Mishra, and V. Sreekanth, "Cavitation and thermal dilepton production in QGP," *Nucl. Phys.*, vol. A875, pp. 181–196, 2012.

[286] ——, "Thermal photons in QGP and non-ideal effects," *JHEP*, vol. 11, p. 106, 2010.

[287] S. Sarkar and A. K. Dutt-Mazumder, "Effect of flow on the quasiparticle damping rate in hot QCD plasma," *Phys. Rev.*, vol. D88, p. 054006, 2013.

[288] S. Sarkar, C. Chattopadhyay, and S. Pal, "Radiative heavy quark energy loss in an expanding viscous QCD plasma," *Phys. Rev.*, vol. C97, no. 6, p. 064916, 2018.

[289] R. Baier, A. H. Mueller, and D. Schiff, "How does transverse (hydrodynamic) flow affect jet-broadening and jet-quenching ?" *Phys. Lett.*, vol. B649, pp. 147–151, 2007.

[290] R. Baier, D. Schiff, and B. G. Zakharov, "Energy loss in perturbative QCD," *Ann. Rev. Nucl. Part. Sci.*, vol. 50, pp. 37–69, 2000.

[291] C. Chattopadhyay, R. S. Bhalerao, J.-Y. Ollitrault, and S. Pal, "Effects of initial-state dynamics on collective flow within a coupled transport and viscous hydrodynamic approach," *Phys. Rev.*, vol. C97, no. 3, p. 034915, 2018.

[292] Z. Qiu and U. Heinz, "Hydrodynamic event-plane correlations in Pb+Pb collisions at $\sqrt{s} = 2.76$ATeV," *Phys. Lett.*, vol. B717, pp. 261–265, 2012.

[293] D. Teaney, "The Effects of viscosity on spectra, elliptic flow, and HBT radii," *Phys. Rev.*, vol. C68, p. 034913, 2003.

[294] K. Dusling and D. Teaney, "Simulating elliptic flow with viscous hydrodynamics," *Phys. Rev.*, vol. C77, p. 034905, 2008.

[295] K. Dusling, G. D. Moore, and D. Teaney, "Radiative energy loss and v(2) spectra for viscous hydrodynamics," *Phys. Rev.*, vol. C81, p. 034907, 2010.

[296] J. Bjorken, "Highly Relativistic Nucleus-Nucleus Collisions: The Central Rapidity Region," *Phys. Rev. D*, vol. 27, pp. 140–151, 1983.

[297] L. M. Abreu, D. Cabrera, F. J. Llanes-Estrada, and J. M. Torres-Rincon, "Charm diffusion in a pion gas implementing unitarity, chiral and heavy quark symmetries," *Annals Phys.*, vol. 326, pp. 2737–2772, 2011.

[298] O. Scavenius, A. Mocsy, I. N. Mishustin, and D. H. Rischke, "Chiral phase transition within effective models with constituent quarks," *Phys. Rev.*, vol. C64, p. 045202, 2001.

Publications

Publications with star marks are included in the thesis.

Published

1. **Balbeer Singh**, Lata Thakur and Hiranmaya Mishra, *Heavy quark complex potential in a strongly magnetized hot QGP medium*, Phys. Rev. D 97 (2018) no.9, 096011, [arXiv:1711.03071 [hep-ph]].*

2. **Balbeer Singh**, Surasree Mazumder and Hiranmaya Mishra, *HQ Collisional energy loss in a magnetized medium*, JHEP 05 (2020), 068, [arXiv:2002.04922 [hep-ph]].*

3. **Balbeer Singh**, Aman Abhishek, Santosh K Das and Hiranmaya Mishra, *Heavy quark diffusion in a Polyakov loop plasma*, Phys.Rev. D 100 (2019) no.11, 114019, [arXiv:1812.05263 [hep-ph]].*

4. **Balbeer Singh** and Hiranmaya Mishra, *Heavy quark transport in a viscous semi QGP*, Phys. Rev. D 101 (2020) no.5, 054027, [arXiv:1911.06764 [hep-ph]].*

5. **Balbeer Singh**, Jitesh R Bhatt and Hiranmaya Mishra, *Probing vorticity in heavy ion collision with dilepton production*, Phys. Rev. D 100 (2019) no.1, [arXiv:1811.08124 [hep-ph]].

6. Saurav D Rindani and **Balbeer Singh**, *Indirect measurement of triple-Higgs coupling at an electron-positron collider with polarized beams* Int. J. Mod. Phys. A 35 (2020), 205011, [arXiv:1805.03417 [hep-ph]].

Submitted Papers

1. **Balbeer Singh**, Manu Kurian, Surasree Mazumder, Hiranmaya Mishra, Vinod Chandra and Santosh K Das, *Momentum broadening of heavy quark in a magnetized thermal QCD medium* [arXiv:2004.11092 [hep-ph]].* [submitted in PRD]

A.5.1 Proceedings

1. **Balbeer Singh**, Lata Thakur and Hiranmaya Mishra, *Effect of strong magnetic field on the complex heavy quark potential* DAE Symp. Nucl. Phys. **62** (2017), 946-947

2. **Balbeer Singh**, Aman Abhishek, Santosh K Das and Hiranmaya Mishra, *Non-perturbative effects on heavy quark drag*, DAE Symp. Nucl. Phys. **64** (2020), 780-781

3. **Balbeer Singh**, Aman Abhishek, Hiranmaya Mishra and Santosh K. Das, *Heavy quark transport coefficients in Polyakov loop background*; DAE High Energy Physics Symposium 2018 (Submitted).